REMOVAL OF TRACE PHARMACEUTICAL RESIDUES BY ADSORPTION ON MODIFIED INORGANIC POROUS MATERIALS

Mr. Nakorn Suriyanon

A Dissertation Submitted in Partial Fulfillment of the Requirements
for the Degree of Doctor of Philosophy Program in Environmental Management
(Interdisciplinary Program)
Graduate School
Chulalongkorn University
Academic Year 2013

Copyright of Chulalongkorn University

บทคัดย่อและแฟ้มข้อมูลฉบับเต็มของวิทยานิพนธ์ตั้งแต่ปีการศึกษา 2554 ที่ให้บริการในคลังปัญญาจุฬาฯ (CUIR)
เป็นแฟ้มข้อมูลของนิสิตเจ้าของวิทยานิพนธ์ที่ส่งผ่านทางบัณฑิตวิทยาลัย
The abstract and full text of theses from the academic year 2011 in Chulalongkorn University Intellectual Repository(CUIR)
are the thesis authors' files submitted through the Graduate School.

การกำจัดสารตกค้างจากยาที่ความเข้มข้นต่ำโดยการดูดซับด้วยตัวดูดซับพอรัสซิลิกาที่มีฟังก์ชันอินทรีย์ชนิดต่างๆ

นายนคร สุริยานนท์

วิทยานิพนธ์นี้เป็นส่วนหนึ่งของการศึกษาตามหลักสูตรปริญญาวิทยาศาสตรดุษฎีบัณฑิต
สาขาวิชาการจัดการสิ่งแวดล้อม (สหสาขาวิชา)
บัณฑิตวิทยาลัย จุฬาลงกรณ์มหาวิทยาลัย
ปีการศึกษา 2556

ลิขสิทธิ์ของจุฬาลงกรณ์มหาวิทยาลัย

Thesis Title	REMOVAL OF TRACE PHARMACEUTICAL RESIDUES BY ADSORPTION ON MODIFIED INORGANIC POROUS MATERIALS
By	Mr. Nakorn Suriyanon
Field of Study	Environmental Management
Thesis Advisor	Assistant Professor Patiparn Punyapalakul, Ph.D.
Thesis Co-advisor	Assistant Professor Chawalit Ngamcharussrivichai, Ph.D.

Accepted by the Graduate School, Chulalongkorn University in Partial Fulfillment of the Requirements for the Doctoral Degree

………………………………………..Dean of the Graduate School
(Associate Professor Amorn Petsom, Ph.D.)

THESIS COMMITTEE

………………………………………..Chairman
(Assistant Professor Chantra Tongcumpou, Ph.D.)

………………………………………..Thesis Advisor
(Assistant Professor Patiparn Punyapalakul, Ph.D.)

………………………………………..Thesis Co-advisor
(Assistant Professor Chawalit Ngamcharussrivichai, Ph.D.)

………………………………………..Examiner
(Associate Professor Jin Anotai, Ph.D.)

………………………………………..Examiner
(Assistant Professor Khemarath Osathaphan, Ph.D.)

………………………………………..External Examiner
(Boonyawan Yoosuk, Ph.D.)

นคร สุริยานนท์ : การกำจัดสารตกค้างจากยาที่ความเข้มข้นต่ำโดยการดูดซับด้วยตัวดูดซับพอรัสซิลิกาที่มีฟังก์ชันอินทรีย์ชนิดต่างๆ (REMOVAL OF TRACE PHARMACEUTICAL RESIDUES BY ADSORPTION ON MODIFIED INORGANIC POROUS MATERIALS) อ.ที่ปรึกษาวิทยานิพนธ์หลัก : ผศ ดร. ปฏิภาณ ปัญญาพลกุล, อ.ที่ปรึกษาวิทยานิพนธ์ร่วม : ผศ.ดร. ชวลิต งามจรัสศรีวิชัย., 249 หน้า.

งานวิจัยนี้มีวัตถุประสงค์เพื่อศึกษาถึงกลไกและประสิทธิภาพในการกำจัดสารตกค้างจากยาที่ความเข้มข้นต่ำโดยการดูดซับด้วยตัวดูดซับพอรัสซิลิกา โดยในการทดลองนี้ได้ทำการศึกษาการสังเคราะห์ตัวดูดซับพอรัสซิลิกาชนิดต่างๆ ได้แก่ HMS SBA-15 MCM-41 และ PMO ศึกษาการต่อติดหมู่ฟังก์ชั่นชนิดอะมิโนและเมอร์แคปโตบนพื้นผิวของตัวดูดซับชนิด HMS และศึกษาการต่อติดหมู่ฟังก์ชั่นแอมมีนที่แตกต่างกันสามชนิดลงบนพื้นผิวของตัวดูดซับชนิด PMO ที่ศึกษาวิเคราะห์คุณสมบัติทางกายภาพและทางเคมีของตัวดูดซับโดยเครื่องมือวิเคราะห์ชั้นสูงชนิดต่างๆ ผลการวิเคราะห์พบว่าตัวดูดซับที่สังเคราะห์ได้มีโครงสร้างรูพรุนที่เป็นระเบียบ จากการทดลองการดูดซับพบว่าประสิทธิภาพของการดูดซับสารตกค้างทางยาชนิด CBZ DCF และ NAP โดยตัวดูดซับชนิด HMS มีค่าเพิ่มขึ้นเมื่อทำการการต่อติดหมู่ฟังก์ชั่นชนิดเมอร์แคปโตบนพื้นผิวของตัวดูดซับ ประสิทธิภาพของการดูดซับสารตกค้างทางยาชนิด CFA และ ACT โดยตัวดูดซับชนิด HMS มีค่าเพิ่มขึ้นเมื่อทำการต่อติดหมู่ฟังก์ชั่นชนิดอะมิโนบนพื้นผิวของตัวดูดซับ ประสิทธิภาพของการดูดซับสารตกค้างทางยาชนิด CFA โดยตัวดูดซับชนิด PMO มีค่าเพิ่มขึ้นเมื่อทำการต่อติดหมู่ฟังก์ชั่นอะมิโนทั้ง 3 ชนิดบนพื้นผิวของตัวดูดซับ ชนิดของหมู่ฟังก์ชั่นและความหนาแน่นของหมู่ฟังก์ชั่นที่ต่อติดบนพื้นผิวของตัวดูดซับมีผลต่อประสิทธิภาพในการดูดซับสารตกค้างทางยาชนิด CFA จากการศึกษาการดูดซับแบบคัดเลือกพบว่า ความสามารถในการดูดซับของสารตกค้างทางยาชนิด DCF CBZ และ NAP โดยตัวดูดซับชนิด HMS และ HMS ที่ต่อติดหมู่ฟังก์ชั่นเมอร์แคปโตขึ้นอยู่กับขนาดของสารตกค้างทางยา และพบว่าความสามารถในการดูดซับของสารตกค้างทางยาชนิด DCF NAP และ CFA โดยตัวดูดซับชนิด HMS ที่มีการต่อติดหมู่ฟังก์ชั่นอะมิโนขึ้นอยู่กับความสามารถในการแตกตัวของสารตกค้างทางยา

สาขาวิชา การจัดการสิ่งแวดล้อม ลายมือชื่อนิสิต..
ปีการศึกษา 2556 ลายมือชื่อ อ.ที่ปรึกษาวิทยานิพนธ์หลัก............................
ลายมือชื่อ อ.ที่ปรึกษาวิทยานิพนธ์ร่วม............................

5287782020: MAJOR ENVIRONMENTAL MANAGEMENT
KEYWORDS: ADSORPTION / PHARMACEUTICAL RESIDUES / PERIODIC MESOPOROUS ORGANOSILICA / DIRECT CO-CONDENSTION / ORGANIC INORGANIC HYBRID MATERIALS

NAKORN SURIYANON: REMOVAL OF TRACE PHARMACEUTICAL RESIDUES BY ADSORPTION ON MODIFIED INORGANIC POROUS MATERIALS. ADVISOR: ASST. PROF. PATIPARN PUNYAPALAKUL, Ph.D., CO-ADVISOR: ASST. PROF. CHAWALIT NGAMCHARUSSRIVICHAI, Ph.D., 249 pp.

The objective of this research work is to study the mechanism and efficiency of mesoporous silica materials in removal of trace pharmaceutical residues by adsorption. HMS, SBA-15, and MCM-41 and PMO were synthesized via surfactant template method. A-HMS and M-HMS were synthesized by surface modification of virgin HMS with amino- and mercapto-organosilanes via co-condensation method. Functionalized PMOs were synthesized by surface modification of PMO with three different types of amino-organosilane. The physicochemical properties of the synthesized materials were investigated by XRD, SEM, TEM, N_2 adsorption-desorption isotherm, TGA, DTA, elemental analysis, FTIR, acid/base titration, water contact angle and zeta potential analysis. XRD patterns showed that the synthesized materials had well ordered hexagonal structure. N_2 adsorption-desorption isotherm showed that the pore sizes of synthesized materials were in the mesoscale. The removal of 5 selected pharmaceuticals (DCF, CBZ, NAP, CFA and ACT) were examined by batch adsorption experiment onto the synthesized materials. The adsorption capacity of HMS for CBZ, DCF and NAP increased after modification with mercapto functional group, whereas its adsorption for CFA and ACT increased after modification with amino functional group. The adsorption capacity of PMO for CFA increased after surface modification with mono-, di- and tri-organosilane. The adsorption capacity of PMO derivatives varied with the type and density of amine functional groups on their surface. In competitive (selective) adsorption study the adsorption capacity of HMS and M-HMS for DCF, CBZ and NAP varied with the molecular sizes of the adsorbates. But the adsorption of A-HMS for acidic pharmaceuticals (DCF, NAP and CFA) varied with the pKa of the adsorbates.

Field of Study: Environmental Management Student's Signature..............................
Academic Year: 2013 Advisor's Signature..............................
Co-advisor's Signature..............................

ACKNOWLEDGEMENTS

I would like to express my gratitude to my thesis advisor, Asst. Prof. Dr. Patiparn Punyapalakul, and my thesis co-advisor, Asst Prof. Dr. Chawalit Ngamcharussrivichai, for their helpful advices, supports, suggestions and encouragement throughout this research work.

I am grateful to Assist. Prof. Dr. Chantra Tongcumpou, chairman of the dissertation committee, Assoc. Prof. Dr. Jin Anotai, Assistant Prof. Dr. Khemarath Osathaphan and Dr. Boonyawan Yoosuk, member of dissertation committee for valuable suggestions. Without the essential contributions of the chairman and the committee member, dissertation would never be completed.

I would like to acknowledge financial support received from NCE-EHWM and graduate school, Chulalongkorn University and the 90th Anniversary of Chulalongkorn University (Ratchadaphiseksomphot Endowment Fund).

I would like to thank NCE-EHWM, Department of Environmental Engineering, Faculty of Engineering, Chulalongkorn University and Department of Chemical Technology, Faculty of Science, Chulalongkorn University for providing laboratory and research facilities.

I would like to thank Dr. Chaiwat Rongsayamanont, Dr. Seelawut Damrongsiri, Dr. Pantip Kayee, Dr. Lada Mathurasa, Dr. Jaruwan Talawat, Dr. Pummarin Khamdahsag, Dr. Pensiri Akkajit, Miss Naphatsarnan Phasukarratchai, Miss Thanatorn Yoadsomsuay, Mrs Prapaporn Luekittisup, Miss Duangjai Khankruer, Mr. Pumis Thuptimdang, Mr. Sermpong Sairiam, Miss Piyanate Nakseedee, Mr. Pharkphum Rakruam, Mr. Ekkachai Kanchantip, Mr. Nattapong Tuntiwiwattanapun, Miss Panaya Kotchaplai, Miss Chantana Intim and all my laboratory partners at NCE-EHWM lab for their kindness and friendship.

My big thankfulness goes, finally, to my father, my mother, my elder brother and my fiancee for their love and support. This work would not have been possible without their moral support.

CONTENTS

Page

ABSTRACT (IN THAI).. iv

ABSTRACT (IN ENGLISH) v

ACKNOWLEDGEMENTS.. vi

CONTENTS.. vii

LIST OF TABLES.. xiv

LIST OF FIGURES.. xvi

LIST OF ABBREVIATIONS.. xxi

CHAPTER I INTRODUCTION.. 1

1.1 State of problem 1

1.2 Objectives.. 4

1.3 Hypotheses.. 5

1.4 Scope of study.. 6

CHAPTER II BACKGROUND AND LITERATURE REVIEWS......... 8

2.1 Pharmaceutical residues.. 8

2.2 Ordered mesoporous silica materials.. 11

- 2.2.1 Silica-based materials.. 12
- 2.2.2 Surfactant template.. 13
- 2.2.3 MCM-41.. 14
- 2.2.4 HMS.. 15
- 2.2.5 SBA-15.. 16
- 2.2.6 Organic-inorganic hybrid materials.. 16
  - 2.2.6.1 Post-synthesis or grafting method............................ 17
  - 2.2.6.2 Co-condensation or direct synthesis........................... 17
- 2.2.7 PMOs.. 18

Page

2.3 Adsorption………………………………………………………….. 19

2.3.1 Transport phenomena………………………………………………. 20

2.3.2 Physical and chemical adsorption………………………………….. 20

2.3.3 Adsorption capacity………………………………………………… 21

2.4 Literature reviews………………………………………………………… 22

2.4.1 Pharmaceutical residues……………………………………………. 22

2.4.2 Adsorption by silica based porous materials………………………. 24

2.4.3 Adsorption of pharmaceutical residue by silica based porous materials…………………………………………………………… 25

CHAPTER III METHODOLOGY………………………………………… 27

3.1 Materials…………………………………………………………………….. 27

3.1.1 Pharmaceutical residues ……………………………………………. 27

3.1.2 Silica source precursors…………………………………………….. 27

3.1.3 Surfactants………………………………………………………….. 27

3.1.4 Organic functional groups………………………………………….. 27

3.1.5 Powdered activated carbon ………………………………………… 28

3.1.6 Others chemical reagents…………………………………………… 28

3.2 Methodology……………………………………………………………….. 28

3.2.1 Phase I: Synthesis and characterization of porous silicas…..……… 28

3.2.2 Phase II: Removal of trace pharmaceutical residues by adsorption on mesoporous silicas ……………………………………………… 30

3.2.3 Phase III: Synthesis and characterization of periodic mesoporous organosilicas………………………………………………………. 31

3.2.4 Phase IV: Removal of Clofibic acid by adsorption on periodic mesoporous organosilicas………………………………………… 31

3.3 Analytical method……….. 31

3.3.1 Pretreatment of samples…………………………………………….. 31

Page

3.3.2 Quantification of pharmaceutical residues………………………… 32

CHAPTER IV SYNTHESIS AND CHARACTERIZATION OF MESOPOROUS SILICAS…………………………………………………........ 33

4.1 Introduction…………………………………………………………... 33

4.2 Method……………………………………………………………… 33

4.2.1 Synthesis of HMS……………………………………………… 33

4.2.2 Synthesis of SBA-15…………………………………………….. 34

4.2.3 Synthesis of MCM-41…………………………………………… 34

4.2.4 Synthesis of amino or mercapto functionalized HMS via direct co-condensation method……………………………………………. 34

4.2.5 Characterization………………………………………………… 35

4.2.5.1 X-ray Diffraction ……………………………………….. 35

4.2.5.2 Scanning electron microscopy micrographs……….……… 35

4.2.5.3 Nitrogen gas adsorption-desorption.................................... 35

4.2.5.4 Thermogravimetric analysis …………... ………………… 36

4.2.5.5 Elemental analysis……………………………………… 36

4.2.5.6 Fourier transform infrared spectroscopy……….………… 36

4.2.5.7 Point of zero charge and hydrophobic/hydrophilic surface characteristics of the adsorbents………………………….. 36

4.3 Results and discussion……………………………………………… 37

4.3.1 X-ray Diffraction………………………………………………… 37

4.3.2 Scanning electron microscopy micrographs………………………. 40

4.3.3 Nitrogen gas adsorption-desorption..……………………………… 44

4.3.4 Thermogravimetric analysis……………………………………….. 47

4.3.5 Elemental analysis………………………………………………… 50

4.3.6 Fourier transform infrared spectroscopy…………………………. 50

Page

4.3.7 Point of zero charge and hydrophobic/hydrophilic surface characteristics of the adsorbents…………………………………… 51

4.4 Conclusions……………………………………………………………….. 52

CHAPTER V REMOVAL OF TRACE PHARMACEUTICAL RESIDUES BY ADSORPTION ON MESOPOROUS SILICAS……….. 54

5.1 Introduction…………………………………………………………… 54

5.2 Method……………………………………………………………….. 54

5.2.1 Adsorption kinetics……………………………………………… 54

5.2.2 Adsorption isotherm evaluation………………………………….. 55

5.2.3 Effects of pH and temperature on the adsorption capacity of adsorbent………………………………………………………… 55

5.2.4 Competitive adsorption………………………………………. 55

5.3 Results and discussion……………………………………………… 55

5.3.1 Adsorption kinetics……………………………………………. 55

5.3.2 Adsorption kinetic models……………………………………... 60

5.3.3 Diffusion mechanism…………………………………………… 68

5.3.4 Adsorption isotherm modeling………………………………… 75

5.3.5 Adsorption mechanisms……………………………………….. 108

5.3.5.1 Effect of surface functional group………………………… 108

5.3.5.2 Effect of the adsorbent's surface area……………………… 110

5.3.5.3 Effect of pH………………………………………………… 112

5.3.5.4 Effect of temperature and thermodynamic parameters……... 116

5.3.5.5 Competitive adsorption…………………..………................. 118

5.4 Conclusions…………………………………………………………. 121

CHAPTER VI SYNTHESIS AND CHARACTERIZATION OF PERIODIC MESOPOROUS ORGANOSILICAS……………………….. 123

Page
6.1 Introduction………………………………………………………… 123
6.2 Method…………………………………………………………… 123
  6.2.1 Synthesis of periodic mesoporous organosilica……………………. 123
  6.2.2 Synthesis of amino functionalized PMO via direct co-condensation method………………………………………………………… 124
  6.2.3 Characterization……………………………………………….. 124
    6.2.3.1 X-ray Diffraction………………………………………… 124
    6.2.3.2 Nitrogen sorption.. 124
    6.2.3.3 Scanning electron microscope…………………………… 125
    6.2.3.4 Transmission electron microscope…………………………. 125
    6.2.3.5 Thermogravimetric analysis and Differential thermal analysis…………………………………………………… 126
    6.2.3.6 Elemental analysis……………………………………….. 126
    6.2.3.7 Fourier transform infrared spectroscopy………………........ 126
    6.2.3.8 Zeta potential…………………………………………….. 126
6.3 Results and discussion……………………………………………… 126
  6.3.1 X-ray Diffraction………………………………….…………… 126
  6.3.2 Nitrogen gas sorption…………………………………………….. 132
  6.3.3 Scanning electron microscope……………………………………. 138
  6.3.4 Transmission electron microscope……………………………….. 141
  6.4.5 Thermogravimetric analysis and Differential thermal analysis…….. 142
  6.3.6 Elemental analysis………………………………………………… 144
  6.3.7 Fourier Transform Infrared Spectroscopy…………………………… 145
  6.3.8 Zeta potential……………………………………………………… 155
6.4 Conclusions………………………………………………………….. 156

CHAPTER VII REMOVAL OF CLOFIBRIC ACID BY ADSORPTION ON PERIODIC MESOPOROUS ORGANOSILICAS……………………. 158

Page

7.1 Introduction………………………………………………………………. 158

7.2 Method……………………………………………………………………. 158

7.2.1 Adsorption kinetics………………………………………………….. 158

7.2.2 Adsorption isotherm evaluation…………………………………….. 159

7.2.3 Effects of pH on the adsorption capacity of adsorbent…………….. 159

7.3 Results and discussion…………………………………………………… 159

7.3.1 Adsorption kinetic…………………………………………………….. 159

7.3.2 Adsorption kinetic models………………………………………….. 161

7.3.3 Diffusion mechanism……………………………………………….. 163

7.3.3.1 Weber and Morris intraparticle diffusion model………….. 163

7.3.3.2 Boyd kinetic model……………………………………….... 165

7.3.3.3 Pore diffusion (by Fick's law)…………………………….. 167

7.3.4 Adsorption isotherms modeling…………………………………….. 167

7.3.5 Adsorption mechanism……………………………………………... 170

7.3.5.1 Effect of functional groups………………………………… 170

7.3.5.2 Effect of the adsorbent's surface area……………………… 172

7.3.5.3 Effect of surface functional groups density……………….. 172

7.3.5.4 Effect of nitrogen contents in the adsorbents……………… 173

7.3.5.5 Effect of pH………………………………………………… 174

7.4 Conclusions………………………………………………………………. 176

CHAPTER VIII CONCLUSIONS AND RECOMMENDATIONS……. 177

8.1 Conclusions……………………………………………………………… 177

8.1 Recommendations………………………………………………………. 180

REFERENCES………………………………………………………………... 181

APENDICES………………………………………………………………… 196

Page

APENDIX A HPLC Chromatograms of pharmaceutical residues………….. 197

APENDIX B Experimental results for removal of trace pharmaceutical residues by adsorption on mesoporous silicas……………….. 201

APENDIX C Experimental results for removal of Clofibic acid by adsorption on periodic mesoporous organosilicas………………………. 239

BIOGRAPHY……………………………………………………………….. 249

LIST OF TABLES

Table Page

2.1 Properties of pharmaceutical compounds……………………………. 10

2.2 Recipes for synthesis of PMOs……………………………………….. 19

4.1 Physicochemical characteristics of HMS, M-HMS, A-HMS, SBA-15, MCM-41 and PAC…………………………………………………. 46

5.1 Kinetic parameters for the adsorption of DCF onto HMS, modified HMS derivatives, SBA-15, MCM-41 and PAC………………………. 63

5.2 Kinetic parameters for the adsorption of CBZ onto HMS, modified HMS derivatives, SBA-15, MCM-41 and PAC………………………. 64

5.3 Kinetic parameters for the adsorption of NAP onto HMS, modified HMS derivatives, SBA-15, MCM-41 and PAC………………………. 65

5.4 Kinetic parameters for the adsorption of CFA onto HMS, modified HMS derivatives, SBA-15, MCM-41 and PAC………………………. 66

5.5 Kinetic parameters for the adsorption of ACT onto HMS, modified HMS derivatives, SBA-15, MCM-41 and PAC………………………. 67

5.6 Isotherm parameters for sorption of DCF…………………………….. 103

5.7 Isotherm parameters for sorption of CBZ…………………………….. 104

5.8 Isotherm parameters for sorption of NAP…………………………….. 105

5.9 Isotherm parameters for sorption of CFA…………………………….. 106

5.10 Isotherm parameters for sorption of ACT…………………………….. 107

5.11 Thermodynamic parameters for sorption of DCF, CBZ, and NAP onto M-HMS, and for sorption of CFA and ACT onto A-HMS at three different temperatures………………………………………... 117

6.1 d_{100} spacings of PMOs samples………………………………………. 127

6.2 Structural properties of functionalized periodic mesoporous organosilicas……………………………………………………….. 134

6.3 BET, KJS and SF pore diameter of PMOs samples…………………. 136

6.4 Total nitrogen content of PMOs functionalized with 1N-, 2N- and 3N 145

Table Page

silane………………………………………………………………..

6.5 Zeta potentials of PMO and PMO derivatives at pH 5, 7 and 9…….. 156

7.1 Kinetic parameters for the adsorption of CFA onto PMO and the functionalized PMO derivatives……………………………………… 162

7.2 Pore diffusion coefficient of the adsorption processes………………. 168

7.3 Isotherm parameters for sorption of CFA……………………………. 169

LIST OF FIGURES

Figure Page

2.1 Fate of pharmaceuticals in the environment 9
2.2 Pharmaceutical compounds detected in the environment 9
2.3 Molecular structures of pharmaceutical compounds 10
2.4 Porous silica phase diagram for cationic surfactant in water 14
2.5 Scheme of S^+I^- and $S^+X^-I^+$ electrostatic interactions in MCM-41 synthesized process 15
2.6 Scheme of S^0I^0 hydrogen bonding interactions in HMS synthesized process. 15
2.7 Scheme of $(S^0H^+)(X^-I^+)$ hydrogen bonding interactions in SBA-15 synthesized process 16
2.8 Synthesis of organic-inorganic hybrid material via grafting method 17
2.9 Synthesis of organic-inorganic hybrid material via co-condensation method 18
2.10 Transport processes of the adsorbate to surface site of the adsorbent 21
3.1 Experimental framework of this study 29
4.1 Low-angle XRD patterns of as-synthesized and calcined HMS 38
4.2 Low-angle XRD patterns of as-synthesized and extracted M-HMS 39
4.3 Low-angle XRD patterns of as-synthesized and extracted A-HMS 39
4.4 Low-angle XRD patterns of as-synthesized and extracted SBA-15 39
4.5 Low-angle XRD patterns of as-synthesized and extracted MCM-41 40
4.6 SEM micrographs of calcined HMS 41
4.7 SEM micrographs of extracted M-HMS 42
4.8 SEM micrographs of extracted A-HMS 42
4.9 SEM micrographs of calcined SBA-15 43
4.10 SEM micrographs of calcined MCM-41 43
4.11 Nitrogen gas adsorption-desorption isotherms plots of calcined or extracted silicate materials 45

Figure Page

4.12 TGA curves of as-synthesized and calcined HMS…………………… 48

4.13 TGA curves of as-synthesized and extracted M-HMS……………… 48

4.14 TGA curves of as-synthesized and calcined SBA-15……………….. 49

4.15 TGA curves of as-synthesized and calcined MCM-41……………… 50

4.16 FTIR spectra of template removed HMS, M-HMS and A-HMS…… 51

5.1 Adsorption kinetics of DCF adsorbed onto the different mesoporous silicates and PAC…………………………………………………….. 56

5.2 Adsorption kinetics of CBZ adsorbed onto the different mesoporous silicates and PAC……………………………………………………. 57

5.3 Adsorption kinetics of NAP adsorbed onto the different mesoporous silicates and PAC…………………………………………………….. 58

5.4 Adsorption kinetics of CFA adsorbed onto the different mesoporous silicates and PAC……………………………………………………. 59

5.5 Adsorption kinetics of ACT adsorbed onto the different mesoporous silicates and PAC…………………………………………………….. 60

5.6 Intraparticle diffusion plot of DCF adsorbed onto HMS, modified HMS derivatives, SBA-15, MCM-41 and PAC…………………….... 70

5.7 Intraparticle diffusion plot of CBZ adsorbed onto HMS, modified HMS derivatives, SBA-15, MCM-41 and PAC…………………….. 71

5.8 Intraparticle diffusion plot of NAP adsorbed onto HMS, modified HMS derivatives, SBA-15, MCM-41 and PAC…………………….. 72

5.9 Intraparticle diffusion plot of CFA adsorbed onto HMS, modified HMS derivatives, SBA-15, MCM-41 and PAC…………………….. 73

5.10 Intraparticle diffusion plot of ACT adsorbed onto HMS, modified HMS derivatives, SBA-15, MCM-41 and PAC…………………….. 74

5.11 Adsorption isotherm of DCF removal according to the Langmuir isotherm model……………………………………………………. 78

5.12 Adsorption isotherm of CBZ removal according to the Langmuir isotherm model……………………………………………………. 79

Figure Page
5.13 Adsorption isotherm of NAP removal according to the Langmuir isotherm model………………………………………………………. 80
5.14 Adsorption isotherm of CFA removal according to the Langmuir isotherm model………………………………………………………. 81
5.15 Adsorption isotherm of ACT removal according to the Langmuir isotherm model………………………………………………………. 82
5.16 Adsorption isotherm of DCF removal according to the Freundlich isotherm model………………………………………………………. 83
5.17 Adsorption isotherm of CBZ removal according to the Freundlich isotherm model………………………………………………………. 84
5.18 Adsorption isotherm of NAP removal according to the Freundlich isotherm model………………………………………………………. 85
5.19 Adsorption isotherm of CFA removal according to the Freundlich isotherm model………………………………………………………. 86
5.20 Adsorption isotherm of ACT removal according to the Freundlich isotherm model………………………………………………………. 87
5.21 Adsorption isotherm of DCF removal according to the D-R isotherm model………………………………………………………………. 88
5.22 Adsorption isotherm of CBZ removal according to the D-R isotherm model………………………………………………………………. 89
5.23 Adsorption isotherm of NAP removal according to the D-R isotherm model………………………………………………………………. 90
5.24 Adsorption isotherm of CFA removal according to the D-R isotherm model………………………………………………………………. 91
5.25 Adsorption isotherm of ACT removal according to the D-R isotherm model………………………………………………………………. 92
5.26 Adsorption isotherm of DCF removal according to the Temkin isotherm model………………………………………………………. 93
5.27 Adsorption isotherm of CBZ removal according to the Temkin isotherm model………………………………………………………. 94

Figure Page

5.28 Adsorption isotherm of NAP removal according to the Temkin isotherm model………………………………………………………. 95

5.29 Adsorption isotherm of CFA removal according to the Temkin isotherm model………………………………………………………. 96

5.30 Adsorption isotherm of ACT removal according to the Temkin isotherm model………………………………………………………. 97

5.31 Adsorption isotherm of DCF removal according to the Linear isotherm model………………………………………………………. 98

5.32 Adsorption isotherm of CBZ removal according to the Linear isotherm model………………………………………………………. 99

5.33 Adsorption isotherm of NAP removal according to the Linear isotherm model………………………………………………………. 100

5.34 Adsorption isotherm of CFA removal according to the Linear isotherm model………………………………………………………. 101

5.35 Adsorption isotherm of ACT removal according to the Linear isotherm model………………………………………………………. 102

5.36 Adsorption capacity of HMS, M-HMS, A-HMS and PAC for DCF, CBZ, NAP, CFA and ACT…………………………………………… 108

5.37 Adsorption capacity of HMS, SBA-15 and MCM 41 for DCF, CBZ, NAP, ACT and CFA………………………………………………… 111

5.38 Adsorption capacity per surface area of HMS, SBA-15 and MCM 41 for DCF, CBZ, NAP, ACT and CFA……………………………….. 112

5.39 Adsorption capacity of HMS, M-HMS, A-HMS and PAC for DCF at pH 5, 7 and 9………………………………………………………… 113

5.40 Adsorption capacity of HMS, M-HMS, A-HMS and PAC for CBZ at pH 5, 7 and 9………………………………………………………… 114

5.41 Adsorption capacity of HMS, M-HMS, A-HMS and PAC for NAP at pH 5, 7 and 9………………………………………………………… 114

5.42 Adsorption capacity of HMS, M-HMS, A-HMS and PAC for CFA at pH 5, 7 and 9………………………………………………………… 115

Figure Page

5.43 Adsorption capacity of HMS, M-HMS, A-HMS and PAC for ACT at pH 5, 7 and 9………………………………………………………. 115

5.44 Adsorption capacity of M-HMS in single solute and mixed solute solutions……………………………………………………………… 118

5.45 Adsorption capacity of A-HMS in single solute and mixed solute solutions…………………………………………………………... 118

5.46 Adsorption capacity of HMS in single solute and mixed solute solutions…………………………………………………………….. 119

5.47 Adsorption capacity of PAC in single solute and mixed solute solutions…………………………………………………………….. 119

6.1 Structural formulas of 1N-, 2N- and 3N-silane…………………….. 125

6.2 Low-angle XRD patterns of as-synthesized and extracted PMO…... 128

6.3 Low-angle XRD patterns of as-synthesized and extracted 1N10PMO 129

6.4 Low-angle XRD patterns of as-synthesized and extracted 1N25PMO 129

6.5 Low-angle XRD patterns of as-synthesized and extracted 1N40PMO 129

6.6 Low-angle XRD patterns of as-synthesized and extracted 2N10PMO 130

6.7 Low-angle XRD patterns of as-synthesized and extracted 2N25PMO 130

6.8 Low-angle XRD patterns of as-synthesized and extracted 2N40PMO 131

6.9 Low-angle XRD patterns of as-synthesized and extracted 3N10PMO 131

6.10 Low-angle XRD patterns of as-synthesized and extracted 3N25PMO 131

6.11 Low-angle XRD patterns of as-synthesized and extracted 3N40PMO 132

6.12 Nitrogen gas adsorption/desorption isotherms of extracted ethanesilicas……………………………………………………... 133

6.13 Pore size distribution of extracted ethanesilicas……………………… 135

6.14 SEM micrographs of extracted virgin PMO………………………….. 139

6.15 SEM micrographs of extracted 1NPMOs……………………………. 139

6.16 SEM micrographs of extracted 2NPMOs……………………………. 140

6.17 SEM micrographs of extracted 3NPMOs……………………………. 140

6.18 TEM microphotographs of PMO, 1N25PMO, 2N25PMO and 3N25PMO……………………………………………………………… 141

Figure Page

6.19 TG/DTA curves of as-synthesized and extracted PMO....................... 143

6.20 TG/DTA curves of as-synthesized and extracted 1N25PMO……… 143

6.21 TG/DTA curves of as-synthesized and extracted 2N25PMO……… 143

6.22 TG/DTA curves of as-synthesized and extracted 3N25PMO……… 144

6.23 FTIR spectra of as-synthesized and extracted PMO………………… 146

6.24 FTIR spectra of as-synthesized and extracted 1N10PMO………….. 147

6.25 FTIR spectra of as-synthesized and extracted 1N25PMO………….. 147

6.26 FTIR spectra of as-synthesized and extracted 1N40PMO………….. 148

6.27 FTIR spectra of as-synthesized and extracted 2N10PMO………….. 148

6.28 FTIR spectra of as-synthesized and extracted 2N25PMO………….. 149

6.29 FTIR spectra of as-synthesized and extracted 2N40PMO………….. 149

6.30 FTIR spectra of as-synthesized and extracted 3N10PMO………….. 150

6.31 FTIR spectra of as-synthesized and extracted 3N25PMO………….. 150

6.32 FTIR spectra of as-synthesized and extracted 3N40PMO………….. 151

6.33 Comparative spectra of extracted 1N10PMO, 1N25PMO and 1N40PMO………………………………………………………… 153

6.34 Comparative spectra of extracted 2N10PMO, 2N25PMO and 2N40PMO………………………………………………………… 154

6.35 Comparative spectra of extracted 3N10PMO, 3N25PMO and 3N40PMO…………………………………………………………. 155

7.1 Adsorption kinetics of CFA adsorbed onto different kinds of mesoporous silicates………………………………………………. 160

7.2 Weber and Morris intraparticle diffusion plot of CFA adsorbed onto the different kinds of PMOs………………………………………. 164

7.3 Boyd kinetic diffusion plot of CFA adsorbed onto the different kinds of PMOs…………………………………………………………. 166

7.4 Adsorption capacity of PMOs with different functional groups……... 170

7.5 Adsorption capacity of PMOs with different functional groups per surface area………………………………………………………… 172

7.6 Adsorption capacity of PMOs with different surface functional group 174

Figure Page

densities per surface area……………………………………………..

7.7 Adsorption capacity of PMOs with different surface functional group densities per nitrogen content………………………………………… 175

7.8 Adsorption capacity of PMOs at different pH……………………….. 175

LIST OF ABBTEVATIONS

ACT	Acetaminophen
A-HMS	Amine-functionalized Hexagonal mesoporous silicate
BET	Branauer Teller Emmett
BJH	Barrett-Joyner-Halenda
BTSEB	1,4-Bis(trimethoxysilylethyl)benzene
BTME	1,2-Bis(trimethoxysilyl)ethane
BTSE	Bis(triethoxysilyl)ethane
CBZ	Carbamazepine
CFA	Clofibic acid
CMC	Critical micelle concentration
CTAC	Hexadecyltrimethylammonium chloride
CTAB	Hexadecyltrimethylammonium bromide
DCAN	Dicloroacetonitrile
D-R	Dubinin-Radushkevich
DCAN	Dicloroacetonitrile
DCF	Diclofenac
DTA	Differential thermo analysis
FTIR	Fourier transform infrared spectroscopy
HANs	Haloacetoniotriles
HMS	Hexagonal mesoporous silicate
HPLC	High-performance liquid chromatography
MCM-41	Mobil crystalline material no-41 or Mobil composition of matter no.41
M-HMS	Mercapto-functionalized hexagonal mesoporous silicate
NAP	Naproxen
NOEC	No observed effect concentration
NSAID	Non-steroidal anti-inflammatory drugs
ODTMA	Octadecyltrimethyl ammonium chloride
ODTMABr	Octadecyltrimethylammonium bromide
PAC	Powdered activated carbon
pH_{pzc}	Point of zero charge

PMO	Periodic mesorpous organosilica
SBA-15	Santa Barbara amorphous-15
SEM	Scanning electron microscope
SPE	Solid phase extraction
STP	Sewage treatment plant
TEM	Transmission electron microscope
TEOS	Tetraethylorthosilicate
TESPTS	Bis[3-(triethoxysilyl)propyl]tetrasulfide
TGA	Thermogravimetric analysis
TMOS	Tetramethylorthosilicate
XRD	X-ray diffraction
1N-silane	3-Aminopropyl)trimethoxysilane
2N-silane	3-[2-(2-Aminoethylamino)ethylamino]propyltrimethoxysilane)
3N-silane	[2-(2-Aminoethylamino)propyl]trimethoxysilane
1NPMOs	Mono-aminopropyl functionalized periodic mesoporous silicas
2NPMOs	Di-aminopropyl functionalized periodic mesoporous silicas
3NPMOs	Tri-aminopropyl functionalized periodic mesoporous silicas

CHAPTER I

INTRODUCTION

1.1 State of problem

Pharmaceuticals such as non-steroidal anti-inflammatory drugs (NSAID), antibiotics, lipid regaulators, sex hormones, antiepileptics, beta-blockers etc., are used worldwide for treatment of diseases in humans and animals. Some of them are used in farming industry too. These pharmaceutical compounds are very often, incompletely metabolized in the bodies of human and animals and their tranform producted might cause a variety of adverse effects, including acute and chronic toxicity to animal and microorganisms in environments [Brigante et al., 2012]. Pharmaceutical residues were reported to be present in wastewater treatment plant, ground water, river and reservoirs at the concentration ranging up to μg/L [Ternes, 1998; Kummerer 2001; Thacker et al., 2005; Tixier et al., 2003; Skadsen et al., 2004; Hua et al., 2006; Clara et al., 2004; Paxeus 2004; Buser et al., 1998; Thomas and Hilton, 2004; Rabiet et al., 2006]. That can be indicated that conventional wastewater treatment plant could not complete remove of pharmaceutical residues.

Chemical treatment (such as ozonation, oxidation), and physicochemical treatment (such as adsorption, membrane filtration, and coagulation) have been used for removal of pharmaceuticals from aqueous solution [Radjenovic et al., 2009; Suarez et al., 2009; Gebhardt and Schroder, 2007; Matamoros et al., 2008; Rosal et al., 2010; Weiss and Reemtsma, 2008; Coelho et al., 2009; Kimura and Watanabe, 2005]. However, adsorption is a preferable method for the removal of pharmaceutical residues [Bui and Choi, 2012], because it has the advantages of producing high-quality treated effluents, is easy and cheap to run, and does not have the problem of undesirable by-products [Al-Ghouti et al., 2009; Brown et al., 2001, Allen et al, 2001]. Powdered activated carbon (PAC) is one of the most popular adsorbents [El

Qada et al., 2006; El Qada et al., 2008]. It contains numerous pores of varying sizes and has different functional groups on its surface. However, PAC has the drawback of the difficulty in regeneration process and has a low selective adsorption of organic adsorbates, especially at low concentrations.

Inorganic materials with mesoporous structures, such as hexagonal mesoporous silicate (HMS), Santa Barbara amorphous-15 (SBA-15) and Mobile crystalline material no-41 (MCM-41), are alternative adsorbents for water treatment [Bui and Choi, 2012]. They possess a high porosity, uniform pore size, orderly arrangement of pore structures, large pore volume, narrow pore size and a high surface area, all of which enhance their adsorption capacity. The presence of a high density of surface silanol groups allows them to be modified easily with various organosilanes to improve the adsorption selectivity to target molecules, and to increase their adsorption capacity [Walcarius et al., 2003; Mercier and Pinnavia, 1999]. Although there have been many research studies on the removal of heavy metals, dyes, phosphate and nitrate anions, haloacetic acids and haloacetonitriles [Lee et al., 2001; Prarat et al., 2011; Punyapalakul et al., 2009; Punyapalakul and Takizawa, 2006], there have been relatively few studies on the adsorptive removal of pharmaceutical residues by functionalized silica-based porous materials [Punyapalakul and Sitthisorn, 2010; Wang et al., 2009].

Periodic mesorpous organosilica (PMO) is a new class of organic-inorganic hybrid materials with organic moieties incorporated into the pore wall network. The distribution of the organic moieties of PMOs should be more homogeneous than the organic-inorganic hybrid materials which are synthesized by grafting and co-condensation method [Xhang et al., 2005; Wahab et al., 200]. Compared with other mesporous silicas, there have been much fewer reports on the research studies related to the synthesis of PMO, its modification with organic funtional groups and its application for the adsorptive removal of undesirable substances. Before our study, there have been no report on the usage of PMO for adsorption of pharmaceutical residues.

In this study, the adsorption capacities and related mechanism about the removal of trace pharmaceutical residues by adsorption on modified inorganic porous materials were reported and can be divided into 4 phases.

In the 1st phase, we report on the synthesis and characterization of silica based mesoporous materials and inorganic-organic hybrid materials. HMS, SBA-15 and MCM-41 were synthesized via surfactant template method. Two inorganic organic hybrid materials namely A-HMS and M-HMS, were synthesized by modifying the surface of virgin HMS with two different types of organosilane, i.e. mercaptoprpyltrimethoxysilnae and aminopropyltrimethosysilane via direct co-condensation method. The physicochemical properties of adsorbents were investigated by low-angle powder x-ray diffraction (XRD), scanning electron microscope (SEM), nitrogen gas adsorption and desorption isotherms, thermogravimetric analysis (TGA), elemental analysis, Fourier transform infrared spectroscopy (FTIR), zeta potential analysis by acid/base tritration and water contact angle analysis by tensiometer.

In the 2nd phase, we report on a study into the removal of a low concentration of five pharmaceutical residues, i.e. Acetaminophen (ACT), Clofibric acid (CFA), Carbamazepine (CBZ), Diclofenac (DCF) and Naproxen (NAP), from aqueous solution by adsorption onto A-HMS and M-HMS in comparison with that obtained with pristine HMS, SBA-15, MCM-41 and PAC. The adsorption mechanism was investigated by analyzing the adsorption kinetics, isotherms and thermodynamics under various conditions, and used in comparison between different adsorbates to simultaneously elucidate the potential effects of the surface functional group, pH and temperature on the adsorption capacity.

In the 3rd phase, PMOs was synthesized via surfactant template method. In this study we modified the surface of PMO via direct-cocondensation method with three different types of organosilane, i.e. mono-, di- and triamino-organoalkoxsysilanes. The physicochemical properties of adsorbents were investigated by XRD, SEM, transmission electron microscope (TEM), nitrogen gas adsorption and desorption isotherms, TGA, differential thermo analysis (DTA), elemental analysis, FTIR and zetapotential analyzer.

In the final phase, we report on a study into the removal of a low concentration of pharmaceutical residue (CFA) from aqueous solution by adsorption onto virgin PMO and PMO which were functionalized with three type of amino-functional groups (mono-, di- and tri-amino propyl functional groups) (1NPMOs, 2NPMOs and 3NPMOs, respectively). The adsorption mechanism was investigated by analyzing the adsorption kinetics and isotherms under various conditions, and used in comparison between different adsorbates to simultaneously elucidate the potential effects of the surface functional group, adsorbent surface area, surface functional groups density, nitrogen contents and pH on the adsorption capacity.

1.2 Objectives

The primary objective of this research was to investigate the removal of 5 pharmaceutical residues (i.e. DCF, CBZ, ACT, CFA and NAP) onto silica-based porous materials and other adsorbents. The sub-objectives were as follows:

Phase 1: Synthesis and characterization of mesoporous silicas.

1. To synthesize and characterize the physicochemical properties of HMS, SBA-15 and MCM-41 which are synthesized via surfactant template method.
2. To synthesize and characterize the physicochemical properties of mercapto-functionalized HMS and amino-functionalized HMS which are functionalized via direct co-condensation method.

Phase 2: Removal of trace pharmaceutical residues by adsorption on mesoporous silicas.

1. To investigate the effects of surface functional groups, surface area, pore size, pH and temperature on adsorption capacities and mechanism of adsorption of pharmaceutical residues onto mesoporous silicas.

2. To investigate the selective adsorption of mixed pharmaceutical residues onto mesoporous silicas.

Phase 3: Synthesis and characterization of periodic mesoporous organosilicas.

1. To synthesize and characterize the physicochemical properties of PMO which synthesized via surfactant template method.
2. To synthesize and characterized the physicochemical properties of amino-functionalized PMOs which functionalized via direct co-condensation methods using organoalkoxysilanes containing one, two and three amino groups.

Phase 4: Removal of Clofibic acid by adsorption on periodic mesoporous organosilicas.

1. To investigate the effects of surface functional groups, surface area, functional group density, nitrogen content and pH on adsorption capacities and mechanism of adsorption of Clofibric acid onto PMOs.

1.3 Hypotheses

The hypotheses of this study were as follows:

Phase 1: Synthesis and characterization of mesoporous silicas.

1. The physicochemical properties of HMS, MCM-41 and SBA-15 which are synthesized from surfactant template are different depending on the characteristics of the reactants and the synthesis protocol.
2. Functionalization HMS with mercaptopropyl-organosilane or aminopropyl-organosilane via direct co-condensation methods has an effect on the physicochemical properties of HMS.

Phase 2: Removal of trace pharmaceutical residues by adsorption on mesoporous silicas.

1. Surface modification of mesoporous silicate materials with hydrophobic functional groups increases the adsorption capacity of adsorbents for pharmaceutical residues.

2. The adsorption capacities of adsorbents can be increased by decreasing the pH of the solution to lower than point of zero charge (pH_{pzc}).

3. The adsorption capacities of silica-based porous materials can be enhanced by increasing temperature.

4. The mechanism of adsorption of each individual pharmaceutical compound in the mixed solution by each adsorbent is different depending on the physico-chemical properties of the adsorbate (surface functional group, molecular structure, molecular weight, molecular size) and of the adsorbent (surface functional group and porous structure).

Phase 3: Synthesis and characterization of periodic mesoporous organosilicas.

1. Functionalized PMO with organoalkoxysilanes containing one, two and three amino groups via direct co-condensation methods have an effect on the physicochemical properties of HMS.

Phase 4: Removal of Clofibic acid by adsorption on periodic mesoporous organosilicas.

1. Surface modification of PMO with organoalkoxysilanes containing one, two and three amino functional groups increases the adsorption capacity of adsorbents for Clofibric acid.

2. The adsorption capacities of PMO and PMO derivatives can be increased by decreasing the pH of the solution to lower than pH_{PZC}.

1.4 Scope of study

The scopes of this study are as follows:

1. Five pharmaceutical compounds were used as the adsorbates in this study.

2. Mesoporous silicas and periodic mesoporous organosilicas were synthesized. These synthesized adsorbents as well as commercial PAC were used as the adsorbents in this study.
3. The physicochemical properties of the adsorbents (i.e. XRD pattern, surface area, average pore size, pore size distribution, surface functional group, nitrogen content, sulfur content, hydrophobic/hydrophilic surface characteristic, surface charge density) were characterized
4. The adsorption study of the single and mixed pharmaceutical compound was done at low concentration (40-200 ppb) to investigate the adsorption mechanism of the adsorbents.

CHAPTER II

BACKGROUND AND LITERATURE REVIEWS

2.1 Pharmaceutical residues

In this decade, pharmaceutical residue has become an interesting topic to environmental scientists and researchers. Large amounts of pharmaceutical compounds have been used for treatments of diseases in both human and animals, and their residues may damage or have effects on ecology. These pharmaceutical compounds are very often, incompletely metabolized in the bodies of human and animals. These metabolites are excreted, distributed and remain in the environment. The fate of pharmaceuticals in the environment is shown in Figure 2.1.

Pharmaceutical residues were reported to be present in wastewater treatment plant, ground water, river and reservoirs at the concentration ranging up to μg/L [Ternes, 1998; Kümmerer 2001; Thacker et al., 2005; Tixier et al., 2003; Skadsen et al., 2004; Hua et al., 2006; Clara et al., 2004b; Paxéus 2004; Buser et al., 1998; Thomas and Hilton, 2004; Rabiet et al., 2006]. According to the data presented in literatures as shown in Figure 2.2, non-steroidal anti-inflammatory drugs , antibiotics, blood lipid lowering agents (or antilipidemics), sex hormones and antiepileptics were the groups of pharmaceutical compounds most frequently detected in the environment. In this study, we did the study on adsorption of only some pharmaceutical compounds in NSAID, antiepileptic and antilipidemic groups. In the NSAID group, the drugs used in this study were DCF, NAP and ACT. In the antiepileptic and antilipidemic groups, the drugs used in this study were CBZ and CFA respectively. The properties and molecular structure of these pharmaceutical compounds are shown in Table 2.1 and Figure 2.3 respectively.

Table 2.1 Properties of pharmaceutical compounds

No	Pharmaceutical	Formula	MW	Log Kow	pKa	Functional group
1	ACT	$C_8H_9NO_2$	151.2 ^{a}	0.46^{d}	9.38 ^{d}	OH
2	CFA	$C_{10}H_{11}O_3Cl$	214.5 ^{b}	2.57 ^{e}	2.84^{b}	COOH
3	CBZ	$C_{15}H_{12}N_2O$	236.27 ^{c}	2.45 ^{e}	13.9 ^{e}	NH_2
4	DCF	$C_{14}H_{11}C_{12}NO_2$	296.15 ^{c}	4.5 ^{e}	4.2 ^{e}	COOH
5	NAP	$C_{14}H_{14}O_3$	230.27^{a}	3.18 ^{f}	4.15 ^{b}	COOH

a: Kim and Tanaka, 2009. b: Sim et al., 2010. c: Munoz et al., 2009. d: Radjenovic et al., 2008. e: Pavlovic et al., 2007. f: Carballa et al., 2005

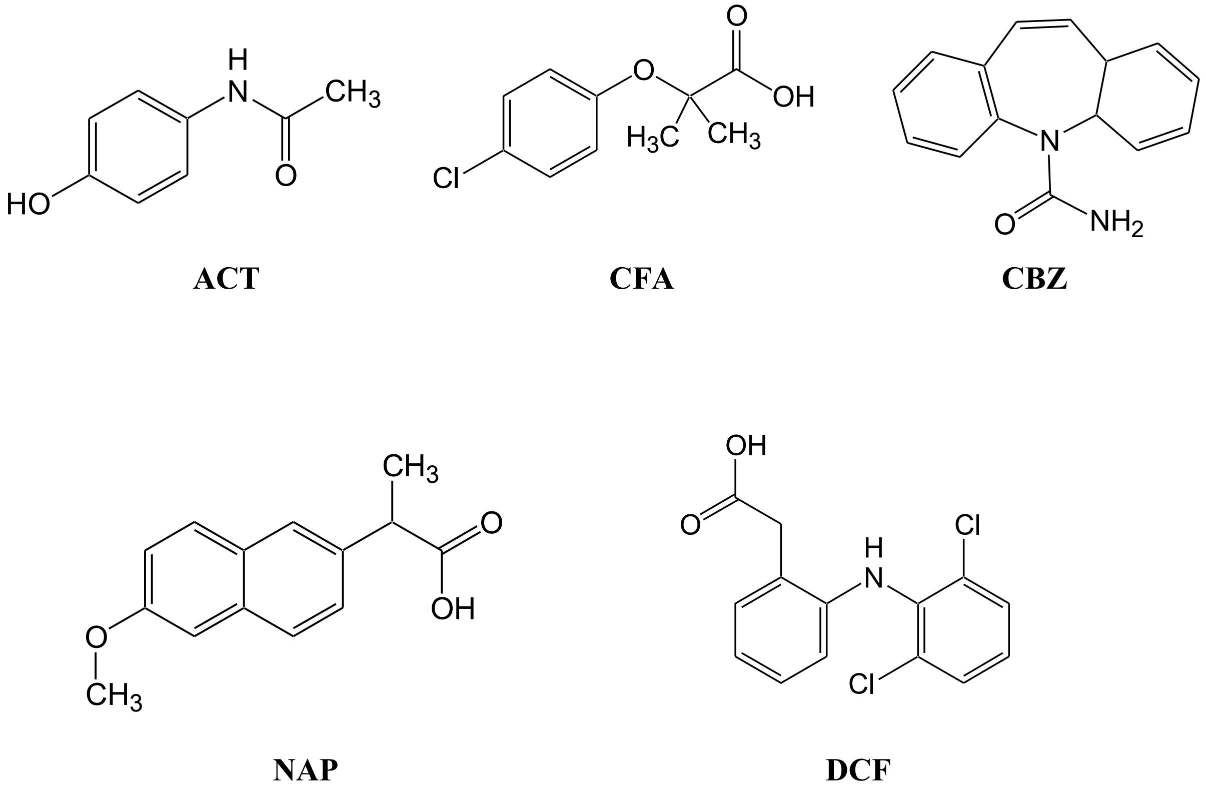

ACT **CFA** **CBZ**

NAP **DCF**

Figure 2.3 Molecular structures of pharmaceutical compounds

So far there has been no report on the direct effects of pharmaceutical residues in the environment on human. Many researchers, who studied the ecotoxicology of pharmaceutical residues, observed that these substances had a relatively limited acute ecotoxicity on the tested organisms. They recommended that attention should be paid to chronic effects of these pharmaceutical residues on bacteria, algae and fish. In a bioaccumulation study, DCF was detectable in the livers, kidneys and gills of fishes. Cytological alterations were observed in these organs even at DCF concentration of 1 µg/L [Triebskorn et al., 2004]. Therefore, DCF have the potential to damage or to have effect on ecology. Based on environmental risk assessment study, NAP and CBZ were classified as compounds toxic or harmful to aquatic environment [Quinn et al., 2008]. From a study on the impact of lipid lowering agents on ecology, it was found that chronic exposure to Bezafibrate, Fenofibrate and Gemfibrozil caused inhibition of population growth of rotifers and crustaceans [Isidori et al., 2005]. Eventhough acute ecotoxicity is unlikely to occur, these pharmaceutical compounds are always found in the environment in complex mixtures where added, and synergistic toxic effects might occur [Farre et al., 2008]. Because the synergistic toxic effect of pharmaceuticals with personal care products on tested organisms was observed in some studies, the toxicity of these pharmaceuticals in complex mixture may occur at concentrations lower than expected [Schnell et al., 2009].

Because the efficiency of biological and physical treatment for removal of pharmaceutical residues is not so good, other more effective treatments have been sought for. Chemical treatment (such as ozonation, oxidation), and physicochemical treatment (such as adsorption, membrane filtration, and coagulation) have been used for removal of pharmaceuticals from aqueous solution [Radjenovic et al., 2009; Suarez et al., 2009; Gebhardt and Schroder, 2007; Matamoros et al., 2008; Rosal et al., 2010; Weiss and Reemtsma, 2008; Coelho et al., 2009; Kimura and Watanabe, 2005]

2.2 Ordered mesoporous silica materials

In the past, a large number of researchers tried to discover or develop, synthesize and characterize porous solid materials with large specific surface areas for application in adsorption, chromatography, catalysis, gas separation, sensor technology etc. The time period of development and investigation of ordered porous materials could be divided into two periods. The first period or the golden age of microporous crystalline zeolite is the period of development and study of microporous materials with pore diameters smaller than 1.5 nm. The second period starting from 1992 is the period of development or synthesis of mesoporous silica materials. In the past, a number of scientists tried to synthesize zeolites having larger surface areas and larger pore sizes but no one was able to synthesize the zeolites with pore size larger than 2 nm (mesopore). Not until 1992 when Mobil oil group was able to synthesize solid materials with pores sized larger than 2 nm in diameter and reported their work for the first time in that year. Since then, a number of researchers in other groups were interested in developing new ordered mesoporous materials. The materials synthesized by the Mobil group were named M41S including MCM 41, MCM-48 and MCM-50. The ordered mesoporous pure silica materials which were synthesized have been widely applied in the fields of science and engineering. It is not wrong to say that the period from 1992 till present is the golden age of mesoporous materials. The synthesis of M41S family inspired several groups of researchers to develop new types of mesoporous materials such as HMS, SBA-15, PMO etc.

2.2.1 Silica-based materials

Since the early 1990s, a large number of microporous and mesoporous silica-based materials have been synthesized and they have a wide range of applications in separation and catalysis processes. These silica materials have many advantages such as having high porosity, very uniform and orderly arranged pore structure, large pore volume, narrow pore size, high surface area and homogeneous surface functional group. In addition these silica materials have the advantage of possibilty of having a particular tailor-made pore size and shape. Another advantage of inorganic adsorbents is that their surfaces can be modified with various organosilanes to improve their adsorption capacity and selective adsorption [Walcarius et al., 2003; Mercier and Pinnavaia, 2000; Chong et al., 2004]. Raman et al have classified organic template for amorphous silicas into two groups according to the nature of template-matrix interactions [Raman et al., 1996]. The first group is surfactant-template in which nature of the template-matrix interaction is via non-covalent bonding. The second group is covalently bonded organic templates. In this study we only focused on porous silica-based adsorbents which were prepared by surfactant-template method.

2.2.2 Surfactant template

Template was defined by Beck et al., as “a central structure about which a network forms in such a way that removal of the template creates a cavity with morphological and/or stereochemical features related to those of the template” [Beck et al., 1992]. Surfactants are bifunctional molecules that contain a hydrophilic head group and a hydrophobic tail [Raman et al., 1996]. As a result of their amphiphilic property, surfactants can associate into supramolecular arrays or micelles. At higher concentration, the micelles aggregate to become a liquid crystal. The liquid crystal can have different shapes, e.g. cylindrical, hexagonal, cubic and lamellar, depending on the concentration of the surfactant. The theory of surfactant template has been developed based on the geometry of micellar shapes. A schematic phase diagram for cationic surfactant in water is shown in Figure 2.4. CMC1 is the critical micelle concentration of the surfactant. At this concentration the individual surfactant molecules will start to form spherical micelles. At higher concentration (CMC2) the spherical micelles can coalesce to form elongated cylindrical micelles. As the concentration of surfactant keeps increasing the micelles will aggregate to form hexagonal liquid crystal, cubic liquid crystal and lamellar liquid crystal respectively. The interaction between the surfactant template and silica source is dictated by the reagents and the synthesis condition. This interaction can affect the physical and chemical properties of the porous materials. The porous materials which are synthesized from surfactant template have a periodic arrangement of pores (or layer), but the inorganic walls (or sheets) are amorphous.

2.2.4 HMS

Hexagonal mesoporous silicate is one of the mesoporous materials which have hexagonal array uniform channel of controlled pore size. HMS was first reported by Tanev and Pinnavia in 1996 [Tanev and Pinnavaia, 1996]. HMS is synthesized by surfactant templating S^0I^0 pathway (Figure 2.6). It is prepared from neutral primary amine surfactant (S^o) which are used as a structure-directing agent such as octylamine, dodecylamine, tetradeclyamine, hexadecylamine and octadeclyamine and molecular silica source (I^o), such as TEOS, TMOS, in neutral pH condition [Mercier and Pinnavia, 2000; Mori and Pinnavia, 2001] The surfactant head group interacts or binds to the inorganic precursor of HMS via hydrogen bonding.

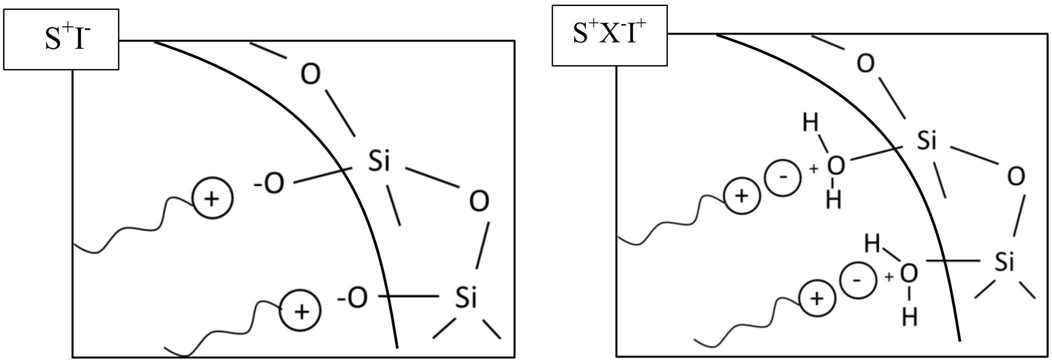

Figure 2.5 Scheme of S^+I^- and $S^+X^-I^+$ electrostatic interactions in MCM-41 synthesized process.

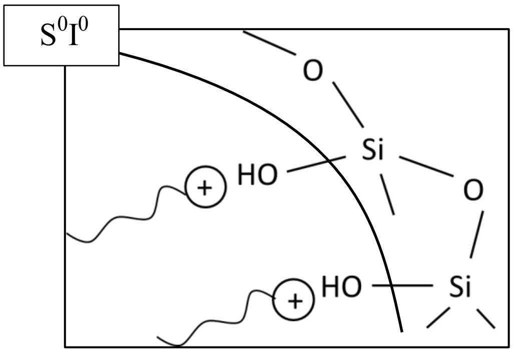

Figure 2.6 Scheme of S^0I^0 hydrogen bonding interactions in HMS synthesized process

2.2.5 SBA-15

Santa barbara amorphous-15 is one of the mesoporous materials which have hexagonal array uniform channel of controlled pore size. SBA-15 was first reported by Zhao et al., in 1998 [Zhao et al., 1998]. SBA-15 is synthesized by surfactant templating $(S^0H^+)(X^-I^+)$ pathway (Figure 2.7). SBA-15 is prepared from nonionic-triblock-copolymer pluronic P123 (S^0) as a structure-directing agent and molecular silica source in acidic condition. Because the synthesis condition is done below the aqueous isoelectric point of silica, cationic silica species is presented as inorganic precursor (I^+). The surfactant head group interacts or binds to the inorganic precursor of SBA-15 via hydrogen bonding and electrostatic attraction.

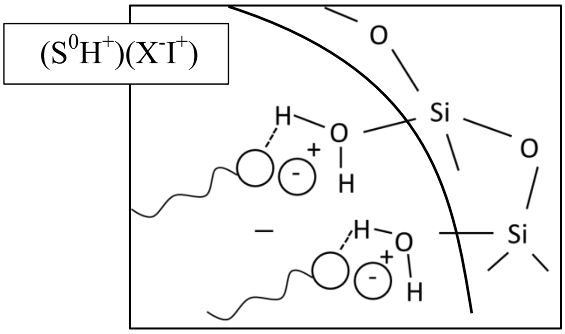

Figure 2.7 Scheme of $(S^0H^+)(X^-I^+)$ hydrogen bonding interactions in SBA-15 synthesized process.

2.2.6 Organic-inorganic hybrid materials

Organic-inorganic hybrid materials are the materials which combine organic unit with inorganic unit in the same materials. Improving the adsorptive properties of inorganic materials by functionalizing them with organic materials is one of the most interesting topic for researchers. Nowadays there are several ways of improving the adsorptive property of materials, and the addition of organic functional groups to the inorganic materials is one of the methods to improve the adsorptive property of the materials.

synthesized by grafting and co-condensation method. This is because the organic functions in the organosilica precursors are directly incorporated into the pore wall network of the materials by two covalent bonds. Because of this advantage, PMOs have increasing popularity among researchers. A large number of researchers are interested to synthesize and study this material.

The synthesis process of PMOs can be categorized into two types according to the type of surfactant directing agent. The First type is the synthesis of PMOs with ionic surfactant (such as CTAC, CTAB, ODTMA : Octadecyltrimethyl ammonium chloride, ODTMABr : Octadecyltrimethylammonium bromide). The second type is the synthesis with non-ionic surfactant (such as P123). The recipes for synthesis of PMOs as reported in other studies are shown in Table 2.2.

Table 2.2 Recipes for synthesis of PMOs

Silica sources	Surfactant	Cosolvents	Reference
BTME	ODTMA	NaOH, H_2O	Inagaki et al., 1999
BTSE	CTAB	NH_4OH, H_2O	Asefa et al., 1999
BTME	ODTMABr	NaOH, H_2O	Park et al., 2001
BTSE	CTAC	NaOH, H_2O	Burleigh et al., 2001
BTESE	CTAB	NH_4OH, H_2O	Wahab et al., 2004
TESPTS	P123	CH_3COOH, CH_3COONa, H_2O	Liu et al., 2007
BTSEB	P123	KCl, HCl, H_2O	Li et al., 2007

2.3 Adsorption

Adsorption is defined as the process of accumulating substances, which are contained in solution, on a suitable interface [Tchobanoglous et al., 2004]. The substance that is removed from the liquid phase at the interface is called adsorbate. And the solid which the adsorbate accumulated is called adsorbent. Adsorption is a preferable method for removal of pharmaceutical residues [Quesada-Penate et al., 2009; Bui and Choi, 2009]. It has the advantage of being easy and cheap to run and not having problem about undesirable byproduct. Tchobanoglous et al classified the adsorbents into three kinds, i.e. activated carbon, synthetic polymeric and silica-based adsorbents [Tchobanoglous et al., 2004]. Powdered Activated Carbon is one of the most popular adsorbents [Dural et al., 2010; Ip et al., 2010; Ahmad and Alrozi, 2010; Ahmad and Rahman, 2010]. It contains numerous pores of varying sizes and has different functional groups on its surface. The only drawback properties of PAC are difficulty in regeneration and low selective adsorption.

2.3.1 Transport phenomena

The actual adsorption process occurs at the surface of the adsorbent. Before the actual adsorption occurs, the adsorbate moves or is transported to the adsorption site. The following are sequential events or phenomenas that occurs during transportation. The first phenomenon is bulk fluid transport. The second phenomenon is film transport or film diffusion. The third phenomenon is intraparticle or pore diffusion. The final event is adsorption (physical or chemical) to the surface of the adsorbent. Figure 2.10 is the diagram showing the process of transport of the adsorbate to the surface of the adsorbent.

2.3.2 Physical and chemical adsorption

The actual adsorption process at the surface of the adsorbent can be classified as physical or chemical, according to the type of the force that attracts the adsorbate's molecules to the surface of the adsorbent. In physical adsorption, the attraction or interaction force can be electrostatic interaction, hydrogen bonding, hydrophobic interaction, Van der Waals force etc. The attraction force in physical adsorption is relatively weak and the adsorption process is reversible. The adsorbates can be released from the surface of the adsorbents by desorption process. On the contrary, the attraction or interaction force in chemical adsorption is chemical bond in which sharing of electrons or transfer of electrons is involved. The chemical attraction force is strong and the adsorption process is irreversible.

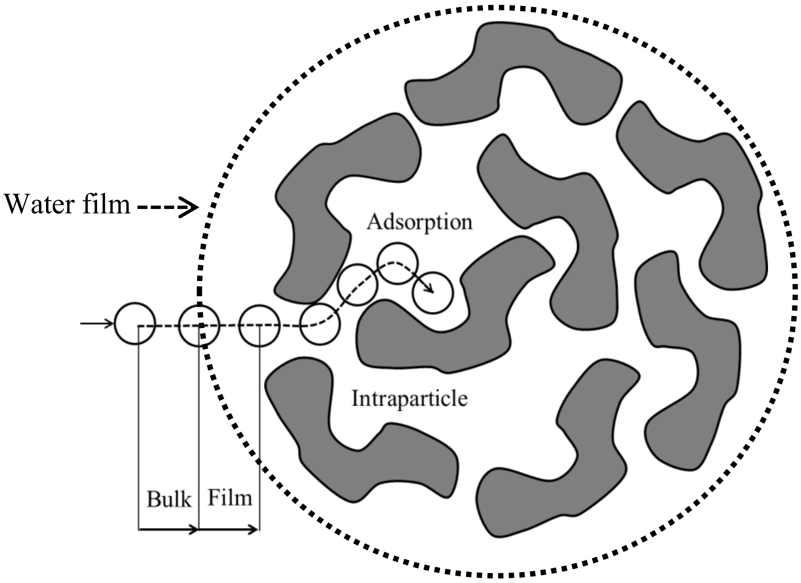

Figure 2.10 Transport processes of the adsorbate to surface site of the adsorbent adapted from Lagrega et al., 2001.

2.3.3 Adsorption capacity

The adsorption capacity of the adsorbent is determined from the mass balance equation. It can be expressed as Eq. (2.1)

$$q = \frac{(C_0 - C_e)}{M} \times V \tag{2.1}$$

Where q is the adsorption capacity (µg/g), C_0 is the initial concentration of the adsorbate (µg/L), C_e is the equilibrium concentration of the adsorbate, V is the volume of the solution (L) and M is the mass of the adsorbent (g)

2.4 Literature reivews

2.4.1 Pharmaceutical residues

Among the drugs in the class of antiepileptics and antidepressants, CBZ is the most frequently detected drug in the environment at high concentration [Fent et al., 2006]. From monitoring study, many researchers reported the detection of CBZ in surface water, ground water, sediment and river around the world [Zhang et al., 2008]. In a survey conducted by Ternes, CBZ was detected in all 30 sewage treatment plant (STP) effluents with a 90 percentile of 3.7 µg/L [Ternes, 1998]. This pharmaceutical was also detected in 24 of 26 samples from 20 rivers with a 90 percentile of 0.82 µg/L. The efficiency of STP in removal of CBZ was found to be very low (4-8 %) [Fent et al., 2006]. CBZ was found to be one of the most persistent pharmaceutical residues, it was hardly eliminated by STP [Gebhardt and Schroder, 2007].

Among the drugs in the class of lipid regulator, CFA is the most frequently detected pharmaceutical in the monitoring study [Fent et al., 2006]. CFA was found in tap water (concentration of 0.27 µg/L) [Ternes, 1998], in Swiss lake surface water (0.55µg/L) [Buser et al., 1998], in German STP effluent (1.6 µg/L) [Ternes, 1998] and in Detroit river water (0.1 µg/L) [Boyd et al., 2003]. From an ecotoxicology study, the no observed effect concentration (NOEC) on Rotifers was found to be 250 µg/L [Santos et al., 2010]. The proportion of male offspring produced by D. *magna* will be increased after exposure to CFA at concentration 10 to 100 µg/L. And at this concentration range the reduction in sperm motility and plasma androgen concentration occurred to Fathead minnow fish (*Pimephalespromelas*). The cytological changes in gills were detected in rainbow trout at the exposure dose of 5 µg/L. The removal efficiency of STP for CFA was around 51± 10 % [Ternes, 1998]. The removal efficiency of Ozonation for CFA was very low (8 %, operating condition 10 min, O_3 1 mg/L in drinking water) [Esplugas et al., 2007]. Membrane bioreactor and conventional activated sludge had no efficiency to remove CFA [Kimura et al., 2005].

NAP was detected in STP effluents and surface water at concentration of 7.96 and 0.25 μg/L respectively [Santos et al., 2010]. It was also detected in drinking water [Santos et al., 2010]. The efficiency of STP in removal of NAP was around 66 ± 7 % [Ternes, 1998]. From an ecotoxicology study, the photoproducts of NAP were found to be more toxic than the parent compounds, regarding both acute and chronic toxicity [Isidori et al., 2005]. NAP could not be dramatically removed by conventional activated sludge [Kimura et al., 2005].

ACT is one of the most commonly consumed pharmaceutical in the world. The annual consumption of ACT in German was around 650 ton/year in year 1999-2001 [Fent et al., 2006]. From monitoring study by several investigators, ACT was found in surface water, eventhough the efficiency of STP in removal of ACT was high (99%). ACT was found in STP effluents and surface water at concentration of 4.3 and 78.17 μg/L respectively [Santos et al., 2010]. The predicted no-effect concentration (PNEC) of ACT was 9.2 μg/L.

In Switzerland and Belgium, DCF was detected in STP effluent at concentration up to 2.4 and 1.42 μg/L respectively. Groundwater contamination with DCF up to 3.5 μg/L was found in samples from the indirect reuse of treated sewage [Daughton and Jones, 2001]. It was also detected in groundwater sample close to a domestic landfill site at the maximum concentration 3.5 μg/L. The removal efficiency of STP for DCF was about 17-69 % [Bendz et al., 2005]. Membrane bioreactor and activated sludge had no efficiency in removal of DCF [Kimura et al., 2005]. DCF could be removed by ozonation but only 24 % of the substrate was mineralized after 1 hr of ozonation [Coelho et al., 2009]. So the undesirable byproduct compounds require further investigation.

2.4.2 Adsorption by Silica based porous materials

Inorganic adsorbents which have mesopore such as HMS, SBA-15 and MCM-41 are alternative adsorbents for water treatment. There have been many research studies on the removal of soluble compounds from water and waste water by functionalized silica-based porous materials.

Punyapalakul and Takisawa (2006) did a study on the adsorption of nonionic surfactant (Triton X-100) and ionic dyes on HMS. They functionalized HMS with three functional groups (ie. amino-, mercapto- and octyl-). They found that the adsorption capacity of TX-100 onto HMS was affected by specific surface area, pore size and grafted organic functional groups. HMS functionalized with mercapto and octyl functional group had higher adsorption capacity than PAC. HMS which grafted amino functional group (A-HMS) had the lowest adsorption capacity because the hydrogen bonding between TX-100 and A-HMS was less significant than hydrophobic adsorption of TX-100 on PAC. In case of dye adsorption, they found that surface charge was the most important attractive force between HMSs and dyes.

Punyapalakul et.al (2009) also did a study on the adsorption of haloacetic acids by inorganic materials. They found that the adsorption capacity of inorganic materials was significantly affected by the crystalline structure of the adsorbents. Hydrogen bonding was the most important attractive force in the adsorption processes. The adsorption capacity of the adsorbents was increased when the pH of the solution decreased due to the electrostatic interaction and hydrogen bonding. Molecular structure of haloacetic acid did not affect the adsorption capacity of the adsorbents. Common electrolytes in tap water had effect on the adsorption capacity and selectivity of PAC but had no effect on the adsorption capacity and selectivity of HMS and functionalized HMS.

Prarat et al. (2011) did a study on the adsorption of haloacetoniotriles (HANs) by functionalized silica-based porous materials. They found that the surface functional groups of the adsorbents largely affected the adsorption capacity of dicloroacetonitrile (DCAN). Among functionalized HMS, 3-mercaptopropyl grafted HMS had the highest adsorption capacity. The adsorption mechanism occurred via an ion-dipole electrostatic interaction. The adsorption capacity of DCAN strongly depended on the pH of the solution. The molecular structure of HANs had effect on the adsorption capacity and selectivity of the 3-mercaptopropyl grafted HMS adsorbents.

2.4.3 Adsorption of pharmaceutical residue by silica based porous materials

Until now very few studies have been done on the removal of pharmaceutical residues by inorganic adsorbents especially functionalized silica-based porous materials.

Bui and Choi (2010) studied the removal of CBZ, CFA, DCF, Ibuprofen and Ketoprofen by SBA-15. They found that the adsorption kinetics and adsorption isotherms were best fit with the pseudo-second order kinetic model and Freundlich isotherm model respectively. The efficiency of SBA-15 in removal of pharmaceutical compounds was found to be highest at pH 3. In the opinion of these investigators mesoporous silica based materials are promising absorbents for removing pharmaceutical from water.

Punyapalakul and Sitthisorn (2010) studied the removal of CBZ and Ciprofloxacin by HMS and functionalized HMS. They did the adsorption study in the concentration range 6 – 9 mg/L. They found that the adsorption kinetic of both pharmaceuticals were compatible with pseudo-second order kinetic model. The adsorption capacity of inorganic adsorbents was lower than PAC. The hydrophobicity and hydrogen bonding were two of the most important attractive force in the adsorption processes. The adsorption capacity was affected by varying the pH of the solution.

Wang et al. (2009) studied the adsorption of drug molecules (Rhodamine 6G and Ibuprofen) onto functionalized MCM-41 in the concentration range around 450 mg/L. They found that surface modification of MCM-41 with hydrophobic functional groups (mercaptopropyl and vinyl) could improve the adsorption capacity of Rhodamine 6G on to MCM-41 due to the favorable interaction with the hydrophobic parts of adsobate. Surface modification of MCM-41 with amine functional group could improve the adsorption capacity of ibuprofen due to hydrogen bonding between carboxylic acid group of ibuprofen and hydrogen molecule in the amine functional group.

So far, there has been almost no study on the removal of pharmaceutical residues by adsorption onto HMS and functionalized HMS except for the above mentioned study by Punyapalakul and Sitthisorn. To get more knowledge about the the adsorption of HMS and functionalized HMS for pharmaceutical residues, we did the adsorption study with more different types and at lower concentration of pharmaceutical compounds (i.e. ACT, CFA, CBZ, DCF and NAP).

Until now PMO has never been used for adsorption of pharmaceutical residues, and has never been functionalized. We therefore synthesized PMO and functionalized it with organosilane, and used these synthesized materials to study the removal of one representative pharmaceutical (CFA).

CHAPTER III

METHODOLOGY

3.1 Materials

3.1.1 Pharmaceutical residues

Acetaminophen was purchased from Sigma-Aldrich. Clofibric acid was purchased from Aldrich. Carbamazepine was purchased from Fluka. Diclofenac was purchased from Sigma. Naproxen was purchased from Sigma-Aldrich.

3.1.2 Silica source precursors

Tetraethylorthosilicate was purchased from Aldrich. Bis(triethoxysilyl)ethane was purchased from Aldrich. Ludox HS-40 (40 wt. % SiO_2) was purchased from Dupont.

3.1.3 Surfactants

Dodecylamine was purchased from Aldrich. Cetyltrimethylammonium chrloride was purchased from Aldrich. Pluronic123 was purchased from BASF.

3.1.4 Organic functional groups

(3-Aminopropyl)triethoxysilane was purchased from Aldrich. (3-Mercaptopropyl)trimethoxysilane was purchased from Sigma. (3-Aminopropyl) trimethoxysilane was purchased from Aldrich. 3-[2-(2-Aminoethylamino) ethylamino]propyltrimethoxysilane was purchased from Aldrich. [2-(2-Aminoethylamino)propyl]trimethoxysilane was purchased from Aldrich.

3.1.5 Powdered activated carbon

Powdered activated carbon (Shirasagi S-10) was purchased from Japan Enviro Chemicals Ltd.

3.1.6 Other chemical reagents

Other chemical reagents used in this study are of the high quality grade (laboratory grade or higher).

3.2 Methodology

The experimental frame work of this study is shown in Figure 3.1. The study was divided into 4 phases. The methodology of each phase is described in this chapter. The overall experimental methods are described in this section. The details of each experiment are described in next chapters (Chapter IV, V, VI and VII).

3.2.1 Phase 1: Synthesis and characterization of mesoporous silicas

The aims of this phase of the study were to synthesize and to characterize silica based mesoporous materials and organic-inorganic hybrid materials. In this study, three kinds of pure silicate inorganic porous materials, namely HMS, MCM-41 and SBA-15, were synthesized. All of them are mesoporous materials which have hexagonal array uniform channel of controlled pore size. Their synthesis pathways were different. HMS was synthesized by surfactant templating S^0I^0 pathway. Primary amine surfactant dodecylamine (S^o) was used at neutral pH as a structure-directing agent for the synthesis of HMS. SBA-15 was synthesized by surfactant templating $(S^0H^+)(X^-I^+)$ pathway. Nonionic-triblock-copolymer pluronic P123 (S^0) was used under acidic conditions as a structure-directing agent for the synthesis of SBA-15. MCM-41 was synthesized by surfactant templating (S^+I^-) pathway. Cationic surfactant CTAC (S^+) was used under basic conditions as a structure-directing agent for the synthesis of MCM-41. TEOS was used as a molecular silica source for the synthesis of all of these materials.

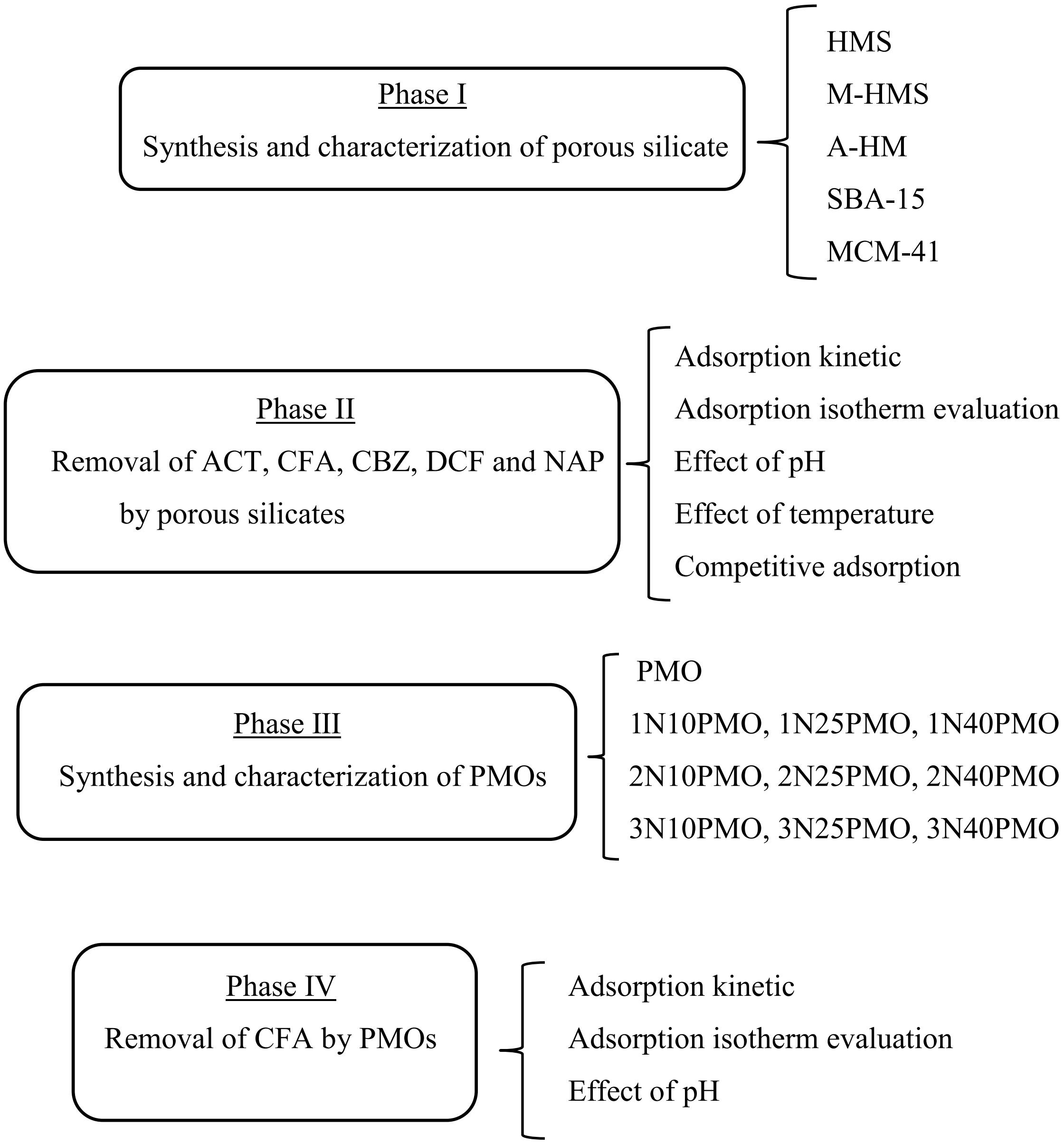
Phase I
Synthesis and characterization of porous silicate
HMS
M-HMS
A-HM
SBA-15
MCM-41
Phase II
Removal of ACT, CFA, CBZ, DCF and NAP by porous silicates
Adsorption kinetic
Adsorption isotherm evaluation
Effect of pH
Effect of temperature
Competitive adsorption
Phase III
Synthesis and characterization of PMOs
PMO
1N10PMO, 1N25PMO, 1N40PMO
2N10PMO, 2N25PMO, 2N40PMO
3N10PMO, 3N25PMO, 3N40PMO
Phase IV
Removal of CFA by PMOs
Adsorption kinetic
Adsorption isotherm evaluation
Effect of pH

Figure 3.1 Experimental framework of this study

In this phase of the study mesoporous organosilica functionalized with organic functional groups were also synthesized. Two types of organic functional group, namely aminopropyl and mercaptopropyl, were incorporated into the surface of HMS by direct co-condensation method.

All of the synthesized adsorbents were then characterized by their physical and elemental properties. These properties were determined by low-angle powder x-ray diffraction, scanning electron microscope, Nitrogen gas adsorption and desorption isotherms, thermogravimetric analysis, differential thermo analysis, elemental analysis, Fourier transform infrared spectroscopy, zetapotential and water contact angle analysis.

3.2.2 Phase 2: Removal of trace pharmaceutical residues by adsorption on mesoporous silicas

The aims of phase II of the study were to find out the most effective adsorbent and, after elucidating the adsorption mechanism, to evaluate the effect of surface functional groups and the effect of pH and temperature on their adsorption capacity, so as to improve its adsorption capacity by surface modification with the appropriate functional groups. In addition, the competitive adsorption of mixed pharmaceutical residues over the synthesized adsorbents and PAC was studied.

Batch experiments were performed to measure the adsorption capacity of each adsorbent for each pharmaceutical residue. The samples were shaken, filtrated, extracted, concentrated and finally the concentration of pharmaceutical residue remaining was measured by High-performance liquid chromatography (HPLC). The adsorption kinetic and the adsorption isotherm studies were done. The adsorption mechanism was investigated by analyzing the adsorption kinetics, isotherms and thermodynamics under various conditions, and used in comparison between different adsorbents to simultaneously elucidate the potential effects of pH and temperature on the adsorption capacity. The procedure for the study in selective or competitive adsorption was the same as for the study in single solute except that in selective adsorption study all of the pharmaceutical compounds were mixed together.

3.2.3 Phase 3: Synthesis and characterization of periodic mesoporous organosilicas

The aim of phase III of the study was to synthesize periodic mesoporous organosilicas as well as amino-functionalized PMOs via direct co-condensation using mono-, di- and triamino-organoalkosysilanes. After synthesis, all of the synthesized PMOs were characterized by XRD, SEM, TEM, Nitrogen gas adsorption and desorption isotherms, TGA, DTA, Elemental Analysis, FTIR, zetapotential and water contact angle analysis.

3.2.4 Phase 4: Removal of Clofibic acid by adsorption on periodic mesoporous organosilicas

The aim of phase IV of the study was to elucidate the adsorption mechanism of PMOs for CFA. The experiment and the procedure for the study were the same as in phase II study. The study was done on only one pharmaceutical compound i.e. CFA.

3.3 Analytical method

3.3.1 Pretreatment of samples

A solid-phase extraction (SPE) was used for extraction and pre-concentration of liquid samples which were taken from the adsorption experiments before quantification process by HPLC. A reversed phase C18 catridges (60 mg, Agela, Japan) were used in this study. Before samples feeding, the catridges were washed as a conditioning or pre-activation step by loading with 20 mL of methanol (loading flow rate = 3 mL/min), followed by 20 mL of DI water at the same loading flow rate. After preconditioning step, the samples were fed into the catridges at loading rate 3 mL/min. After that the cartridges were washed with 10 mL of DI water at flow rate 3 mL/min before evaporation process. The catridges were then left to dry under flow of nitrogen for 30 min. The drugs were eluted from the catridges by 10 mL of methanol

(1 mL/min) and the liquid samples were then dehydrated again by nitrogen gas. The volume of the samples was then adjusted to 0.5 mL by methanol before moving to the step of quantification analysis.

3.3.2 Quantification of pharmaceutical residues

The quantities of pharmaceutical residue in the solutions were measured by reverse phase Agilent 1100 HPLC with a UV detector. The column type used in this study was Agilent C18 column (4x250 mm, 5 µm). A mixture of dihydrogenphosphate potassium salt (KH_2PO_4, 25 mM) and acetonitile were used as mobile phase in chromatography process. The ratio of KH_2PO_4 to acetonitrile in the eluent was 30:40. The flow rate of an isocratic eluent was 0.8 mL/min. Column temperature was controlled at 25 ^{o}C. In this study Ibuprofen was utilized as the surrogate standard. The percentage of recovery of every pharmaceutical residue was higher than 90%. The chromatogram of pharmaceutical residues is shown in appendix A.

CHAPTER IV

SYNTHESIS AND CHARACTERIZATION OF MESOPOROUS SILICAS

4.1 Introduction

In this chapter we report on the synthesis of HMS, SBA-15 and MCM-41 via surfactant template method. We also report on the synthesis of two inorganic organic hybrid materials namely A-HMS and M-HMS which were synthesized by modifying the surface of virgin HMS with two different types of organosilane, i.e. mercaptoprpyltrimethoxysilnae and aminopropyltrimethosysilane via direct co-condensation method. The physicochemical properties of adsorbents were investigated by low-angle powder x-ray diffraction, scanning electron microscope, nitrogen gas adsorption and desorption isotherms, thermogravimetric analysis, Elemental analysis, Fourier transform infrared spectroscopy, zeta potential analysis by acid/base tritration and water contact angle analysis by tensiometer. The synthesized and characterized materials were used as the adsorbents in removal of pharmaceutical residues by adsorption in phase II (chapter 5).

4.2 Method

4.2.1 Synthesis of the HMS

Synthesis of pure silica HMS materials was carried out as described by Tanev et al. (1996). 0.27 mol of dodecylamine was dissolved into a mixture of 9.09 mol of ethanol and 29.6 mol of deionized water under stirring. After that, 1.0 mol of tetraethoxysilane was added. The reaction mixture was stirred for 18 h at room temperature. The solid product was recovered by filtration and washed thoroughly with deionized water. The product was dried at room temperature overnight and then the material was calcined at 650 ^{o}C for 4 h.

4.2.2 Synthesis of SBA-15

SBA-15 was prepared under acidic conditions according to the synthesis procedure described by Zhao et al. (1998). 0.017 mol of Pluronic P123 was dissolved into a mixture of 6.1 mol of HCl and 165 mol of deionized water under stirring. After that, the homogeneous solution was heated to 40 °C. Then 1 mol of tetraethoxysilane was added dropwise under stirring. The mixture was stirred for 24 h at ambient temperature. After that, it was kept at 100 °C for 24 h under static condition. The solid product was recovered by filtration and washed thoroughly with deionized water. The product was dried at room temperature overnight and then the material was calcined at 540 °C for 5 h.

4.2.3 Synthesis of MCM-41

MCM-41 was synthesized under basic conditions following the procedure described by Kim et al. (1997). Solution A was prepared by dissolving 12.5 g of hexadecyltrimethylammonium chloride into a mixture of 0.725 g of NH_4OH and 37.5 g of deionized water under stirring. Simultaneously solution B was prepared by adding 35 g of Ludox HS-40 to the mixture of 4.68 g of NaOH and 112.32 g of deionized water under stirring in a separate vial at 80 °C for 2 h. Solution B was then added to solution A and mixed vigorously at room temperature for 1 h. The reaction gel was then kept at 100 °C for 24 h. After that, the gel was cooled in a water bath and its pH was adjusted to 11 with acetic acid. After pH adjustment, the gel was kept in the oven at 100 °C for another 24 h. The pH of the gel was adjusted again, for the second time, and was kept again, for the last time, in the oven at 100 °C for 24 h. The target solid product was recovered by filtration and washed thoroughly with deionized water. The product was dried at room temperature overnight and then the material was calcined at 650 °C for 8 h.

4.2.4 Synthesis of amino or mercapto functionalized HMS via direct co-condensation method

Modification of HMS with either 3-aminopropyltriethoxy or 3-mercaptopropyltrimethoxy (for amine- or mercapto- modification,respectively) was performed by a co-condensation method following the procedure described by Lee et al. (2001). 0.25 mol of dodecylamine was dissolved into a mixture of 10.25 mol of ethanol and 50 mol of deionized water under stirring. After that, 1.0 mol of tetraethoxysilane was added. The stirring was continued for 30 min. Then 0.25 mol of either 3-mercaptopropyltrimethoxysilane or 3-aminopropyltriethoxysilane was added. The mixture was vigorously stirred for 18 h at room temperature. The solid product was recovered by filtration and washed thoroughly with deionized water. The product was dried at room temperature overnight and then the residual organosilanes and surfactant were removed by soxhlet extraction with ethanol for 72 h.

4.2.5 Characterization

4.2.5.1 X-ray Diffraction

Low-angle powder XRD patterns of synthesized adsorbents were obtained from a Bruker AXS Model D8 Discover with CuKα radiation (40 kv, 40 mA) at 2ϴ angle of 0.5 – 10 ^{o}. The scan speed was 0.04 ^{o}/min.

4.2.5.2 Scanning electron microscopy micrographs

The SEM Micrographs of the materials were observed at 1000, 5000, 10000 and 20000 magnifications through scanning electron microscope model JEOL-JSM5410LV.

4.2.5.3 Nitrogen gas adsorption-desorption

Nitrogen gas adsorption and desorption isotherms were obtained using Micromeritics ASAP 2020 version 1.04H. Before analysis the samples were dehydrated at 150 ^{o}C for 4 h under nitrogen condition and then the measurements were performed at 77 K. The pore size distribution was obtained using BJH (Barrett-Joyner-Halenda) model. The specific surface area of the materials was computed with the BET (Branauer Teller Emmett) model within a range of relative pressure, p/p_0 = 0.05 – 0.3. The total pore volume was taken from the volume of Nitrogen adsorbed at a relative pressure P/P_0 = 0.995 single point.

4.2.5.4 Thermogravimetric analysis

Thermogravimetry analysis was performed with a Mettler-851e from ambient temperature to 1,000 ^{o}C at a heating rate 20 ^{o}C/min under flow of nitrogen (20 mL/min).

4.2.5.5 Elemental analysis

The amount of sulfur was directly measured by a LECOS132 sulfur analyzer. A Shimadzu UV 1601S UV-Visible spectrophotometer was used to determine the amount of nitrogen, via absorbance at a wavelength of 220 nm after digesting adsorbents, in autoclave, by potassium persulfate under base conditions as reported [Smart et al., 1983].

4.2.5.6 Fourier transform infrared spectroscopy

The presence of organofunctional groups on the HMS surface was confirmed by FTIR on a Nicolet Impact 410 FTIR spectrophotometer.

4.2.5.7 Point of zero charge and hydrophobic/hydrophilic surface characteristics of the adsorbents

Point of zero charge of the adsorbents were determined by acid-base titration. Tensiometer (Dataphysics DCAT-11) was used, in a powder contact angle mode, to determine the hydrophobic/hydrophilic characteristics of the adsorbent surface.

4.3 Results and discussion

4.3.1 X-ray Diffraction

Figure 4.1 shows the XRD patterns of the as-synthesized and calcined HMS. To evaluate the structural property of the porous materials, the XRD (100) interplanar diffraction spacing (d_{100}) [Qiao et al., 2003], was calculated from the following equation

$$d_{100} = \frac{1.5406}{2 \sin \theta} \qquad (4.1)$$

where θ was the scanning diffraction angle (radian) corresponding to diffraction peak (100).

The XRD pattern of the HMS showed a single broad diffraction peak (d_{100}) reflection at $2\Theta = 2.0563\ ^{o}$, corresponding to a lattice spacing of 42.93 Å. The higher order Bragg reflections was not found in the diffraction pattern. This pattern and the lattice spacing proved that the synthesized material was the porous silicate which has orderly hexagonal frame work [Tanev et al., 1996]. The calcined sample exhibited a much higher intensity than the as-synthesized sample. This indicated that the material had a more orderly structure after the surfactant template removal [Zhao et a., 1997].

In case of HMS derivatives, namely M-HMS and A-HMS, their XRD patterns were similar to the pattern of virgin HMS (Figure 4.2 and 4.3). But the position and the magnitude of the reflection peak of the HMS derivatives were different from those of the virgin HMS. In case of M-HMS the extracted material showed a single broad diffraction peak (d_{100}) reflection at $2\Theta = 2.6564\ ^{o}$, corresponding to a lattice spacing of 33.23 Å. And in case of A-HMS, the XRD pattern of the extracted material showed a small diffraction peak at $2\Theta = 2.4922\ ^{o}$. Functionalization of HMS caused the diffraction peak (d_{100}) to shift to a higher diffraction angle. In case of M-HMS, the peak shifted from $2\Theta = 2.0563\ ^{o}$ to $2.6564\ ^{o}$. In case of A-HMS, the peak shifted from

material was affected by the modification with aminopropyl functional groups. Functionalization of HMS with different functional groups gave different results on the morphology of the HMS material. The adding of different types of organosilane into the starting reaction mixture could lead to the difference in condensation rate of the synthesized materials. The difference in condensation rate could explain the difference in morphology of the synthesized materials.

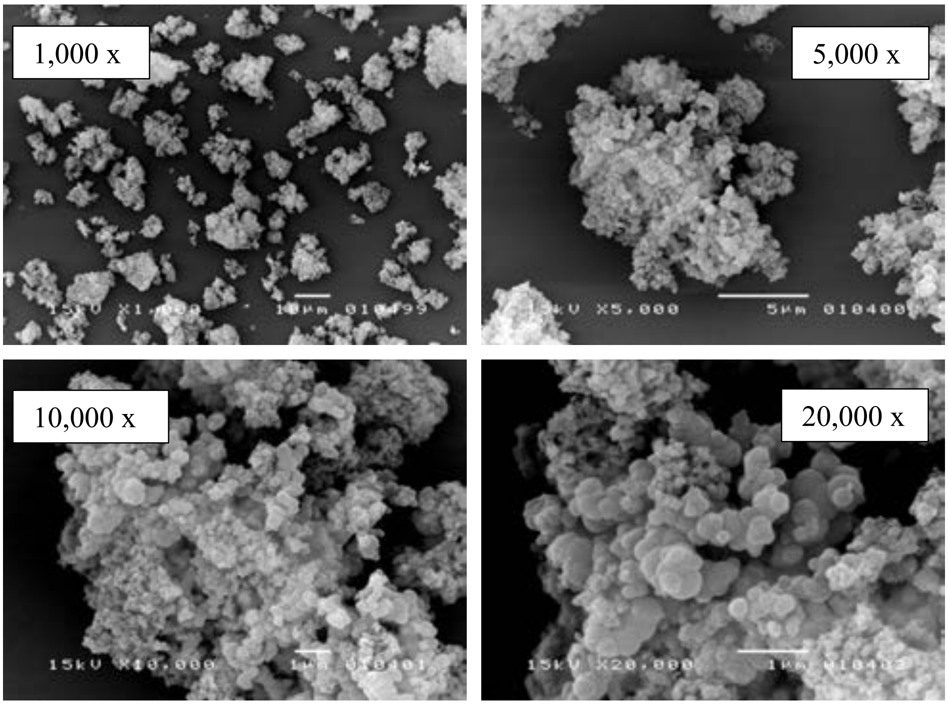

Figure 4.6 SEM micrographs of calcined HMS

The SEM images of calcined SBA-15 are shown in Figure 4.9. The morphology of SBA-15 was found to be very different from those of HMS and HMS derivatives. It consisted of larger particles which looked like bundles of threads. The particles consisted of many ropelike domains of relatively uniform size which aggregated into wheat-like macrostructures.

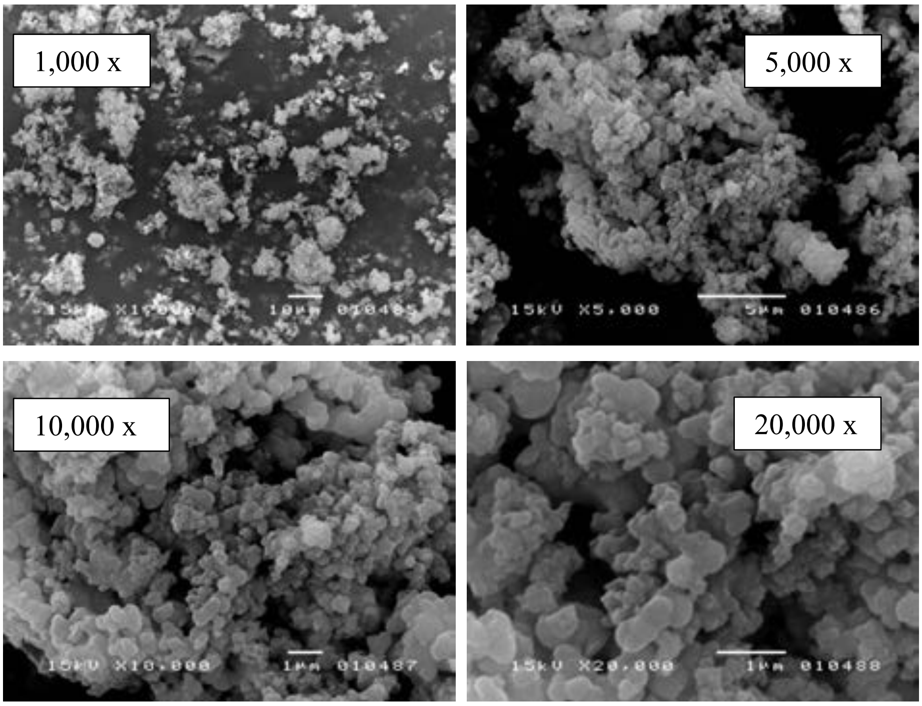
1,000 x
5,000 x
10,000 x
20,000 x
15kV X5,000 5μm 010486
15kV X10,000 1μm 010487
15kV X20,000 1μm 010488

Figure 4.7 SEM micrographs of extracted M-HMS

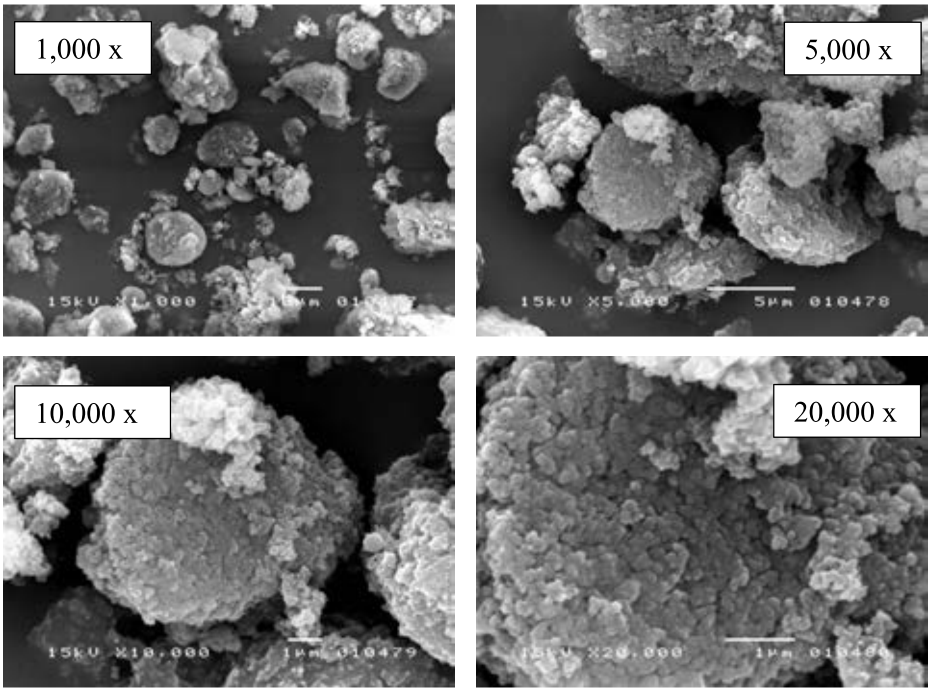
1,000 x
5,000 x
10,000 x
20,000 x
15kV X5,000 5μm 010478
15kV X10,000 1μm 010479
15kV X20,000 1μm

Figure 4.8 SEM micrographs of extracted A-HMS

Figure 4.10 illustrates SEM micrographs of MCM-41. The morphology of MCM-41 was found to be different from the other materials. It consisted mostly of irregularly shaped particles.

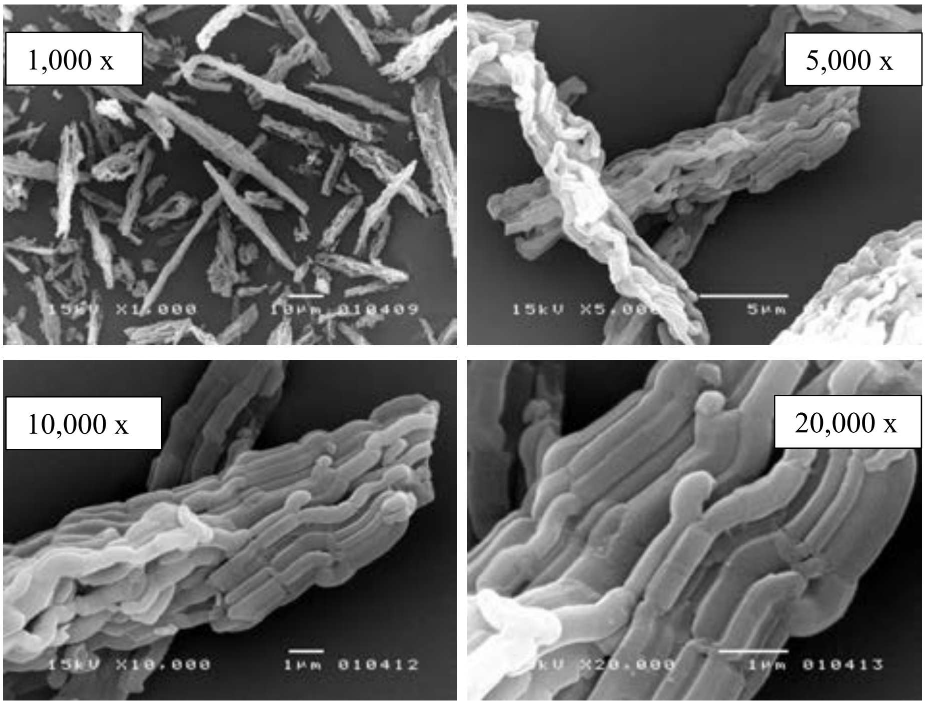
1,000 x
5,000 x
10,000 x
20,000 x
15kV X10,000 1µm 010412
1µm 010413
5µm

Figure 4.9 SEM micrographs of calcined SBA-15

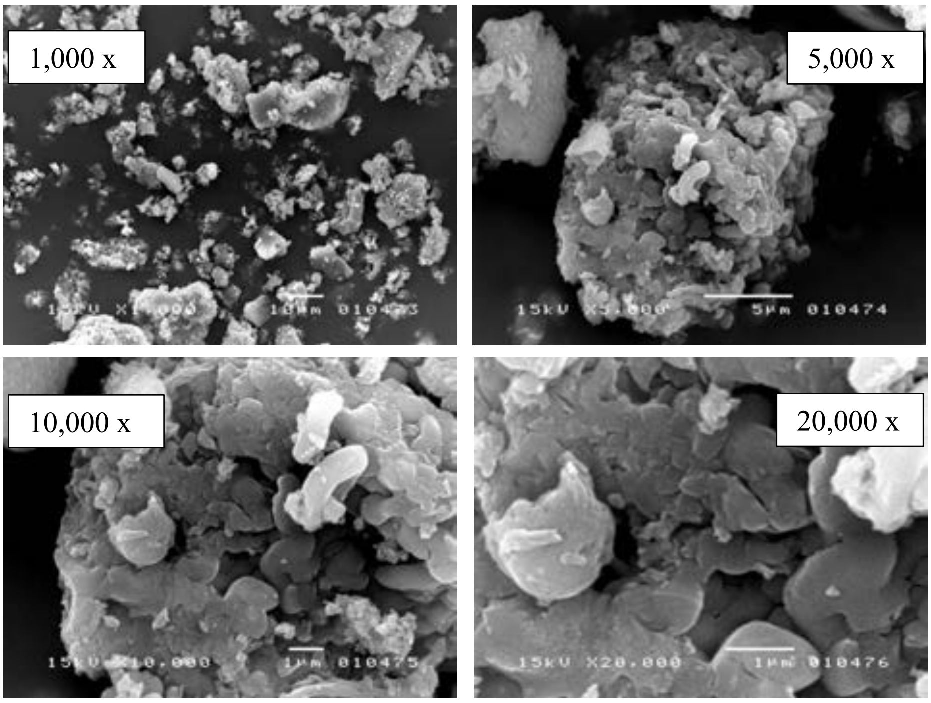
1,000 x
5,000 x
10,000 x
20,000 x
15kV 5µm 010474
1µm 010475
15kV X20,000 1µm 010476

Figure 4.10 SEM micrographs of calcined MCM-41

4.3.3 Nitrogen gas adsorption-desorption

Nitrogen gas adsorption-desorption isotherms of the calcined or the extracted porous silicate materials are shown in Figure 4.11. All of the silicate materials exhibited type IV isotherms demonstrating the preservation of the orderly mesostructures of the former samples. The isotherms demonstrated the presence of framework-confined pores at P/P_0 around 0.1 to 0.5 for HMS, M-HMS, A-HMS and MCM-41. But in case of SBA-15 the shift of the filling of framework-confined was found at the P/P_0 range 0.5 to 0.9. The shift of relative pressure of the materials can be used to explain the framework pore size [Pauly and Pinnavaia, 2001, Lee et al., 2001]. It could be concluded from this study that among the silicate materials, SBA-15 had the biggest frame work pore size.

The BET specific surface area and the BJH pore diameter of all adsorbents are shown in Table 4.1. It could be derived from the BET analysis that the pore sizes of all adsorbents except SBA-15, were in the mesoporous scale ranging from 19.0 Å (PAC) up to 33.5 Å (MCM-41). SBA-15 had a much larger pore size (80.6 Å). The pore diameter size was broadly ordered (largest to smallest) as: SBA-15 >> MCM-41 ≈ HMS > M-HMS > A-HMS > PAC. The BET surface area ranged from 712 m2/g (HMS) up to 980 m^2/g (PAC). A-HMS had a much smaller surface area (262 m^2/g). The surface area was not congruent with the pore size but ordered (largest to smallest) as: PAC > M-HMS > SBA-15 > MCM-41 > HMS >> A-HMS.

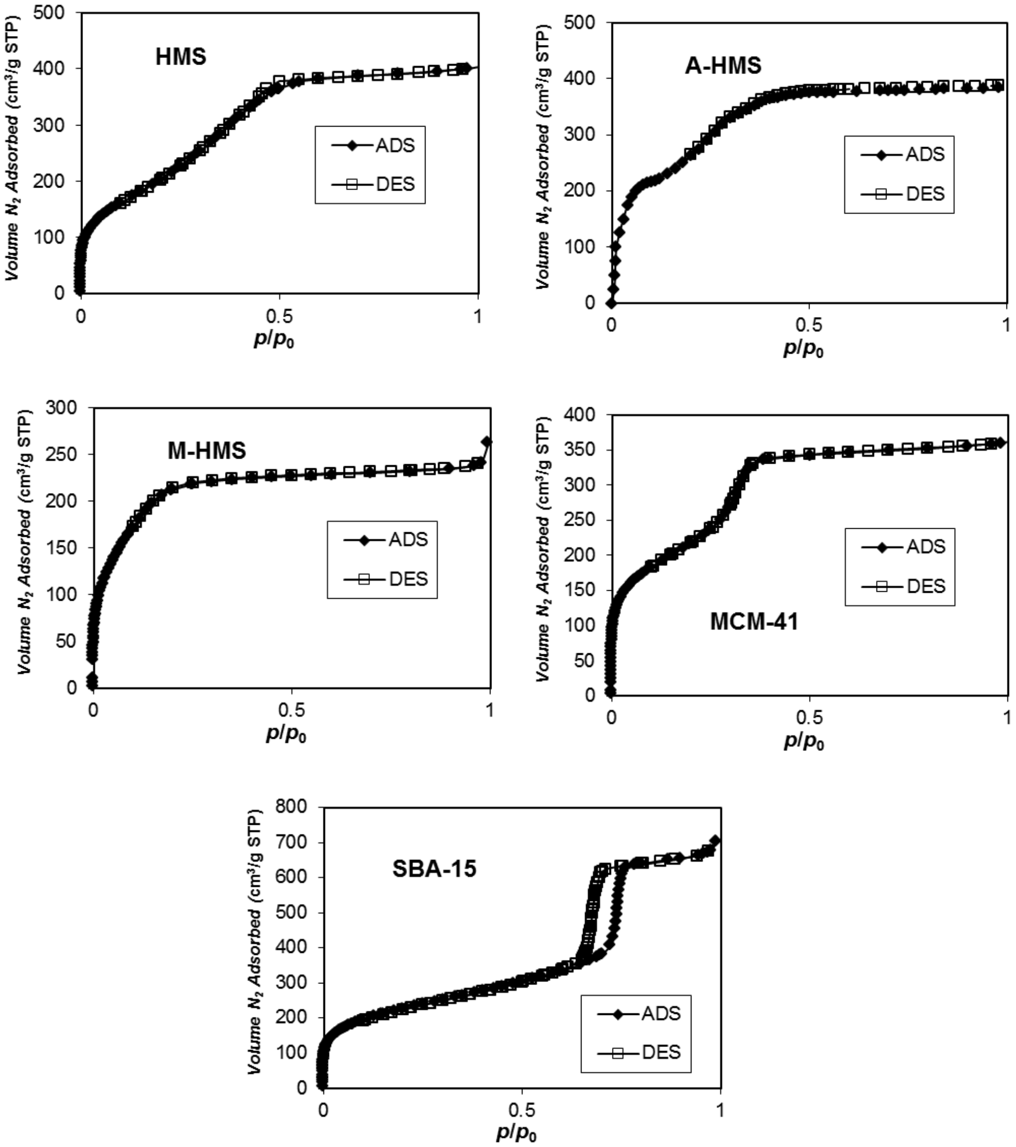

Figure 4.11 Nitrogen gas adsorption-desorption isotherms plots of calcined or extracted silicate materials**.**

Table 4.1 Physicochemical characteristics of HMS, M-HMS, A-HMS, SBA-15, MCM-41 and PAC

Adsorbents	**Surface functional groups**[a]	**Surface characteristics**	**Mean pore diameter (Å)**	**BET surface area (m^2/g)**[a]	**pH$_{PZC}$**[b]	**Contact angle (Degree)**
HMS	Silanol	Hydrophilic	32.8	712	4.5-5.5	45.06
M-HMS	Mercapto and Silanol	Hydrophobic	26.6	912	6.2	89.65
A-HMS	Amino and Silanol	Hydrophilic	23.4	262	9.5	40.18
SBA-15	Silanol	Hydrophilic	80.6	890	4.8	-
MCM-41	Silanol	Hydrophilic	33.5	755	5.6	-
PAC	Carboxyl, phenyl and oxygen-containing groups	Hydrophobic	19.0	980	9.5	58.34

[a] Determined by BET analysis of N_2 adsorption-desorption
[b] pH of net zero charge

4.3.4 Thermogravimetric analysis

TGA of the silicate materials was performed from room temperature to 1,000 ^{o}C. TGA of virgin HMS was carried out on the as-synthesized and calcined materials. The TG curves are shown in Figure 4.12. The as-synthesized material exhibited the total weight loss of 34.8 % during heating from room temperature to 1,000 ^{o}C. The calcined samples exhibited the total weight loss of 6.9 %. The as-synthesized material exhibited a greater weight loss probably because it contained a larger amount of surfactant template. Tanev et al. (1996) divided the TG curve of HMS in to 3 portions. The 1st portion represented the TG curve from 20 to 150 ^{o}C. The weight loss occurring in this temperature range could be attributed to desorption of water. The 2nd portion represented the curve from 150 to 300 ^{o}C. The weight loss occurring in this temperature range was probably due to decomposition and combustion of the surfactant template. The last portion represented the TG curve from 300 ^{o}C to 520 ^{o}C. The weight loss occurring in this portion was attributed to dehydroxylation of the surface. From our study, the total weight loss occurring between of 20 ^{o}C and 150 ^{o}C was less in the as-synthesized than in the calcined samples. We thought the weight loss in this temperature range correlated with the hydrophobic/hydrophilic properties of the surface of the materials. In case of the as-synthesized sample, its hydrophobic property could be explained by the presence of a large amount of surfactant templates inside it. Because the as-synthesized sample did not pass through the template removal process it contained a large amount of hydrophobic tails of the surfactant micelles and had a smaller surface area. Because of this, the as-synthesized material was more hydrophobic. Between 150 ^{o}C and 300 ^{o}C, the total weight loss of around 30 % was observed in the as-synthesized samples. But in the calcined samples, the weight loss was very little (less than 1 %). This could be explained by the complete removal of the surfactant template from the calcined samples. From 520 ^{o}C to 1,000 ^{o}C, all of the samples exhibited very little weight loss (less than 1.5 %) caused by the condensation of the silicate walls of the materials.

The band at 2850-2965 cm^{-1} which is ascribed to the C-H stretching was seen in A-HMS and M-HMS, but not in virgin HMS. The presence of the band at this wavelength can be used as an evidence to confirm that the HMS has been functionalized.

In this study, however, the band at 2560 cm^{-1} which is ascribed to the S-H stretching in M-HMS and the band at 3300-3400 cm^{-1} which is ascribed to the N-H stretching in A-HMS were not seen. The absence of the band at 2560 cm^{-1} in case of M-HMS might be due to the low sensitivity of FTIR in detecting S-H stretching. The absence of the band at 3300-3400 cm^{-1} in case of A-HMS, might be due to the hiding of this band by the physisorption of water molecules.

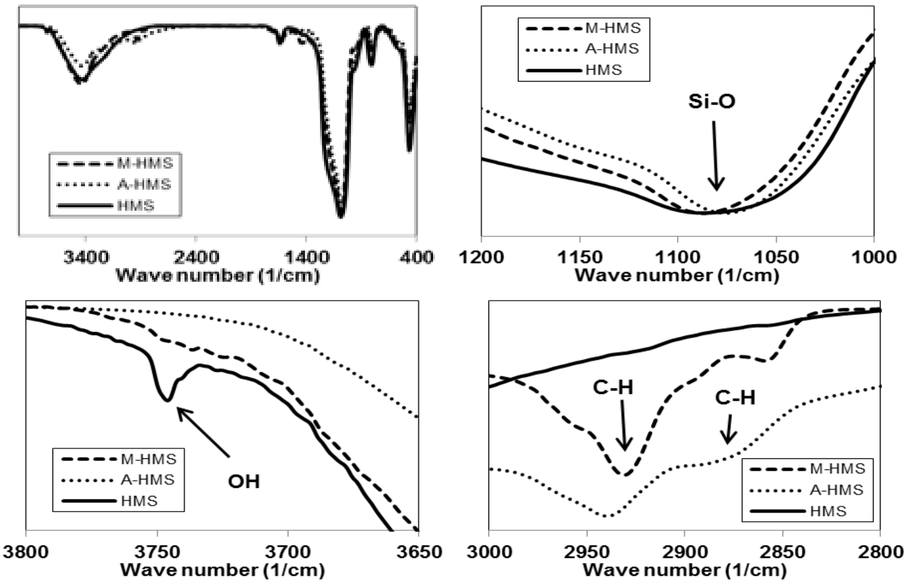

Figure 4.16 FTIR spectra of template removed HMS, M-HMS and A-HMS.

4.3.7 Point of zero charge and hydrophobic/hydrophilic surface characteristics of the adsorbents

In this study, the point of zero charge was determined by acid/base titration technique and the hydrophobic/hydrophilic characteristics of the adsorbents were revealed by water contact angle as determined by tensiometer. The pH_{ZPC} and the water contact angle of the adsorbents are summarized in Table 4.1. The pH_{ZPC} of the adsorbents were found to range from 4.5 to 9.5. And from the water contact angle data obtained in this study, it can be concluded that M-HMS was the most hydrophobic, and A-HMS the most hydrophilic adsorbents.

4.4 Conclusions

The powder X-ray diffraction (XRD) pattern of the synthesized materials showed the pattern of porous materials with well ordered hexagonal frame work. The template removed materials had the structure more well ordered than the as-synthesized materials indicating that the materials had a more well ordered structure after removal of surfactant templates. The SEM micrograph showed that HMS and M-HMS had similar morphology. Both had uniform aggregates of small distinct particles (diameter 0.1 to 0.2 micron). But A-HMS had different morphology. It had particles which looked like sponge balls. These sponge balls consisted of aggregates of small particles. The small particles of A-HMS were a little bit smaller than those of HMS and M-HMS. The morphology of SBA-15 and MCM-41 was found to be very different from those of HMS and HMS derivatives. SBA-15 had larger particles which looked like bundles of threads. These particles consisted of many ropelike domains of relatively uniform size which aggregated into wheat-like macostructures. MCM-41 had mostly irregularly shaped particles. The BET analysis showed that the synthesized materials had different pore sizes. The pore diameter size was broadly ordered (largest to smallest) as: SBA-15 >> MCM-41 ≈ HMS > M-HMS > A-HMS > PAC. The BET surface area ranged from 712 m^2/g (HMS) up to 980 m^2/g (PAC) except for the much smaller surface area for A-HMS (262 m^2/g). The surface area was not congruent with the pore size but ordered (largest to smallest) as: PAC > M-HMS > SBA-15 > MCM-41 > HMS >> A-HMS. Elemental analyses of extracted HMS derivatives showed that the total nitrogen content in A-HMS was 1.48 % and the sulfur content in M-HMS was 9.84 %. The content of amino group in A-HMS was 1.06 mmol/g and the content of mercapto group in M-HMS was 3.08 mmol/g. The results of elemental and thermogravimetric analysis and FTIR spectra confirmed the presence of organic functional groups in the functionalized that we synthesized. The water contact angle analysis by tensiometer showed that M-HMS was the most hydrophobic and A-HMS the most hydrophilc. Surface characteristics of the adsorbents were changed after functionalization with organic functional groups.

CHAPTER V

REMOVAL OF TRACE PHARMACEUTICAL RESIDUES BY ADSORPTION ON MESOPOROUS SILICAS

5.1 Introduction

In this chapter, we report on a study into the removal of a low concentration of five pharmaceutical residues (DCF, CBZ, NAP, CFA and ACT) from aqueous solution by adsorption onto amino- or mercapto- functionalized HMS (A-HMS and M-HMS, respectively) in comparison with that obtained with pristine HMS, SBA-15, MCM-41 and PAC. The adsorption mechanism was investigated by analyzing the adsorption kinetics, isotherms and thermodynamics under various conditions, and used in comparison between different adsorbates to simultaneously elucidate the potential effects of the surface functional group, pH and temperature on the adsorption capacity.

5.2 Methods

5.2.1 Adsorption kinetics

Adsorption assays were performed as batch experiments with the test pharmaceutical compound diluted to a concentration of 100 μg/L. The pH of the solution was controlled at 7 using 0.01 M phosphate buffer and the ratio of adsorbent to pharmaceutical solution was fixed at 2 g/L. The mixture was agitated in a rotary shaker at 25°C at 150 rpm. The adsorption kinetics were evaluated by measuring the concentration of each pharmaceutical compound at different time intervals. The liquid taken from the adsorption mixture was filtered through a polytetrafluoroethylene syringe filter (Chrom Tech, US). The filtrate was concentrated by SPE using a 60 mg C18 cartridge (Agela, Japan) and the concentration of pharmaceutical residue remaining was measured on an Agilent 1100 HPLC with a UV detector. Taking of the liquid samples and their measurements continued until the concentrations of pharmaceutical residues reached equilibrium point.

5.2.2 Adsorption isotherm evaluation

Adsorption isotherm assays were performed as for the adsorption kinetic study above; except that the concentrations of pharmaceutical compounds were varied from 40 to 200 µg/L and samples were only taken at the equilibrium time (determined in the adsorption kinetic study above).

5.2.3 Effects of pH and temperature on the adsorption capacity of adsorbent

The effect of varying the pH or temperature on the adsorption capacity of each adsorbent was evaluated in the same manner as per the adsorption isotherm study above, except for the former the pH of the solution was adjusted to 5 or 9 using 0.01 M phosphate buffer, and for the latter a temperature of 15, 25 or 40 ^{o}C was used at pH 7.0.

5.2.4 Competitive adsorption

The competitive adsorption of each individual pharmaceutical compound over HMS, M-HMS, A-HMS and PAC was investigated in a mixed-solute solution. The range of initial concentrations and the adsorption conditions used in this study were the same as those applied to the single solute experiment above.

5.3 Results and discussion

5.3.1 Adsorption kinetics

The kinetics of Pharmaceuticals adsorption are shown in Figure 5.1 , 5.2, 5.3, 5.4 and 5.5 as the amount of adsorbate adsorbed (q_t) over time (µg/g.min). For all six adsorbents, the concentration of all pharmaceuticals in the solution decreased rapidly in the first 30 min and then gradually decreased thereafter until they reached equilibrium within 10 h.

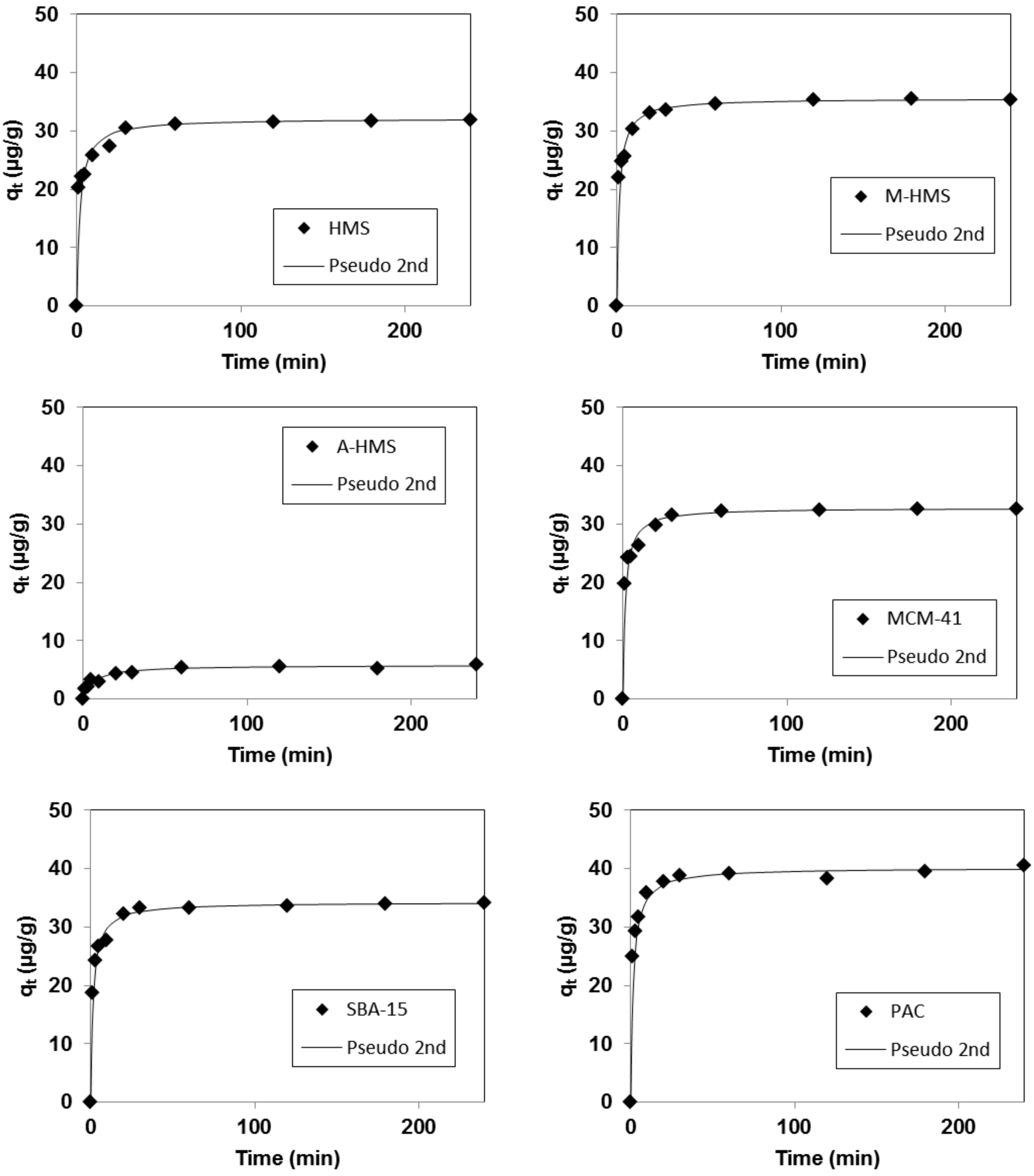

Figure 5.1 Adsorption kinetics of DCF adsorbed onto the different mesoporous silicates and PAC (pH 7, 25 ^{o}C and IS 0.01M).

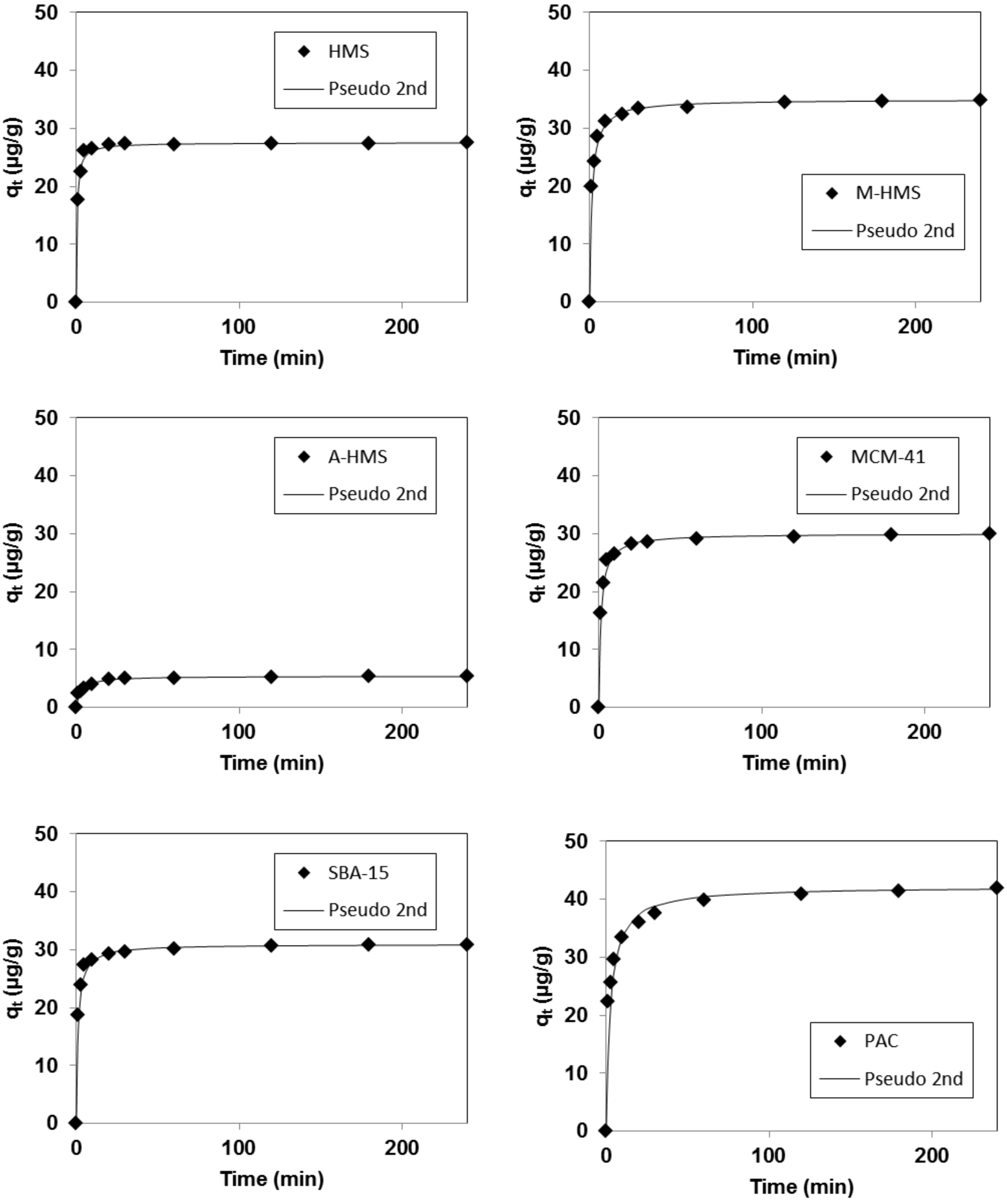

Figure 5.2 Adsorption kinetics of CBZ adsorbed onto the different mesoporous silicates and PAC (pH 7, 25 °C and IS 0.01M).

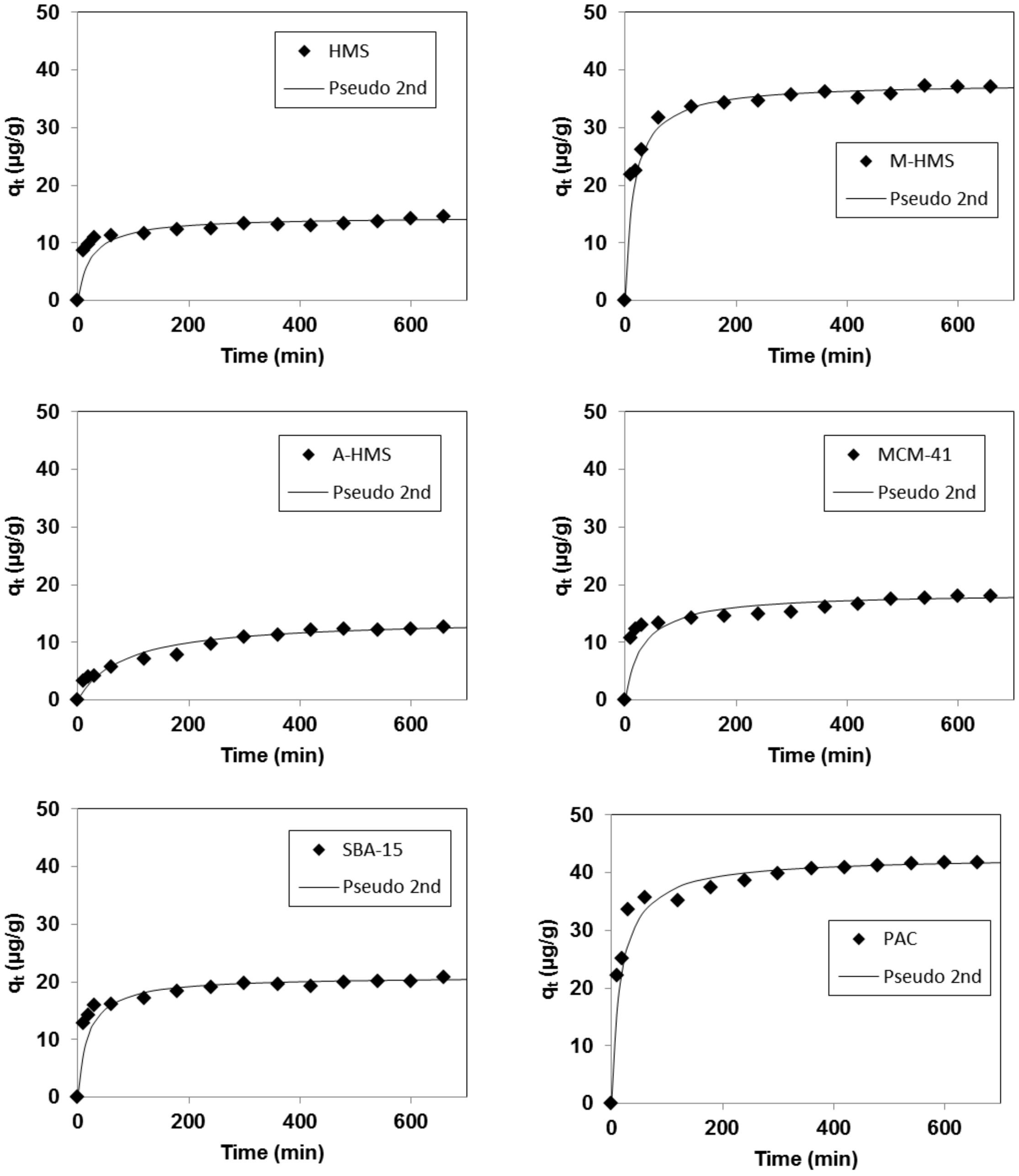

Figure 5.3 Adsorption kinetics of NAP adsorbed onto the different mesoporous silicates and PAC (pH 7, 25 °C and IS 0.01M).

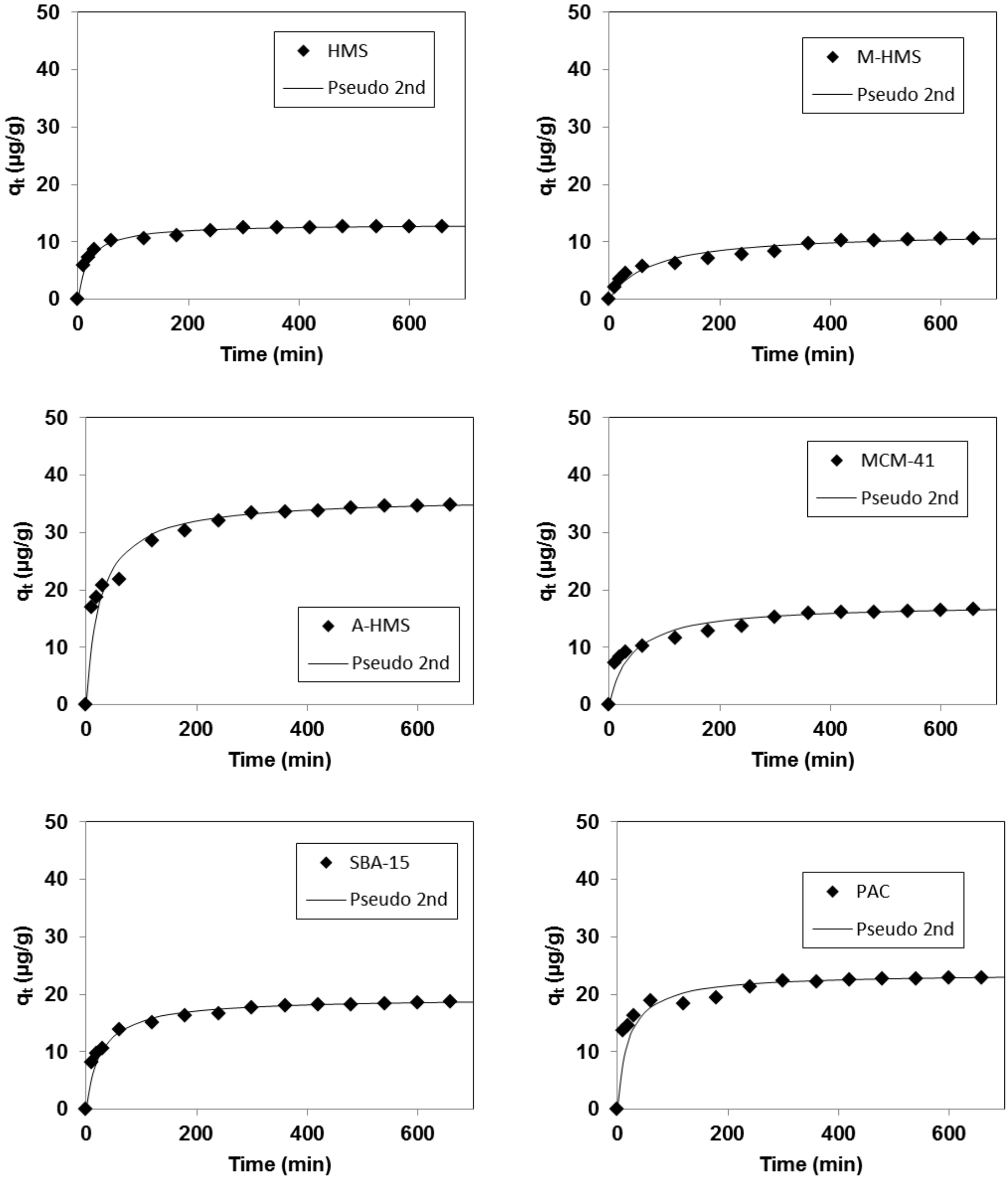

Figure 5.4 Adsorption kinetics of CFA adsorbed onto the different mesoporous silicates and PAC (pH 7, 25 °C and IS 0.01M).

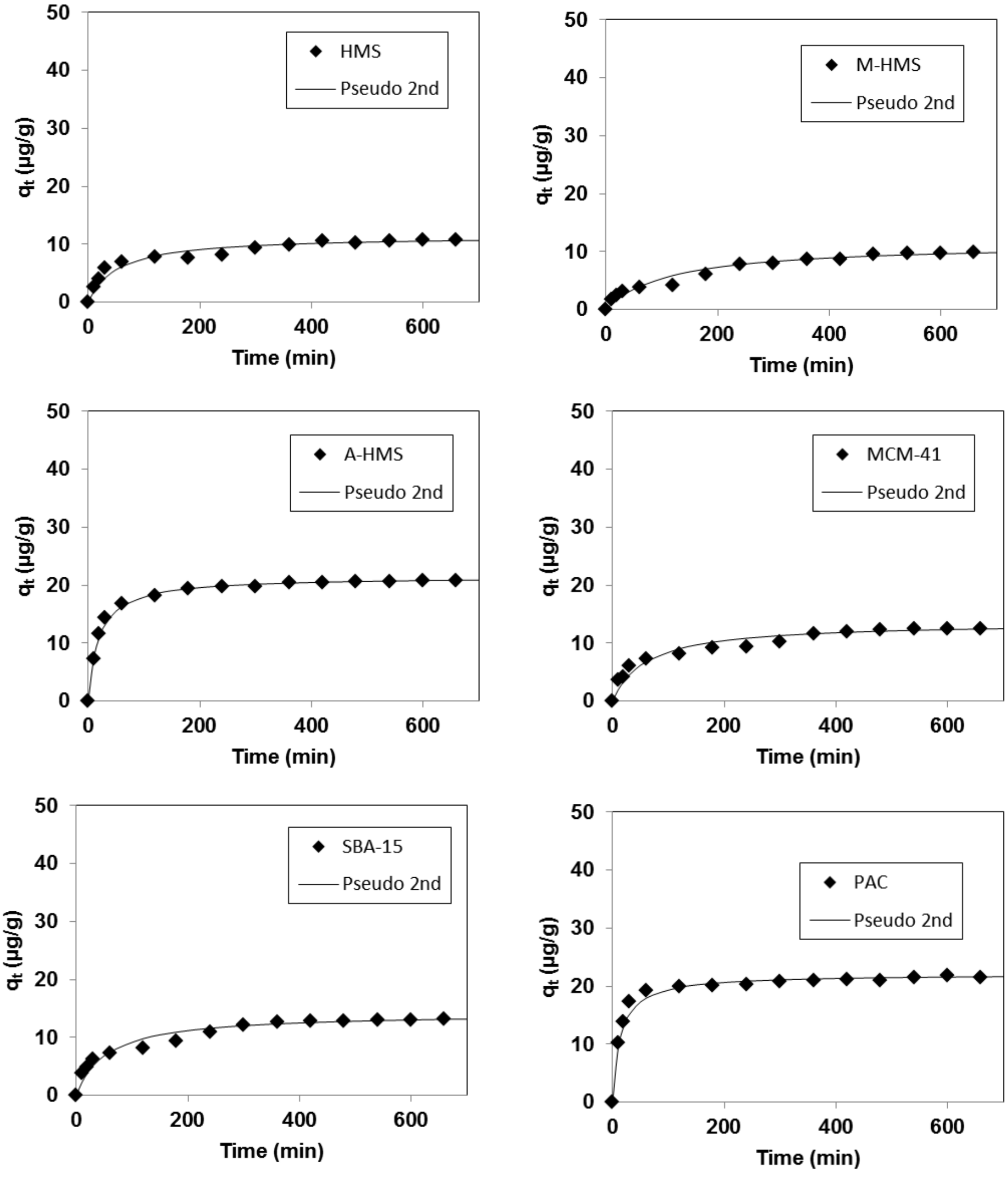

Figure 5.5 Adsorption kinetics of ACT adsorbed onto the different mesoporous silicates and PAC (pH 7, 25 °C and IS 0.01M).

5.3.2 Adsorption kinetic models

To evaluate the efficiency of adsorption process pseudo-second-order and Ritchie-second-order kinetic models were used for interpretation of the experimental data. The pseudo-second order equation [Ho and Mckay, 1999] can be defined as in Eq. (5.1):

$$\frac{t}{q_t} = \frac{1}{k_2 q_e^2} + \frac{t}{q_e} \tag{5.1}$$

where k_2 is the pseudo-second order rate constant (g/µg.min), which is determined from the plots of t/q_t versus t. The plot of pseudo-second order kinetic model for the adsorption of pharmaceuticals on the adsorbate are shown in appendix B. Furthermore, the initial adsorption rate (h) and half equilibrium time ($t_{0.5}$) that are obtained from this model can be expressed as in Eq. (5.2) and (5.3), respectively [Pan et al., 2011]:

$$h = k_2 q_e^2 \tag{5.2}$$

$$t_{0.5} = \frac{1}{k_2 q_e} \tag{5.3}$$

The Ritchie-second-order equation [Ritchie, 1997] can be expressed as in Eq. (5.4)

$$\frac{1}{q_t} = \frac{1}{k_r q_e t} + \frac{1}{q_e} \tag{5.4}$$

where k_r is the Ritchie-second-order rate constant (1/min), and is derived from the plots of $1/q_t$ versus $1/t$. The plot of Ritchhie-second order kinetic model for the adsorption of pharmaceuticals on the adsorbate are shown in appendix B.

The calculated parameters for each adsorbent and kinetic model, and the respective correlation coefficients (R^2) for the data and model, are summarized for the adsorption of DCF, CBZ, NAP, CFA and ACT in Table 5.1, 5.2, 5.3, 5.4 and 5.5 respectively. From the correlation coefficients, the adsorption of all of these pharmaceuticals onto the silicate materials and onto PAC is most likely represented by pseudo-second-order kinetics. Therefore, it is assumed that chemisorption is involved in the adsorption process [Pan et al., 2011].

In case of the adsorption of DCF, CBZ and NAP the calculated parameters showed that among the porous silicates, the initial adsorption rate was highest in M-HMS, whilst it was by the far the slowest in A-HMS. Overall, PAC showed the fastest initial adsorption rate, which were ranked (in descending order) as PAC > M-HMS > SBA-15 > MCM-41 > HMS > A-HMS. In case of the adsorption of CFA, A-HMS showed the fastest initial adsorption rate. The initial adsorption rates of the adsorbents for CFA were ranked as A-HMS > PAC > SBA-15 > HMS > MCM-41 > M-HMS. In case of the adsorption of ACT, the initial adsorption rates of the adsorbents were ranked as PAC > A-HMS > SBA-15 > MCM-41 > HMS > M-HMS.

Table 5.1 Kinetic parameters for the adsorption of DCF onto HMS, modified HMS derivatives, SBA-15, MCM-41 and PAC.

Adsorbents	$q_{e,\exp}$ **(µg/g)**	**Pseudo-second order**					**Ritchie**		
		$k_2 x10^3$ **(g/µg.min)**	$q_{e,cal}$ **(µg/g)**	h **(µg/g.min)**	$t_{0.5}$ **(min)**	R^2	k_r **(L/min)**	$q_{e,cal}$ **(µg/g)**	R^2
HMS	31.93	16.4	32.16	32.15	1.90	0.999	1.874	29.33	0.701
M-HMS	35.59	19.6	35.59	35.59	1.43	0.998	1.676	33.33	0.799
A-HMS	5.89	28.2	5.82	5.82	6.09	0.996	0.569	4.64	0.798
SBA-15	34.18	19.7	34.26	34.25	1.49	0.998	1.255	32.79	0.945
MCM-41	32.64	21.1	32.80	32.79	1.45	1.000	1.612	30.86	0.867
PAC	40.55	15.9	40.16	40.16	1.57	0.997	1.667	38.46	0.911

Table 5.2 Kinetic parameters for the adsorption of CBZ onto HMS, modified HMS derivatives, SBA-15, MCM-41 and PAC.

Adsorbents	$q_{e,\mathrm{exp}}$ (µg/g)	**Pseudo-second order**					**Ritchie**		
		k_2x10^3 (g/µg.min)	$q_{e,\mathrm{cal}}$ (µg/g)	h (µg/g.min)	$t_{0.5}$ (min)	R^2	k_r (L/min)	$q_{e,\mathrm{cal}}$ (µg/g)	R^2
HMS	27.59	27.6	27.59	27.55	0.53	1.000	1.739	27.78	0.982
M-HMS	34.79	20.7	34.98	34.97	1.38	0.999	1.338	33.67	0.947
A-HMS	5.36	66.7	5.41	5.41	2.77	0.998	0.933	4.778	0.763
SBA-15	30.94	30.3	30.97	30.96	1.07	0.999	1.567	30.40	0.985
MCM-41	29.93	25.8	30.03	30.03	1.29	0.999	1.209	29.33	0.984
PAC	41.87	9.10	42.20	42.19	2.60	0.998	1.236	38.17	0.848

Table 5.3 Kinetic parameters for the adsorption of NAP onto HMS, modified HMS derivatives, SBA-15, MCM-41 and PAC.

Adsorbents	$q_{e,\mathrm{exp}}$ **(µg/g)**	**Pseudo-second order**					**Ritchie**		
		k_2x10^3 **(g/µg.min)**	$q_{e,\mathrm{cal}}$ **(µg/g)**	h **(µg/g.min)**	$t_{0.5}$ **(min)**	R^2	k_r **(L/min)**	$q_{e,\mathrm{cal}}$ **(µg/g)**	R^2
HMS	14.61	2.92	14.56	0.62	23.52	0.996	0.169	13.37	0.873
M-HMS	37.44	1.73	37.73	2.46	15.35	0.999	0.126	36.10	0.887
A-HMS	12.82	0.85	14.08	0.17	82.99	0.988	0.038	10.55	0.835
SBA-15	20.99	2.59	20.96	1.14	18.43	0.998	0.167	19.61	0.878
MCM-41	18.29	1.72	18.59	0.69	31.25	0.994	0.166	16.45	0.785
PAC	41.88	1.41	42.74	2.57	16.61	0.999	0.108	41.15	0.938

Table 5.4 Kinetic parameters for the adsorption of CFA onto HMS, modified HMS derivatives, SBA-15, MCM-41 and PAC.

Adsorbents	$q_{e,\mathrm{exp}}$ **(µg/g)**	**Pseudo-second order**					**Ritchie**		
		$k_2 x10^3$ **(g/µg.min)**	$q_{e,\mathrm{cal}}$ **(µg/g)**	h **(µg/g.min)**	$t_{0.5}$ **(min)**	**R^2**	k_r **(L/min)**	$q_{e,\mathrm{cal}}$ **(µg/g)**	**R^2**
HMS	12.80	3.99	13.11	0.69	19.13	0.999	0.082	12.56	0.989
M-HMS	10.69	1.14	11.68	0.16	74.94	0.989	0.028	9.92	0.982
A-HMS	34.82	1.09	36.10	1.42	25.50	0.999	0.089	32.79	0.839
SBA-15	18.92	1.95	19.38	0.73	26.43	0.999	0.074	17.95	0.934
MCM-41	16.77	1.41	17.54	0.43	40.40	0.996	0.079	15.06	0.843
PAC	23.32	2.13	23.64	1.19	19.90	0.998	0.140	21.93	0.849

Table 5.5 Kinetic parameters for the adsorption of ACT onto HMS, modified HMS derivatives, SBA-15, MCM-41 and PAC.

Adsorbents	$q_{e,\text{exp}}$ **(µg/g)**	**Pseudo-second order**					**Ritchie**		
		$k_2 x10^3$ **(g/µg.min)**	$q_{e,\text{cal}}$ **(µg/g)**	h **(µg/g.min)**	$t_{0.5}$ **(min)**	R^2	k_r **(L/min)**	$q_{e,\text{cal}}$ **(µg/g)**	R^2
HMS	10.78	1.67	11.47	0.22	52.26	0.993	0.034	10.44	0.980
M-HMS	9.93	0.78	11.43	0.10	112.6	0.977	0.025	8.26	0.915
A-HMS	21.08	2.44	21.46	1.13	19.06	0.999	0.053	21.65	0.991
SBA-15	13.19	1.30	14.20	0.26	54.00	0.995	0.042	12.06	0.930
MCM-41	12.67	1.22	13.59	0.23	60.33	0.992	0.040	11.44	0.929
PAC	21.92	3.27	22.08	1.59	13.86	0.999	0.089	21.93	0.986

5.3.3 Diffusion mechanism

The kinetic data were then analyzed by the Weber and Morris intraparticle diffusion models to determine the diffusion mechanism and to find the rate-limiting step in the adsorption process. In a solid-liquid adsorption, the dynamic process can be described in three steps. The first step is film diffusion, which represents the transport of adsorbate's molecules to the external surface of the adsorbent. The second step is pore diffusion or intraparticle diffusion, which represents the diffusion of the adsorbate's molecules to an adsorption site through the liquid filled pores. The third step is adsorption of the adsorbate's molecules at a site on the surface (internal or external) of the adsorbent. The activation energy for this step depends on the type of binding process (physical or chemical). Among these 3 steps the slowest step is the rate limiting step in the adsorption process. The adsorption process at the active site (step3) is relatively fast when compared with the other two [Al-Mhutaseb et al., 2011; Tong et al., 2011; Cheung et al., 2007] and is not considered to be the rate limiting step. Only diffusion (either film diffusion or pore diffusion) is the rate limiting step in the adsorption process. The overall rate of adsorption is controlled by either film or intraparticle diffusion or a mixture of both [Al-Mhutaseb et al., 2011; Tong et al., 2011; Cheung et al., 2007].

The Weber and Morris intraparticle diffusion model [Weber and Morris, 1963] can be expressed as in Eq. (5.5):

$$q_t = k_p t^{1/2} + C \qquad (5.5)$$

where k_p is the intraparticle diffusion rate constant (μg/g.min$^{1/2}$) and C is a constant relating to the thickness of the boundary layer (μg/g), which is determined from the plot of q_t versus $t^{1/2}$.

As shown in Figure 5.6, 5.7, 5.8, 5.9 and 5.10, the intraparticle plots reveal an asymptote pattern that can be subdivided into a multi-linearity pattern of three stages in the adsorption process of the mesoporous adsorbents and PAC. The first, sharper stage is attributed to the diffusion of pharmaceuticals from the solution through the boundary layer to the external surface of the adsorbents. The second stage represents the intraparticle or pore diffusion stage during which the pharmaceuticals move into the interior of the sorbent particles and adsorb onto the interior sites of the adsorbents. Lastly, the third stage is the final equilibrium [Pan et al., 2011; Zou et al., 2011; Han et al., 2011; Wan Ngah and Hanafiah, 2008; Guan et al., 2011; Ahmad and Alrozi et al., 2011; Ip et al., 2010].

For all adsorbents, the adsorption plots of DCF, CBZ, NAP and CFA did not pass through the origin and so the intraparticle diffusion was not the only rate-limiting step. Rather, the external mass transfer played an important role in the adsorption process [Al-Ghouti et al., 2009; Kumar and Guar, 2011]. But in case of the adsorption of ACT, the adsorption plots for all adsorbents seemed to pass through the origin. This suggested that pore diffusion was the rate-limiting step in ACT adsorption.

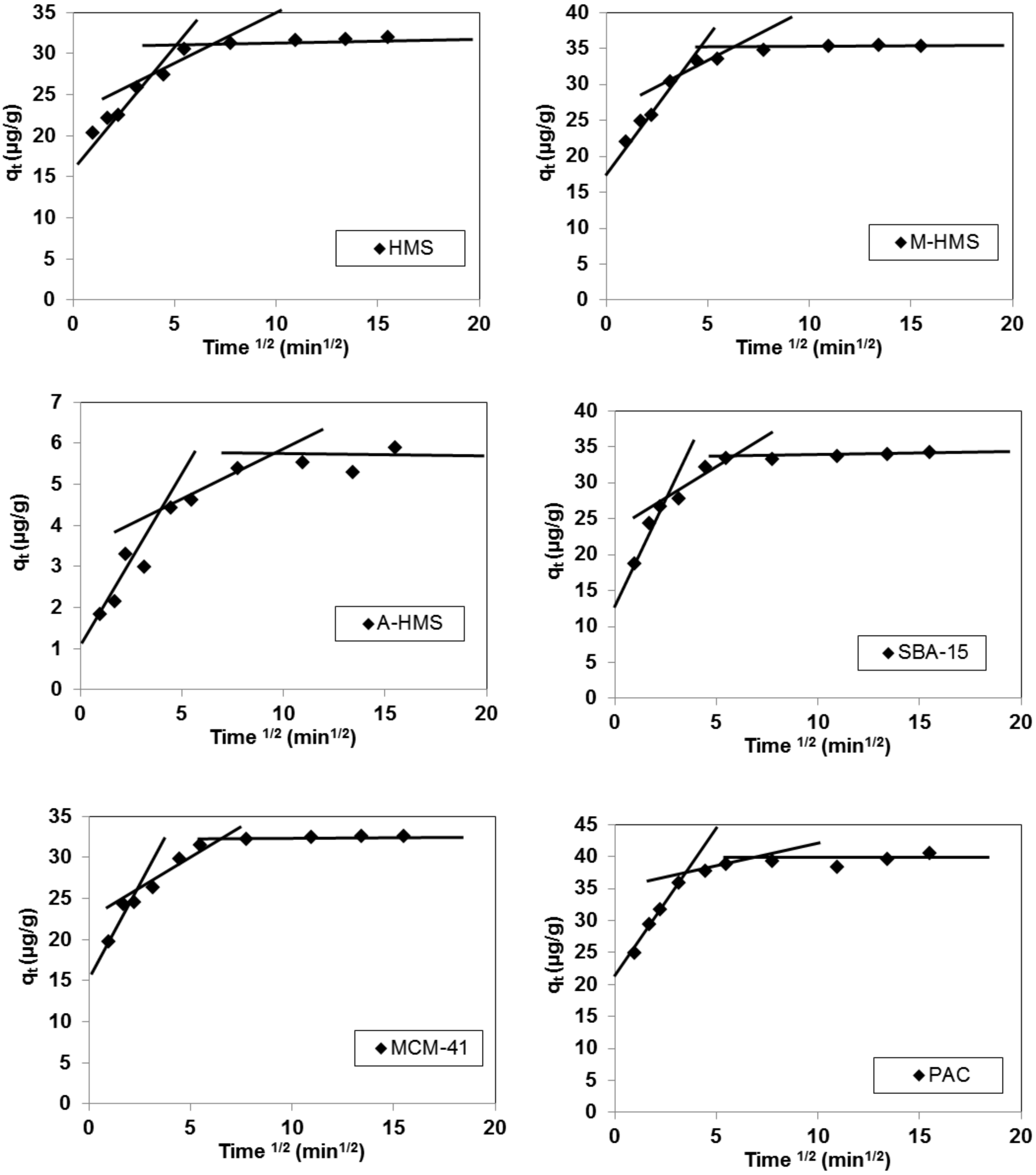

Figure 5.6 Intraparticle diffusion plot of DCF adsorbed onto HMS, modified HMS derivatives, SBA-15, MCM-41 and PAC (pH 7, 25 °C and IS 0.01M).

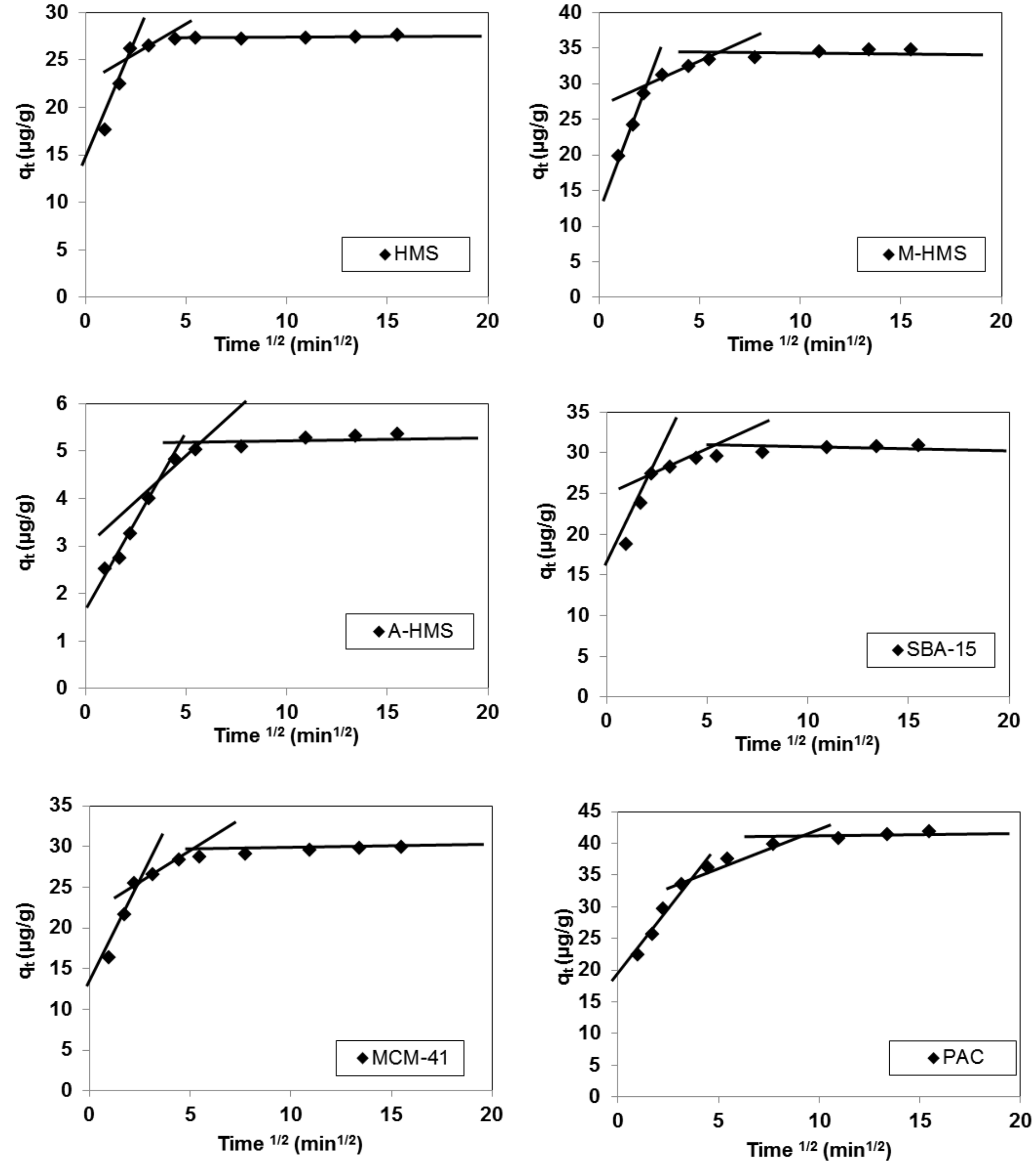

Figure 5.7 Intraparticle diffusion plot of CBZ adsorbed onto HMS, modified HMS derivatives, SBA-15, MCM-41 and PAC (pH 7, 25 °C and IS 0.01M).

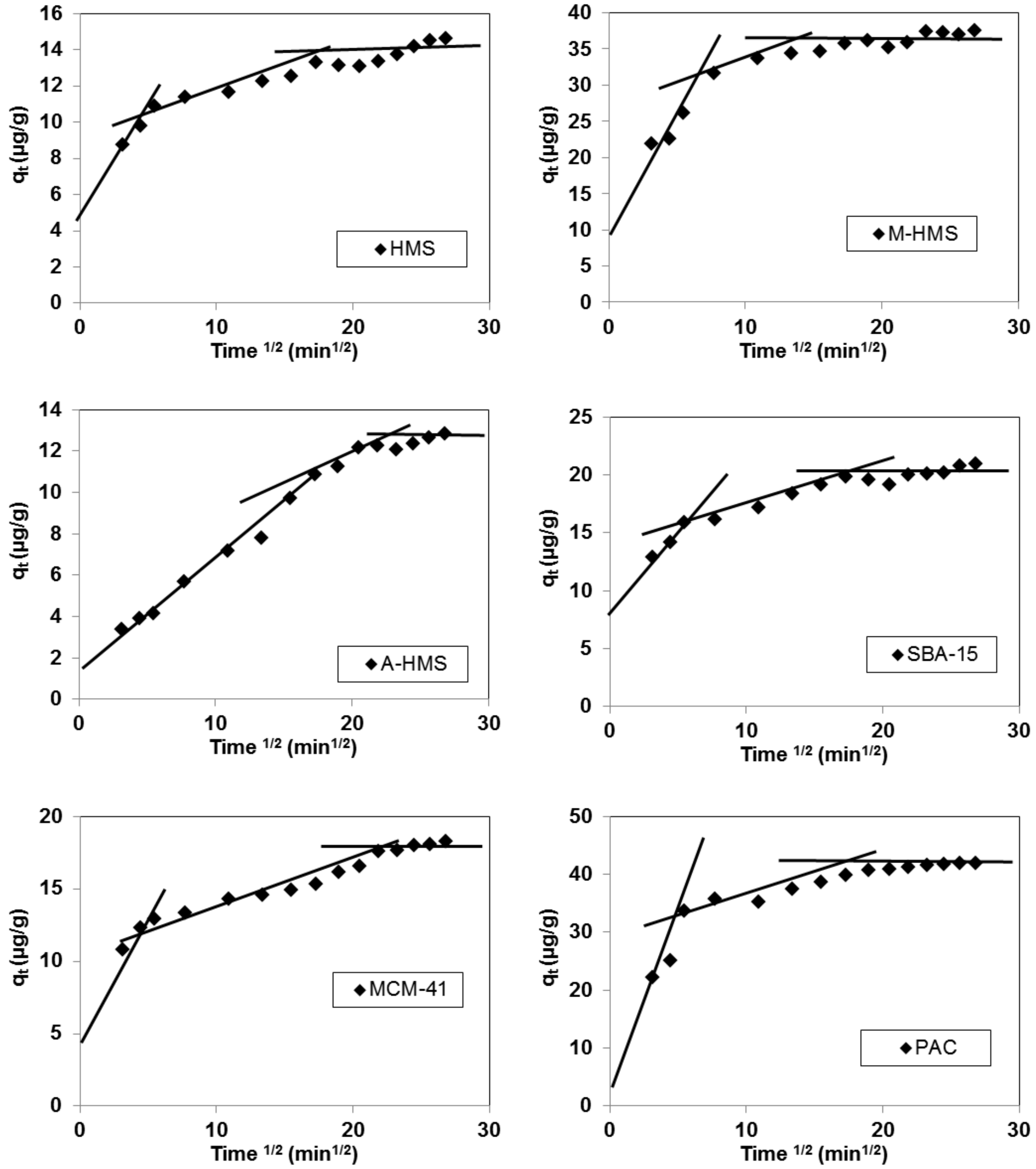

Figure 5.8 Intraparticle diffusion plot of NAP adsorbed onto HMS, modified HMS derivatives, SBA-15, MCM-41 and PAC (pH 7, 25 ^{o}C and IS 0.01M).

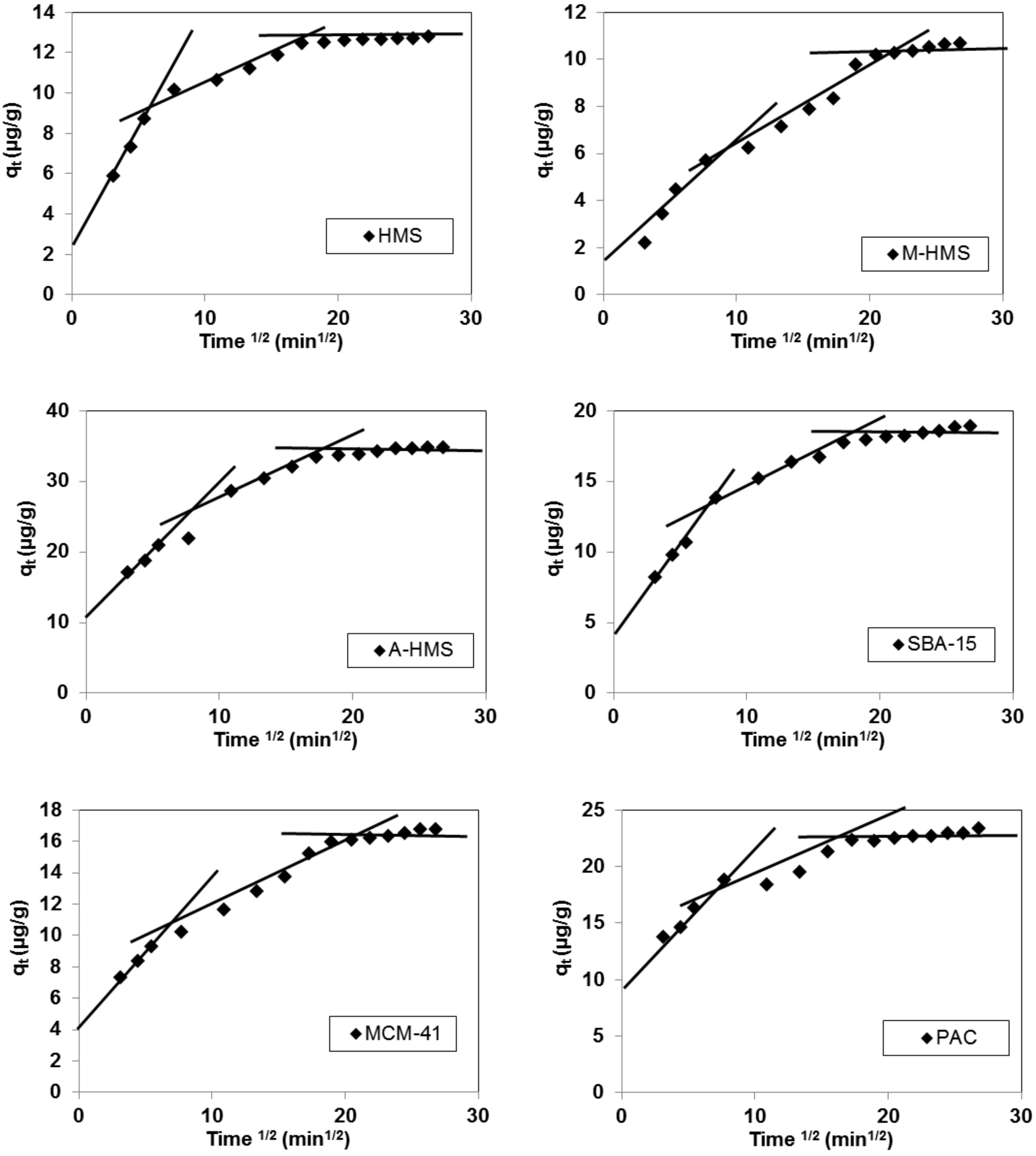

Figure 5.9 Intraparticle diffusion plot of CFA adsorbed onto HMS, modified HMS derivatives, SBA-15, MCM-41 and PAC (pH 7, 25 °C and IS 0.01M).

.

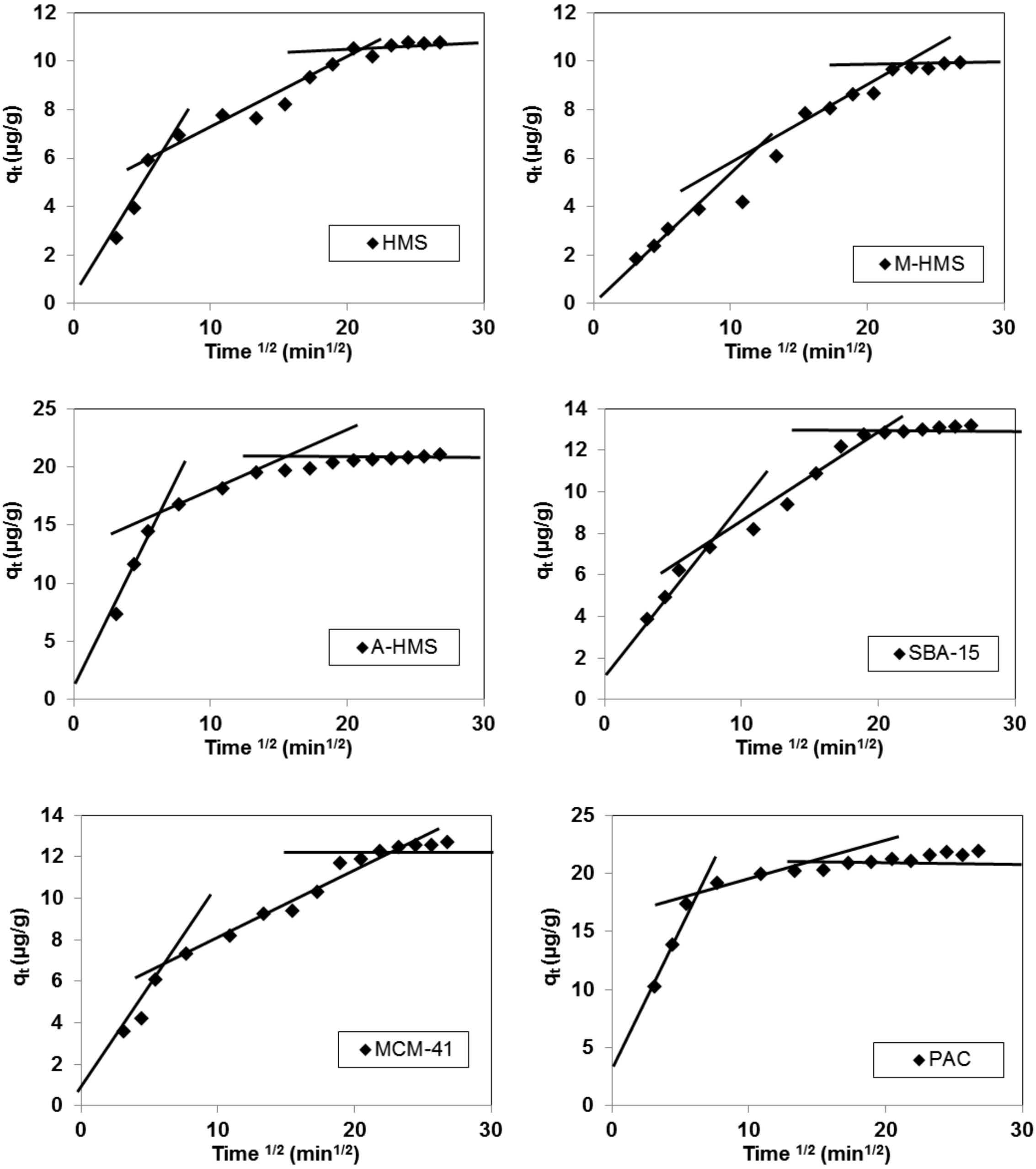

Figure 5.10 Intraparticle diffusion plot of ACT adsorbed onto HMS, modified HMS derivatives, SBA-15, MCM-41 and PAC (pH 7, 25 °C and IS 0.01M).

5.3.4 Adsorption isotherm modeling

The adsorption isotherm data were analyzed by five mathematical isotherm models (Langmuir, Freundlich, Dubinin-Radushkevich (D-R), Temkin and Linear isotherm), to model the adsorption of each pharmaceutical compound onto the mesoporous adsorbents.

The linear form of the Langmuir isotherm [Langmuir, 1916] can be described as Eq. (5.6):

$$\frac{1}{q_e} = \frac{1}{q_m} + \frac{1}{k_L q_m C_e} \tag{5.6}$$

where q_m is the maximum adsorption capacity (µg/g) and k_L is the Langmuir constant (L/µg). The dimensionless separation factor R_L, which is used to predict the favorability of an adsorption system, can be described as Eq. (5.7):

$$R_L = \frac{1}{1+K_L C_o} \tag{5.7}$$

where C_0 is the initial concentration of pharmaceuticals (µg/L). The plot of Langmuir isotherm model for the adsorption of pharmaceuticals on the adsorbate are shown in Figure 5.11, 5.12, 5.13, 5.14 and 5.15.

The linear form of the Freundlich isotherm [Freundlich, 1906] can be described as Eq. (5.8):

$$\ln q_e = \ln k_F + \frac{1}{n} \ln C_e \tag{5.8}$$

where k_F is the Freundlich constant and n is the adsorption intensity (dimensionless). The plot of Freundlich isotherm model for the adsorption of pharmaceuticals on the adsorbate are shown in Figure 5.16, 5.17, 5.18, 5.19 and 5.20.

The linear form of the D-R isotherm [Dubinin and Radushkevich, 1947; Fu et al., 2008] can be described as Eqs. (5.9) and (5.10):

$$\ln q_e = \ln q_m - B\varepsilon^2 \tag{5.9}$$

$$\varepsilon = RT\ln\left(1 + \frac{1}{C_e}\right) \tag{5.10}$$

where q_m is the maximum adsorption capacity (μg/g), B is a constant related to the mean free energy of sorption per mol of adsorbent (mol^2/J^2), ε is the Polanyi potential, *R* is the gas constant (8.314 J/mol.K) and *T* is the Kelvin (absolute) temperature (K). The plot of D-R isotherm model for the adsorption of pharmaceuticals on the adsorbate are shown in Figure 5.21, 5.22, 5.23, 5.24 and 5.25.The mean free energy, *E*, of sorption per mol of adsorbent when it is transferred to the surface of the adsorbate can be computed using the following relationship [Hobson, 1969]:

$$E = \frac{1}{(-2\beta)^{0.5}} \tag{5.11}$$

The linear form of the Temkin isotherm [Temkin and Pyzhev, 1940] can be described as Eq. (5.12):

$$q_e = \frac{RT}{b_T}\ln A_T + \frac{R_T}{b_T}\ln C_e \tag{5.12}$$

where A_T (L/g) and b_T (J/mol) are the Temkin constants. The plot of Temkin isotherm model for the adsorption of pharmaceuticals on the adsorbate are shown in Figure 5.26, 5.27, 5.28, 5.29 and 5.30.

The Linear isotherm [Samuel and Osman, 1987] can be described as Eq. (5.13):

$$q_e = K_p C_e \tag{5.13}$$

where $K_p$is the linear constant (L/g). The plot of Linear isotherm model for the adsorption of pharmaceuticals on the adsorbate are shown in Figure 5.31, 5.32, 5.33, 5.34 and 5.35.

The calculated parameters and the correlation coefficients (R^2) for adsorption of pharmaceuticals (i.e. DCF, CBZ, NAP, CFA and ACT) onto the different adsorbents are shown in Table 5.6, 5.7, 5.8, 5.9 and 5.10 respectively. For the adsorption of DCF, CBZ, NAP and CFA, the Linear isotherm model gave the highest, and the Freundlich model the second highest R^2values for all adsorbents except for A-HMS with DCF, NAP and CFA, where the Langmuir model was slightly better correlated than the Linear and the Freundlich models. Nevertheless, the Linear and the Feundlich models still fitted the data on the adsorption of A-HMS well. For the adsorption of ACT the Langmuir model gave the highest, and the Freundlich model the second highest R^2 values for all adsorbents except for PAC, where the Linear isotherm model was slightly better correlated than the Langmuir and the Freundlich models. Nevertheless, the Langmuir and Freundlich models still fitted the data on the adsorption of PAC well. In conclusion, the Linear and the Freundlich models fitted the adsorption data of DCF, CBZ, NAP and CFA very well. For the adsorption of ACT, the Langmuir model was better correlated. The Freundlich model also fitted the ACT adsorption data well.

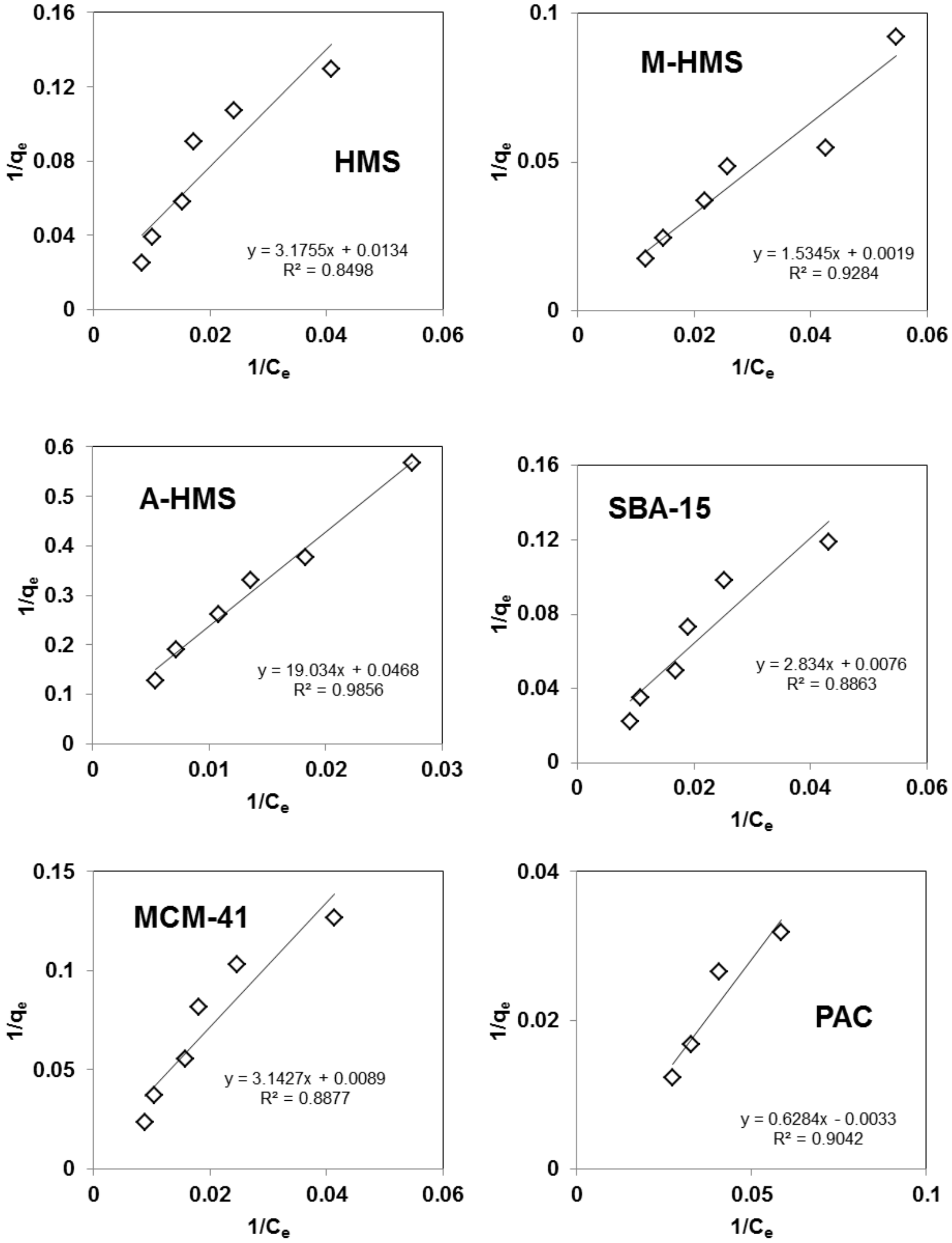

Figure 5.11 **A**dsorption isotherm of DCF removal according to the Langmuir isotherm model (pH 7, 25 ^{o}C and IS 0.01M).

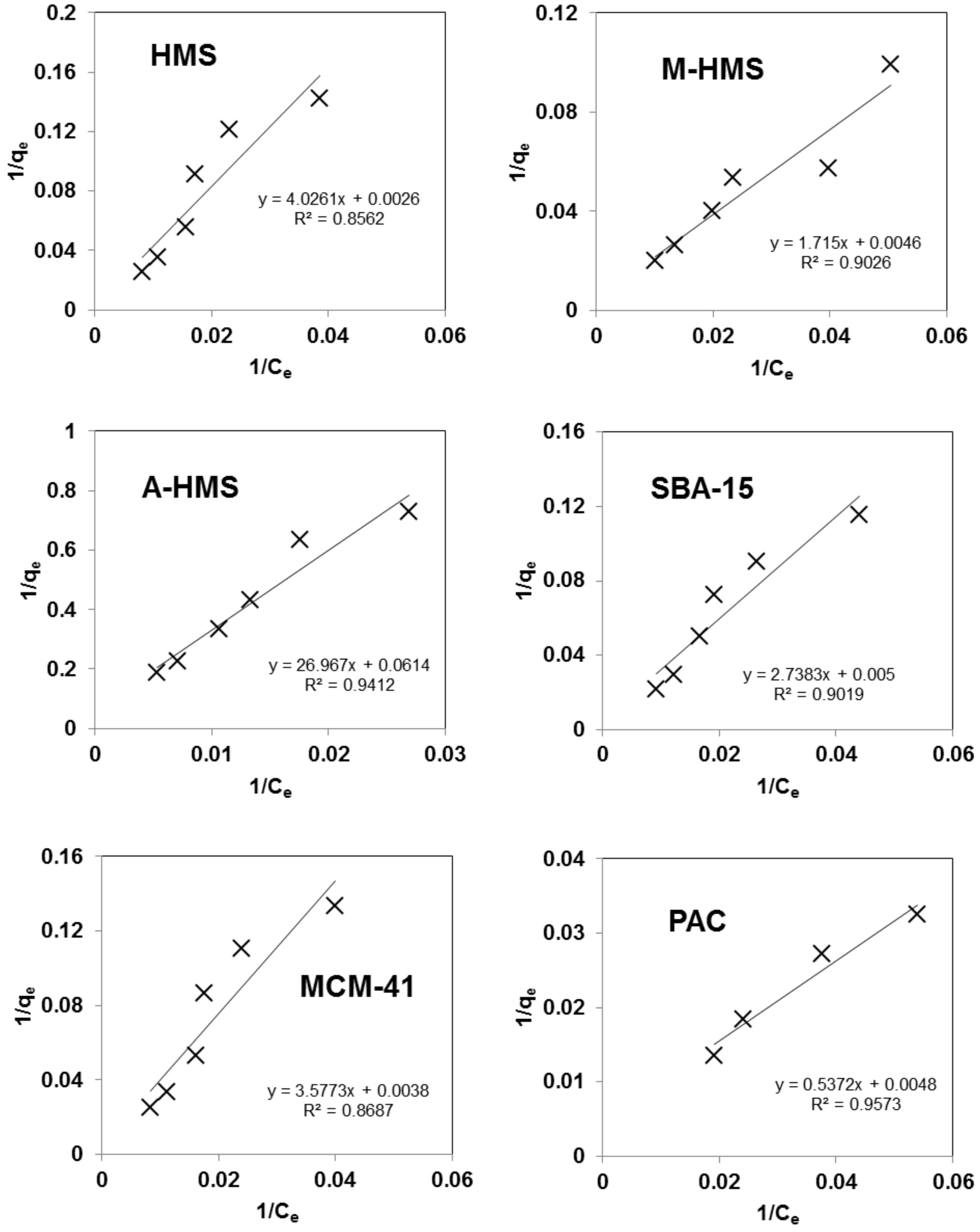

Figure 5.12 **A**dsorption isotherm of CBZ removal according to the Langmuir isotherm model (pH 7, 25 °C and IS 0.01M).

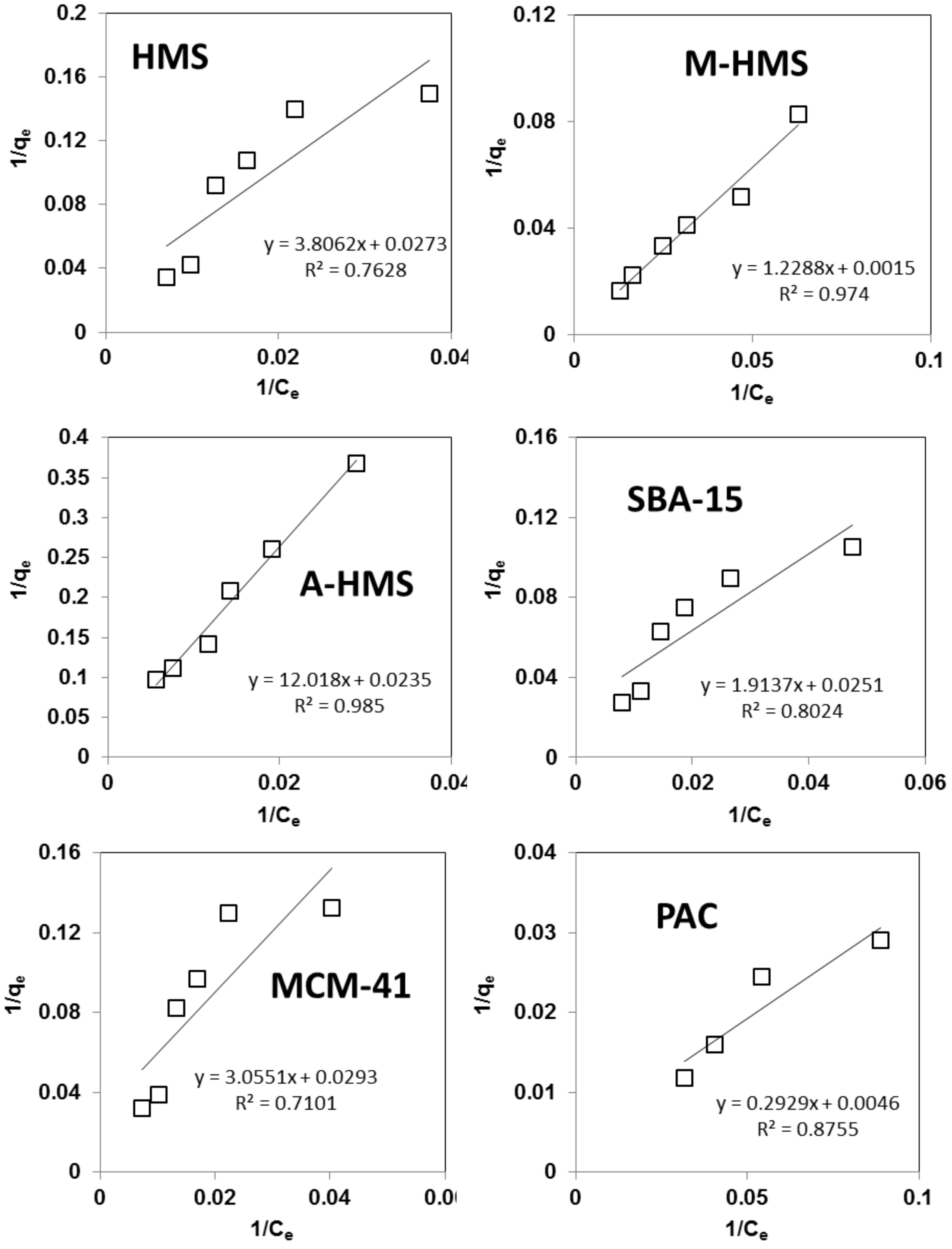

Figure 5.13 **A**dsorption isotherm of NAP removal according to the Langmuir isotherm model (pH 7, 25 ^{o}C and IS 0.01M).

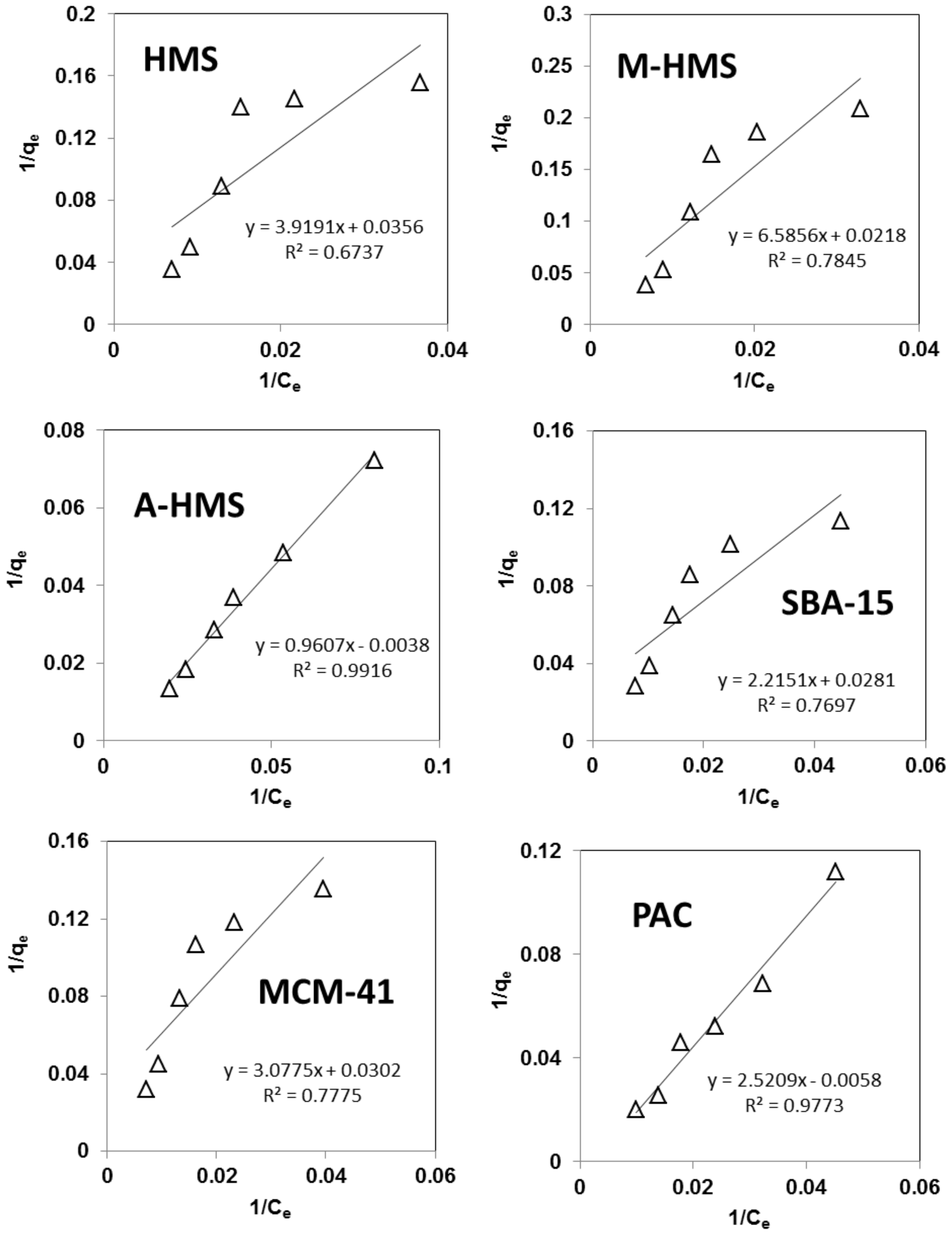

Figure 5.14 **A**dsorption isotherm of CFA removal according to the Langmuir isotherm model (pH 7, 25 °C and IS 0.01M).

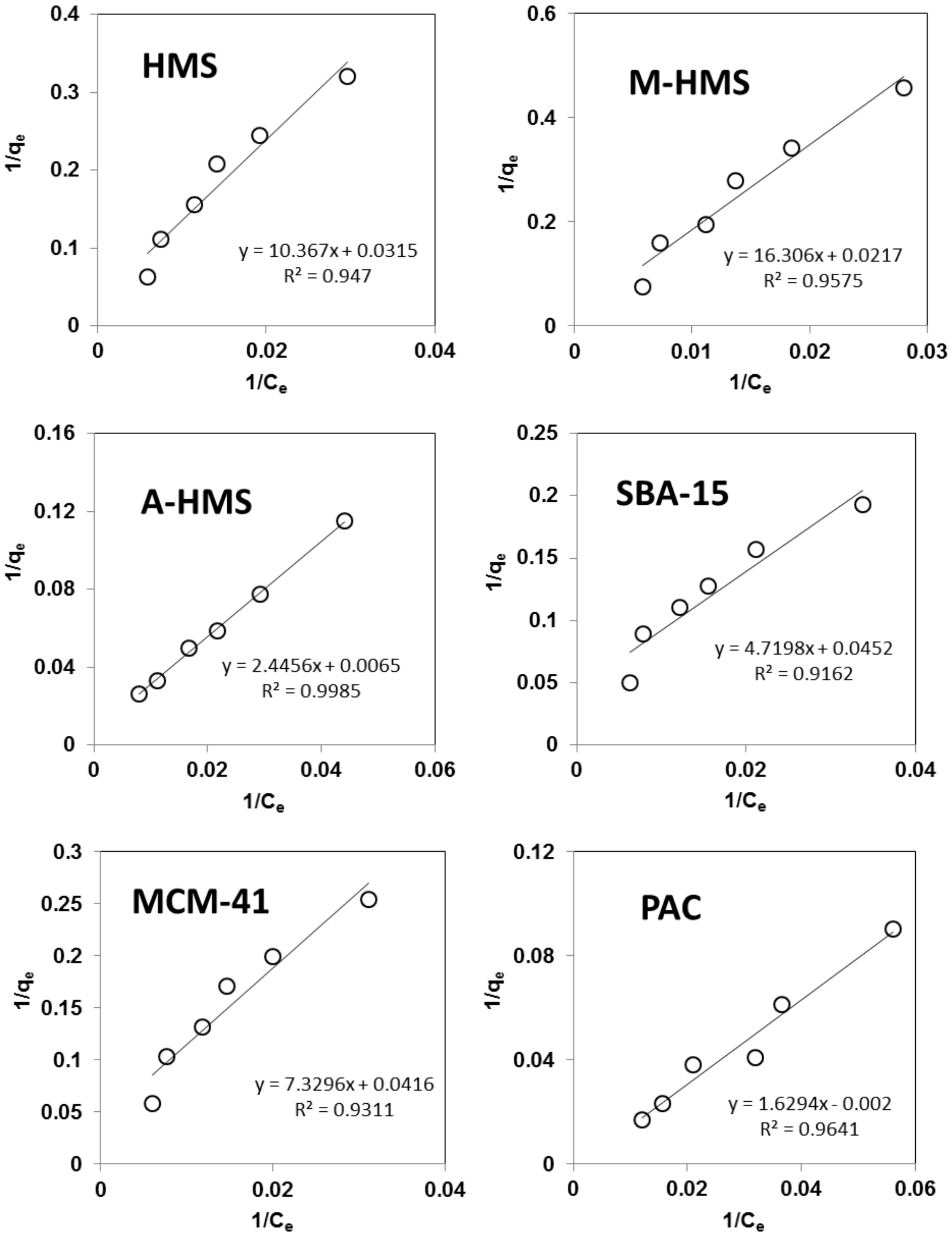

Figure 5.15 Adsorption isotherm of ACT removal according to the Langmuir isotherm model (pH 7, 25 °C and IS 0.01M).

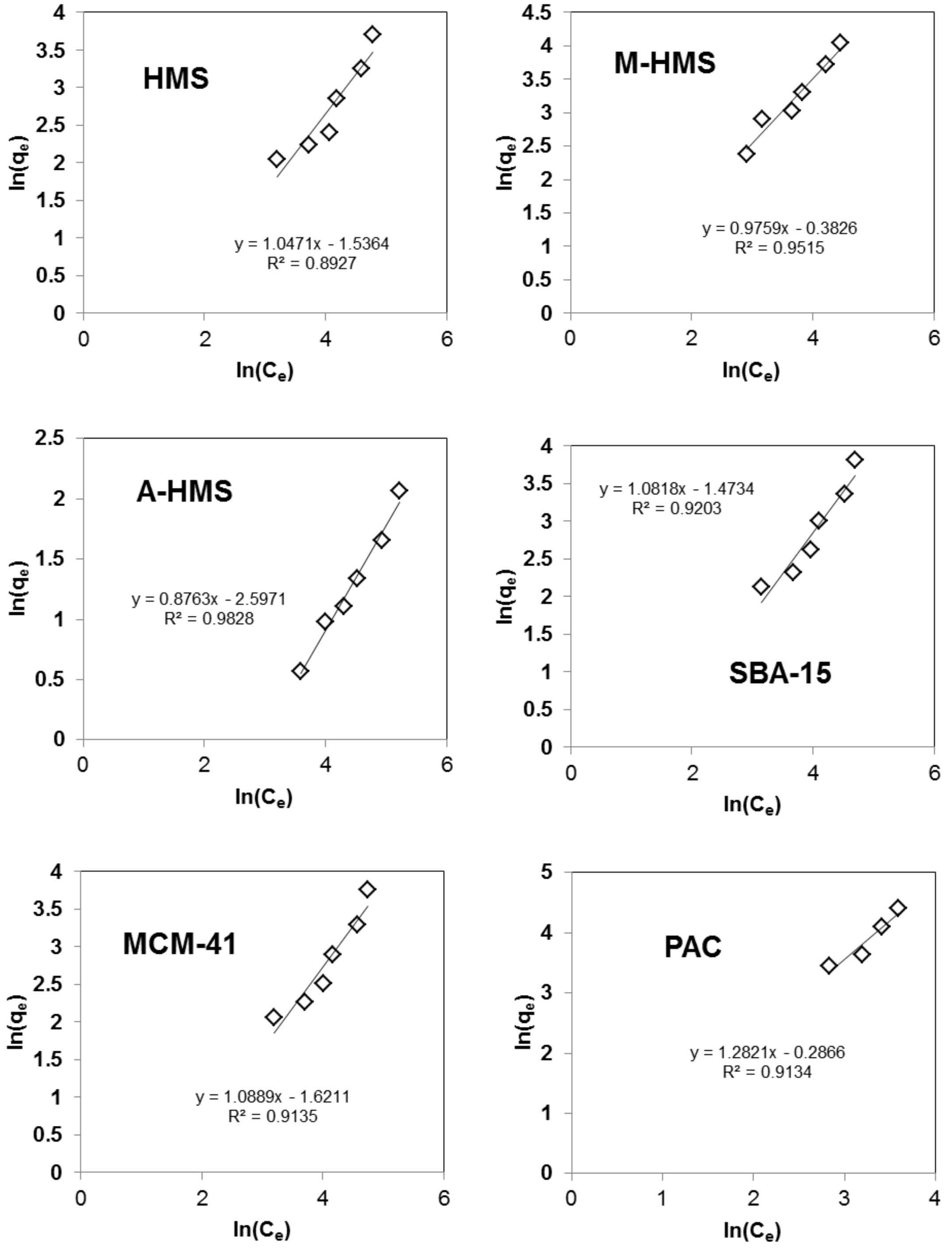

Figure 5.16 Adsorption isotherm of DCF removal according to the Freundlich isotherm model (pH 7, 25 °C and IS 0.01M).

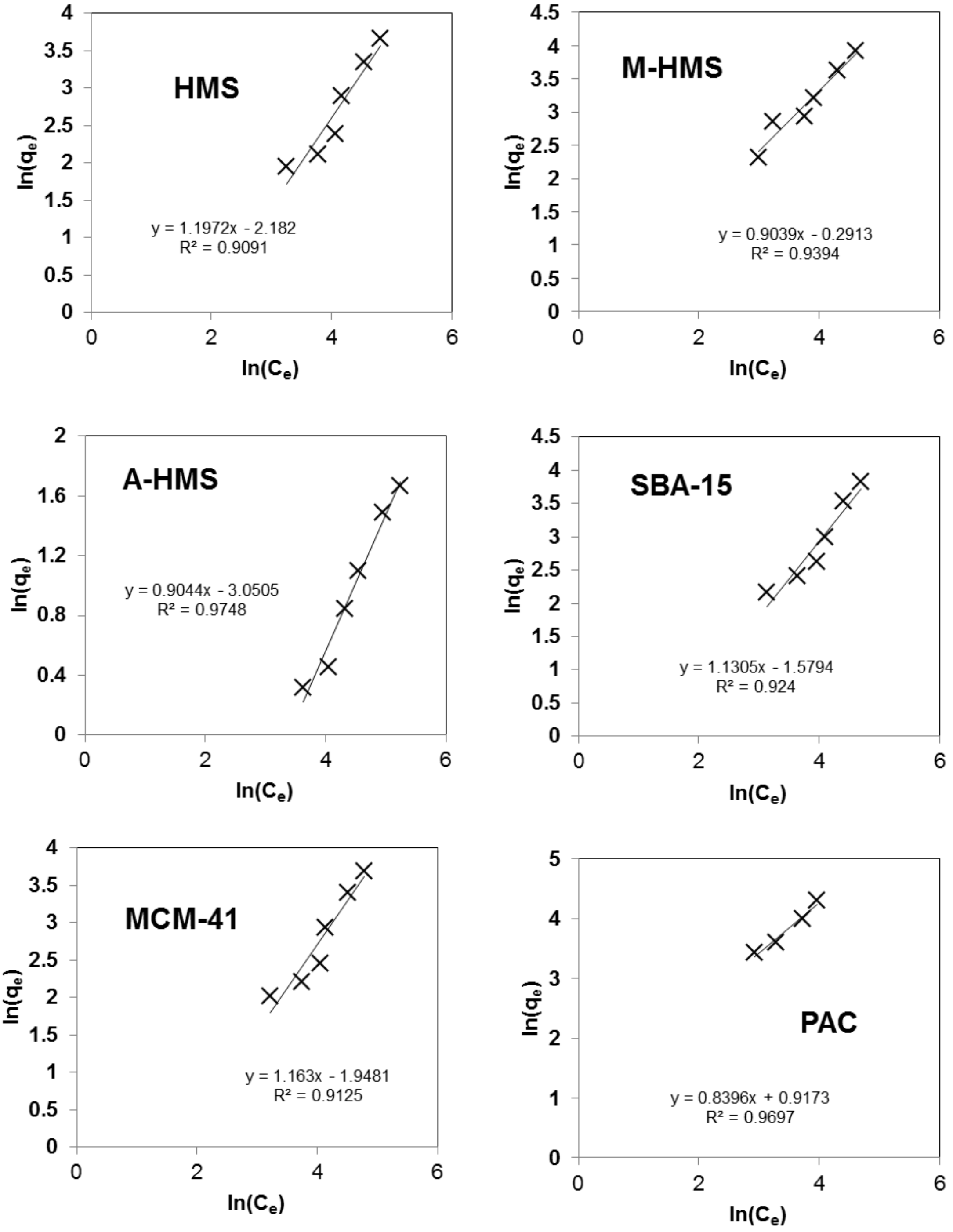

Figure 5.17 Adsorption isotherm of CBZ removal according to the Freundlich isotherm model (pH 7, 25 °C and IS 0.01M).

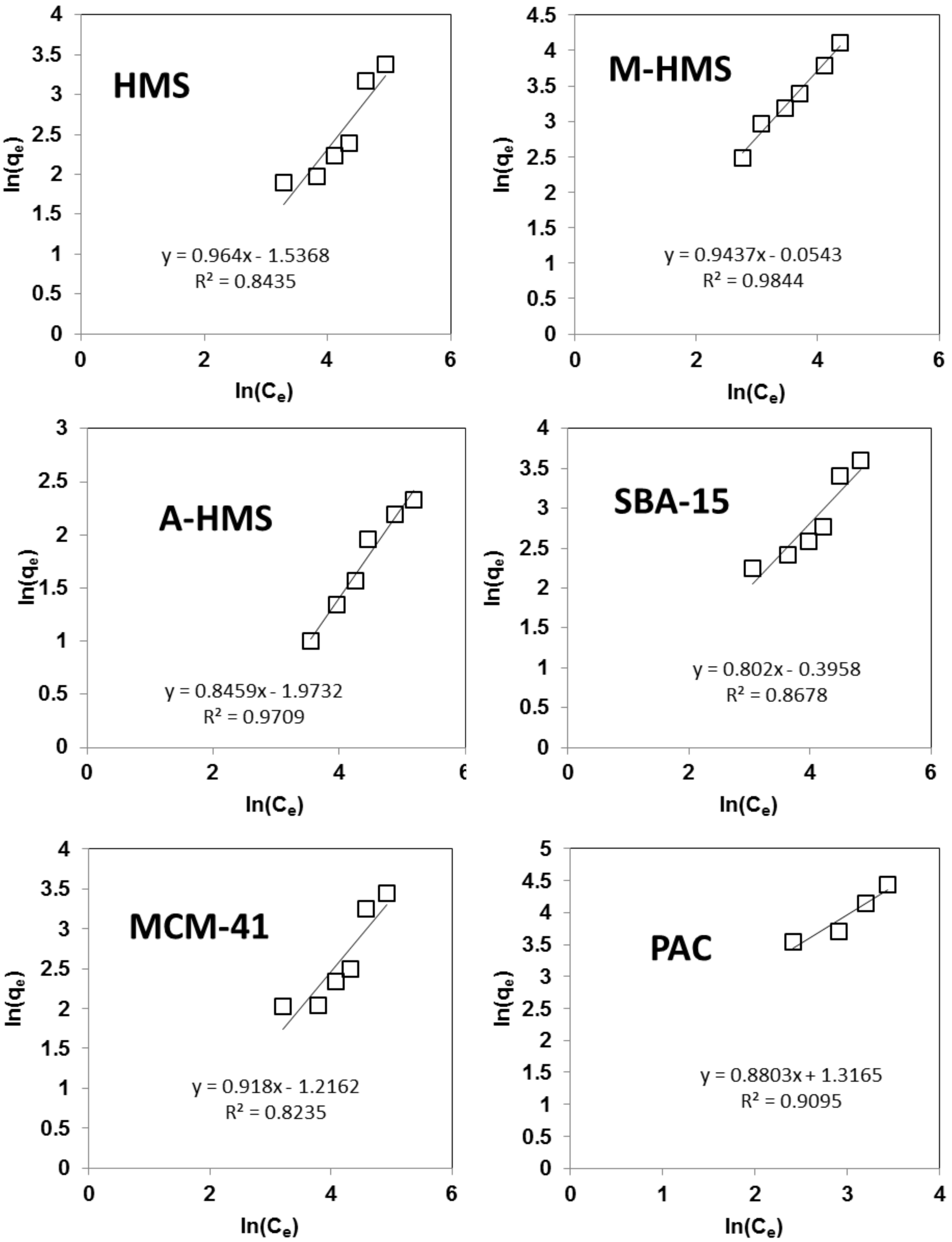

Figure 5.18 Adsorption isotherm of NAP removal according to the Freundlich isotherm model (pH 7, 25 °C and IS 0.01M).

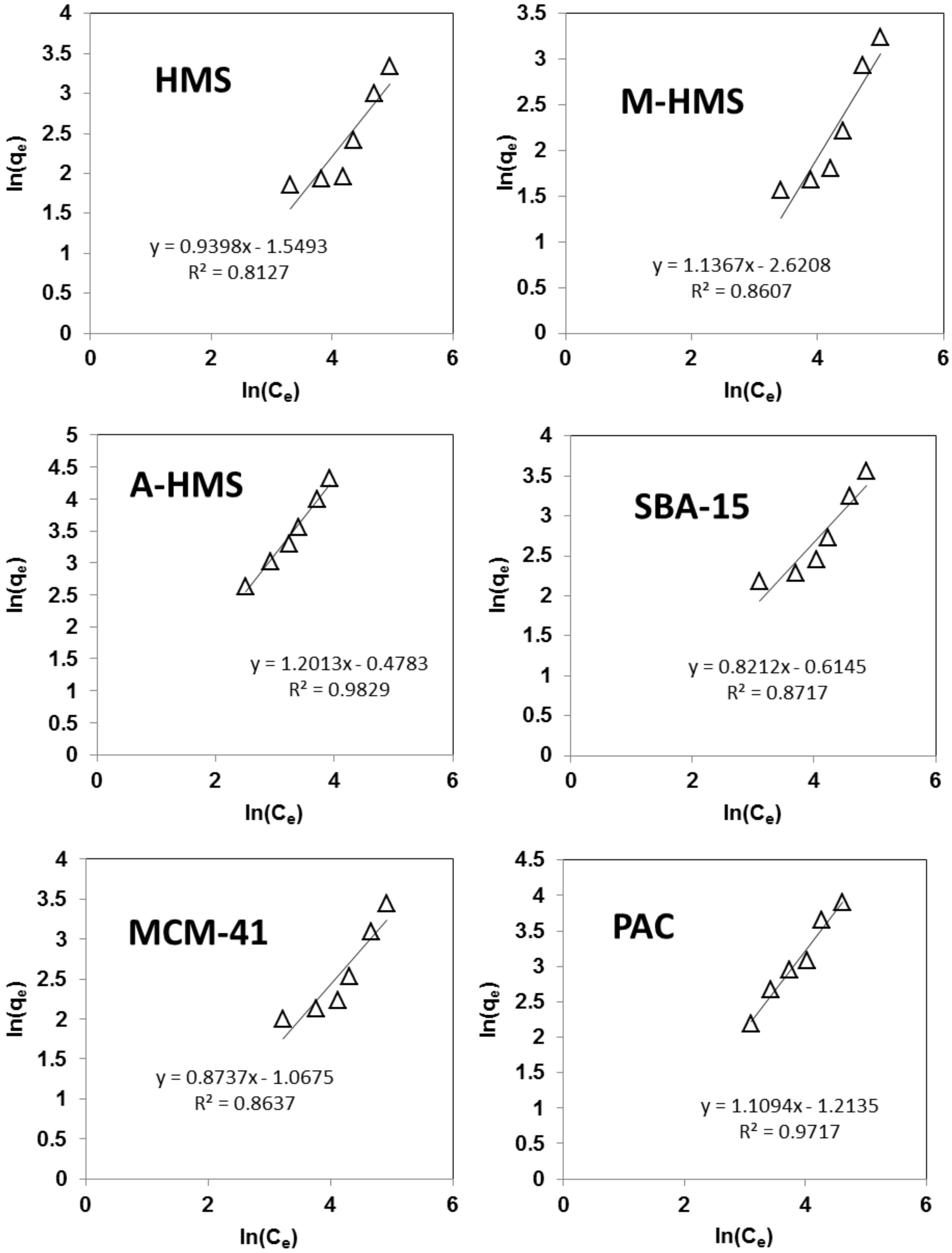

Figure 5.19 Adsorption isotherm of CFA removal according to the Freundlich isotherm model (pH 7, 25 °C and IS 0.01M).

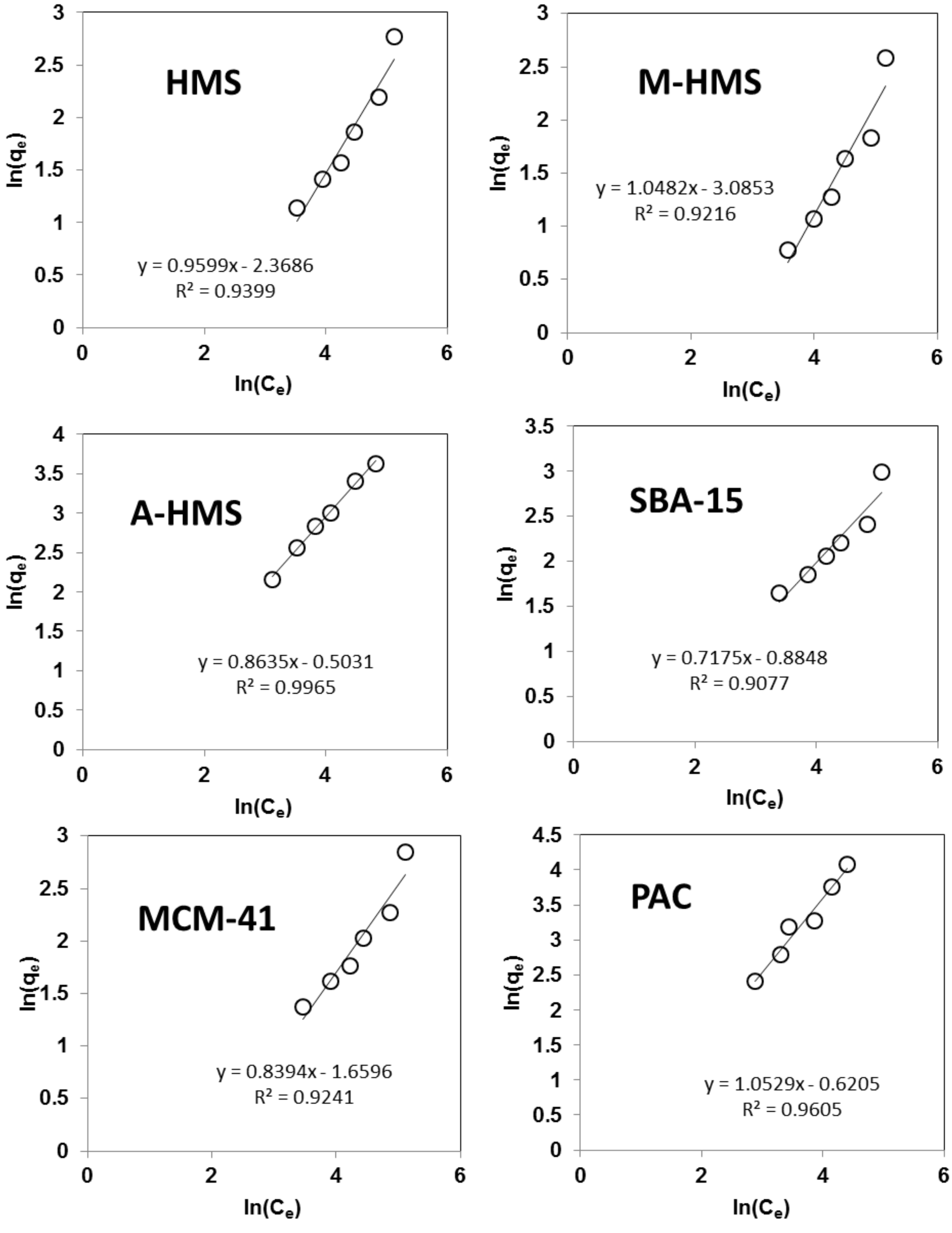

Figure 5.20 Adsorption isotherm of ACT removal according to the Freundlich isotherm model (pH 7, 25 ^{o}C and IS 0.01M).

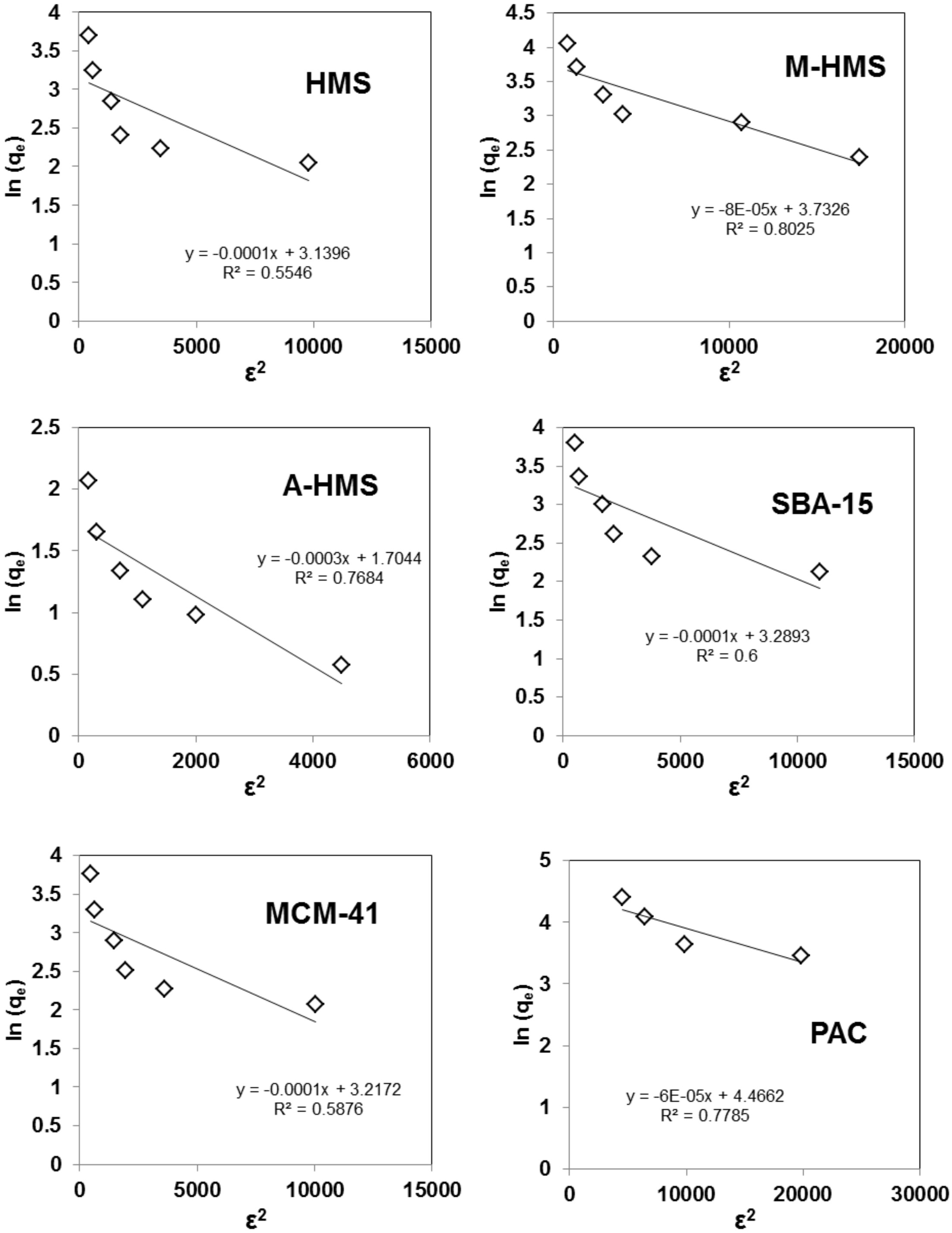

Figure 5.21 **A**dsorption isotherm of DCF removal according to the D-R isotherm model (pH 7, 25 °C and IS 0.01M).

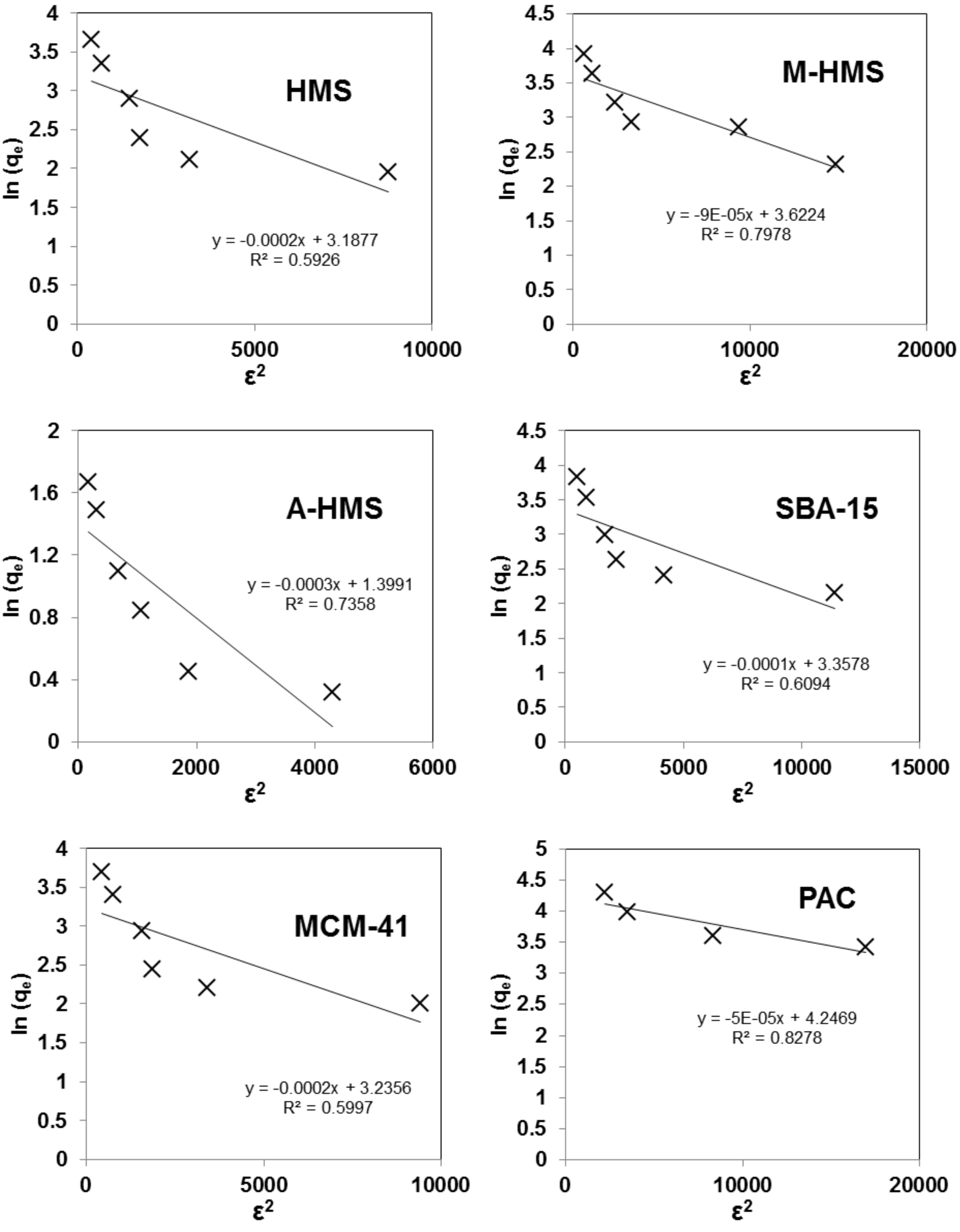

Figure 5.22 Adsorption isotherm of CBZ removal according to the D-R isotherm model (pH 7, 25 °C and IS 0.01M).

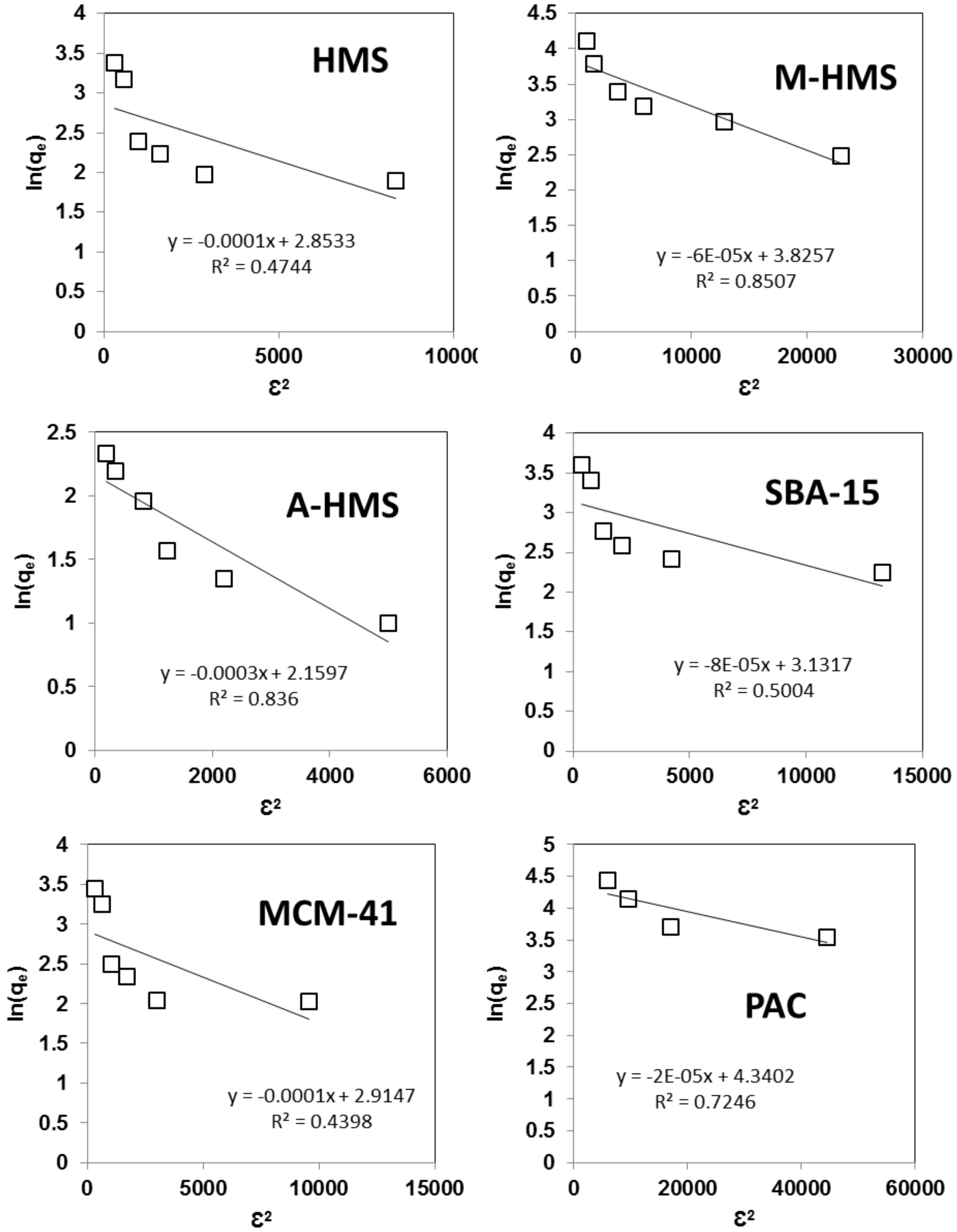

Figure 5.23 **A**dsorption isotherm of NAP removal according to the D-R isotherm model (pH 7, 25 °C and IS 0.01M).

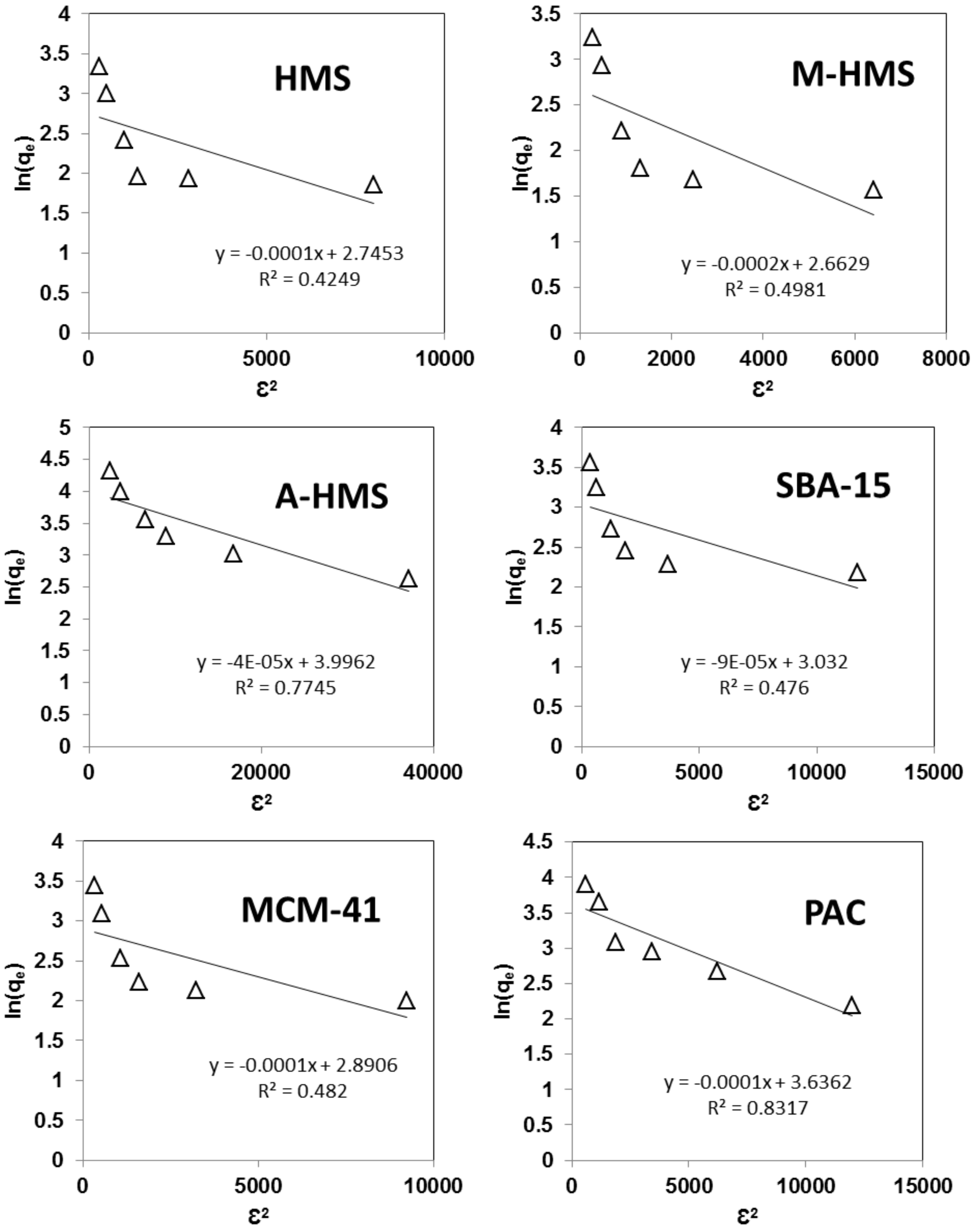

Figure 5.24 Adsorption isotherm of CFA removal according to the D-R isotherm model (pH 7, 25 ^{o}C and IS 0.01M).

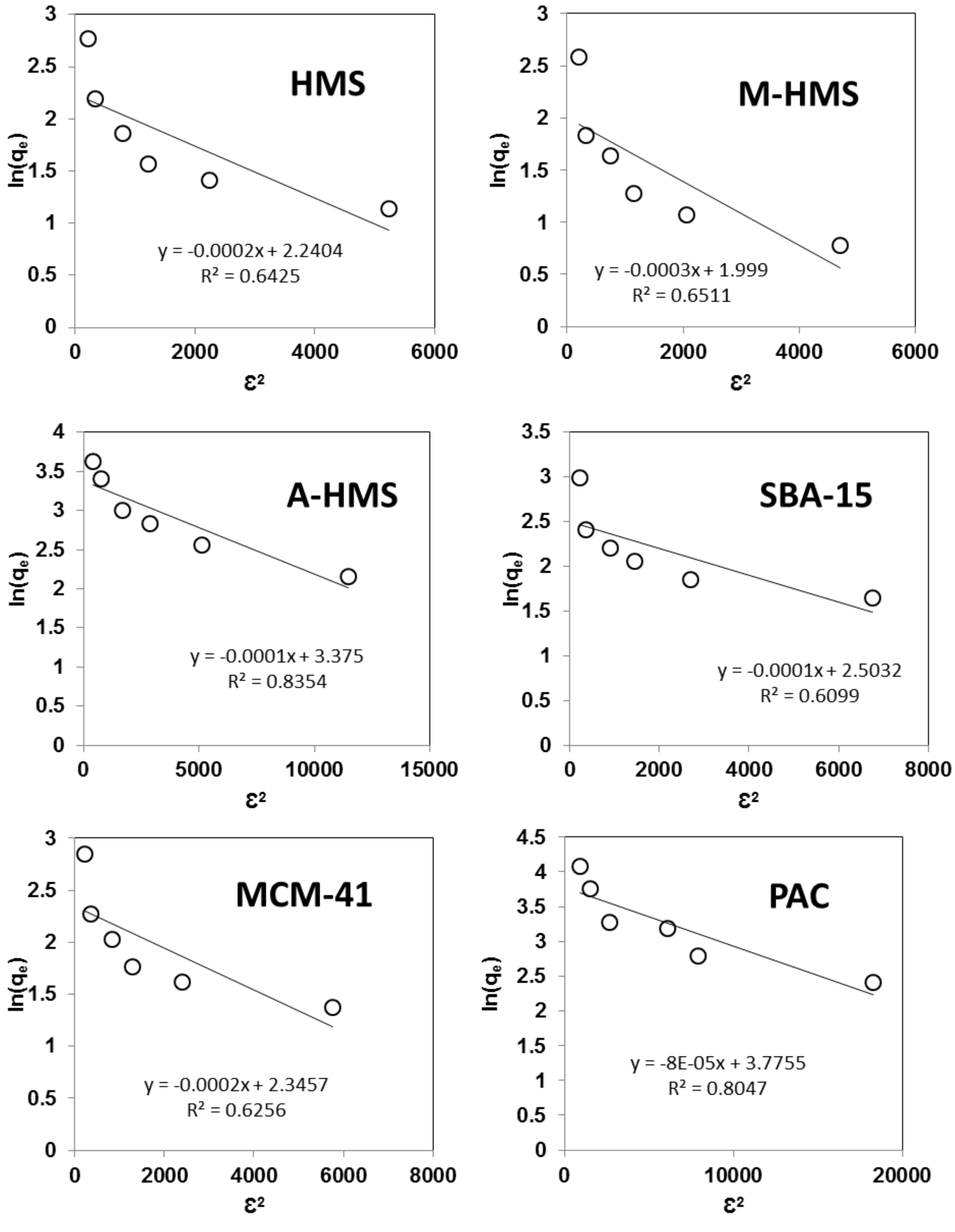

Figure 5.25 **A**dsorption isotherm of ACT removal according to the D-R isotherm model (pH 7, 25 ^{o}C and IS 0.01M).

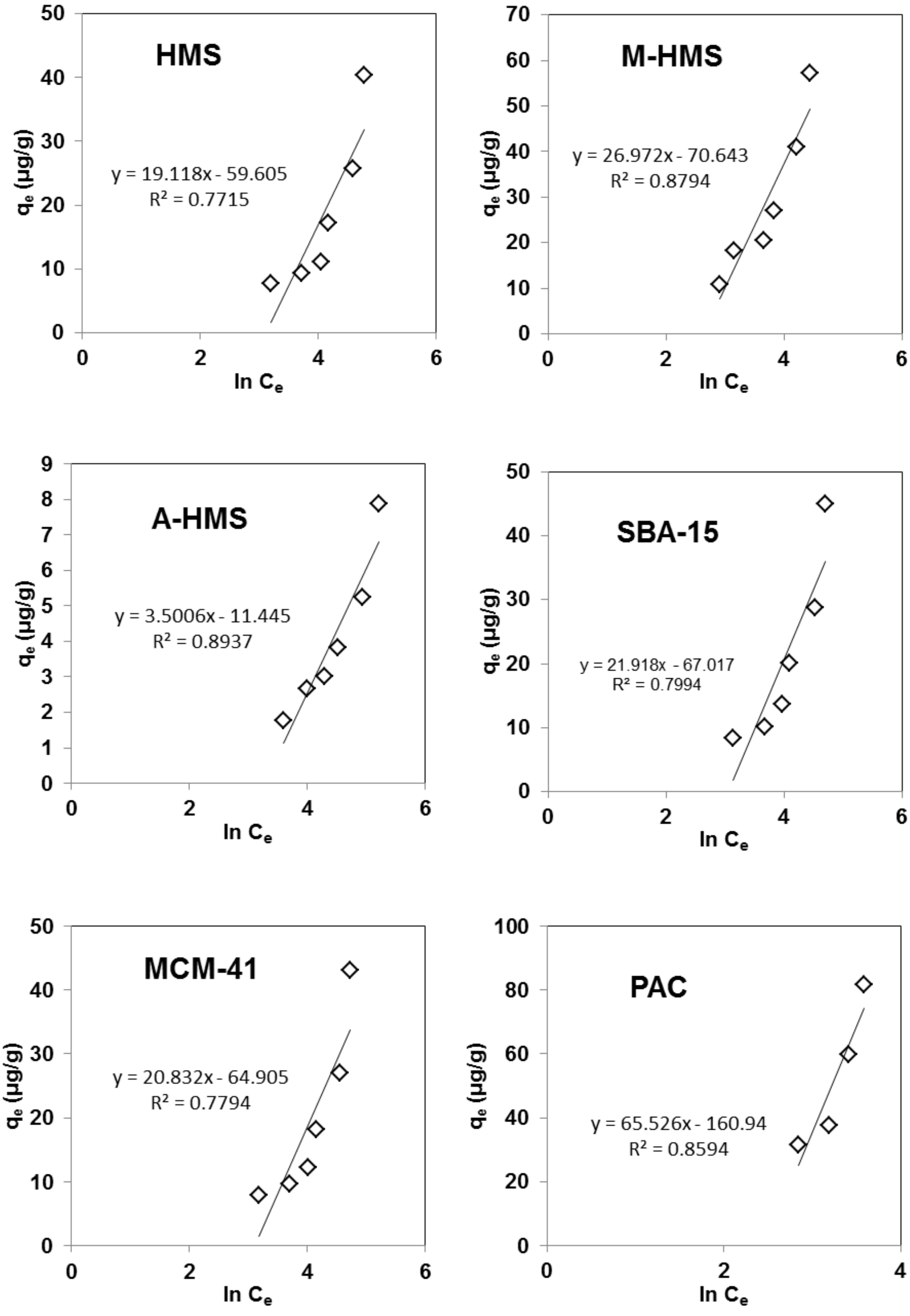

Figure 5.26 **A**dsorption isotherm of DCF removal according to the Temkin isotherm model (pH 7, 25 °C and IS 0.01M).

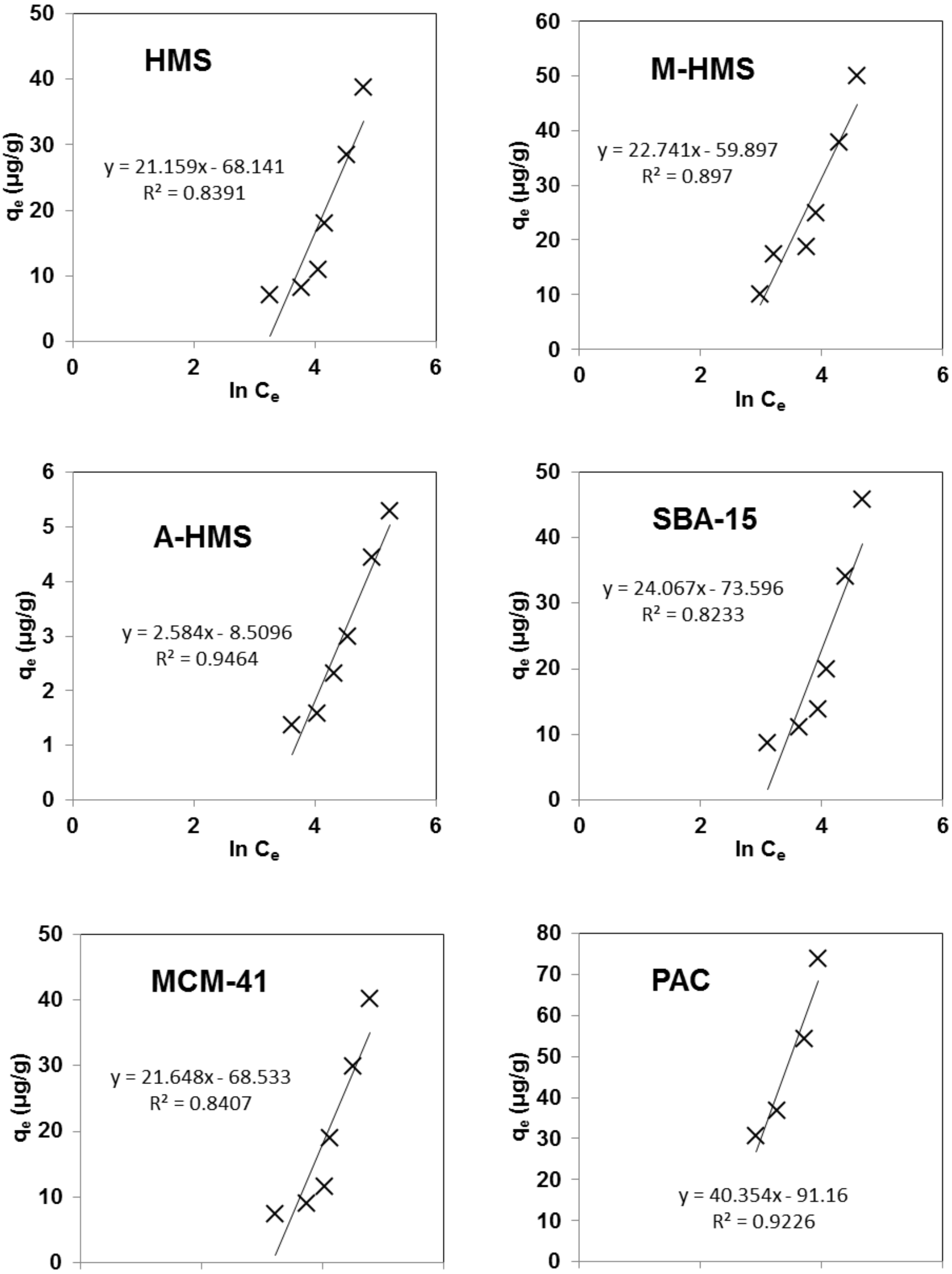

Figure 5.27 Adsorption isotherm of CBZ removal according to the Temkin isotherm model (pH 7, 25 °C and IS 0.01M).

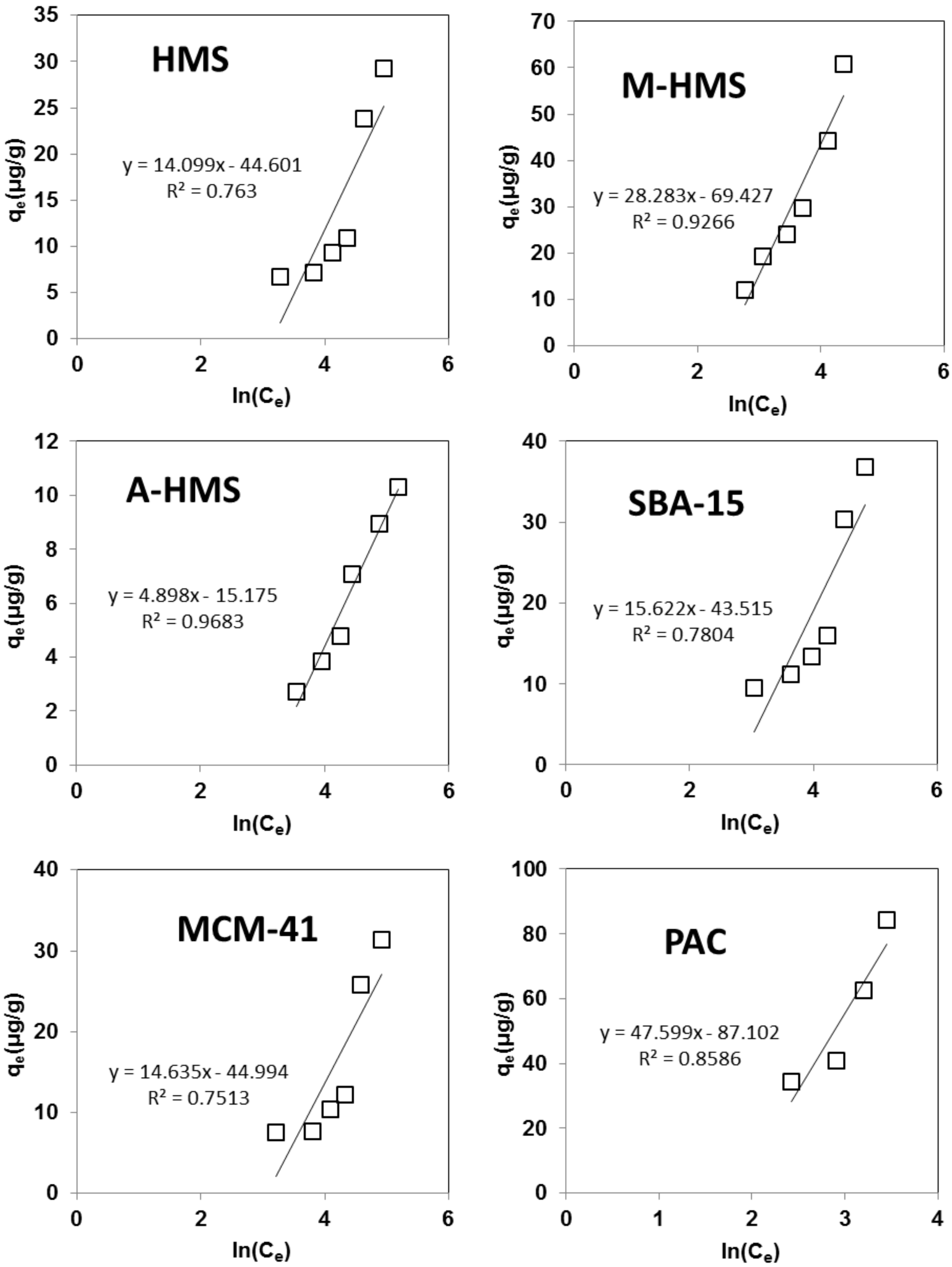

Figure 5.28 Adsorption isotherm of NAP removal according to the Temkin isotherm model (pH 7, 25 °C and IS 0.01M).

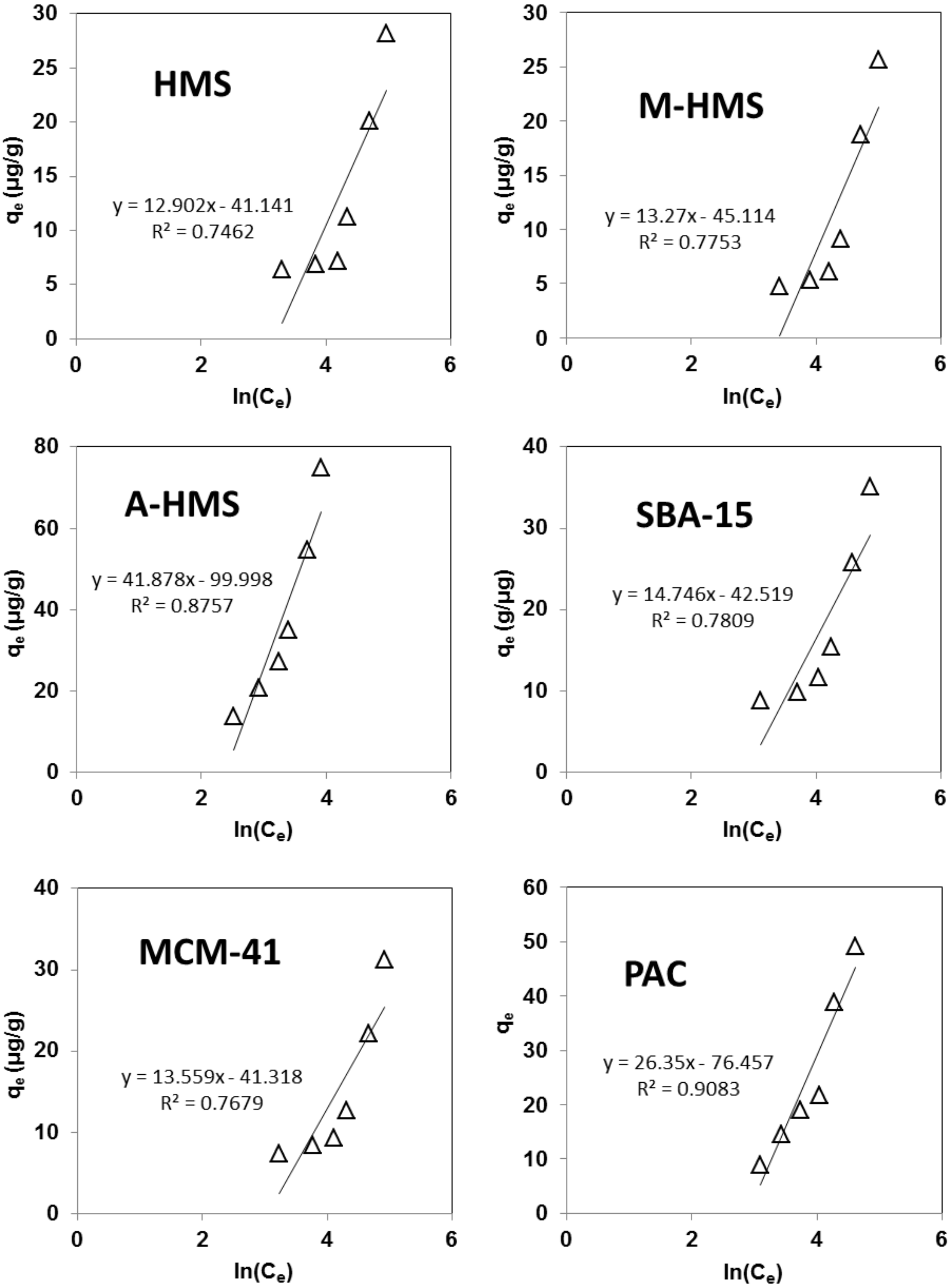

Figure 5.29 **A**dsorption isotherm of CFA removal according to the Temkin isotherm model (pH 7, 25 ^{o}C and IS 0.01M).

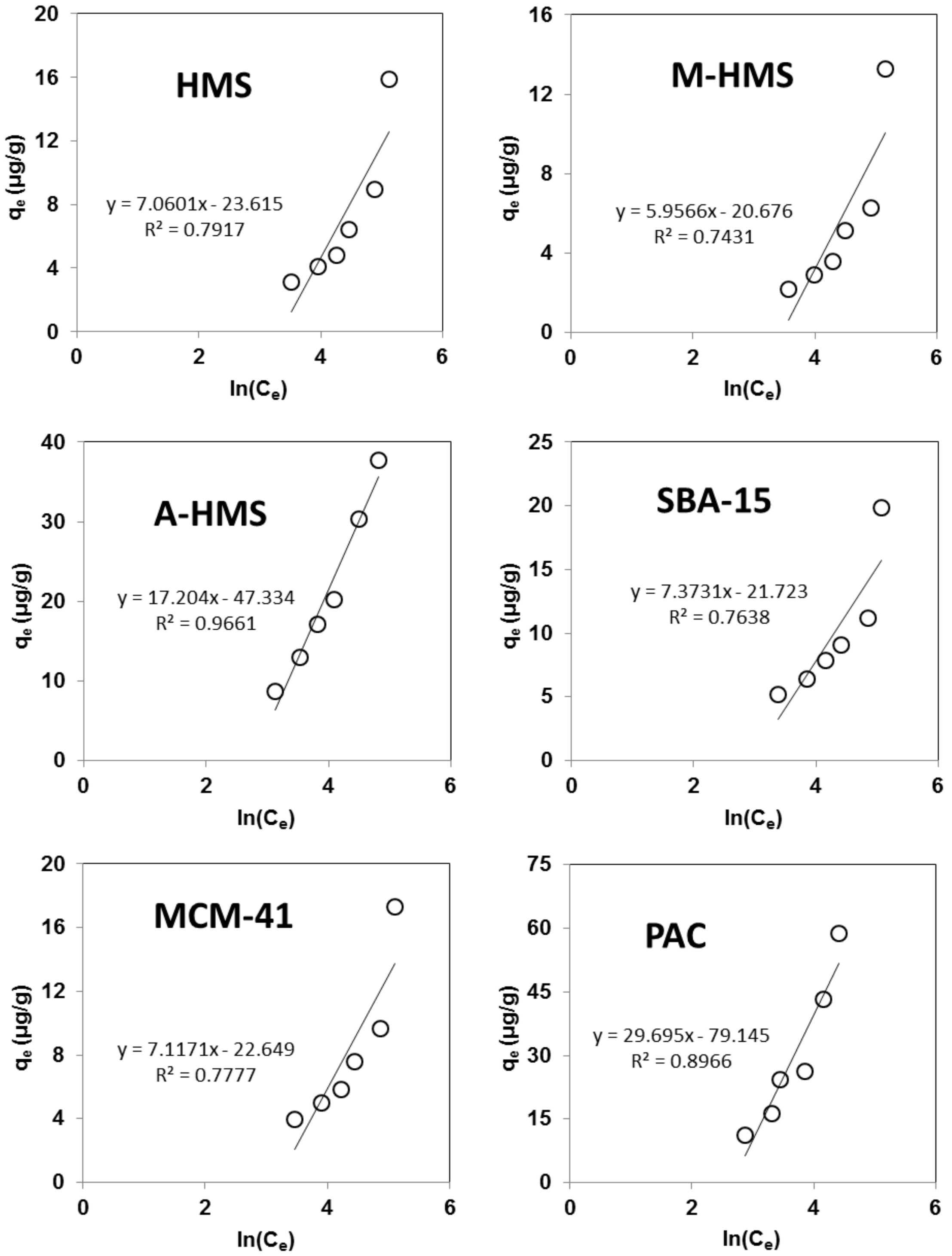

Figure 5.30 **A**dsorption isotherm of ACT removal according to the Temkin isotherm model (pH 7, 25 °C and IS 0.01M).

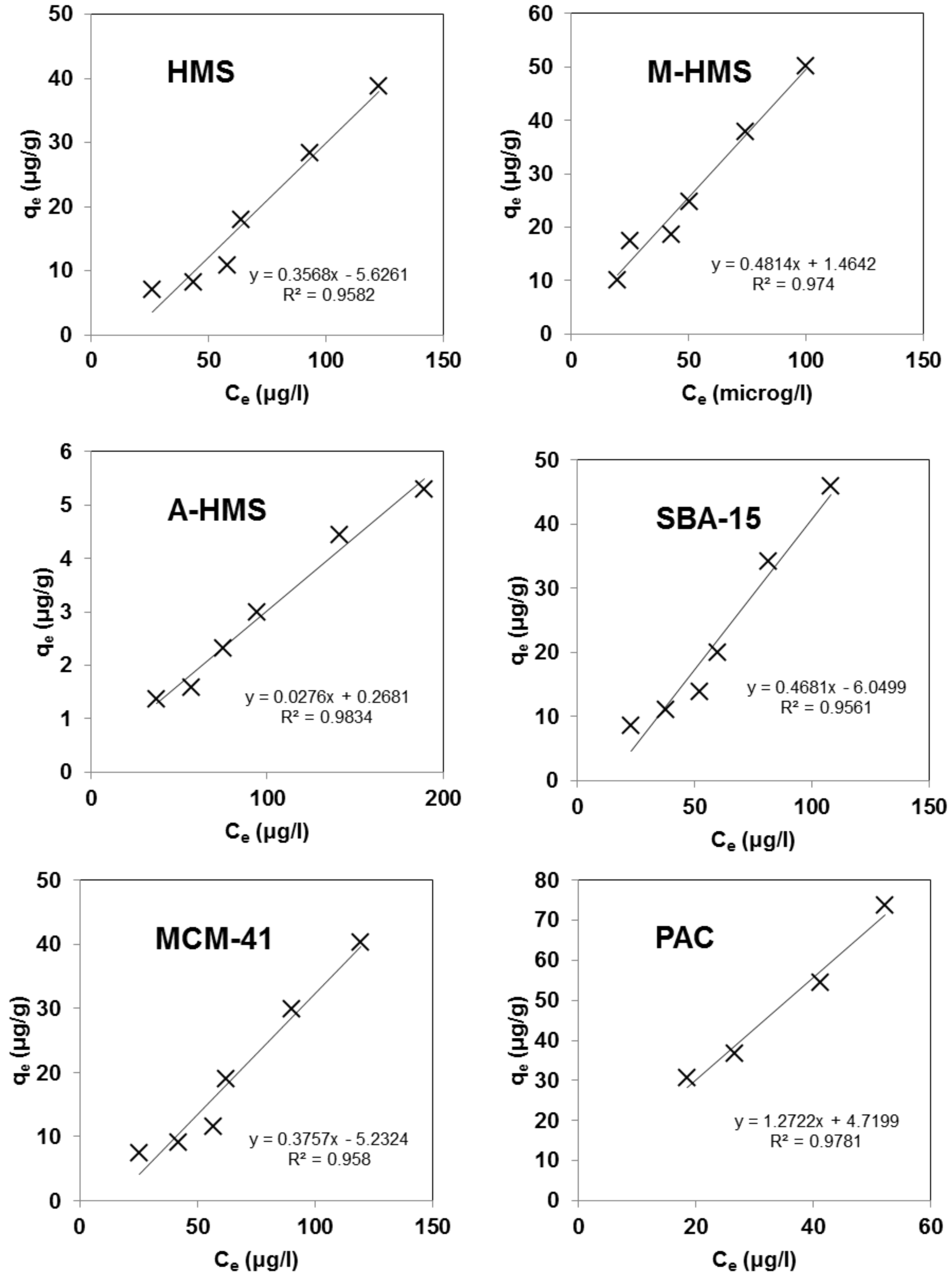

Figure 5.32 **A**dsorption isotherm of CBZ removal according to the Linear isotherm model (pH 7, 25 °C and IS 0.01M).

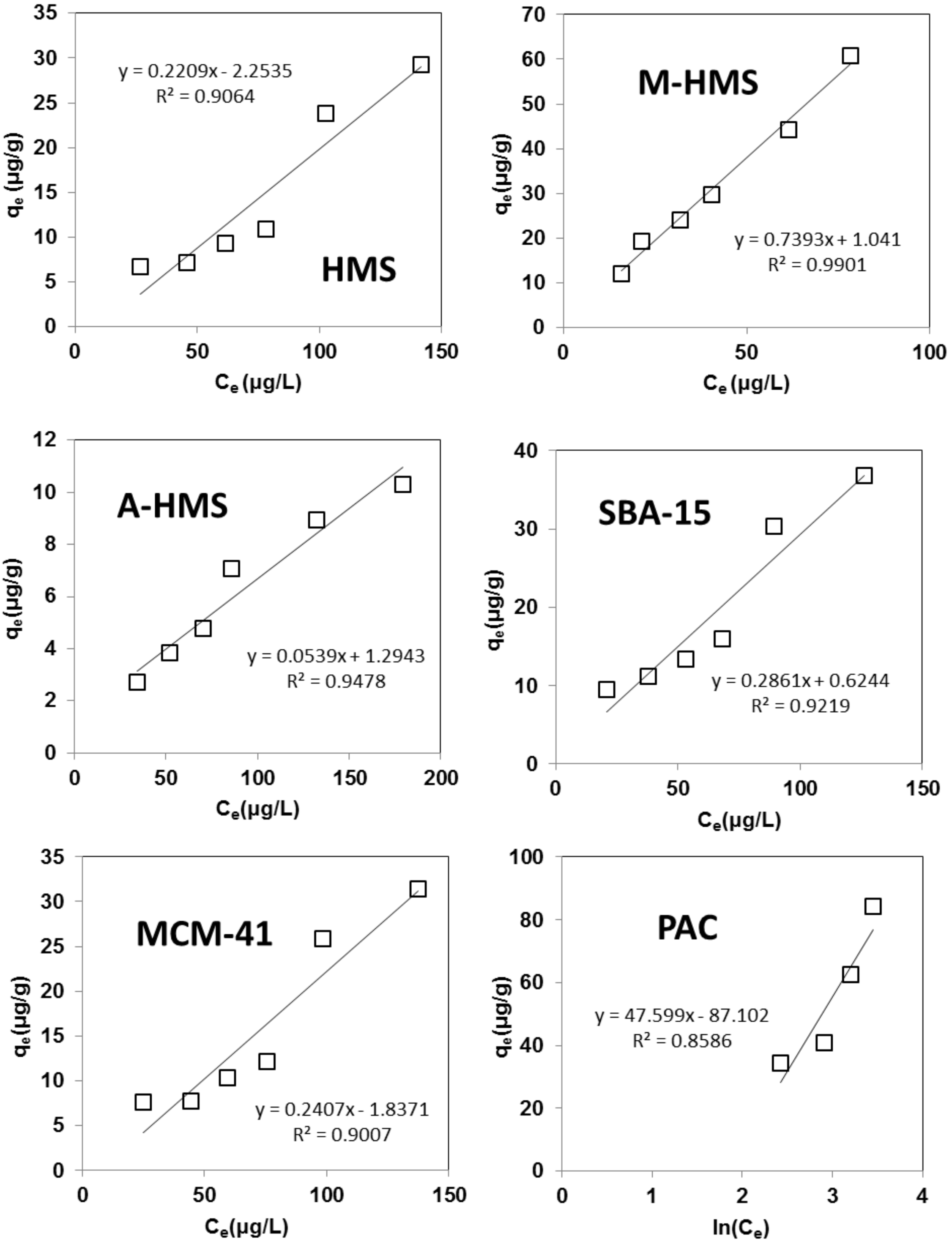

Figure 5.33 Adsorption isotherm of NAP removal according to the Linear isotherm model (pH 7, 25 °C and IS 0.01M).

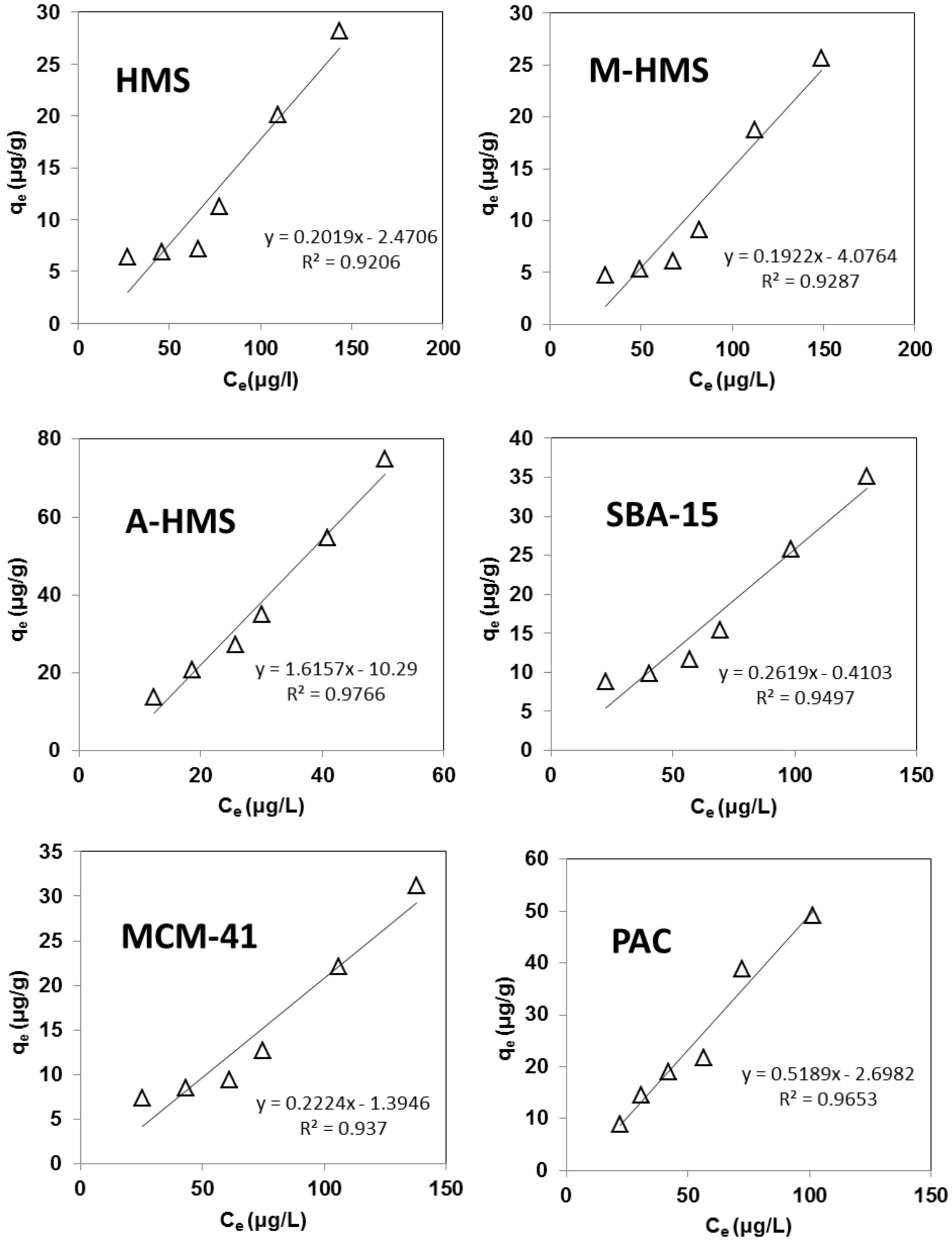

Figure 5.34 **A**dsorption isotherm of CFA removal according to the Linear isotherm model (pH 7, 25 ^oC and IS 0.01M).

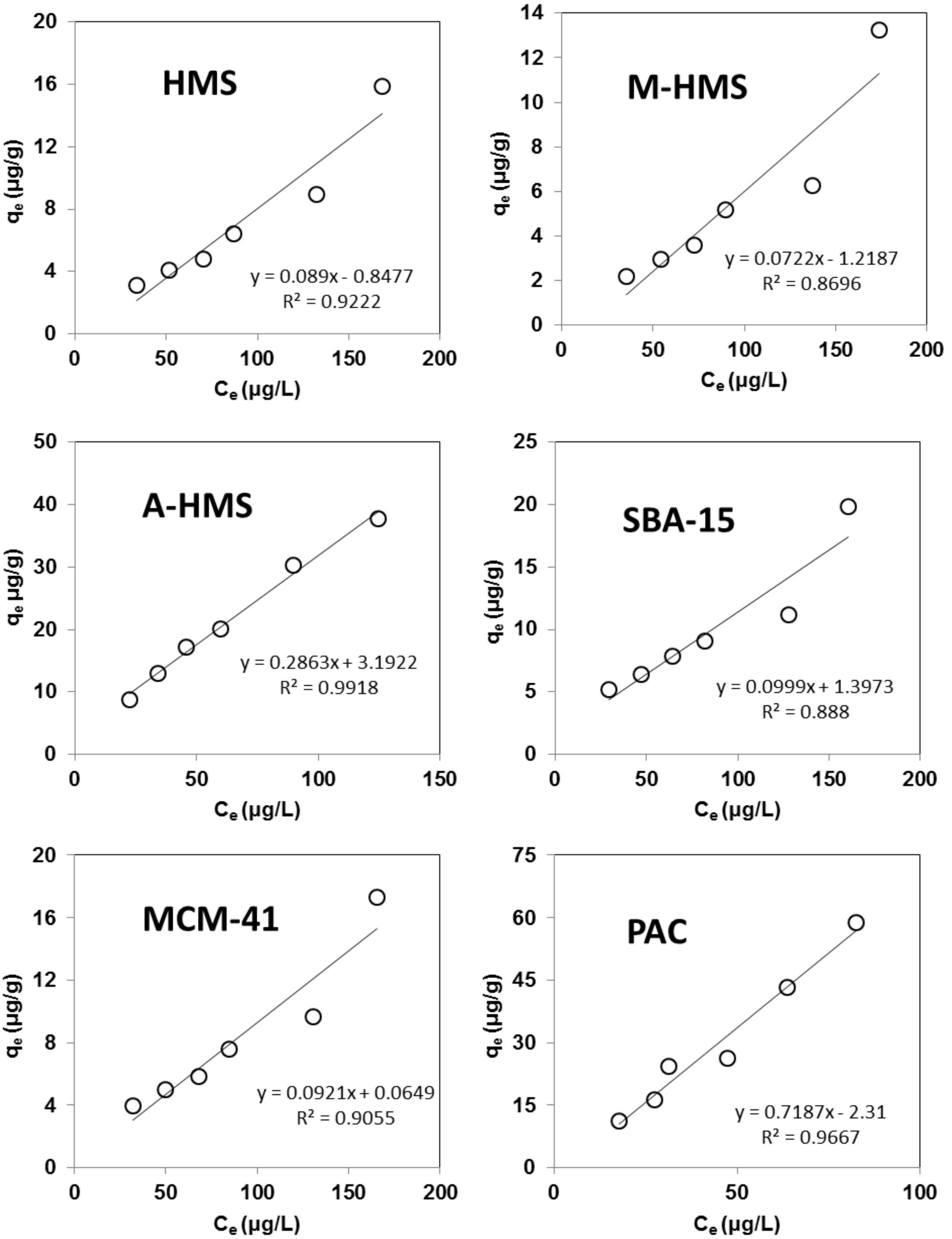

Figure 5.35 Adsorption isotherm of ACT removal according to the Linear isotherm model (pH 7, 25 °C and IS 0.01M).

Table 5.6 Isotherm parameters for sorption of DCF (pH 7, 25 °C and IS 0.01M).

Adsorbents	**Langmuir**			**Freundlich**			**D-R**			**Temkin**			**Linear**	
	k_L (10^3.L/µg)	q_m (µg/g)	R^2	n	k_F	R^2	q_m (µg/g)	B $(mmol/j)^2$	R^2	A_T (10^3.J/µg)	b_T (J/mol)	R^2	Kp (L/µg)	R^2
HMS	4.22	74.6	0.850	1.173	5.747	0.893	23.1	1.00	0.555	44.26	129.6	0.879	0.340	0.920
M-HMS	1.24	526.3	0.928	1.025	0.682	0.952	41.8	5.00	0.803	72.87	91.9	0.879	0.651	0.970
A-HMS	2.46	21.4	0.986	1.141	0.074	0.983	5.50	3.00	0.768	38.03	707.8	0.894	0.039	0.980
SBA-15	2.68	131.6	0.886	0.924	0.229	0.920	26.8	0.10	0.600	47.00	113.0	0.799	0.412	0.930
MCM-41	2.83	112.4	0.888	0.918	0.198	0.914	25.0	1.00	0.588	44.35	118.9	0.779	0.381	0.921
PAC	6.40	109.9	0.940	0.736	0.599	0.950	117.6	0.80	0.807	72.11	27.8	0.918	2.879	0.955

Table 5.7 Isotherm parameters for sorption of CBZ (pH 7, 25 °C and IS 0.01M).

Adsorbents	Langmuir			Freundlich			D-R			Temkin			Linear	
	k_L $(10^3.L/\mu g)$	q_m $(\mu g/g)$	R^2	n	k_F	R^2	q_m $(\mu g/g)$	B $(mmol/j)^2$	R^2	A_T $(10^3.J/\mu g)$	b_T (J/mol)	R^2	Kp $(L/\mu g)$	R^2
HMS	0.65	384.6	0.856	0.835	0.113	0.909	24.2	2.00	0.593	39.94	117.1	0.839	0.357	0.958
M-HMS	2.68	217.4	0.903	1.106	0.747	0.939	37.4	0.90	0.798	71.80	109.0	0.897	0.481	0.974
A-HMS	2.28	16.3	0.941	1.106	0.047	0.975	4.05	3.00	0.736	37.14	958.8	0.946	0.028	0.983
SBA-15	1.83	200.0	0.902	0.885	0.206	0.924	28.7	1.00	0.609	46.98	102.9	0.823	0.468	0.956
MCM-41	1.06	263.2	0.869	0.860	0.143	0.913	25.4	2.00	0.600	42.18	114.5	0.841	0.376	0.958
PAC	4.04	416.7	0.965	1.072	1.852	0.976	91.0	0.70	0.792	78.60	44.0	0.925	1.389	0.977

Table 5.8 Isotherm parameters for sorption of NAP (pH 7, 25 °C and IS 0.01M).

Adsorbents	Langmuir			Freundlich			D-R			Temkin			Linear	
	k_L (10^3.L/μg)	q_m (μg/g)	R^2	n	k_F	R^2	q_m (μg/g)	B $(mmol/j)^2$	R^2	A_T (10^3.J/μg)	b_T (J/mol)	R^2	Kp (L/μg)	R^2
HMS	7.17	36.63	0.763	1.04	0.22	0.841	17.34	100	0.474	42	175.73	0.763	0.221	0.985
M-HMS	1.22	666.67	0.974	1.06	0.95	0.984	45.86	6.00	0.851	86	87.60	0.927	0.739	0.990
A-HMS	1.96	42.55	0.985	1.18	0.14	0.971	8.67	300	0.836	45	505.83	0.968	0.054	0.948
SBA-15	13.12	39.85	0.802	1.25	0.67	0.868	22.91	8.00	0.500	62	158.59	0.780	0.286	0.922
MCM-41	9.59	34.13	0.710	1.09	0.30	0.824	18.44	100	0.440	46	169.29	0.751	0.241	0.900
PAC	15.71	217.39	0.876	1.14	3.73	0.909	76.72	2.00	0.725	160	52.05	0.859	2.561	0.944

Table 5.9 Isotherm parameters for sorption of CFA (pH 7, 25 °C and IS 0.01M).

Adsorbents	**Langmuir**			**Freundlich**			**D-R**			**Temkin**			**Linear**	
	k_L $(10^3.L/\mu g)$	q_m $(\mu g/g)$	R^2	n	k_F	R^2	q_m $(\mu g/g)$	B $(mmol/j)^2$	R^2	A_T $(10^3.J/\mu g)$	b_T (J/mol)	R^2	Kp $(L/\mu g)$	R^2
HMS	9.08	28.09	0.674	1.06	0.21	0.813	15.57	100	0.425	41.22	192.03	0.746	0.202	0.921
M-HMS	3.31	45.87	0.785	0.88	0.07	0.861	14.34	200	0.498	33.38	186.70	0.775	0.192	0.929
A-HMS	3.96	263.16	0.992	0.83	0.62	0.983	54.39	4.00	0.775	91.83	59.16	0.876	1.616	0.977
SBA-15	2.22	35.59	0.770	1.22	0.54	0.872	20.74	9.00	0.476	56.09	167.86	0.781	0.262	0.949
MCM-41	9.81	33.11	0.778	1.14	0.34	0.863	18.00	100	0.482	47.49	182.73	0.768	0.222	0.937
PAC	11.14	172.42	0.977	1.03	0.30	0.972	37.95	100	0.832	54.94	94.03	0.908	0.519	0.965

Table 5.10 Isotherm parameters for sorption of ACT (pH 7, 25 °C and IS 0.01M).

Adsorbents	**Langmuir**			**Freundlich**			**D-R**			**Temkin**			**Linear**	
	k_L $(10^3.L/\mu g)$	q_m $(\mu g/g)$	R^2	n	k_F	R^2	q_m $(\mu g/g)$	B $(mmol/j)^2$	R^2	A_T $(10^3.J/\mu g)$	b_T (J/mol)	R^2	Kp $(L/\mu g)$	R^2
HMS	3.04	31.75	0.947	1.04	0.09	0.940	9.40	200	0.643	35.27	350.9	0.792	0.089	0.922
M-HMS	1.33	46.08	0.958	0.95	0.05	0.922	7.38	300	0.651	31.08	[illegible]	0.743	0.072	0.869
A-HMS	2.66	153.85	0.999	1.16	0.60	0.997	29.22	100	0.835	63.84	144.0	0.966	0.286	0.992
SBA-15	9.58	22.12	0.916	1.39	0.41	0.901	12.22	100	0.610	82.54	336.0	0.764	0.099	0.888
MCM-41	5.67	24.04	0.931	1.19	0.19	0.924	10.44	200	0.626	41.49	348.1	0.778	0.092	0.905
PAC	1.23	500.0	0.964	0.95	0.54	0.961	43.62	8.00	0.805	69.58	83.43	0.897	0.718	0.967

5.3.5 Adsorption mechanisms

5.3.5.1 Effect of surface functional group

The adsorption capacity of PAC, HMS and the functionalized HMS adsorbents at pH 7 are shown in Figure 5.36. Analysis of that for HMS and the functionalized derivatives allows the effect of different surface functional groups, hydroxyl (silanol), mercapto and amino, on the adsorption capacity of the adsorbents to be inferred. At this pH (7), the molecules of DCF (pK_a = 4.15), NAP (pK_a = 3.18) and CFA (pK_a =2.84) are negatively charged whilst those of CBZ (pK_a = 13.9) and ACT (pK_a = 9.38) are neutral.

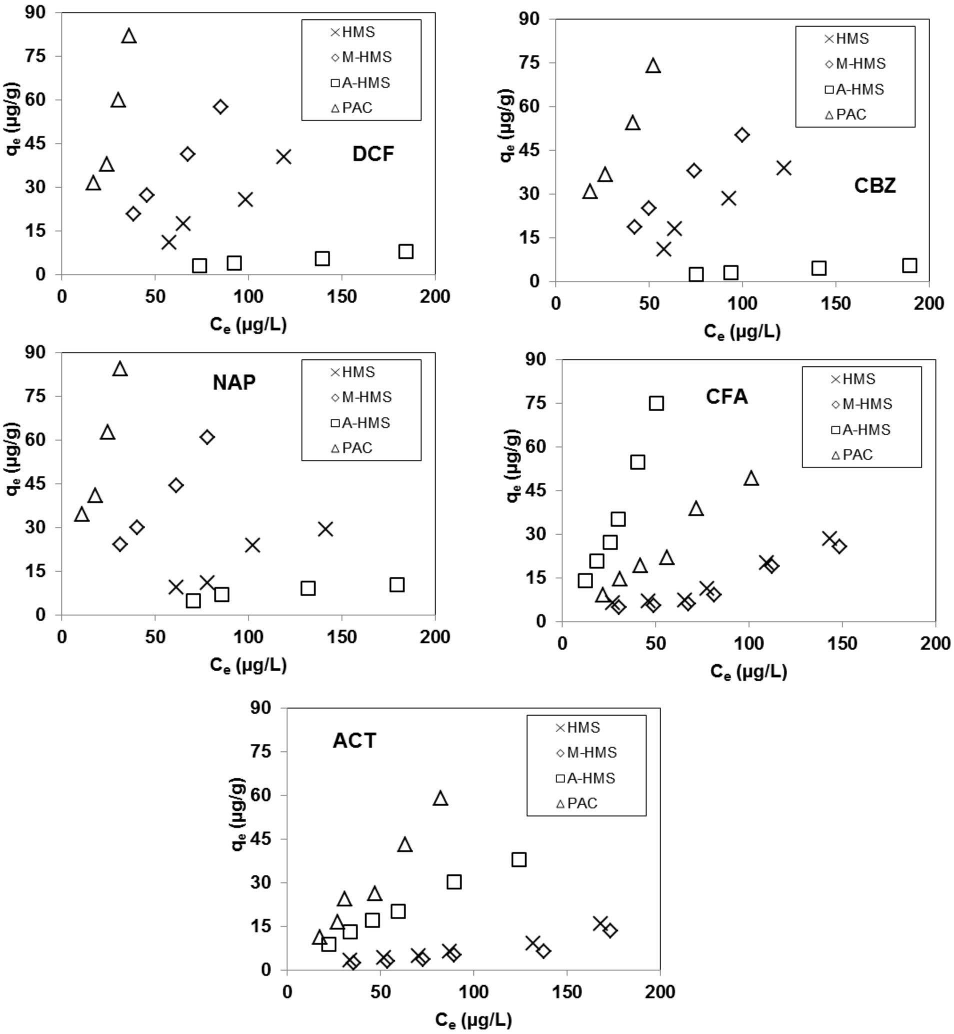

Figure 5.36 Adsorption capacity of HMS, M-HMS, A-HMS and PAC for DCF, CBZ, NAP, CFA and ACT (pH 7, 25 °C and IS 0.01M).

For adsorption of all pharmaceuticals, there are three possible mechanisms for their adsorption onto HMS and the functionalized HMS derivatives. The first mechanism is electrostatic interaction (by Coulomb's law) between the deprotonated (negatively charged) DCF, NAP or CFA molecules and the surface charges of the adsorbents and also could be dipole-ion interactions between the neutral CBZ or ACT molecules and the surface charges of the adsorbents. The second mechanism is hydrogen bonding, a form of dipole-dipole interaction, and the third mechanism is hydrophobic interactions such as Van der Waals interaction, π-π electron acceptor-donor, etc.

At pH 7, A-HMS has a net positive surface charge, but HMS and M-HMS have a net negative surface charge, so it is expected that electrostatic interactions should enhance the adsorption of DCF and NAP onto A-HMS, giving a higher adsorption capacity, but decrease that onto HMS and M-HMS. In contrast, M-HMS had a higher adsorption capacity than either HMS or A-HMS, and so other mechanisms (hydrogen bonding and hydrophobic interaction) play a more significant role than electrostatic interaction forces in the adsorption of DCF and NAP. One possible explanation for this finding lies in the water affinity. Because the concentrations of DCF and NAP used in this study were low, there could be competition between water and DCF (or NAP) molecules for adsorption onto the adsorbents. Compared with HMS and A-HMS, the higher adsorption capacity of M-HMS would then be due to its higher hydrophobic property that can reduce the competitive interference or competition of water in the adsorption of DCF (or NAP). The adsorption capacities of pristine HMS and A-HMS for DCF (or NAP) were suggested to be due to hydrogen bonding between carboxylic part of DCF (or NAP) and free silanol group and/or amino functional group on HMS and A-HMS respectively.

From this study, the adsorption capacities of the adsorbents for CBZ, showed a similar trend as for DCF and NAP, being (highest to lowest adsorption capacity) M-HMS > HMS > A-HMS, and so the modification of HMS with mercapto- functional groups increased the adsorption capacity for CBZ, presumably through enhanced hydrogen bonding and hydrophobic interactions.

The adsorption capacities of the silica based adsorbents for CFA and ACT showed a trend different from those for CBZ, DCF and NAP. The adsorption capacities of the adsorbents for CFA and ACT were ranked in descending order as A-HMS > HMS > M-HMS. The adsorption capacity of a silica based adsorbent for CFA and ACT was increased after modification with amino functional group, but not increased after modification with mercapto functional group. The increase in adsorption capacity of the adsorbent after modification with amino functional group could be explained by the enhancement of the electrostatic interaction between the pharmaceutical residues and the adsorbents, and also possibly by enhanced hydrogen bonding.

Compared with PAC, A-HMS had a better adsorption for CFA, but for other pharmaceuticals PAC had a better adsorption than HMS and functionalized HMS, perhaps due to the complexity of the surface functional groups of PAC inducing various interactions, such as electrostatic, Van der Waals forces and covalent bonding.

5.3.5.2 Effect of the adsorbent’s surface area

Comparative analysis of the adsorbent capacity of HMS, SBA-15 and MCM-41 allows the effect of the adsorbent surface area on the adsorption of pharmaceuticals to be inferred. All adsorbents have hexagonal structure and the same functional group (i.e. silanol group) but they have different average pore sizes and different BET surface areas. The average pore sizes of HMS, SBA-15 and MCM-41 are 32.8, 80.6 and 33.5 Å respectively. The molecular sizes of CBZ and DCF were calculated by ACD/ChemSketch12 Freeware. The calculations showed that DCF has the molecular size of 9.7x9.6 Å. CBZ has the molecular size of 8.6x9.8 Å. NAP has the molecular size of 11.87x4.48 Å. CFA has the molecular size of 9.04x3.35 Å. And ACT has the molecular size of 8.27x2.97 Å. The accessibility of the adsorbates is therefore not affected by the pore size of the adsorbents because the average pore sizes of all adsorbents are bigger than the molecular size of both pharmaceuticals. The BET surface areas of SBA-15, MCM-41 and HMS are 890, 755 and 712 m^2/g respectively (Table 4.1). SBA-15 had the highest and HMS had the lowest adsorption capacity for all pharmaceuticals, respectively (Figure 5.37). The difference in adsorption capacity of adsorbents might be caused by the difference of their specific surface areas. SBA-15 has more surface area than MCM-41 and HMS. When the adsorption capacities of all mesoporous silicate adsorbents were considered as per BET surface area (Fig. 5.38), it was found that their adsorption capacities were not different. From this finding it can be concluded that the adsorption capacities of the adsorbents vary directly with their surface areas.

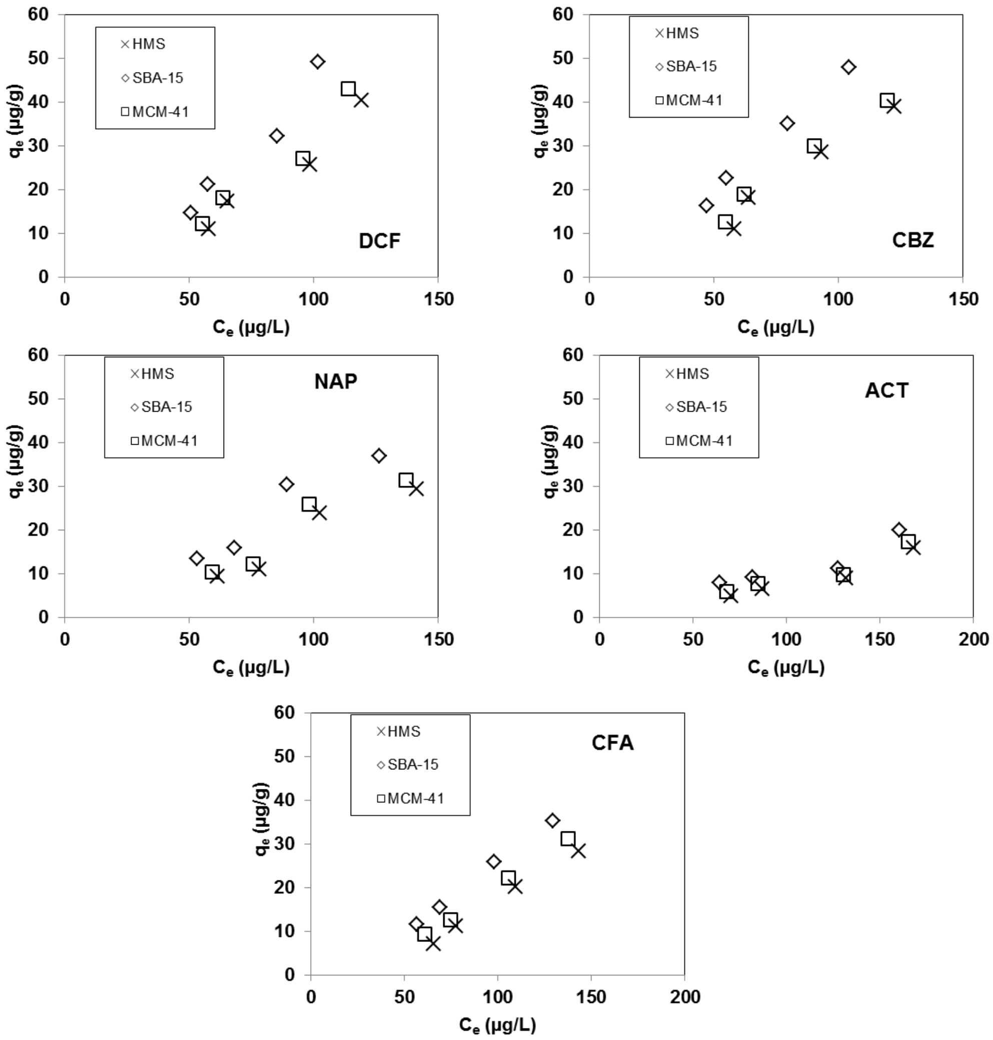

Figure 5.37 Adsorption capacity of HMS, SBA-15 and MCM 41 for DCF, CBZ, NAP, ACT and CFA (pH 7, 25 °C and IS 0.01M).

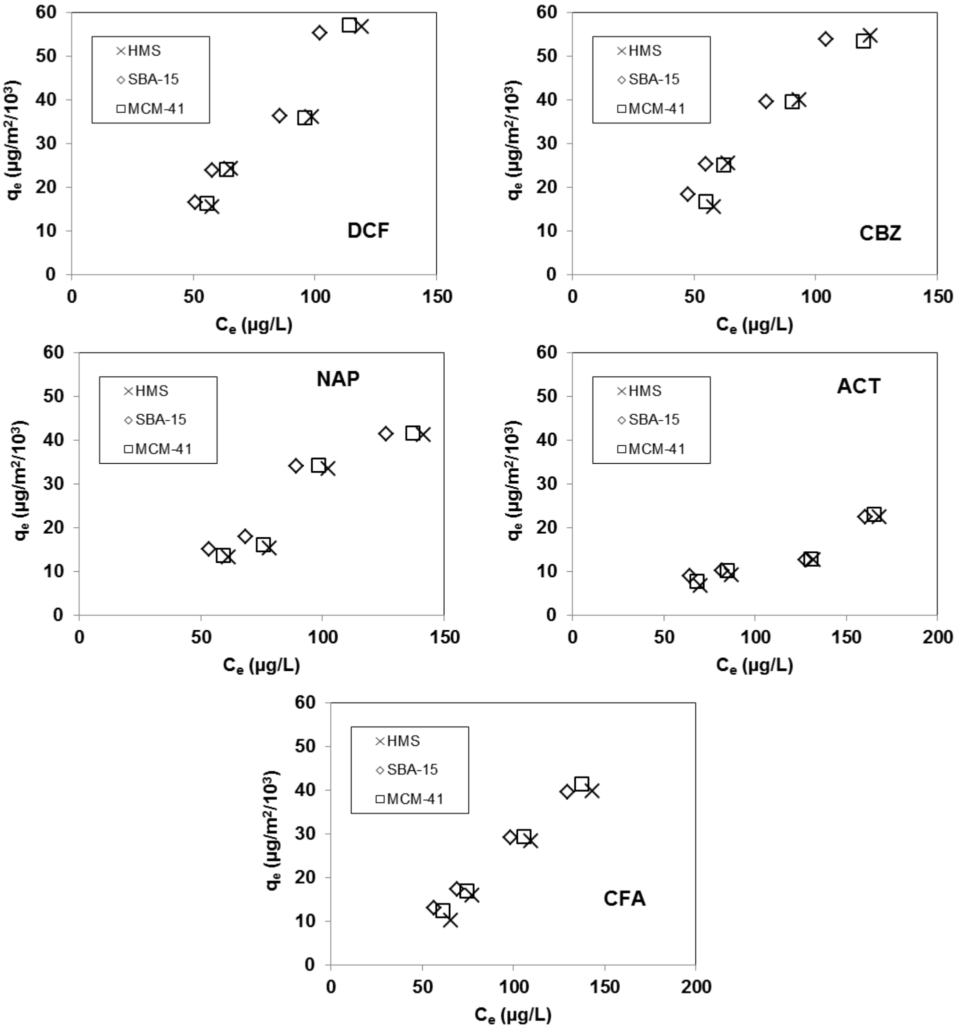

Figure 5.38 Adsorption capacity per surface area of HMS, SBA-15 and MCM 41 for DCF, CBZ, NAP, ACT and CFA (pH 7, 25 °C and IS 0.01M).

5.3.5.3 Effect of pH

The adsorption of pharmaceuticals onto PAC, HMS and the functionalized HMS derivatives were performed at pH 5, 7 and 9 to study the effect of pH on their adsorption capacity. The adsorption capacity of the mesoporous silicates, but not PAC, was dependent on the pH, being highest at pH 5 (Figure 5.39, 5.40, 5.41, 5.42 and 5.43). At pH 5 the surface of HMS and M-HMS had a net positive charge, while DCF, NAP and CFA had a net negative charge, resulting in better adsorption capacity due to the enhanced electrostatic interactions and hydrogen bonds. When the pH was higher than the pH at the point of zero charge, the surface of the adsorbents are negatively charged causing an electrostatic repulsion between the adsorbents and adsorbates. In the case of A-HMS, at pH 5 the surface charge is already negative, but it still has a net higher negative charge density than at higher pH values because the pH_{PZC} is equal to 9.5, which may explain why at pH 9 the adsorption capacity was the lowest.

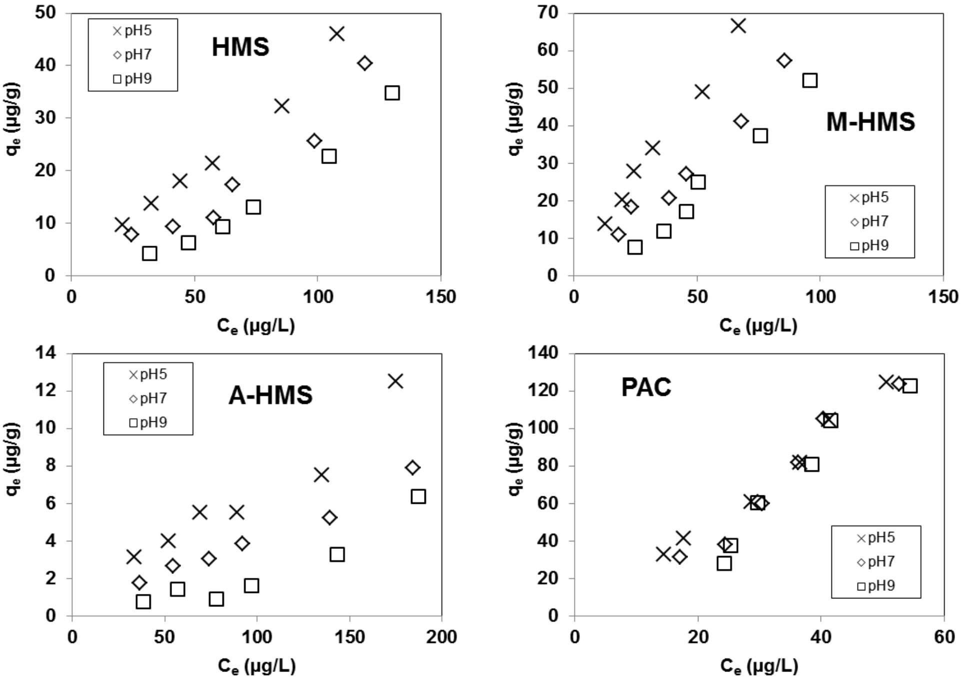

Figure 5.39 Adsorption capacity of HMS, M-HMS, A-HMS and PAC for DCF at pH 5, 7 and 9 (25 °C and IS 0.01M).

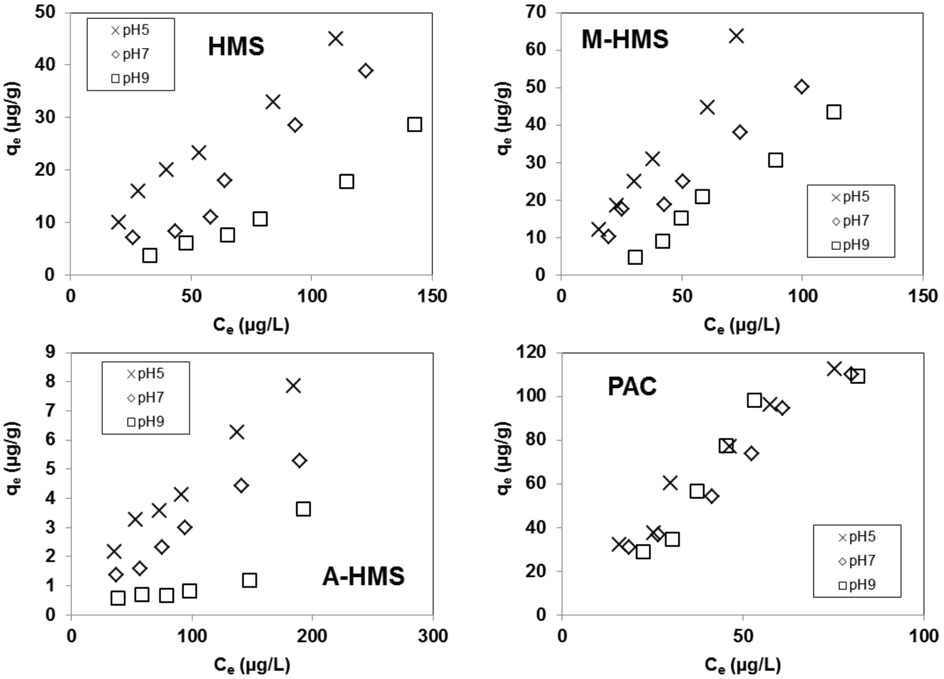

Figure 5.40 Adsorption capacity of HMS, M-HMS, A-HMS and PAC for CBZ at pH 5, 7 and 9 (25 °C and IS 0.01M).

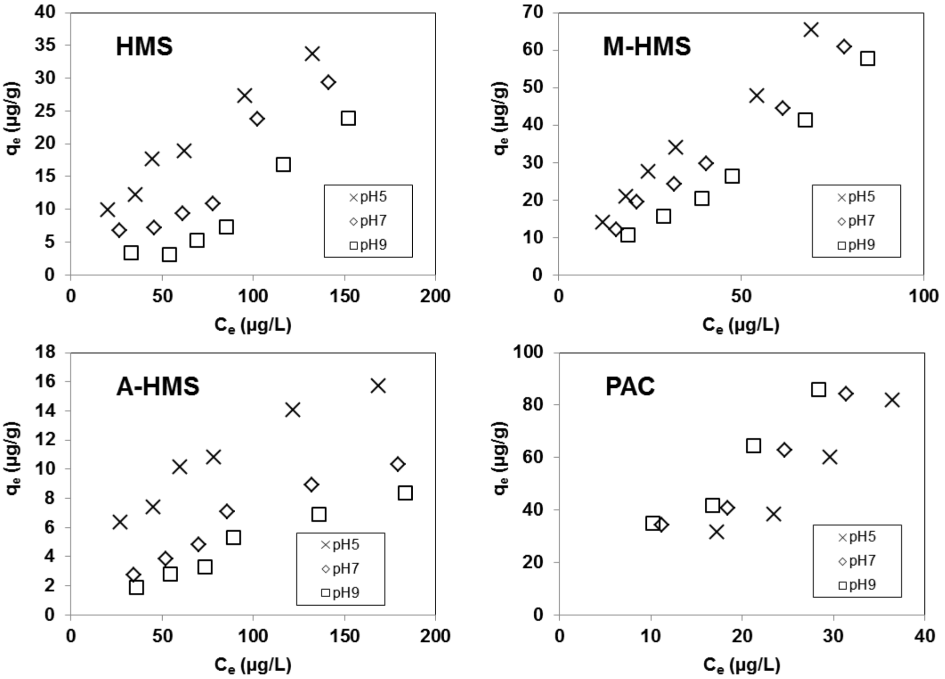

Figure 5.41 Adsorption capacity of HMS, M-HMS, A-HMS and PAC for NAP at pH 5, 7 and 9 (25 °C and IS 0.01M).

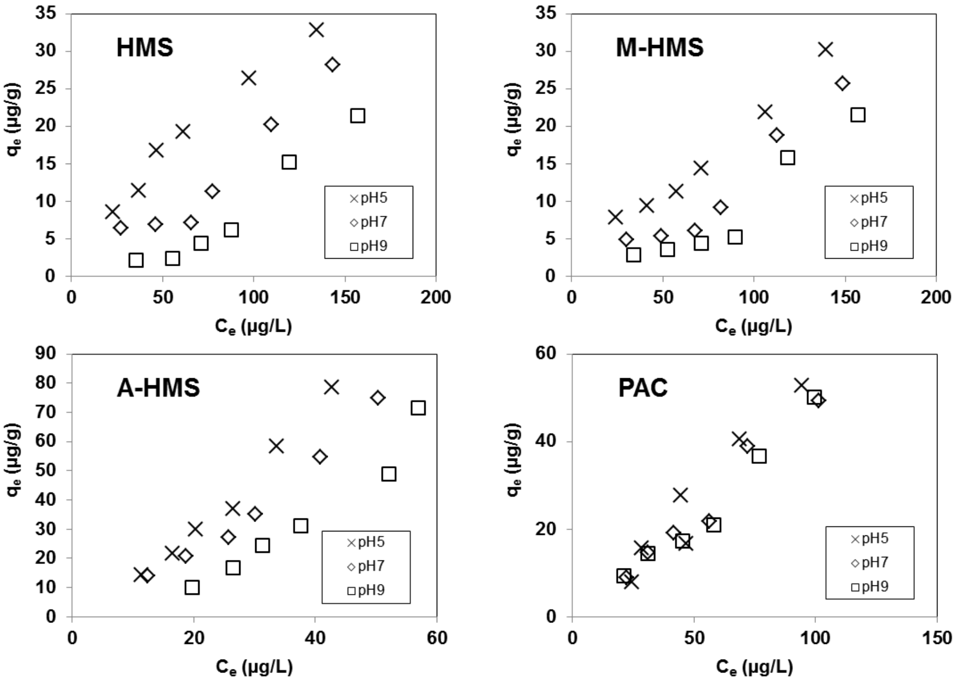

Figure 5.42 Adsorption capacity of HMS, M-HMS, A-HMS and PAC for CFA at pH 5, 7 and 9 (25 °C and IS 0.01M).

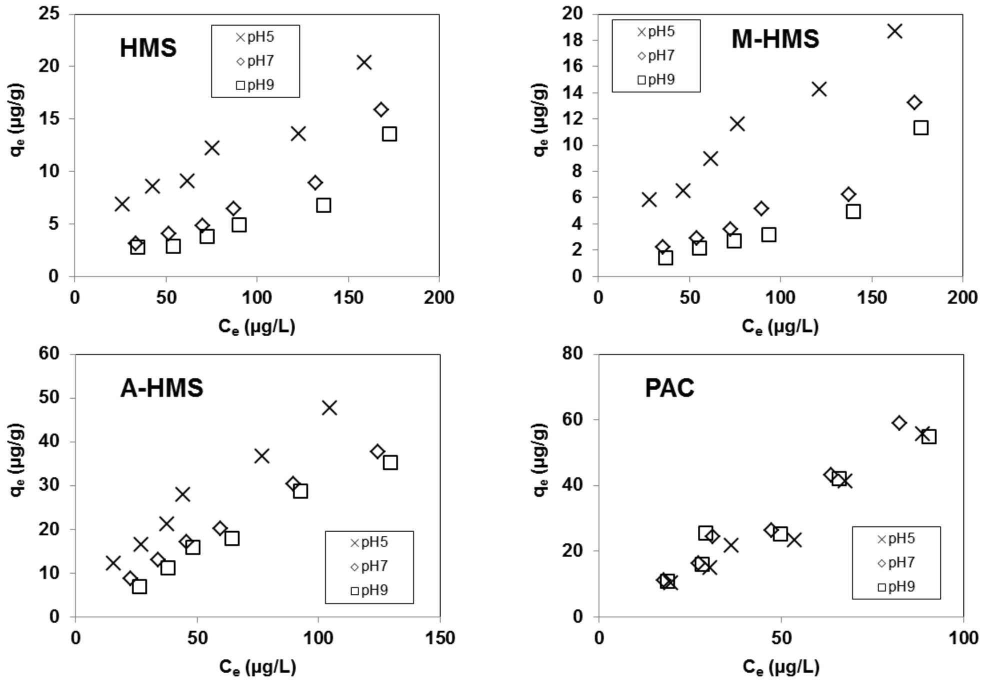

Figure 5.43 Adsorption capacity of HMS, M-HMS, A-HMS and PAC for ACT at pH 5, 7 and 9 (25 °C and IS 0.01M).

For CBZ and ACT, which have a net neutral charge over the tested pH range, the adsorption capacities of M-HMS, A-HMS and HMS were found to be highest at pH 5 and lowest at pH 9. This is consistent with the report that a pH lower than pH_{PZC}, when the silica surface has a net positive charge, is favorable for hydrogen bonding, whereas at a pH higher than pH_{PZC}, the silica surface is negatively charged and less favorable for hydrogen bonding, and so a decreased adsorption capacity is seen [Bui and Choi, 2009]. In conclusion, the adsorption of pharmaceuticals by HMS and the functionalized HMS derivatives varies with the pH. Electrostatic interactions and hydrogen bonding are the main mechanisms that account for the adsorption changes at different pH values.

In the case of PAC, there is no consistent relationship between its adsorption capacity for pharmaceuticals with respect to pH changes, presumably due to the various types of surface functional groups and variable amounts of each functional group on the PAC surface. This variation in the surface functional groups will consequently cause variations in the electrostatic interactions and other forces involved in the adsorption process.

5.3.5.4 Effect of temperature and thermodynamic parameters

To study the effect of temperature, we did the experiment only with the most effective adsorbent. M-HMS was used to study the effect of temperature on the adsorption of DCF, CBZ and NAP. A-HMS was used in the study of CFA and ACT adsorption. The adsorption of phamaceuticals onto the adsorbents were assayed at 15, 25 and 40 ^{o}C to study the effect of temperature and to evaluate the Gibbs free energy of the adsorption (ΔG^{o}), heat of the adsorption (ΔH^{o}), and standard entropy changes (ΔS^{o}). The thermodynamic equations [Pan et al., 2011] used for the calculation are presented in Eqs. (5.14) and (5.15):

$$\ln\left(\frac{q_e}{C_e}\right) = \frac{\Delta S^o}{R} - \frac{\Delta H^o}{RT} \quad (5.14)$$

$$\Delta G^o = \Delta H^o - T\Delta S^o \quad (5.15)$$

where R is the gas constant (8.314 J/mol.K) and T is the absolute temperature (K). ΔH^o and ΔS^o were determined from the slope and intercept of the plots between $\ln(q_e/C_e)$ versus $1/T$. ΔG^o was calculated from equation(14).The values of ΔG^o, ΔH^o and ΔS^o are summarized in Table 5.11. For the adsorption of all pharmaceuticals onto the adsorbents, the magnitude of the Gibbs free energies of the adsorption (ΔG^o) increased when temperature was increased suggesting that the adsorption is more favorable at high temperature. The negative value of the energies indicated that the adsorption process was spontaneous in nature. The positive value of adsorption heats (ΔH^o) suggested that the adsorption process was endothermic. The positive value of standard entropy changes (ΔS^o) suggested that the randomness at the solid-solution interface increased during the adsorption process.

Table 5.11 Thermodynamic parameters for sorption of DCF, CBZ, and NAP onto M-HMS, and for sorption of CFA and ACT onto A-HMS at three different temperatures.

Pharmaceutical	**Adsorbents**	**Temperature (K)**	**ΔG^o (J/mole)**	**ΔH^o (J/mole)**	**ΔS^o (J/mole.K)**
DCF	**M-HMS**	288 298 313	-99.43 -307.49 -619.59	5,893	20.81
CBZ	**M-HMS**	288 298 313	-125.51 -3519.5 -6916.2	6,396	22.64
NAP	**M-HMS**	288 298 313	-299.99 -512.53 -831.35	5,821	21.25
CFA	**A-HMS**	288 298 313	-30.01 -344.21 -815.52	9,019	31.42
ACT	**A-HMS**	288 298 313	-81.79 -424.55 -938.69	9,789	34.28

5.3.5.5 Competitive adsorption

The adsorption capacities of M-HMS, A-HMS, HMS and PAC for each pharmaceutical compound in single solute and mixed solute solution are shown in Figure 5.44, 5.45, 5.46 and 5.47 respectively.

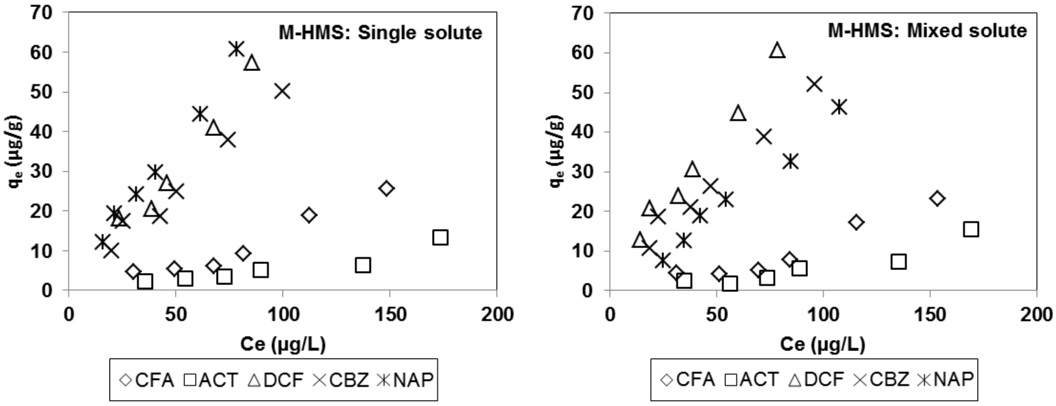

Figure 5.44 Adsorption capacity of M-HMS in single solute and mixed solute solutions (pH 7, 25 °C and IS 0.01M).

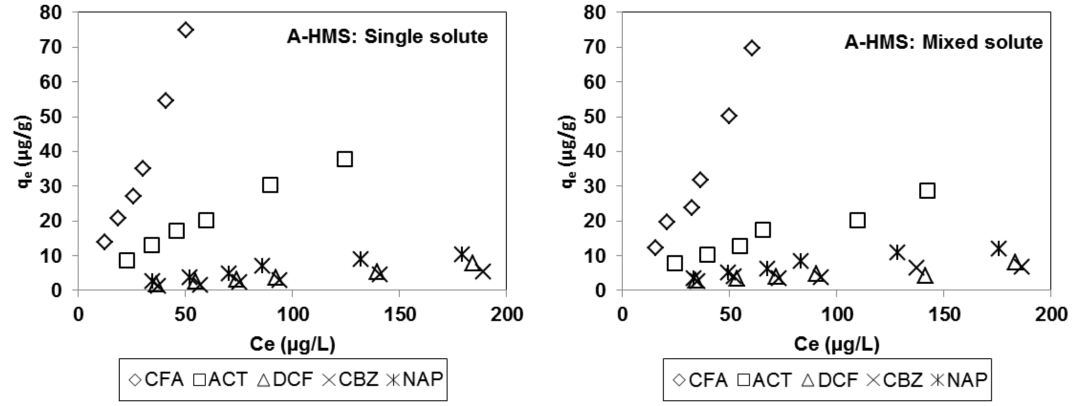

Figure 5.45 Adsorption capacity of A-HMS in single solute and mixed solute solutions (pH 7, 25 °C and IS 0.01M).

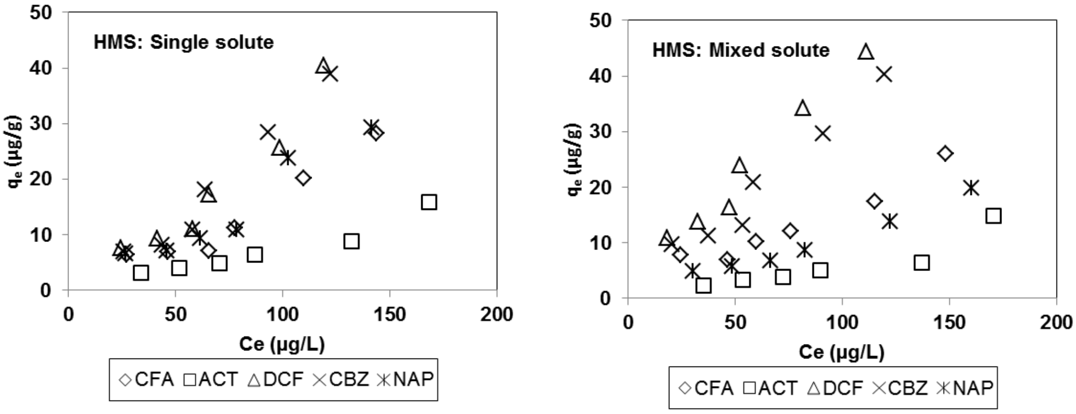

Figure 5.46 Adsorption capacity of HMS in single solute and mixed solute solutions (pH 7, 25 °C and IS 0.01M).

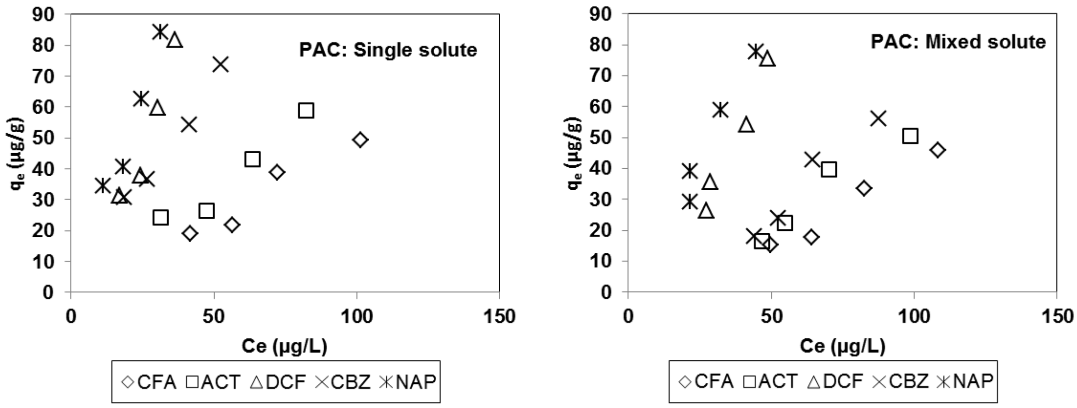

Figure 5.47 Adsorption capacity of PAC in single solute and mixed solute solutions (pH 7, 25 °C and IS 0.01M).

From this study, the adsorption capacities of M-HMS for each pharmaceutical in single solute and in mixed solute solutions showed different trends, being (highest to lowest adsorption capacity) NAP > DCF > CBZ > CFA > ACT in single solute solution, and DCF > CBZ > NAP > CFA > ACT in mixed solute solution. Considering the adsorption of M-HMS for DCF, CBZ and NAP in which the same mechanism (i. e. hydrogen bonding and hydrophobic interaction) played role in the adsorption process , the adsorption capacities in mixed solute solution were ranked (highest to lowest) as DCF > CBZ > NAP. This could be explained by competition between DCF, CBZ and NAP to adsorb to the adsorbent, where the adsorption capacities might be related to the molecular size of the adsorbates. The molecular sizes of the adsorbates (biggest to smallest) are ranked as NAP > CBZ > DCF. Because DCF has a smaller molecular size than CBZ and NAP, it has a faster movement velocity to get access to the inner surface functional group of the adsorbent and win over the other two pharmaceutical compounds in the adsorption competition. Similarly, because CBZ has a smaller molecular size than NAP, it moves faster and win over NAP in the adsorption competition. The adsorption competition is therefore a good explanation for a higher adsorption capacity of M-HMS for DCF than for CBZ and NAP, and a higher adsorption for CBZ than for NAP in the mixed solute solution. From this study, M-HMS was found to have a slightly lower adsorption capacity for NAP in the mixed solute solution than in the single solute solution, whereas the adsorption capacity of M-HMS for DCF and for CBZ in mixed solute solution was slightly higher than in the single solute solution.

From this study, the adsorption capacities of A-HMS for each pharmaceutical in single solute and in mixed solute solution showed a similar trend, being (from highest to lowest) CFA > ACT > NAP > DCF > CBZ. The adsorption capacity of A-HMS for CFA and for ACT in the mixed solute solution was slightly lower than in the single solute solution. But the adsorption capacity of A-HMS for NAP, for DCF and for CBZ in the mixed solute solution was slightly higher than in the single solute solution. For the adsorption of pharmaceuticals which have negatively charged molecules, (CFA, NAP and DCF), it was found that the adsorption capacities might correlate with the pK_a value of the adsorbates. The pK_a values of CFA, NAP and DCF are 2.87, 4.15 and 4.20 respectively. It was found that the adsorbate which had lower pK_a value had a higher adsorption capacity than the adsorbate which had higher pK_a value. So it could be concluded that the selective adsorption of A-HMS for acidic pharmaceuticals, which have negatively charged molecules, depends on their pK_a values.

From this study, the ranking of adsorption capacities of HMS (from highest to lowest) was found to be DCF > CBZ > NAP> CFA > ACT in the single solute solution, and to be DCF > CBZ> CFA > NAP > ACT in the mixed solute solution. Considering the adsorption of M-HMS for DCF, CBZ and NAP in which the same mechanism (i. e. hydrogen bonding and hydrophobic interaction) played role in the adsorption process, the adsorption capacities in mixed solute solution were ranked (highest to lowest) as DCF > CBZ > NAP. The adsorption capacity of HMS for DCF and for CBZ in mixed solute solution was found to be slightly higher than in the single solute solution, whereas the adsorption capacity for NAP in mixed solute solution was slightly lower than in the single solute solution. These findings were similar to those found in the adsorption of M-HMS. These results could be explained by competition between DCF, CBZ and NAP to adsorb to the adsorbent, where the adsorption capacities might be related to the molecular size of the adsorbates.

The adsorption capacities of PAC for each pharmaceutical in single solute solution and in mixed solute solution showed a similar trend, being NAP > DCF > CBZ > ACT > CFA. The adsorption capacities of PAC or all pharmaceuticals were found to be lower in mixed solute solution than in single solute solution. We could not correlate the adsorption capacities of PAC for each pharmaceutical with anything such as the molecular sizes of the pharmaceuticals or the the pK_a values of the acidic pharmaceuticals that can explain the selective adsorption of PAC.

5.4 Conclusion

Fom the adsorption kinetics study, it was found that the adsorption of all pharmaceuticals onto all adsorbents decreased rapidly in the first 30 min and reach equilibrium within 10 h. The adsorption of all pharmaceuticals followed the pseudo-second order kinetic model. The initial adsorption rate for DCF, CBZ and NAP was highest in M-HMS. But for CFA and ACT, A-HMS had the highest initial adsorption rate. Intraparticle diffusion was not the only rate-limiting step in the adsorption process of DCF, CBZ, NAP and CFA. Rather, the external mass transfer played an important role in the adsorption process of these compounds. But in the adsorption process of ACT, pore diffusion was the rate-limiting step. From the adsorption isotherm data analysis, it was found that the adsorption data of DCF, CBZ, NAP and CFA best fitted the Linear isotherm model. But for the adsorption data of ACT, the Langmuir model was better correlated. Freundlich model also fitted well and was the second best fitted model for the adsorption data of all pharmaceutials. From the adsorption mechanism study, the adsorption capacities, at pH 7, of the adsorbents for CBZ, DCF and NAP was found to be ranked (highest to lowest adsorption capacity) as M-HMS > HMS > A-HMS. The modification of HMS with mercapto functional groups increased its adsorption capacity presumably through enhanced hydrogen bonding and hydrophobic interactions. The adsorption capacities of the adsorbents for CFA and ACT were ranked in descending order as A-HMS > HMS > M-HMS. The adsorption capacity of HMS was increased after modification with amino functional group. This could be explained by the enhancement of electrostatic interaction between pharmaceutical residues and the adsorbents, and also possibly by enhanced hydrogen bonding and hydrophobic interaction. Comparative analysis of the adsorption capacity of HMS, SBA-15 and MCM-41 showed that the adsorption capacities of the pure silicate adsorbents varied directly with their surface areas. The adsorption study of pharmaceuticals onto the adsorbents at various pH (5, 7 and 9) showed that the adsorption of pharmaceuticals onto HMS and functionalized HMS derivatives varied with pH. The main mechanisms for the adsorption changes at different pH values were electrostatic interactions and hydrogen bonding. There was no consistent relationship between the adsorption capacity of PAC for pharmaceuticals with respect to pH changes. This was presumably due to the presence of various types of surface functional groups and variable amounts of each functional group on the PAC surface. The results of the study on adsorption of the adsorbent for pharmaceuticals in mixed solute solution suggested that in the process of adsorption of HMS and M-HMS for DCF, CBZ and NAP in which hydrogen bonding and hydrophobic interactions were the main mechanism of adsorption, there was a competition between each pharmaceutical to adsorb to M-HMS and HMS. The adsorption capacities might be related to the molecular size of the adsorbates. The selective adsorption of A-HMS for acidic pharmaceuticals such as DCF, NAP and CFA which have negatively charged molecules, varied with their pk_a values.

CHAPTER VI

SYNTHESIS AND CHARACTERIZATION OF PERIODIC MESOPOROUS ORGANOSILICAS

6.1 Introduction

In this chapter, we report on the synthesis of periodic mesoprous organosilica via surfactant template method as well as the modification of the surface of PMO with three different types of organosilane, i.e. mono-, di- and triamino-organoalkosysilanes via direct-cocondensation method. The physicochemical properties of adsorbents were investigated by low-angle powder x-ray diffraction, scanning electron microscope, transmission electron microscope, nitrogen gas adsorption and desorption isotherms, thermogravimetric analysis, differential thermal analysis, elemental analysis, Fourier transform infrared spectroscopy and zeta potential analysis. The synthesized and characterized materials were used as the adsorbents in removal of pharmaceutical residues by adsorption in phase IV (chapter 7).

6.2 Method

6.2.1 Synthesis of PMO

Synthesis of virgin PMO materials was carried out as described by Burleigh et al. (2001). First hexadecyltrimethylammonium chloride was dissolved in deionized water under stirring in a polypropylene vessel. Then NaOH solution was added dropwise into the beaker and stirred for 10 min. Then bis(triethoxysilyl)ethane was added to the beaker and the mixture of structure directing agent and molecular silica source was stirred at room temperature for 12 h. The white precipitates were recovered by filtration, washed thoroughly with deionized water and dried at 100 ^{o}C for 12 h. The mother gel composition was 1.0 BTSE : 0.12 CTAC : 1.0 NaOH : 230 H_2O. The surfactant in the as-synthesized sample was removed by a solvent extraction method. 1.0 g of the as-synthesized sample was placed in 350 mL of acidified ethanol (1 M HCl) and refluxed for 10 hr.

6.2.2 Synthesis of functionalized PMO via direct co-condensation method

Synthesis of functionalized PMO via direct co-condensation method was carried out as described by Burleigh et al (2001). The procedure of synthesis of the functionalized PMO was quite the same as of the virgin PMO except that the amounts of molecular silica source in the composition were different. The mother gel composition in this case was (1.0-x) BTSE : x R'Si(OR)$_4$: 0.12 CTAC : 1.0 NaOH : 230 H_2O, where x is the proportion of the organosilane in the silica source which was equal to 0.1, 0.25, and 0.40. The organosilane that was used to functionalize the materials in this study was (3-aminopropyl)trimethoxysilane or 1N-silane, 3-[2-(2-aminoethylamino)ethylamino]propyltrimethoxysilane) or 2N-silane and [2-(2-aminoethylamino)propyl]trimethoxysilane or 3N-silane. The structural formulas of organosilane which were used in this study are shown in Figure 6.1. After adjustment of the pH of the solution with NaOH, the mixture of molecular silica source, BTSE and functionalized organosilane, were simultaneously mixed together for 10 min in a separate vial before adding to the mixed solution. The procedure after that was the same as in the synthesis of virgin PMO.

6.2.3 Characterization

6.2.3.1 X-ray Diffraction

XRD patterns of synthesized adsorbents were obtained from a Bruker AXS Model D8 Discover with CuKα radiation (40 kv, 40 mA) at 2Θ angle of 0.5 – 10 ^{o}. The scan speed was 0.04 ^{o}/min.

6.2.3.2 Nitrogen gas sorption

Nitrogen gas adsorption and desorption isotherms were obtained using Micromeritics ASAP 2020 version 1.04H. Before analysis the samples were dehydrated at 150 °C for 4 h under nitrogen condition and then the measurements were performed at 77 K. The pore size distribution was obtained using Barrett Joyner Halenda (BJH) model. The specific surface area of the materials was computed with the BET model within a range of relative pressure, $P/P_0 = 0.05 - 0.3$. The total pore volume was derived from the volume of nitrogen adsorbed at a relative pressure $P/P_0 = 0.995$ single point.

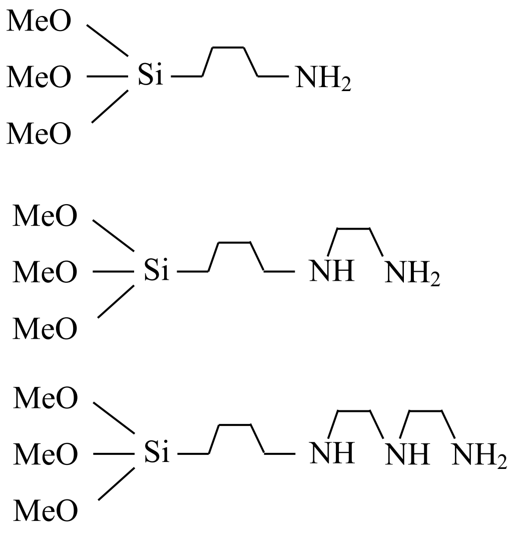

(3-Aminopropyl)trimethoxysilane or 1N-silane

3-[2-(2-Aminoethylamino)ethylamino]-propyltrimethoxysilane) or 2N-silane

[2-(2-Aminoethylamino)propyl]-trimethoxysilane or 3N-silane

Figure 6.1 Structural formulas of amine organosilane (1N-, 2N- and 3N-silane).

6.2.3.3 Scanning electron microscope

The SEM micrographs of the materials were observed at 3,500 magnifications through scanning electron microscope model JEOL-JSM5410LV.

6.2.3.4 Transmission electron microscope

The TEM microphotographs were carried out at 120,000 magnifications on JEOL-JEM2100 electron operating at 200 kV.

6.2.3.5 Thermogravimetric analysis and differential thermal analysis

TGA and DTA were performed with a Mettler-851e from ambient temperature to 1,100 °C at a heating rate 8 °C/min under flow of nitrogen (50 mL/min).

6.2.3.6 Elemental analysis

The amount of nitrogen was measured by a LECO-CHN-2000 CHN analyzer.

6.2.3.7 Fourier transform infrared spectroscopy

The presence of organic moieties in the materials and the efficiency of surfactant template removal method were confirmed by FTIR on a Nicolet Impact 410 FTIR spectrophotometer.

6.2.3.8 Zeta potential

Zeta potential of the adsorbents were measured by a Malvern Zetasizer NanoZS with He-Ne laser source, λ =633 nm. The ratio of adsorbent to solution was fixed at 2 g/L. The sample was sonicated for 10 min before analysis. The pH of the solution was controlled at 5, 7 and 9 using 0.01 M phosphate buffer.

6.3 Results and discussion

6.3.1 X-ray Diffraction

Figure 6.2 shows the XRD patterns of as-synthesized and extracted PMOs materials. To evaluate the structural property of the adsorbent, the XRD (100) interplanar diffraction spacing (d_{100}), was calculated from the following equation

$$d_{100} = \frac{1.5406}{2\sin\theta} \qquad (6.1)$$

where Θ is the scanning diffraction angle (radian) corresponding to diffraction peak (100). The d_{100} spacing of all materials is shown in Table 6.1.

Table 6.1 d_{100} spacings of PMOs samples.

Sample	As-synthesized (Å)	Extracted (Å)
PMO	43.02	43.00
1N10PMO	43.97	42.95
1N25PMO	41.86	41.28
1N40PMO	39.77	39.97
2N10PMO	42.10	42.35
2N25PMO	41.32	42.68
2N40PMO	41.34	40.28
3N10PMO	39.83	38.57
3N25PMO	39.04	39.45
3N40PMO	39.41	38.83

In case of virgin PMO, the as-synthesized and extracted material displayed a typical hexagonal structure, with the XRD patterns featuring one main correlation reflection (100) at $2\Theta = 2.055\ ^{o}$. Unlike the virgin PMO from the other study which used 1, 2-bis(trimethoxysilyl)ethane as the silica source and used octadecyl trimethylammonium chloride as the surfactant directing agent, we did not see the other clear diffraction peaks corresponding to other reflection lines such as (002), (101), (110), (103), (112) which could be used as an index or an evidence or a proof of a 3D-hexagonal lattice [Inagaki et al.,1999]. The prominent peak in our virgin PMO samples was found at the same angle as in the HMS material but its intensity was higher. From the diffraction pattern seen in our study, we could index our virgin PMO material as a hexagonal lattice. The intensity of the extracted PMO sample was much higher than the as-synthesized sample. This indicated that the extracted PMO had a more well-ordered structure after surfactant template removal. We also found that the d_{100} spacing values of the as-synthesized and those of the extracted materials were not different. This suggested that there was no matrix contraction upon the surfactant extraction of the virgin PMO.

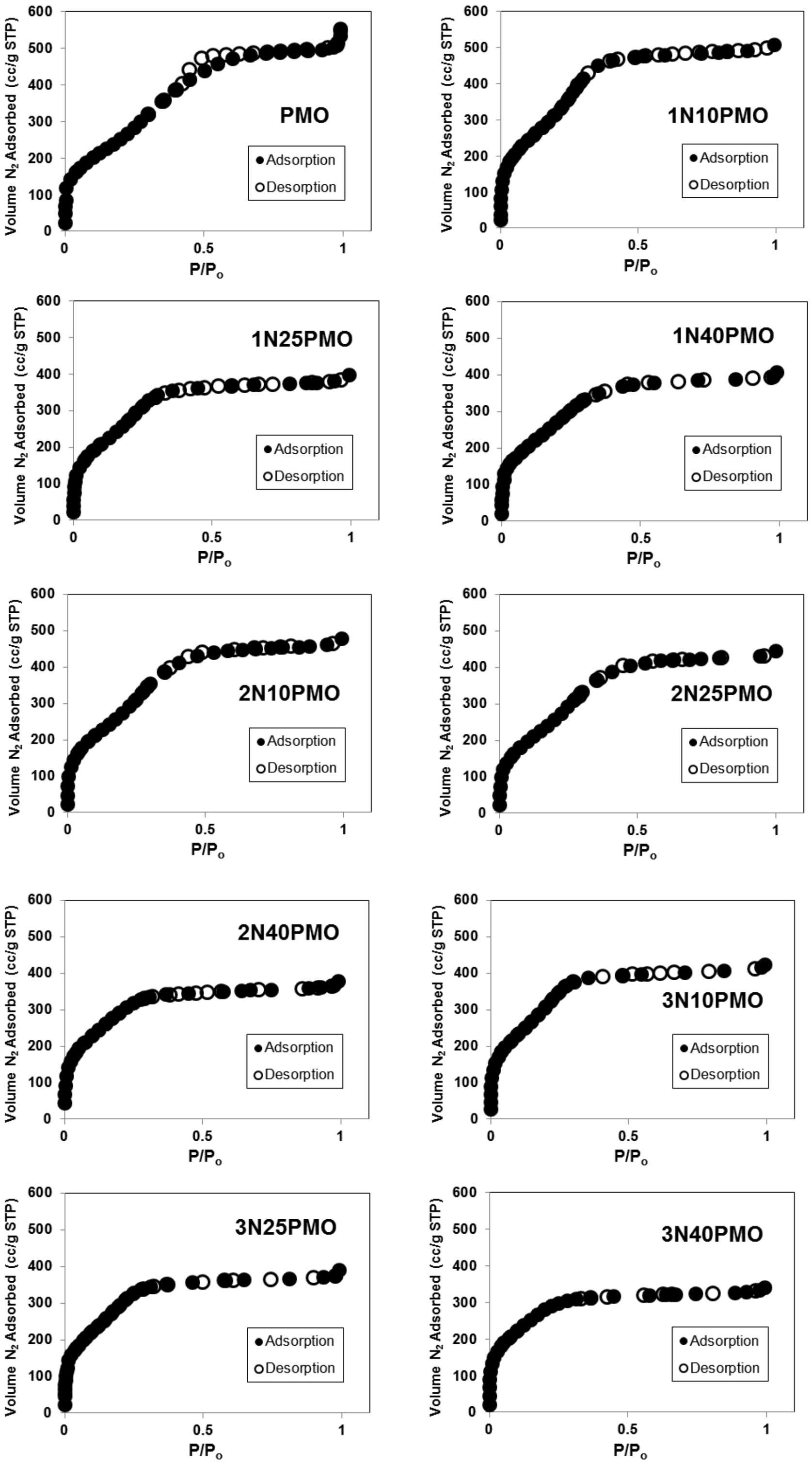

Figure 6.12 N_2 adsorption/desorption isotherms of extracted ethanesilicas.

Table 6.2 Structural properties of functionalized periodic mesoporous organosilicas.

Sample	BET surface area (m^2/g)	Total pore volume (cm^3/g)	Pore diameter[a] (Å)
PMO	1252	0.851	26.5
1N10PMO	1176	0.723	26.0
1N25PMO	1095	0.611	23.5
1N40PMO	1086	0.601	21.5
2N10PMO	1122	0.735	25.5
2N25PMO	1086	0.682	25.3
2N40PMO	963	0.581	20.5
3N10PMO	1230	0.652	23.5
3N25PMO	1188	0.601	20.5
3N40PMO	1037	0.524	20.0

[a] Determined from BJH pore size distribution

In regard to the structural properties of PMO functionalized with amine organosilane, it was found that the BET surface area and the pore volume of the functionalized PMO decreased as the concentration of added amine organosilane increased. This could be explained by the occupying of the pore framework by the terminal organic functional groups protruding into the terminal surface of the pores [Saad et al., 2008]. However these functionalized materials still have larger surface area than other mesoporous materials which were functionalized with amine-functional group such as HMS, MCM-41 or SBA-15 [Prarat et al., 2011, Saad et al., 2008, Hamoudi et al., 2010]. The corresponding pore sizes of PMO, 1N10PMO, 1N25PMO and 1N40PMO materials were 26.5 Å, 26.0 Å, 23.5 Å and 21.5 Å respectively. It was found that further increasing of the concentration of organosilane in the reaction mixture resulted in reduction of the pore diameter of 1NPMOs materials. Dimos et al [Dimos et al., 2008] said that the systematic reduction of the specific surface area and pore diameter of the materials provided evidence that the pores were filled with organic molecules which were dispersed uniformly throughout the pores.

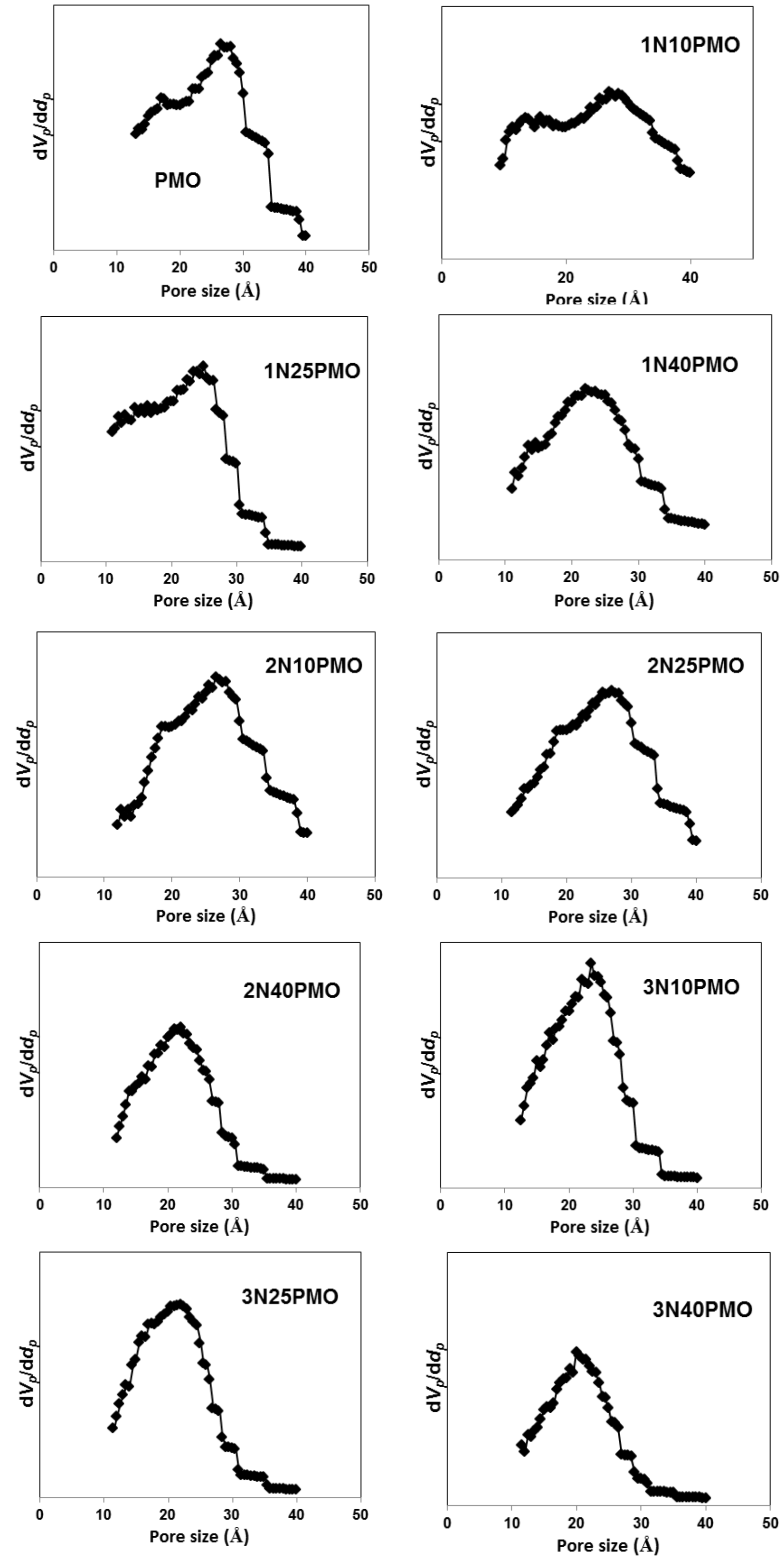

Figure 6.13 BJH pore size distribution of extracted ethanesilicas.

To study the change of the structural properties, the pore center distance in hexagonal geometry or the unit cell parameter (a_0) and the pore wall thickness (w) [Burliegh et al., 2001] of the materials were calculated from the following equation

$$a_0 = \sqrt{({d_{100}}^2 + r^2)} \qquad (6.2)$$

$$w = a_0 - 2 * r \qquad (6.3)$$

where θ is the scanning diffraction angle (radian) corresponding to diffraction peak (100) and r is pore radius (Å). The calculated parameters for each material are summarized in Table 6.3.

Table 6.3 Pore center distance (a_0) and pore wall thickness (w) of functionalized periodic mesoporous organosilicas.

Sample	Pore center distance (Å)	Pore wall thickness (Å)
PMO	44.99	18.49
1N10PMO	44.88	18.88
1N25PMO	42.92	19.42
1N40PMO	41.38	19.89
2N10PMO	44.23	18.73
2N25PMO	44.51	19.21
2N40PMO	41.56	21.06
3N10PMO	40.32	16.82
3N25PMO	40.76	20.26
3N40PMO	39.91	21.41

It was found that the pore center to pore center distance of virgin PMO and PMOs functionalized with 1N-silane were within the range of 41.39 Å to 44.99 Å. Virgin PMO have the highest a_0 value. The pore center to pore center distance values and the average pore diameters of the materials seemed to decrease as the amount of added 1N-silane was increased. The pore thickness of these materials also increased when the concentration of added 1N-silane was increased. The functionalized PMOs (1N10PMO, 1N25PMO and 1N40PMO) had greater values of pore thickness than the virgin PMO. In other words, the wall of the pores of all functionalized PMOs was thicker than those of the virgin PMO.

The same relationship between the surface area, as well as between the pore volume and the concentration of added silane as found in the PMOs functionalized with 1N-silane was also found in PMOs functionalized with 2N-silane. The pore diameters of 2N10PMO, 2N25PMO and 2N40PMO were 25.5 Å, 25.3 Å and 20.5 Å respectively (Table 6.2). The pore diameters of virgin 2N10PMO and 2N25PMO were not different significantly. But the pore diameter of 2N40PMO was around 5 Å smaller than the other materials. The pore center to pore center distance of 2NPMOs was shorter than that of the virgin PMO. The pore center to pore center distance value of 1NPMOs seemed to be not different from that of 2NPMOs with the same concentration of added amine organosilane. The 2NPMOs had greater values of pore thickness than the virgin PMO, and also the values of their pore thickness seemed to be greater than those of 1NPMOs with the same concentration of added silane. The functional groups, when added to the materials, made the wall of the pore to become thicker. The pore wall thickness of the 1NPMOs and 2NPMOs varied with the concentration of added amine organosilane. This was consistent with the result of XRD pattern study that showed the decrease in the peak intensity as the concentration of added organosilane was increased. (The peak intensity of 1NPMO compared with that of virgin PMO were: PMO > 1N10PMO > 1N25PMO > 1N40PMO). The same trend of peak intensity was also found in the XRD patterns of 2NPMO and 3NPMO). There was no relationship between the thickness of the wall of the pores and the types of the added functional groups.

The same relationship between the surface area, as well as between the pore volume and the concentration of added silane as found in PMOs funcionalized with 1N-silane or 2N-silane was also found in PMO functionalized with 3N-silane. Among all PMOs functionalized with organosilane, 3NPMO had the smallest pore diameter. At any concentration of added organisilane, 3NPMO had smaller pore diameter than other ethanesilicas. The pore diameter of 3N10PMO, 3N25PMO and 3N40PMO were 23.5 Å, 20.5 Å and 20.0 Å respectively. The pore center to pore center distances of all 3NPMOs, namely 3N10PMO, 3N25PMO and 3N40PMO, were almost equal (40.3 ± 0.4 Å). The pore center to pore center distance of 3NPMOs was shortest when compared with 1NPMOs and 2NPMOs. The pore wall thickness of 3NPMOs was not significantly different from the pore wall thickness of 1NPMOs and 2NPMOs. The relationship between the pore wall thickness and the concentration of loaded organosilane was found to be similar in all cases of PMO functionalization. The increase of wall thickness varied directly with the increase of silane concentration.

6.3.3 Scanning electron microscope

The SEM images of PMO and PMO derivatives are shown in Figure 6.14 - 6.17. The morphologies of PMO and functionalized PMOs consisted mostly of irregularly shaped particles with smooth surface. The particle size of PMO was around 1 to 10 μm. Both virgin PMO and functionalized PMOs consisted of particles with many different sizes and many different shapes. They both consisted of small and large particles mixed together. The striking difference between virgin PMO and functionalized PMOs was that the proportion of large to small particles in functionalized PMO was greater than the proportion in virgin PMO. The particles of functionalized PMOs seemed to be larger than those of virgin PMO. Another difference between virgin PMO and functionalized PMOs was the presence of spherical particles of various sizes, among the irregularly shaped particles, only in functionalized PMOs. The spherical particles were not seen in virgin PMO. The proportion of spherical to non-spherical particles increased with an increase in the concentration of added organosilane. Functionalized PMOs with different functional groups seemed to have no difference in the proportion of spherical to non-spherical particles. There was an explanation for the formation of spheres in functionalized PMO in Zhu's paper [Zhu et al., 2007]. With hydrophilic pendant groups, the organotrialkoxysilane can interact with each other through the hydrogen bond. The condensation of hydrolyzed ethane silica species around the surfactant micelles may be slowed down because of the steric hindrance of the existence of hydrogen bonds between the organosilanes. The slow condensation rate of silane species is helpful for the formation of sphere, therefore, the spheres with smooth surfaces can be formed in the presence of organotrialkoxysilane.

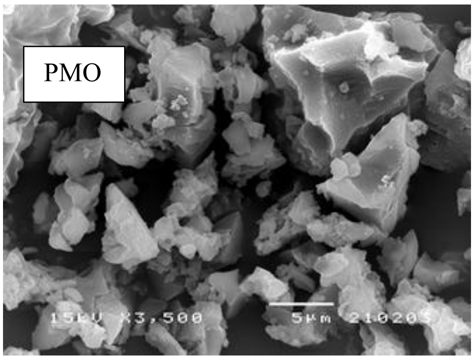
PMO
15kV X3,500 5μm 210205

Figure 6.14 SEM micrographs of extracted virgin PMO

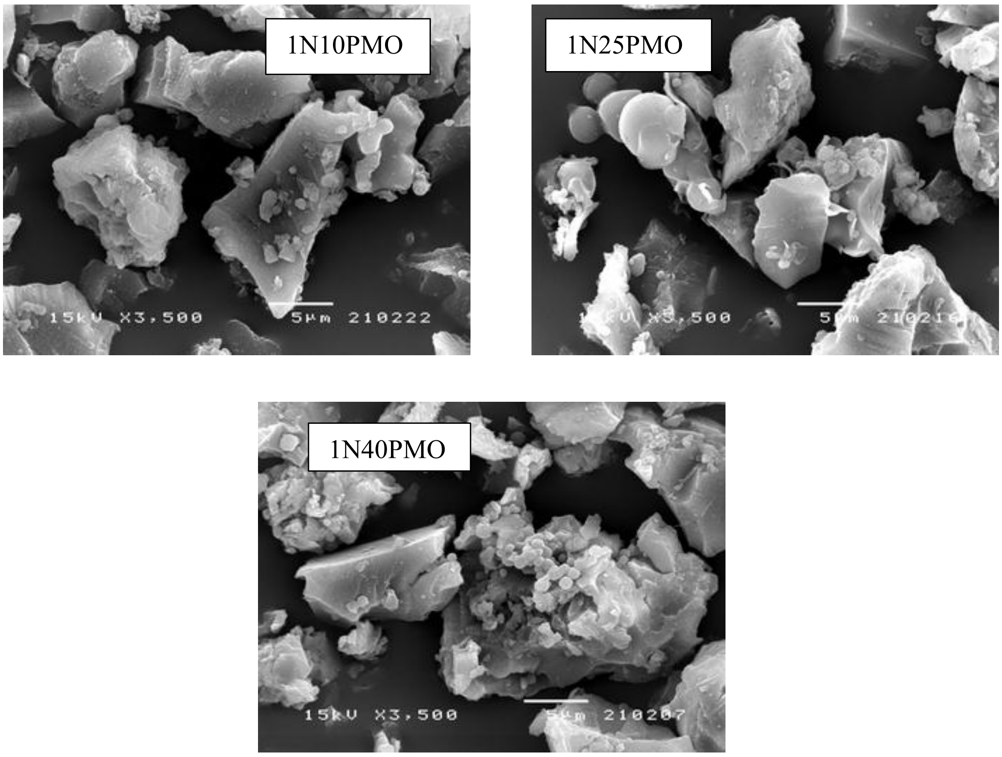
1N10PMO
15kV X3,500 5μm 210222
1N25PMO
15kV X3,500 5μm 210216
1N40PMO
15kV X3,500 5μm 210207

Figure 6.15 SEM micrographs of extracted 1NPMOs

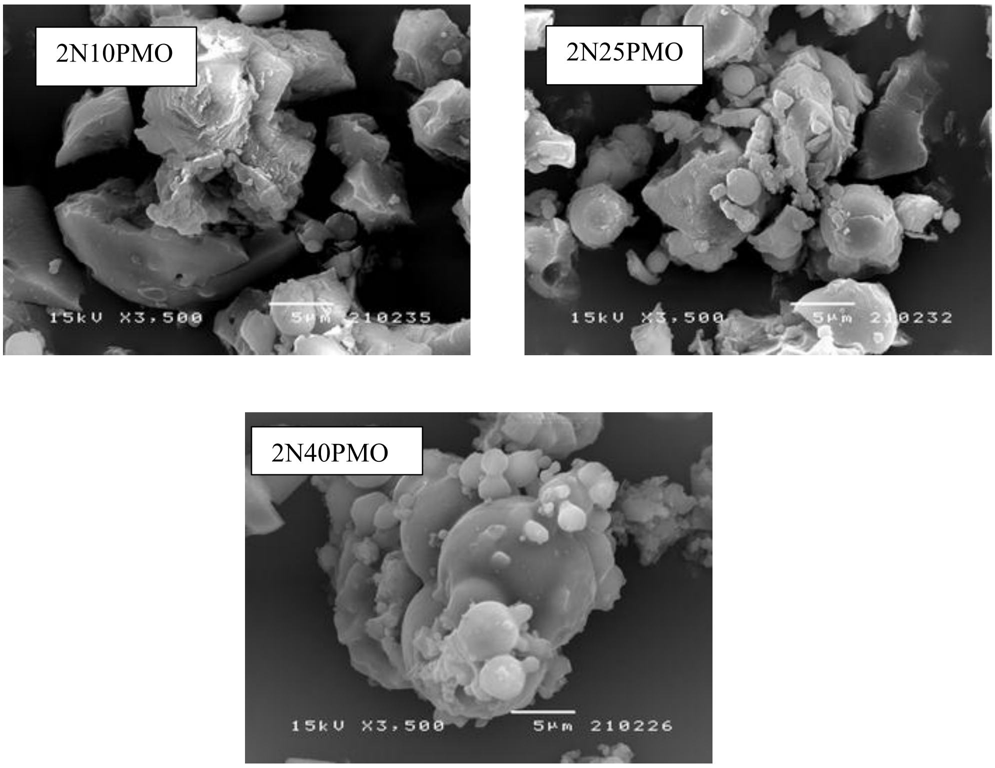
2N10PMO
15kV X3,500 5μm 210235
2N25PMO
15kV X3,500 5μm 210232
2N40PMO
15kV X3,500 5μm 210226

Figure 6.16 SEM micrographs of extracted 2NPMOs

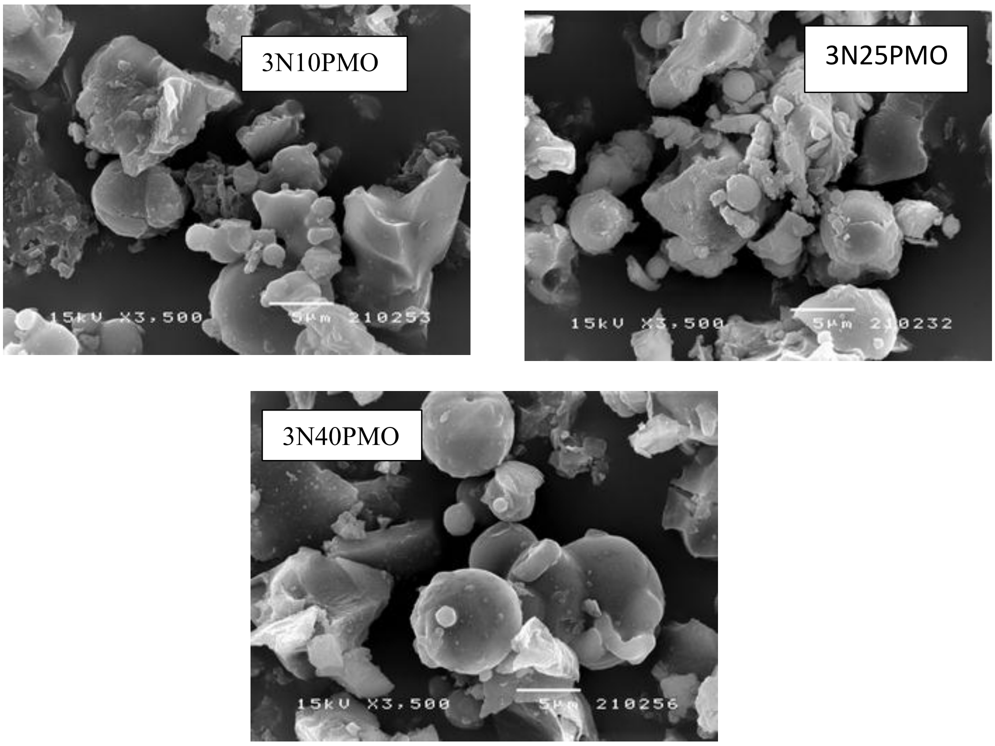
3N10PMO
15kV X3,500 5μm 210253
3N25PMO
15kV X3,500 5μm 210232
3N40PMO
15kV X3,500 5μm 210256

Figure 6.17 SEM micrographs of extracted 3NPMOs

6.3.4 Transmission electron microscope

TEM microphotographs of PMO, 1N25PMO, 2N25PMO and 3N25PMO are shown in Figure 6.18. The well ordered meso-structure of PMO and PMO derivatives was confirmed by TEM images. This was consistent with the results of nitrogen gas adsorption-desorption isotherms and x-ray diffraction patterns studies.

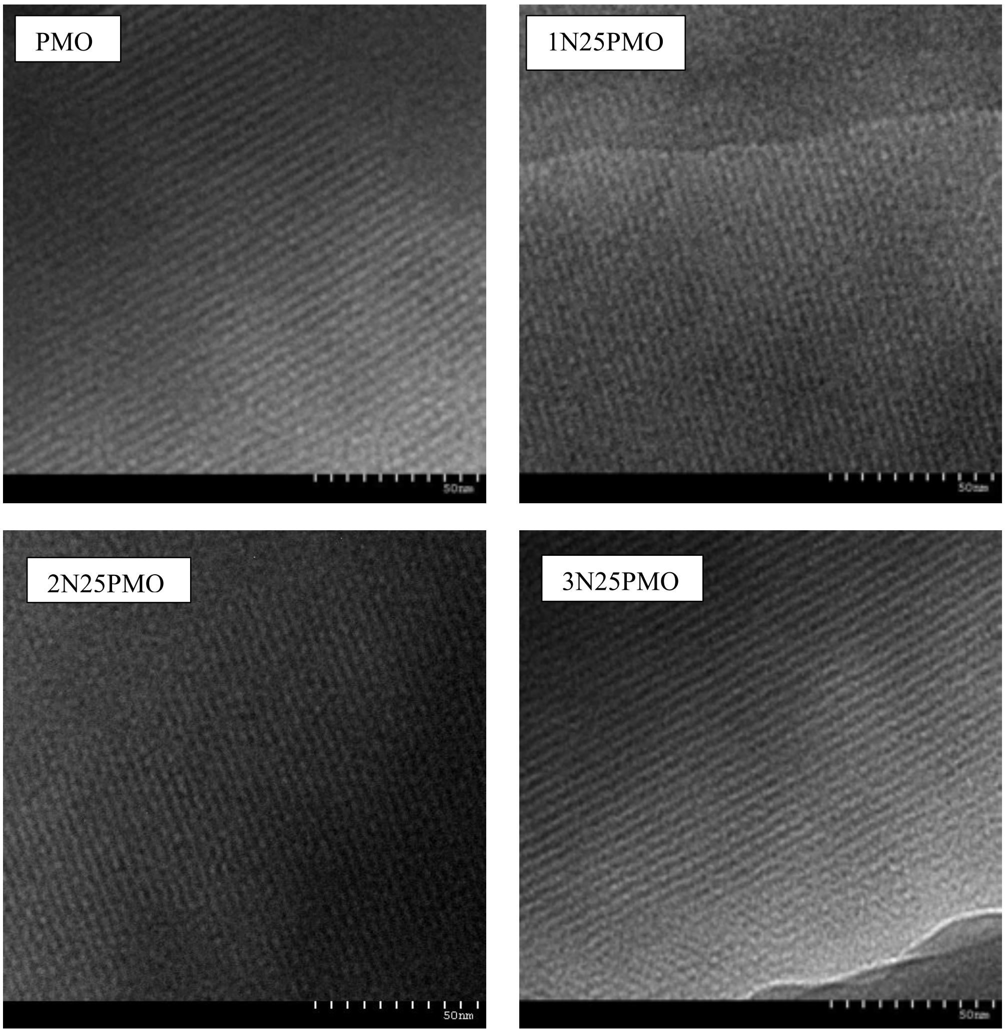
PMO
50nm
1N25PMO
50nm
2N25PMO
50nm
3N25PMO
50nm

Figure 6.18 TEM microphotographs of PMO, 1N25PMO, 2N25PMO and 3N25PMO.

6.4.5 Thermogravimetric analysis and Differential thermal analysis

TGA of PMO and PMO functionalized with organosilane was performed from room temperature to 1,100 °C. TGA of these organosilica was carried out on the as-synthesized and extracted materials.

The TG curves of as-synthesized and extracted PMOs are shown in Figure 6.19. The as-synthesized and extracted samples exhibited the total weight loss of 37.11% and 19.78 % respectively. The as-synthesized samples exhibited a greater weight loss than the extracted samples probably because they contained larger amount of surfactant templates. The DTA curve of the extracted PMO exhibited the first major endothermic peak at temperature around 52 °C. This peak was conformed to the weight loss of 1.07 % at temperature below 80 °C which was attributed to desorption of ethanol and water. At the temperature range from 100 to 500 °C, there were some small peaks but no major loss was shown in this range of temperature. This suggested that the surfactant template was completely removed from the porous material. The second major endothermic peak of the sample was found at the temperature around 590 °C. This inflection point corresponded to the decomposition of the ethylene group of the mesoporous organo-silica material [Zhang et al., 2005]. Burleigh et al (2001) said that it was hard to identify the peak which represented the decomposition of amine groups because the functional groups decomposed at the same temperature as the surfactant. Surprisingly the functionalized sample exhibited a significant weight gain at temperatures around 700 °C. At that high temperature, the DTA curve exhibited an exothermic peak. This interesting finding of weight gain could be attributed to nitridation phenomenon which was related to the forming of silicon oxynitride at the frame work of the organo porous material [Zhang et al., 2005]

The TG and DTA curves of the as-synthesized and extracted samples of 1N25PMO, 2N25PMO and 3N25PMO are shown in Figure 6.20, 6.21 and 6.22 respectively. The TG and DTA curves of extracted 2N25PMO and 3N25PMO samples had the shapes similar to those of the extracted 1N25PMO. The total weight losses of these materials were about the same ranging from 21.30 to 25.52 %. The nitridation phenomenon was also found in these functionalized PMOs at the same temperature (around 700 °C) as found in the extracted PMO. The magnitudes and numbers of DTA peaks in these functionalized PMOs at the temperature range under 700 °C were only slightly different.

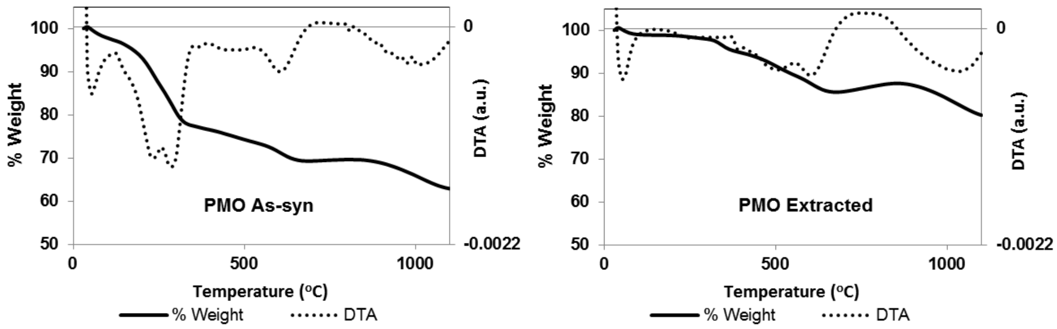

Figure 6.19 TG/DTA curves of as-synthesized and extracted PMO.

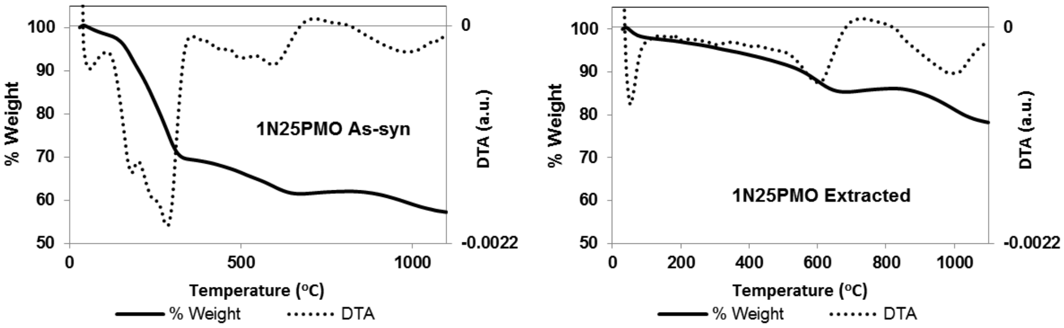

Figure 6.20 TG/DTA curves of as-synthesized and extracted 1N25PMO.

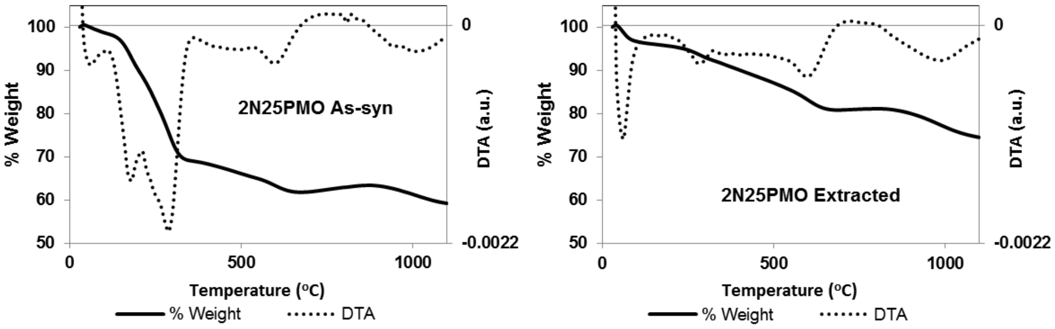

Figure 6.21 TG/DTA curves of as-synthesized and extracted 2N25PMO.

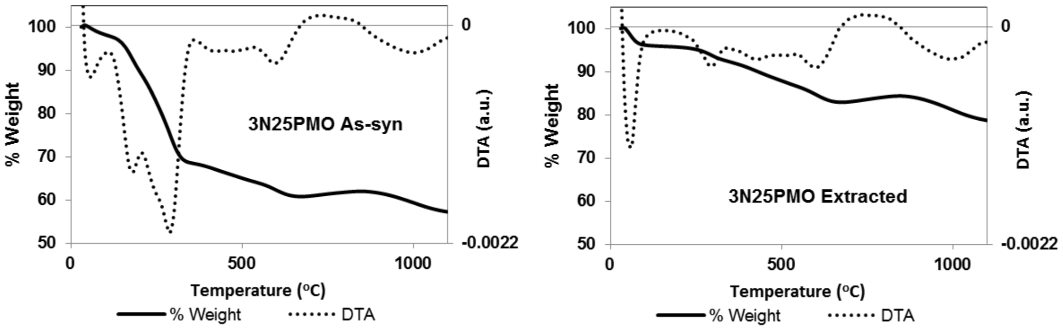

Figure 6.22 TG/DTA curves of as-synthesized and extracted 3N25PMO.

6.3.6 Elemental analysis

In this study, elemental analyses of extracted PMOs functionalized with 1N-, 2N- and 3N- silane, were used for quantitative determinations of organic functional groups in these materials. The total nitrogen content in extracted PMOs is shown in Table 6.4. The total nitrogen contents of PMOs functionalized with 1N-silane were found to range from 0.36 % to 1.09 %. 1N40PMO had the highest total nitrogen content. In regard to the structural properties of PMO functionalized with n-silane, it was found that the total nitrogen content of the functionalized PMO increased as the concentration of added N-silane was increased.

The same relationship between the total nitrogen content and the concentration of added silane as found in PMOs funcionalized with 1N-silane was also found in PMO functionalized with 2N- and 3N-silane. The total nitrogen content of 2N10PMO, 2N25PMO and 2N40PMO were 0.57 %, 1.08 % and 1.42 % respectively. The total nitrogen content of 3N10PMO, 3N25PMO and 3N40PMO were 0.60 %, 1.31 % and 1.78 % respectively. Among all of the functionalized PMOs, 3NPMO had the highest total nitrogen content. At any same concentration of added organisilane, 3NPMO had higher total nitrogen content than 2NPMO and 1NPMO.

Table 6.4 Total nitrogen content of PMOs functionalized with 1N-, 2N- and 3N silane.

Adsorbents	**Nitrogen content**	
	%	**mmol/g**
1N10PMO	0.36	0.257
1N25PMO	0.76	0.545
1N40PMO	1.09	0.779
2N10PMO	0.57	0.414
2N25PMO	1.08	0.770
2N40PMO	1.42	1.013
3N10PMO	0.58	0.410
3N25PMO	1.31	0.934
3N40PMO	1.78	1.274

6.3.7 Fourier Transform Infrared Spectroscopy

FTIR spectrum of the as-synthesized and extracted PMO is displayed in Figure 6.23. For as-synthesized material, the intensities of the bands assigned to the CTAC surfactant was found at 2857 cm^{-1} and 2937 cm^{-1} [Zhu et al., 2006]. This spectrum also showed three weak bands at ca. 1465, 1480, and 1490 cm^{-1}. The adsorption band at 1465 cm^{-1} was attributed to the methylene symmetric bending mode of the hexadecyltrimethylammonium ion. The bands at 1480 cm^{-1} and 1490 cm^{-1} belonged to the bending of the asymmetric head group of methyl (CH_3-N^+) [Diaz et al., 2000]. The presence of these 5 peaks in the IR spectrum could be used to identify the surfactant template which was present in the organo-sample before solvent extraction. These bands in the FTIR-spectrum of the extracted PMO samples greatly decreased in their intensities or almost disappeared. This suggested that most of the surfactant templates were removed by the solvent extraction method. Similar findings were found in the FTIR spectrum of the as-synthesized and extracted samples of 1NPMOs, 2NPMOs and 3NPMOs (Figure 6.24 to 6.32). The 5 peaks in the FTIR spectrum that could be used for identification of surfactant templates were present in the as-synthesized samples but not present in the extracted samples, indicating that the surfactant templates were completely or almost completely removed by solvent extraction.

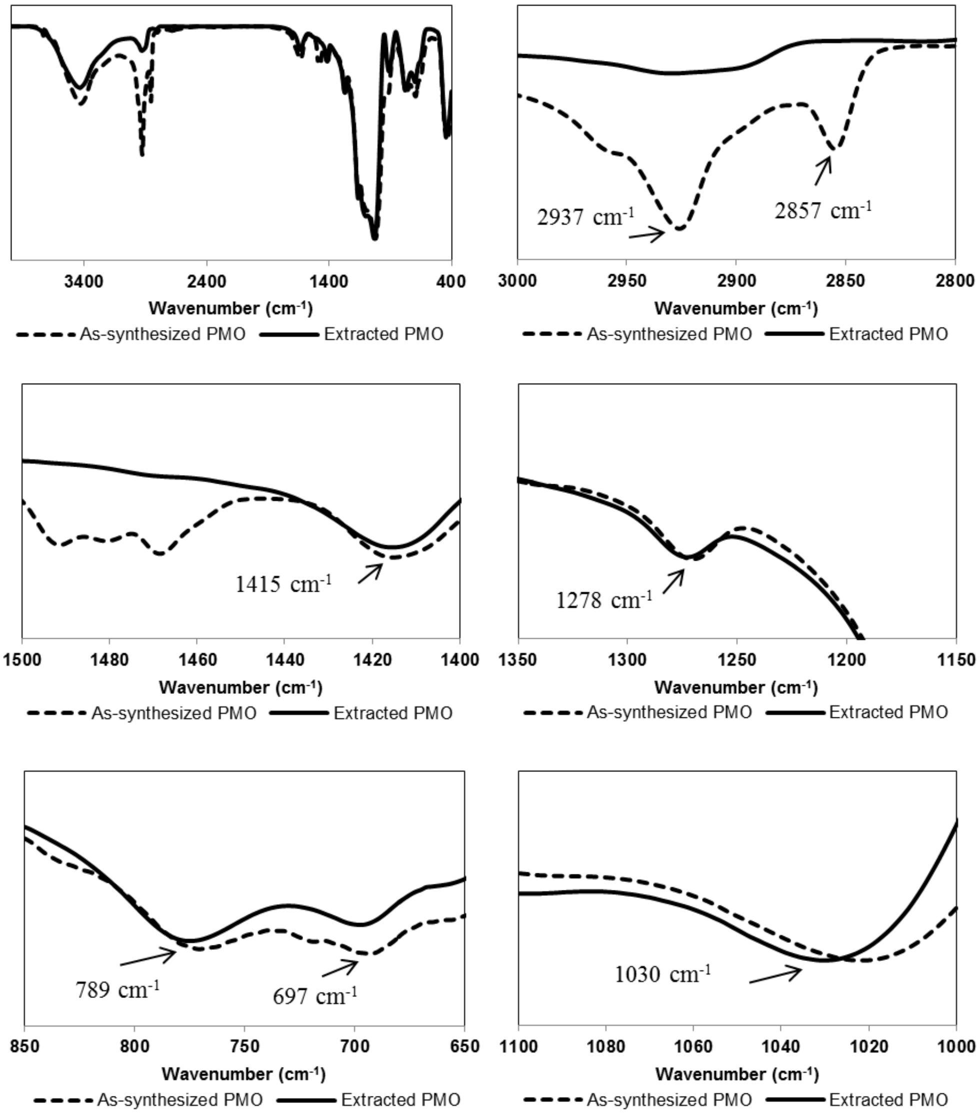

Figure 6.23 FTIR spectra of as-synthesized and extracted PMO

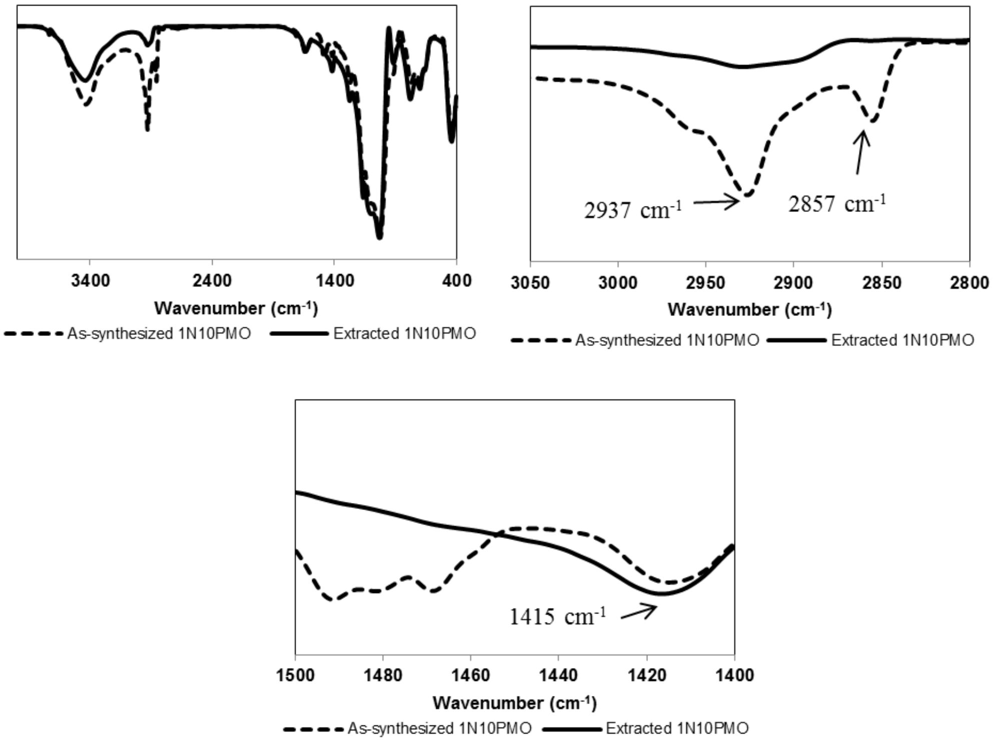

Figure 6.24 FTIR spectra of as-synthesized and extracted 1N10PMO

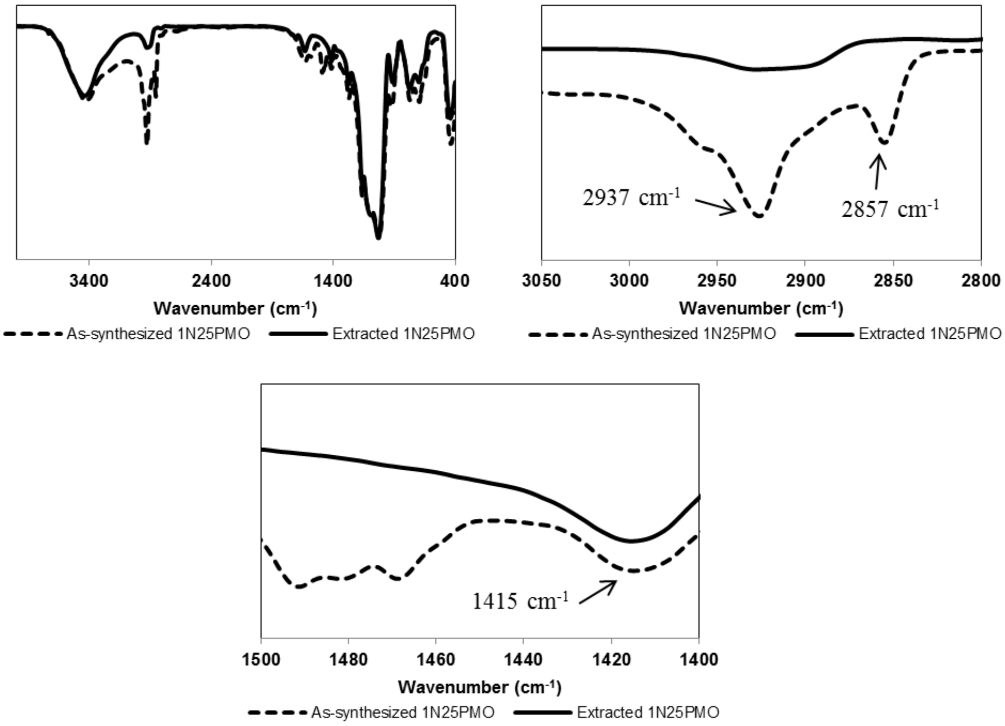

Figure 6.25 FTIR spectra of as-synthesized and extracted 1N25PMO

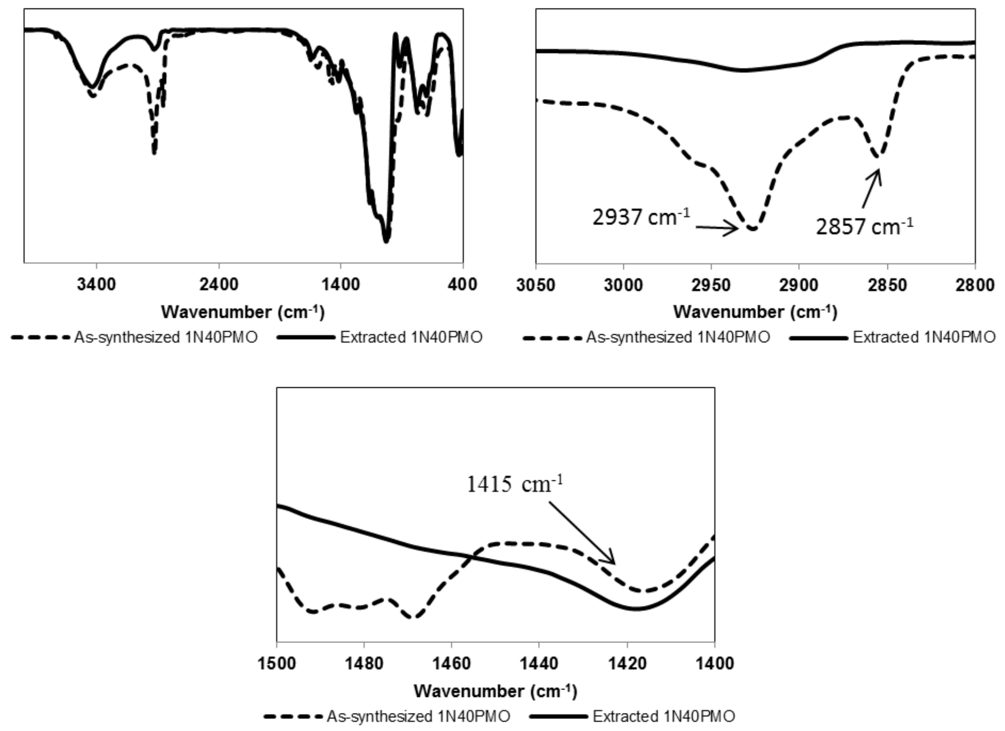

Figure 6.26 FTIR spectra of as-synthesized and extracted 1N40PMO

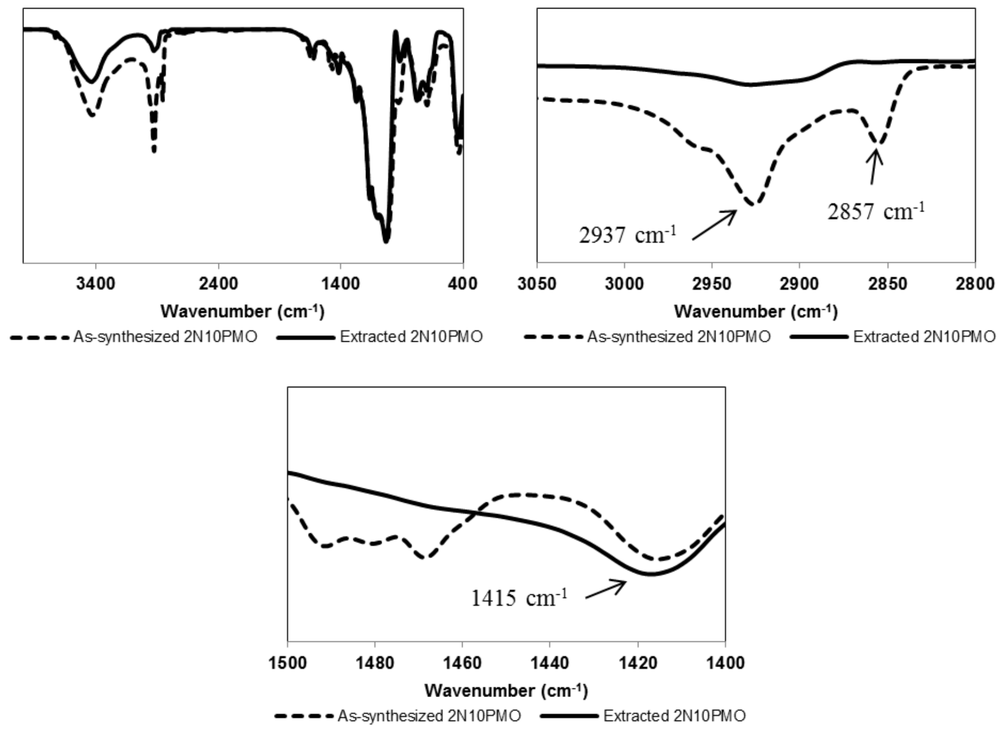

Figure 6.27 FTIR spectra of as-synthesized and extracted 2N10PMO

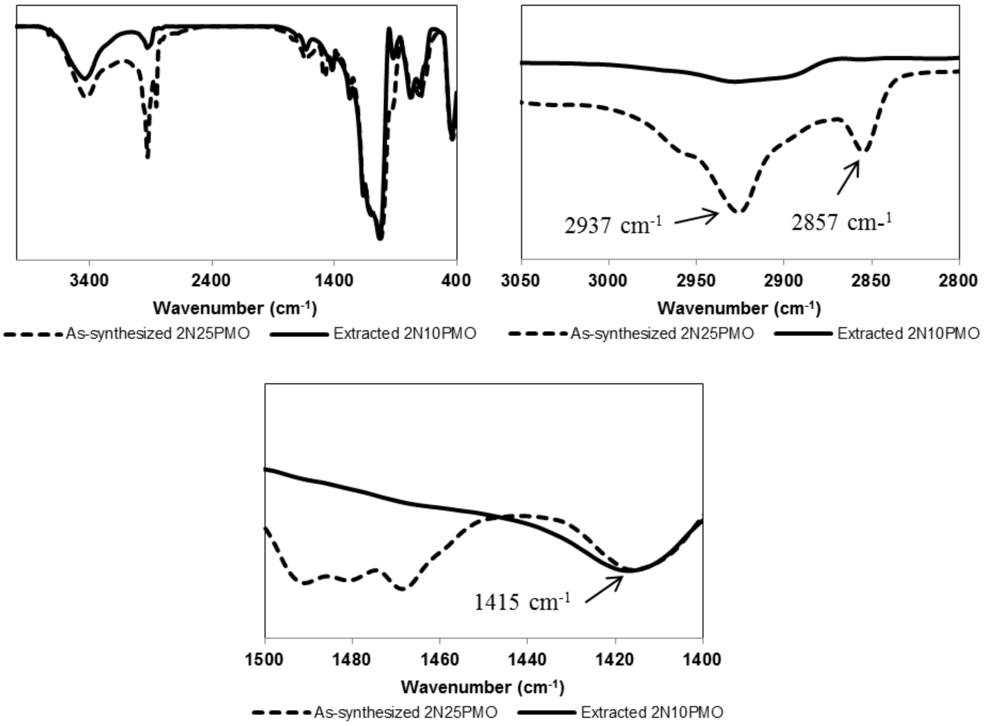

Figure 6.28 FTIR spectra of as-synthesized and extracted 2N25PMO

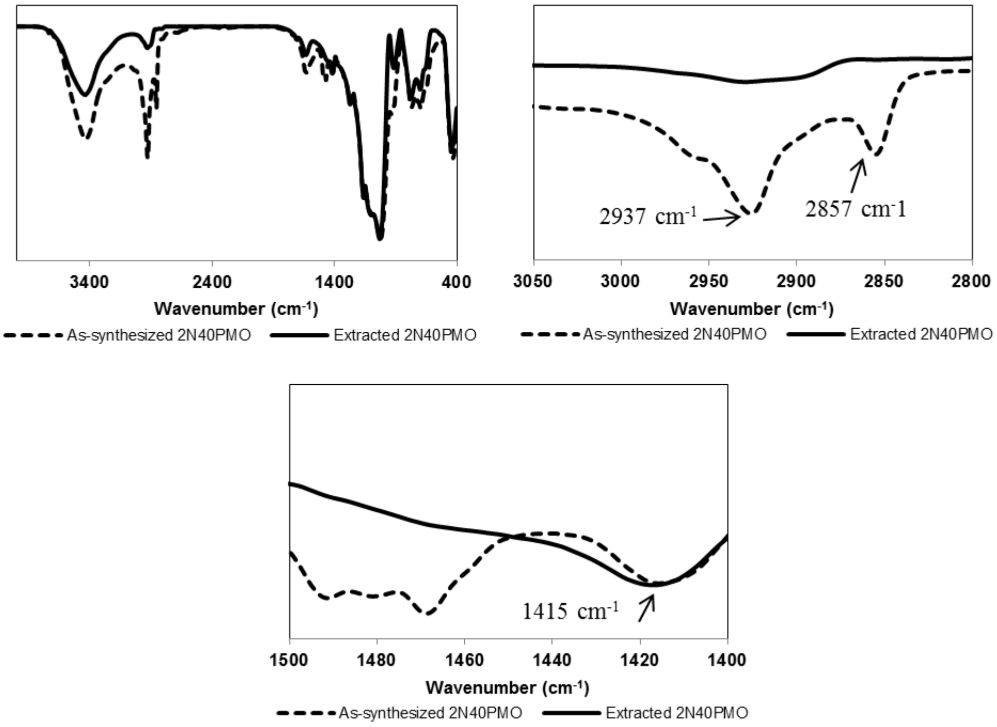

Figure 6.29 FTIR spectra of as-synthesized and extracted 2N40PMO

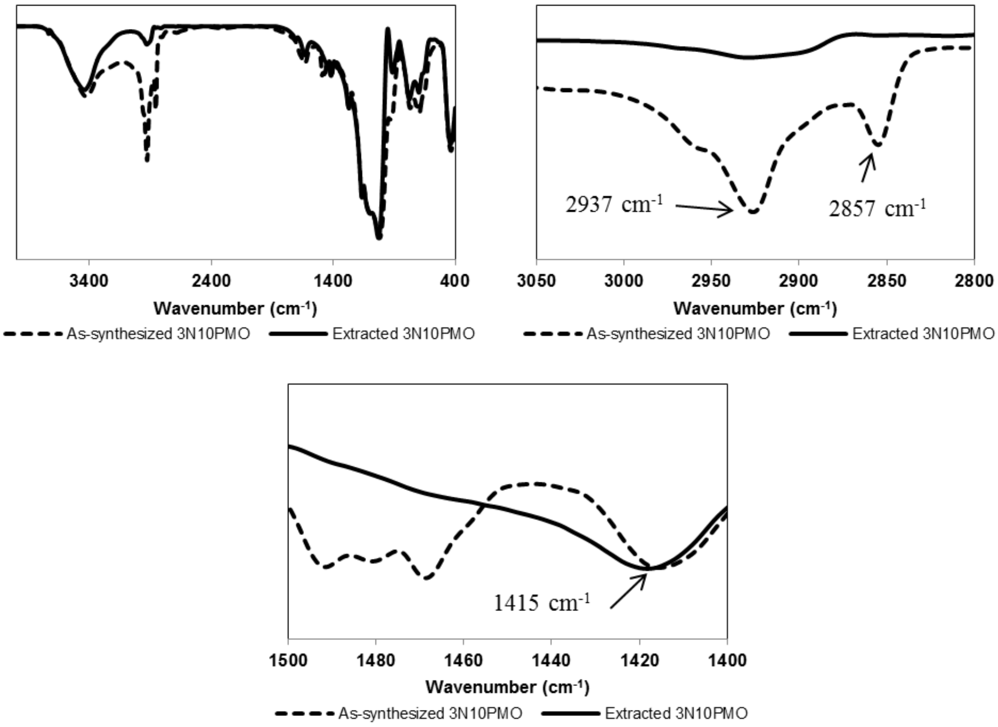

Figure 6.30 FTIR spectra of as-synthesized and extracted 3N10PMO

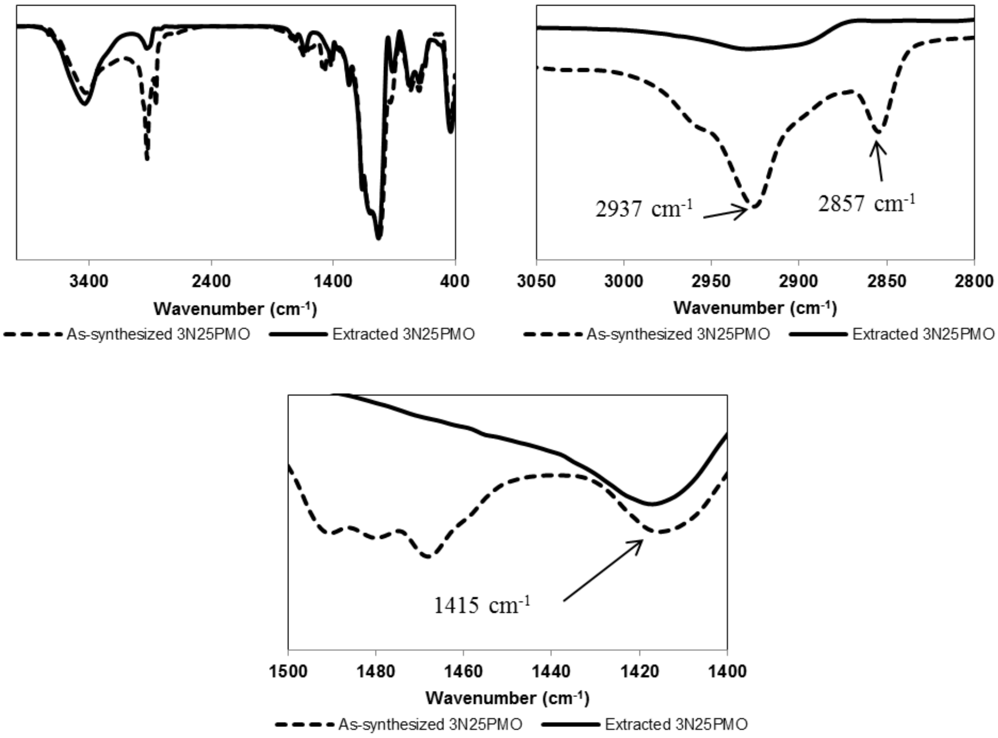

Figure 6.31 FTIR spectra of as-synthesized and extracted 3N25PMO

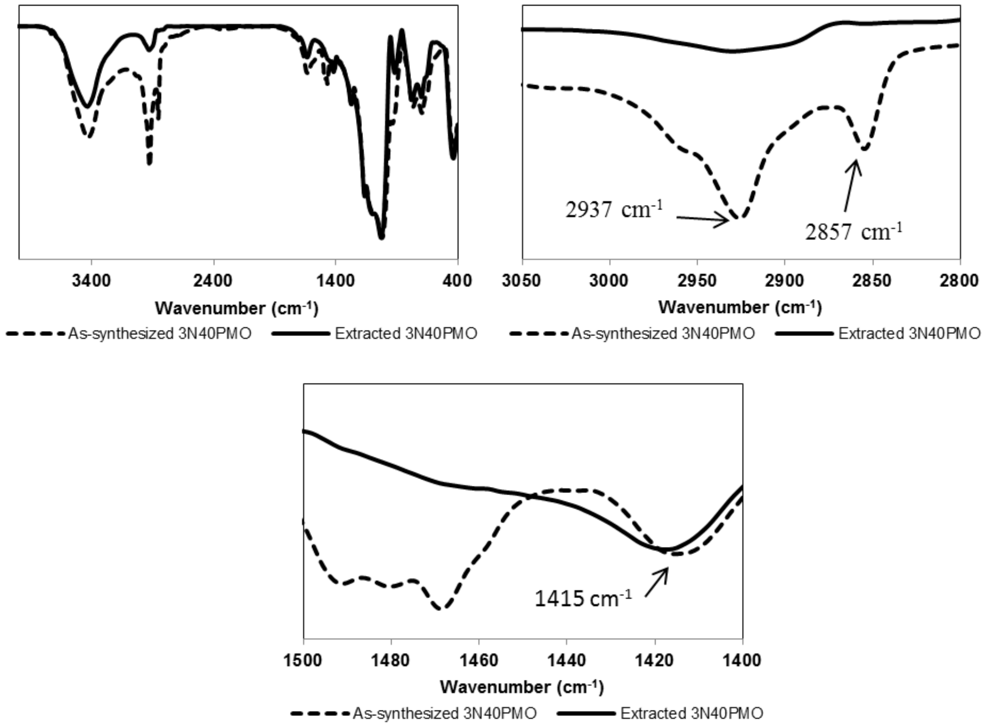

Figure 6.32 FTIR spectra of as-synthesized and extracted 3N40PMO

The band at 1415 cm^{-1} could be assigned to vibration of C-H of the bridging ethylene group [Zhang et al., 2005]. The band at 789 cm^{-1} was ascribed to the C-H stretching. The adsorption band at 697 cm^{-1} and 1278 cm^{-1} were assigned to the vibration of Si-C bonding [Wahab et al., 2004]. The bands from 1100 cm^{-1} - 1000 cm^{-1} were ascribed to the vibration of Si-O-Si stretching [Parambadath et al., 2011]. The presence of Si-O-Si stretching indicated the hydrolysis and condensation of BTSE. The vibration of Si-O-Si stretching was also found in the spectrum of HMS but the band was present at higher wave number (1088 cm^{-1}). This might be caused by the difference in silica source precursors in the synthesis processes of virgin PMO and HMS.

Figure 6.33, 6.34 and 6.35 show the comparative spectra of extracted 1NPMO, 2NPMO and 3MPMO at different concentrations of added organosilane. The stretching of the N-H at 3300 - 3400 cm^{-1} was not identified in any functionalized PMOs. This might be caused by the physisorption of water molecules which were present at the band around 3440 cm^{-1}. Figure 6.33 show the desorption bands at 789 cm^{-1}, 1415 cm^{-1} and 2930 cm^{-1} which were attributed to the vibration of C-H bond were found in the spectra of the extracted virgin and functionalized PMOs at all 3 concentrations of added organosilane. The adsorption band at 697 cm^{-1} and 1278 cm^{-1} which were assigned to the vibration of Si-C bonding and the adsorption bands from 1000 cm^{-1} - 1100 cm^{-1} which were ascribed to the vibration of Si-O-Si stretching were shown in figure 7.33, 7.34, and 7.35 respectively. Margolese et al (2000) reported that the vibration at 2900 cm^{-1} corresponding to C-H stretch vibrations increased as the concentration of functional groups in the initial mixture was increased. But in our study, we did not see this type of relationship between the pattern of IR spectrum and the concentration of the added organic functional groups. These different findings could be explained by the difference in the types of silica precursors used in the synthesis processes. In Margolese's study, pure silica was used as the source of silica. The carbon which was detected by IR spectrum came from organic functional groups only. But in our study, BTSE was used as the silica source. The carbon detectable by IR spectrum could come from two sources: from the remaining organic bridging group in the silica source and from the organic functional groups. The relationship between the pattern of IR spectrum and the concentration of the added organic functional groups was therefore obvious in Margolese's study, but not so obvious in our study. The FTIR data could be used to confirm the presence of organic moieties in the materials and also to confirm the efficiency of surfactant template removal by solvent extraction.

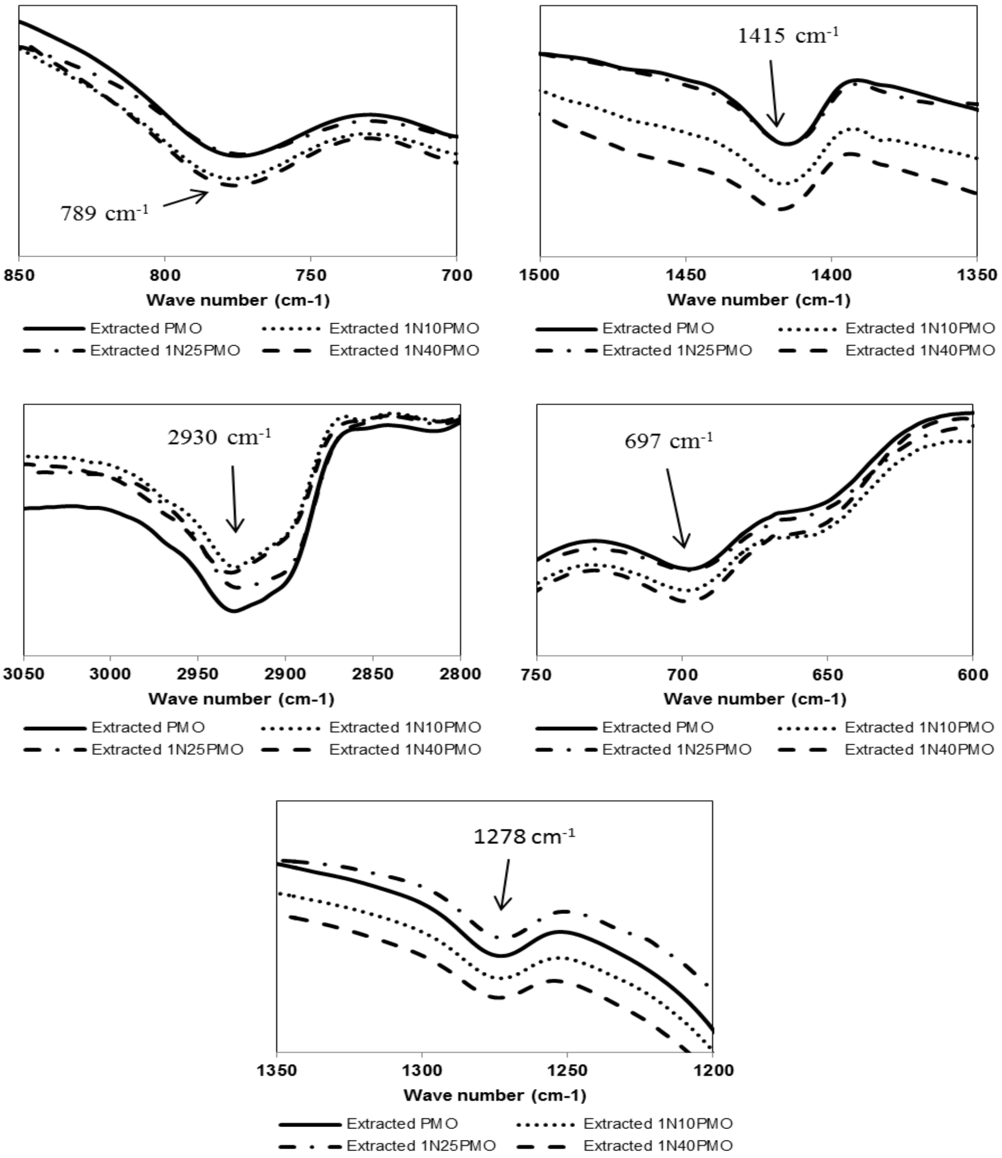

Figure 6.33 Comparative spectra of extracted 1N10PMO, 1N25PMO and 1N40PMO.

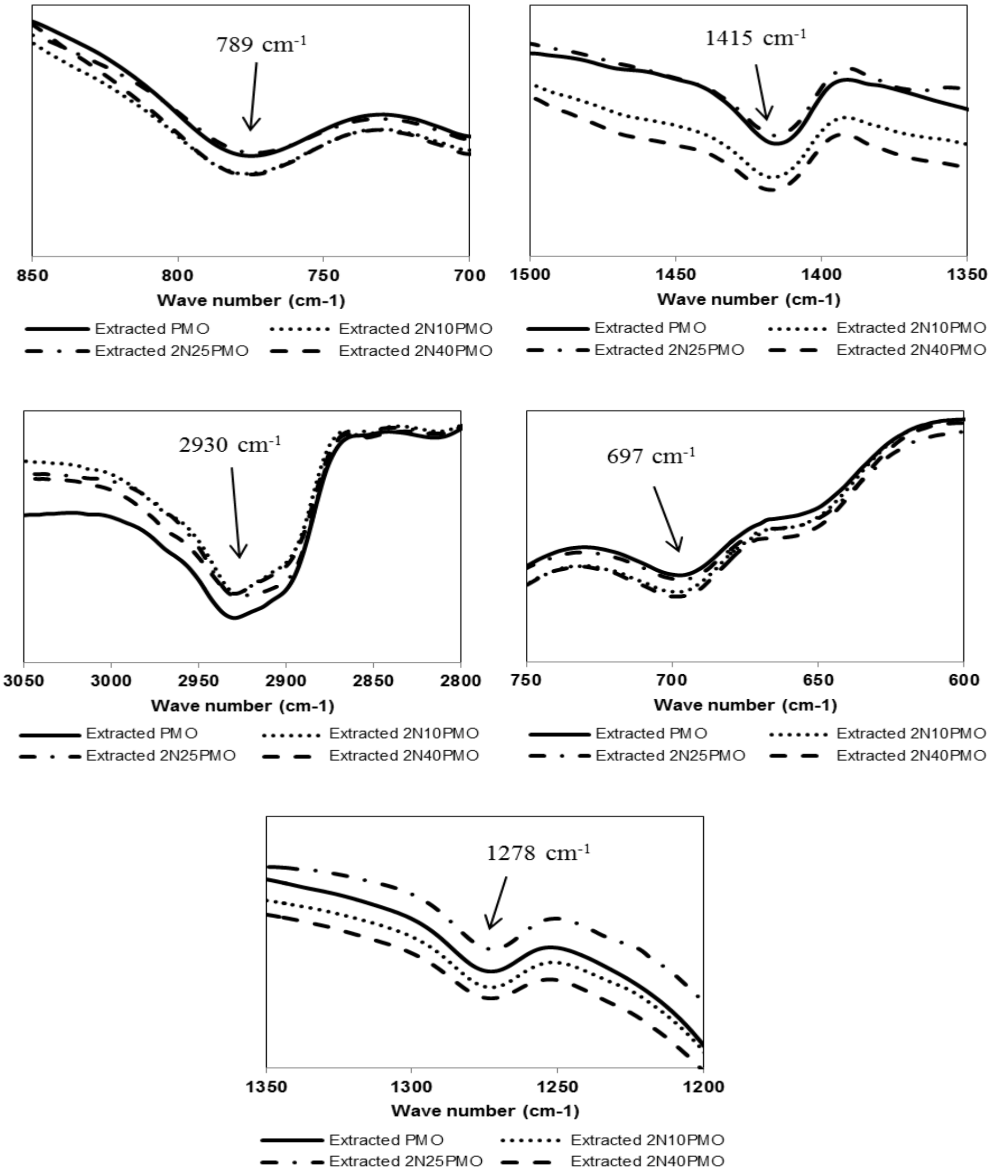

Figure 6.34 Comparative spectra of extracted 2N10PMO, 2N25PMO and 2N40PMO.

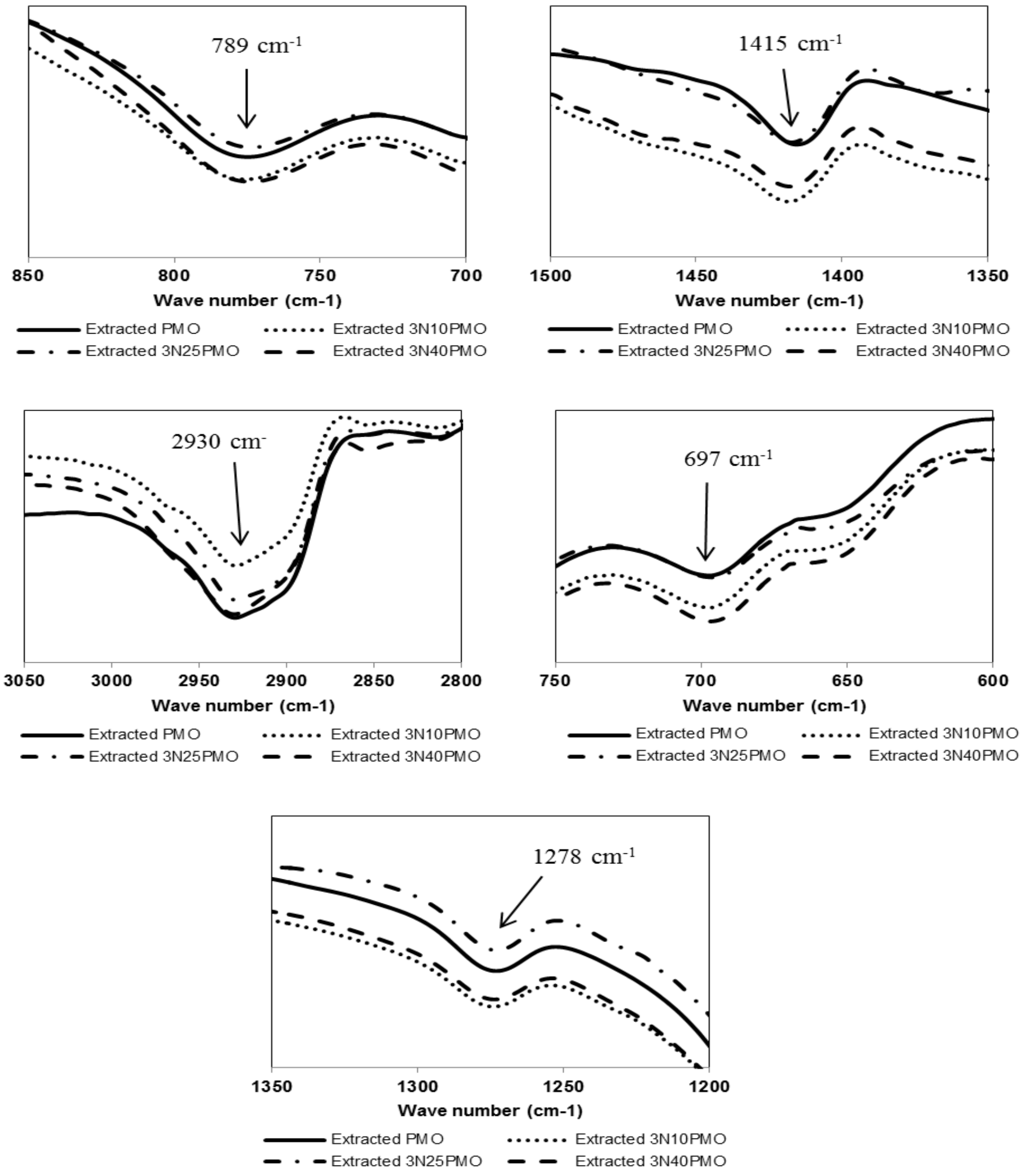

Figure 6.35 Comparative spectra of extracted 3N10PMO, 3N25PMO and 3N40PMO.

6.3.8 Zeta potential

In this study, the zeta potential of PMO and PMO derivatives were measured at pH 5, 7 and 9. The zeta potentials of all adsorbents are shown in table 6.5. The zeta potentials of these adsorbents at pH 5 ranged from -4.36 mV (PMO) up to +14.97 mV (2N40PMO) , at pH 7 from -8.46 mV (PMO) to 5.32 mV (2N40PMO) and at pH 9 from -19.30 (3N10PMO) to -7.99 mV (1N40PMO) .

Table 6.5 Zeta potentials of PMO and PMO derivatives at pH 5, 7 and 9.

Adsorbents	**Zeta potential (mv) at pH**		
	5	**7**	**9**
PMO	-4.36	-8.46	-10.29
1N10PMO	-1.59	-6.76	-18.43
1N25PMO	8.71	-4.89	-16.50
1N40PMO	10.01	3.12	-7.99
2N10PMO	7.77	-3.43	-10.29
2N25PMO	9.61	0.59	-8.41
2N40PMO	14.97	4.58	-5.86
3N10PMO	9.95	-1.11	-19.30
3N25PMO	11.28	1.96	-15.75
3N40PMO	14.70	5.32	-8.03

6.4 Conclusions

The laboratory studies to determine the physico-chemical properties of the PMO materials that we synthesized showed the following results. The XRD diffraction pattern showed evidence of a hexagonal lattice in the virgin PMO material that we synthesized. The addition of aminosilane had very little effect on the d_{100} spacing values of PMOs materials indicating stable mesophase formation in basic aqueous media. The N_2 adsorption-desorption isotherm showed that these materials had very large specific surface areas and pore volume. Their specific surface areas ranged from 963.5 m^2/g to 1252 m^2/g and their pore volumes ranged from 0.524 cm^3/g to 0.85 cm^3/g. The BET surface area and the pore volume of the functionalized PMO slightly decreased as the concentration of added n-silane increased. However these functionalized materials still have larger surface area than other materials which were functionalized with mono-amine such as HMS, MCM-41 or SBA-15. The pore sizes of these materials were in the mesoscale. Increasing of the concentration of organosilane in the reaction mixture resulted in reduction of the pore diameter of the materials. The SEM showed that the morphologies of PMO and functionalized PMO consisted mostly of irregularly shaped particles with smooth surface. The particle size of PMOs was around 1 to 10 micron. The TEM images confirmed that the synthesized PMO and PMO derivatives had well ordered meso-structure. Thermogravimetric analysis and FTIR spectrum indicated that most of the surfactant templates were removed by the solvent extraction method. Elemental analysis showed that the total nitrogen contents of PMOs functionalized with N-silane ranged from 0.36 % to 1.78 % respectively.

CHAPTER VII

REMOVAL OF CLOFIBRIC ACID BY ADSORPTION ON PERIODIC MESOPOROUS ORGANOSILICAS

7.1 Introduction

In this chapter, we report on a study into the removal of a low concentration of pharmaceutical residue (Clofibric acid) from aqueous solution by adsorption onto virgin PMO and PMO which were functionalized with three type of amino-functional groups (1N-amine , 2N-amine and 3N-amine functional groups) (1NPMOs, 2NPMO and 3NPMOS, respectively). The adsorption mechanism was investigated by analyzing the adsorption kinetics and isotherms under various conditions, and used in comparison between different adsorbates to simultaneously elucidate the potential effects of the surface functional group, adsorbent surface area, surface functional groups density, nitrogen contents and pH on the adsorption capacity.

7.2 Method

7.2.1 Adsorption kinetics

Adsorption assays were performed as batch experiments with the test pharmaceutical compound diluted to a concentration of 100 μg/L. The pH of the solution was controlled at 7 using 0.01 M phosphate buffer and the ratio of adsorbent to pharmaceutical solution was fixed at 2 g/L. The mixture was agitated in a rotary shaker at 25^{o}C at 150 rpm. The adsorption kinetics were evaluated by measuring the CFA concentration at different time intervals. The liquid taken from the adsorption mixture was filtered through a polytetrafluoroethylene syringe filter (Chrom Tech, US). The filtrate was concentrated by SPE using a 60 mg C18 cartridge (Agela, Japan) and the concentration of pharmaceutical residue remaining was measured on an Agilent 1100 HPLC with a UV detector. Taking of the liquid samples and their measurements continued until the concentrations of pharmaceutical residues reached equilibrium point.

7.2.2 Adsorption isotherm evaluation

Adsorption isotherm assays were performed as for the adsorption kinetic study above; except that the concentrations of pharmaceutical compounds were varied from 40 to 200 µg/L and samples were only taken at the equilibrium time (determined in the adsorption kinetic study above).

7.2.3 Effects of pH on the adsorption capacity of adsorbent

The effect of varying the pH on the adsorption capacity of each adsorbent was evaluated in the same manner as per the adsorption kinetic study above, except for the former the pH of the solution was adjusted to 5 or 9 using 0.01 M phosphate buffer, and for the latter the pH of the solution was controlled at 7.

7.3 Results and discussion

7.3.1 Adsorption kinetic

The kinetics of CFA adsorption are shown in Figure 7.1 as the amount of adsorbate adsorbed (q_t) over time (µg/g.min). For all adsorbents, the concentration of CFA in the solution decreased rapidly in the first 30 min and then gradually decreased thereafter until they reached equilibrium within 4 h.

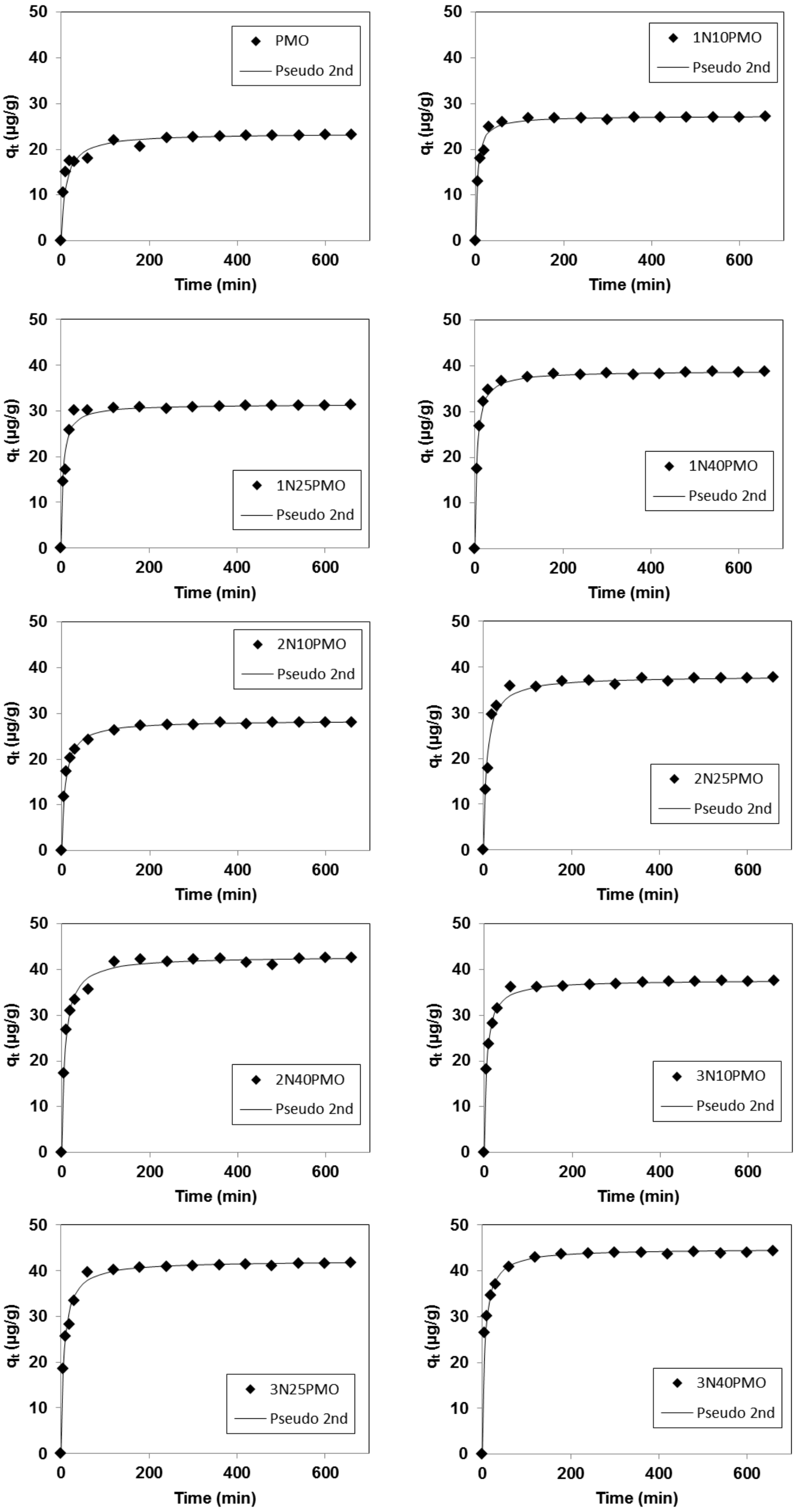

Figure 7.1 Adsorption kinetics of CFA adsorbed onto different kinds of mesoporous silicates (pH 7, 25 °C and IS 0.01M).

7.3.2 Adsorption kinetic models

To evaluate the efficiency of adsorption process pseudo-second-order and Ritchie-second-order kinetic models were used for interpretation of the experimental data.

The calculated parameters for each adsorbent and kinetic model, and the respective correlation coefficients (R^2) for the data and model, are summarized in Table 7.1. From the correlation coefficients, the adsorption of CFA onto the silicate materials is most likely represented by pseudo-second-order kinetics. Therefore, it is assumed that chemisorption is involved in the adsorption process [Pan et al., 2011].

The initial adsorption rates (h) of virgin PMO and PMOs functionalized with 1N-silane were found to range from 2.18 µg/g.min to 8.14 µg/g.min. Virgin PMO has the lowest h value. The h values of the adsorbents seemed to increase as the amount of added n-silane was increased. The half equilibrium time ($t_{0.5}$) of these adsorbents seemed to decrease when the concentration of added n-silane was increased. The functionalized PMOs (1N10PMO, 1N25PMO and 1N40PMO) had lower $t_{0.5}$ than the virgin PMO. The same pattern of relationship between the initial adsorption rate and the concentration of added silane was also found in PMOs functionalized with 2N-silane and 3N-silane. The initial adsorption rates and half equilibrium time of the adsorbents had no relationship with the types of the added functional groups. The results of this study suggested that the surface functional groups of the adsorbent had an effect on the adsorption process. The surface modification with 1N-amine, 2N-amine and 3N-amine functional groups improved the adsorption ability of the silica based porous materials.

Table 7.1 Kinetic parameters for the adsorption of CFA onto PMO and the functionalized PMO derivatives (pH 7, 25 °C and IS 0.01M).

Adsorbents	**$q_{e,\mathrm{exp}}$ (µg/g)**	**Pseudo-second order**					**Ritchie**		
		k_2x10^3 (g/µg.min)	**$q_{e,\mathrm{cal}}$ (µg/g)**	**h (µg/g.min)**	**$t_{0.5}$ (min)**	**R^2**	**k_r (L/min)**	**$q_{e,\mathrm{cal}}$ (µg/g)**	**R^2**
PMO	23.17	3.94	23.53	2.18	10.79	0.999	0.552	22.72	0.954
1N10PMO	27.16	8.18	27.32	6.11	4.47	0.997	0.397	27.32	0.993
1N25PMO	31.30	6.72	31.45	6.64	4.74	0.998	0.158	31.95	0.947
1N40PMO	38.80	5.50	38.91	8.33	4.67	0.996	0.166	40.00	0.980
2N10PMO	28.14	4.29	28.49	3.49	8.17	0.999	0.141	29.07	0.988
2N25PMO	37.70	3.39	38.02	4.91	7.74	0.998	0.098	39.37	0.979
2N40PMO	42.69	3.21	42.92	5.91	7.27	0.996	0.135	43.10	0.986
3N10PMO	37.56	4.68	37.74	6.67	5.66	0.999	0.173	38.17	0.988
3N25PMO	41.73	3.49	42.19	6.23	6.78	0.998	0.150	41.66	0.976
3N40PMO	44.43	4.05	44.84	8.14	5.51	0.996	0.191	44.44	0.996

7.3.3 Diffusion mechanism

The kinetic data were then analyzed by the Weber and Morris intraparticle diffusion and the Boyd kinetic models to determine the diffusion mechanism and to find the rate-limiting step in the adsorption process and also analyzed by the pore diffusion model to determine the pore diffusion coefficients of the adsorbents.

7.3.3.1 Weber and Morris intraparticle diffusion model

The Weber and Morris intraparticle diffusion model [Weber, 1963] can be expressed as in Eq. (7.1):

$$q_t = k_p t^{1/2} + C \qquad (7.1)$$

where k_p is the intraparticle diffusion rate constant (µg/g.min$^{1/2}$) and C is a constant relating to the thickness of the boundary layer (µg/g), which is determined from the plot of q_t versus $t^{1/2}$.

The intraparticle diffusion plot of CFA adsorbed onto different kinds of PMO is shown in Figure 7.2. The CFA adsorption plots for PMO, 1N10PMO, 1N25PMO, 1N40PMO, 2N10PMO, 2N25PMO and 2N40PMO passed through the origin. This suggested that pore diffusion is the rate-limiting step of the adsorption process for these adsorbents (i.e. PMO, 1NPMOs and 2NPMOs). But for 3N40PMO, 3N25PMO and 3N40PMO the adsorption plots did not pass through the origin. Thus, the intraparticle diffusion was not the only rate-limiting step for 3NPMOs. Rather, the external mass transfer played an important role in their adsorption process.

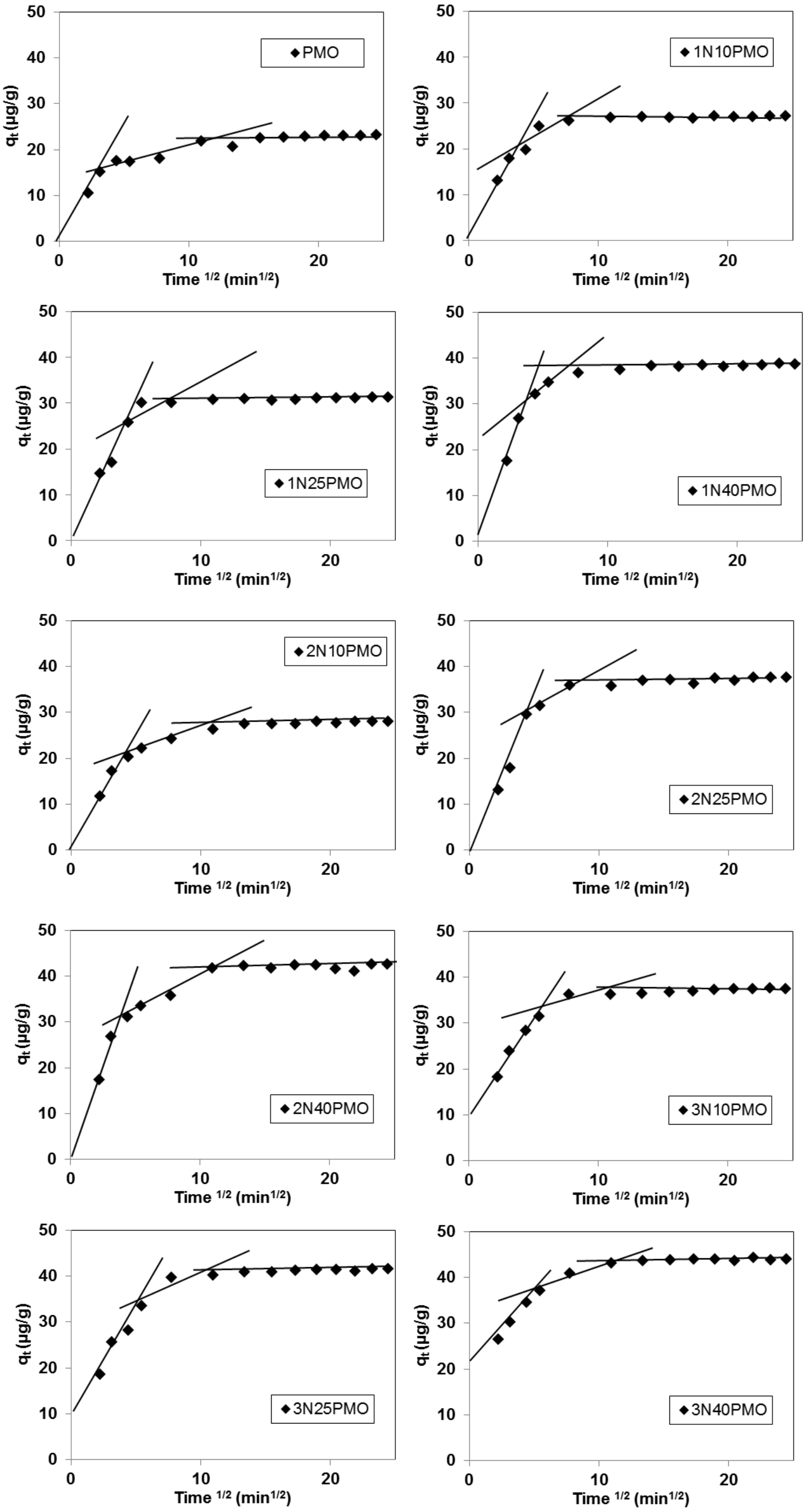

Figure 7.2 Weber and Morris intraparticle diffusion plot of CFA adsorbed onto the different kinds of PMOs (pH 7, 25 °C and IS 0.01M).

7.3.3.2 Boyd kinetic model

The Boyd kinetic model [Boyd et al., 1947; Reichenberg, 1953] can be expressed as in Eqs. (7.2-7.5):

$$F = 1 - \frac{6}{\pi^2} \sum_{n=1}^{\infty} \frac{1}{n^2} \exp(-n^2 Bt) \qquad (7.2)$$

$$F = \frac{q_t}{q_e} \qquad (7.3)$$

$$Bt = \left(\sqrt{\pi} - \sqrt{\pi - \left(\frac{\pi^2 F}{3} \right)} \right)^2 \quad \text{(for F < 0.85)} \qquad (7.4)$$

$$Bt = -0.4977 - \ln(1 - F) \quad \text{(for F > 0.85)} \qquad (7.5)$$

Where F is the fraction of pharmaceuticals adsorbed at any time point compared with the equilibrium point. The Boyd kinetic equation was applied to identify the rate-limiting step of the adsorption process. The slowest step is represented by the plot between *Bt* versus *t*. If the plots are linear and passes through the origin, then pore diffusion is the slowest step. For all adsorbents the Boyd plots of CFA passed through the origin (Figure 7.3). Thus, pore diffusion was the rate-limiting step of the adsorption process in all cases.

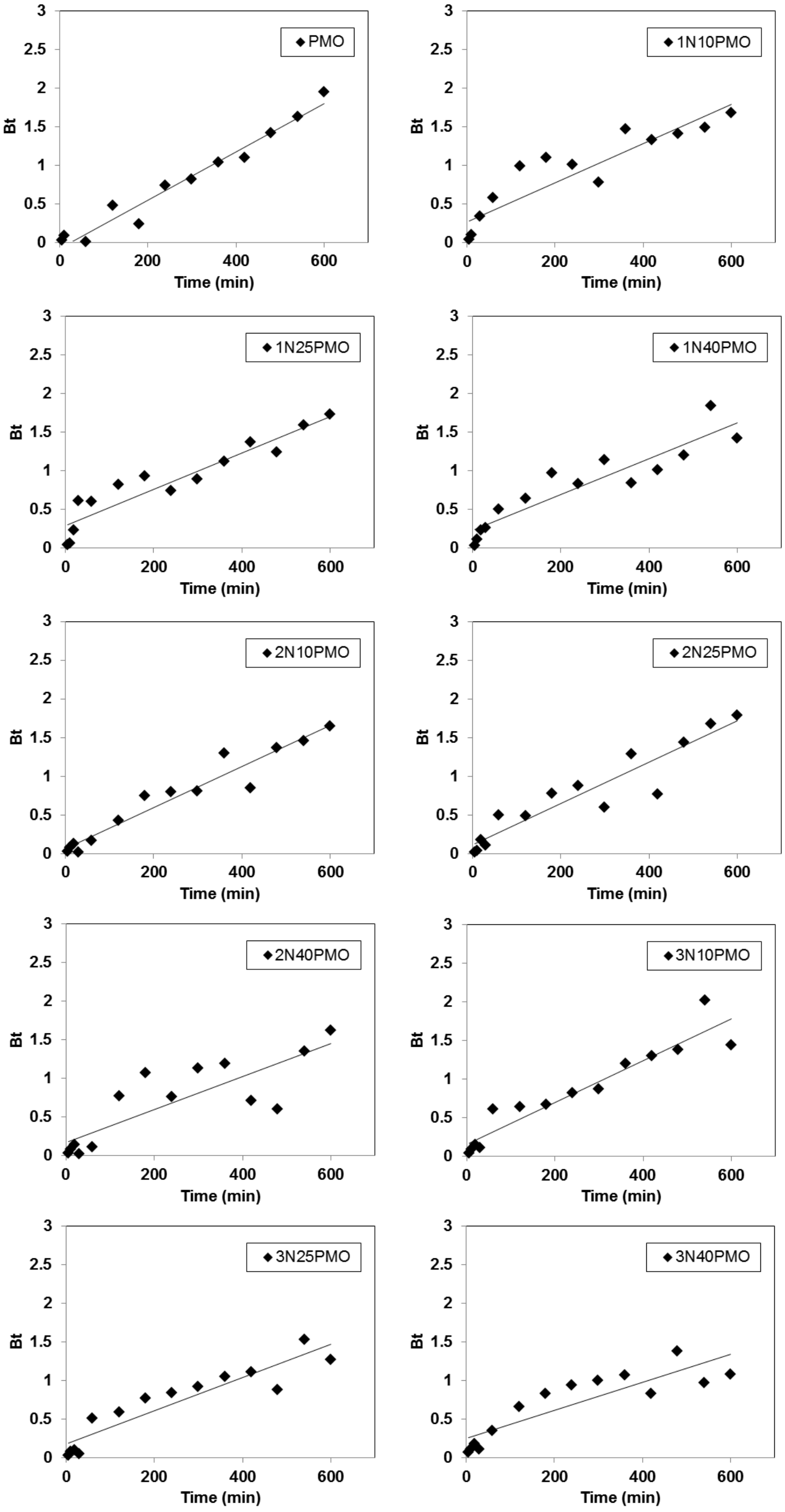

Figure 7.3 Boyd kinetic diffusion plot of CFA adsorbed onto the different kinds of PMOs (pH 7, 25 °C and IS 0.01M).

7.3.3.3 Pore diffusion (by Fick's law)

The pore diffusion model [Vermeulen, 1953] can be expressed as in Eq. (7.6):

$$\log\left(1-\left(\frac{q_t}{q_e}\right)^2\right) = \frac{4\pi Dt}{2.303d^2} \tag{7.6}$$

where D is the pore diffusion coefficient (cm^2/min) of the adsorption process, which is determined from the slope of the plot of $\log\left(1-\left(\frac{q_t}{q_e}\right)^2\right)$ versus t.

The calculated pore diffusion coefficients of all adsorbents are shown in Table 7.2. Virgin PMO has the highest D value. The D values of the materials seemed to decrease as the amount of added 1N-silane was increased. The functionalized PMOs (1N10PMO, 1N25PMO and 1N40PMO) had lower D values than the virgin PMO. The same pattern of relationship between the pore diffusion coefficient and the concentration of added silane was also found in PMOs functionalized with 2N-silane and 3N-silanes. Pore diffusion coefficient had no relationship with the types of the added functional groups. The results of this study suggested that the surface functional groups of the adsorbent had an effect on the pore diffusion process. The reduction of pore diffusion coefficient of the materials by the increasing concentration of the added organosilane could be explained by the reduction of the pore size as they were filled with organic molecules which were dispersed uniformly throughout the pores.

7.3.4 Adsorption isotherms modeling

The adsorption isotherm data were analyzed by five mathematical isotherm models (Langmuir, Freundlich, Dubinin-Radushkevich, Temkin and Linear isotherm), to model the adsorption of CFA onto the PMO and PMO derivative materials.

Table 7.2 Pore diffusion coefficient of the adsorption processes (pH 7, 25 °C and IS 0.01M).

Adsorbents	**Pore diffusion coefficient, D (x10^{-10} cm^2/min)**
PMO	7.88
1N10PMO	6.78
1N25PMO	6.59
2N40PMO	6.23
2N10PMO	6.96
2N25PMO	6.78
2N40PMO	6.05
3N10PMO	7.14
3N25PMO	5.86
3N40PMO	5.13

The calculated parameters and the correlation coefficients (R^2 value) for adsorption of CFA onto the different adsorbents are shown in Table 7.3. The Freundlich isotherm gave the highest correlation coefficient for PMO, 1N25PMO and 1N40PMO. The Langmuir isotherm gave the highest correlation coefficient for 1N10PMO, 2N10PMO, 2N25PMO, 3N10PMO and 3N40PMO. The Temkin isotherm gave the highest correlation coefficient for 2N40PMO. The Linear isotherm gave the highest correlation coefficient for 3N25PMO.

From this study the adsorption of each individual adsorbent for CFA was found to be best fitted to different isotherm models. No single model can best describe the adsorption of all adsorbents for CFA. The Langmuir isotherm model gave the highest correlation coefficients (R^2 value) for 5 of the 10 PMO adsorbents which were included in this study. The other models gave the highest correlation coefficients (R^2 value) for only 3 or less than 3 adsorbents. It could be concluded that the Langmuir isotherm model is the best model to describe the adsorption of CFA onto PMO and functionalized PMOs.

Table 7.3 Isotherm parameters for sorption of CFA (pH 7, 25 °C and IS 0.01M).

Adsorbents	Langmuir			Freundlich			D-R			Temkin			Linear	
	k_L (L/mg)	q_m (μg/g)	R^2	n	k_F	R^2	q_m (μg/g)	B (mmol/j)^2	R2	A_T (J/mg)	b_T (J/mol)	R^2	Kp (L/μg)	R^2
PMO	0.94	500	0.986	0.991	0.437	0.988	34.41	100	0.761	59.9	104.1	0.928	0.464	0.985
1N10PMO	2.00	384.61	0.933	0.887	0.470	0.912	41.73	60.0	0.639	70.9	73.39	0.928	1.038	0.892
1N25PMO	2.49	384.61	0.934	0.917	0.665	0.944	44.84	40.0	0.661	83.1	70.90	0.817	1.162	0.939
1N40PMO	8.03	166.67	0.990	0.868	1.031	0.994	34.41	30.0	0.890	118.5	56.45	0.948	1.919	0.991
2N10PMO	5.55	175.44	0.916	0.963	0.736	0.897	42.18	40.0	0.619	83.0	76.40	0.739	1.083	0.878
2N25PMO	5.69	344.83	0.992	1.107	2.324	0.989	56.49	20.0	0.820	158.9	71.92	0.931	1.564	0.991
2N40PMO	3.94	625.00	0.957	1.012	2.727	0.972	87.94	30.0	0.986	160.6	50.62	0.998	2.440	0.982
3N10PMO	6.53	125.00	0.994	0.748	0.558	0.979	62.37	30.0	0.803	103.1	49.91	0.865	2.381	0.962
3N25PMO	4.03	555.56	0.994	0.981	2.269	0.994	65.87	20.0	0.871	178.9	59.22	0.961	2.384	0.995
3N40PMO	4.33	909.09	0.997	0.932	3.477	0.996	85.83	10.0	0.893	224.4	44.70	0.956	4.607	0.996

7.3.5 Adsorption mechanism

7.3.5.1 Effect of functional groups

The adsorption capacity of PMO and the functionalized PMO adsorbents at pH 7 are shown in Figure 7.4. Analysis of that for PMO and the functionalized derivatives allows the effect of different surface functional groups, hydroxyl (silanol), 1N-amine, 2N-amine and 3N-amine, on the adsorption capacity of the adsorbents to be inferred.

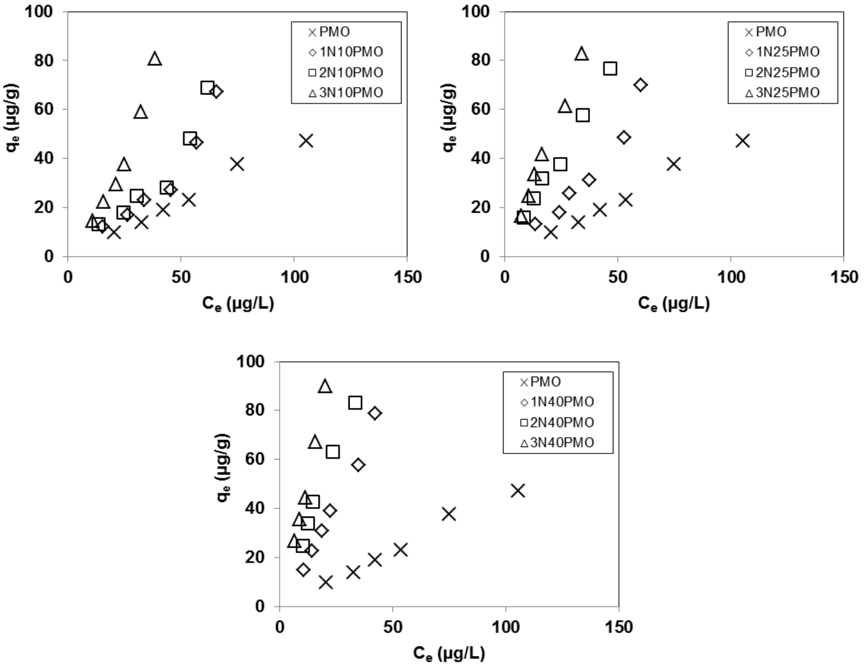

Figure 7.4 Adsorption capacity of PMOs with different functional groups (pH 7, 25 °C and IS 0.01M).

For adsorption of CFA, there are three possible mechanisms for their adsorption onto PMO and the functionalized PMO derivatives. The first mechanism is electrostatic interaction (by Coulomb's law) between the deprotonated CFA molecules and the surface charges of the adsorbents. The second mechanism is hydrogen bonding, a form of dipole-dipole interaction, and the third mechanism is hydrophobic interactions such as Van der Waals interaction, ¶-¶ electron acceptor-donor, etc. In this study, the adsorption capacities of functionalized PMOs were found to be higher than the virgin PMO. At pH 7 CFA's molecules have negative charges. The molecules of PMO, 1N10PMO, 1N25PMO, 2N10PMO and 3N10PMO also have net negative surface charges, but the molecules of the rest of functionalized PMOs have net positive surface charges (See Table 6.5). The enhancement of the adsorption of CFA onto the adsorbents which have positive surface charges (i.e. 1N40PMO, 2N25PMO, 2N40PMO, 3N25PMO and 3N40PMO) could be explained by the electrostatic interaction between the CFA's and the adsorbent's molecules. From the measurement in this study, PMO was found to have a zeta potential of -8.46 mv. Compared with all other adsorbents, PMO has the highest negative surface charges. The electrostatic repulsion between the adsorbent's and CFA's molecules is therefore highest when the adsorbent is PMO. The enhancement of the adsorption of CFA after surface modification of the adsorbents having negative surface charge (1N10PMO, 1N25PMO, 2N10PMO and 3N10PMO) could therefore be explained by the reduction in electrostatic repulsion. The increase in adsorption capacity of functionalized PMOs after modification with 1N-amine, 2N-amine or 3N-amine functional groups could be explained by either the enhancement of the electrostatic interaction or the reduction of the electrostatic repulsion between the CFA's and adsorbent's molecules.

The adsorption capacities of the adsorbents for CFA were ranked (highest to lowest adsorption capacity) as 3NPMOs > 2NPMOs > 1NPMOs > PMO. This could be explained by the electrostatic interaction. The zeta potential of the adsorbents functionalized with the different types (but same concentration) of organosilane was different. The zeta potentials of the adsorbents functionalized with different types of organosilane were ranked (highest to lowest) as 3NPMOs > 2NPMOs > 1NPMOs. This might be related to the differences in length and amount of nitrogen contents of the functional groups which were dispersed at the adsorbents surface. The zeta potential of the extracted 3NPMOs samples was higher than the extracted 1NPMOs and 2NPMOs samples because 3N-amine functional group is longer and contains higher amount of nitrogen content than 1N-amine and 2N-amine functional groups. The adsorption capacity of 3NPMOs was highest because their zeta potential was highest, or in other words higher than 2NPMOs and 1NPMOs. So it could be concluded that the adsorption capacity of the functionalized PMOs was affected by the type of added amine functional groups (i.e. 1N-amine, 2N-amine or 3N-amine).

7.3.5.2 Effect of the adsorbent's surface area

Comparative analysis of the adsorbent capacity of PMO and PMO derivatives (Figure 7.5) allows the effect of the adsorbent's surface area on the adsorption of CFA to be inferred. From this study, the adsorption capacities per surface area and per weight of the adsorbents for CFA showed a similar trend, being (highest to lowest adsorption capacity) 3NPMOs > 2NPMOs > 1NPMOs > PMO. So it could be concluded that the adsorption capacities of functionalized PMOs were increased because of the modification with organic amine functional groups, not because of the difference in their surface areas.

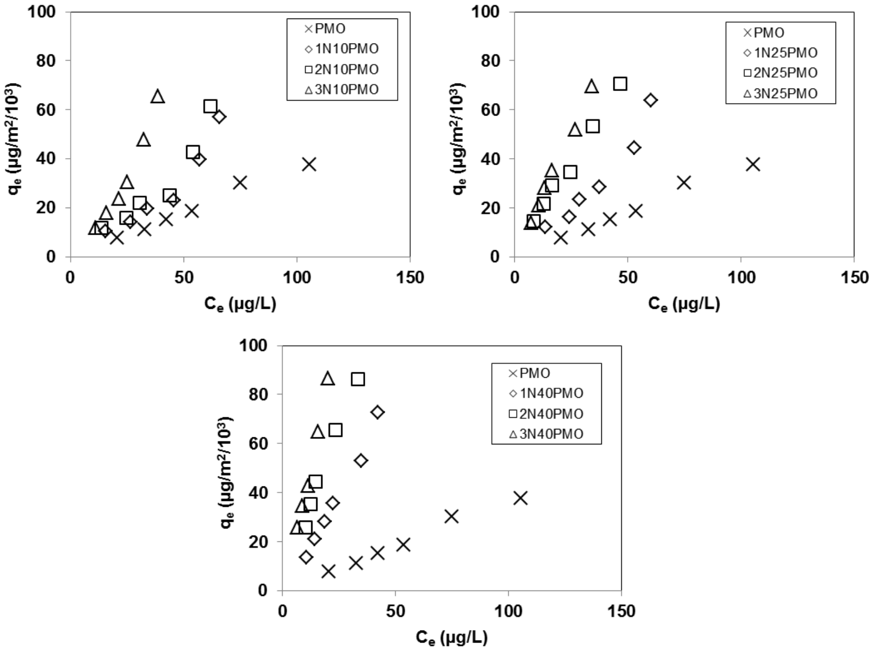

Figure 7.5 Adsorption capacity of PMOs with different functional groups per surface area (pH 7, 25 °C and IS 0.01M).

7.3.5.3 Effect of surface functional groups density

Figure 7.6 showed the adsorption capacities per surface area of CFA onto PMO and functionalized PMOs. As shown in this figure, the adsorption capacity of PMO functionalized with 1N-silane increased as the concentration of added 1N-silane increased (1N40PMO > 1N25PMO > 1N10PMO). This could be correlated with the increase in density of the 1N-amine functional groups on the adsorbent's surface. The increase in concentration of the 1N-silane in the reaction mixture leads to the increase in density of the amine functional groups at the adsorbent's surface. The increased amount of organic functional groups also increased the zeta potential of the adsorbents. The same pattern of relationship between the adsorption capacity and the concentration of added silane was also found in PMOs functionalized with 2N-silane (2N40PMO > 2N25PMO > 2N10PMO) and 3N-silane (3N40PMO > 3N25PMO > 3N10PMO). So it could be concluded that the adsorption capacity of the functionalized PMOs was affected by the density of 1N-amine, 2N-amine and 3N-amine functional groups on the adsorbent's surface.

7.3.5.4 Effect of nitrogen contents in the adsorbents

The adsorption capacities of the adsorbents per nitrogen contents in the adsorbents were determined to evaluate the effect of the nitrogen contents in the adsorbents on their adsorption capacities. The adsorption capacities of the adsorbents per nitrogen content are shown in Figure 7.7. The adsorption capacities per nitrogen content of the adsorbents with different concentrations of added organosilane were different. PMO functionalized with the 10% of organosilane had higher adsorption capacity per nitrogen content than PMO functionalized with higher concentrations of organosilanes (1N10PMO > 1N25PMO > 1N40PMO, 2N10PMO > 2N25PMO > 2N40PMO and 3N10PMO > 3N25PMO >3N40PMO). 1N10PMO had higher adsorption capacities per nitrogen content than 1N25PMO and 1N40PMOs. There was no relationship between the adsorption capacities per nitrogen content and the density of the organic functional groups. The adsorption capacities per weight or per surface area of the adsorbents functionalized with higher concentration of added organosilane were increased because of the increased amount of organic functional groups on the surface of the adsorbent, not because of the increased amount of nitrogen contents in the adsorbent. This study results suggested that nitrogen contents, from functionalization process with organic amine functional groups were not all present on the surface of the adsorbents, some of them were present in the silica wall of the adsorbents.

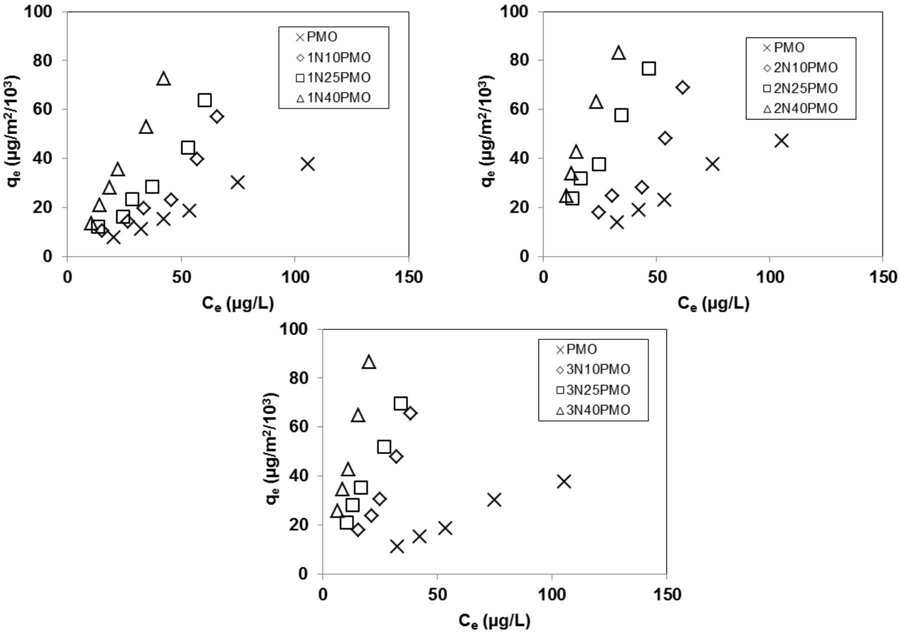

Figure 7.6 Adsorption capacity of PMOs with different surface functional group densities per surface area (pH 7, 25 °C and IS 0.01M).

7.3.5.5 Effect of pH

The adsorption of CFA onto PMO and functionalized PMO derivatives were performed at pH 5, 7 and 9 to study the effect of pH on their adsorption capacity. The adsorption capacity of the periodic mesoporous organosilicas was dependent on the pH. Their adsorption capacity was highest at pH 5 and lowest at pH 9 (Figure 7.8). The adsorption capacity of the adsorbents were decreased when the pH of the solution were increased. This could be explained by electrostatic interaction between CFA and the adsorbents. It could be due to either the reduction of electrostatic attraction or the increase of electrostatic repulsion. At pH 5, some adsorbents had a net negative surface charge but the others had a net positive surface charge (Table 6.5). At pH 9, all had negative surface charge. For all adsorbents, the number of negative charges on the surface of the adsorbents was increased when the pH of the solution was increased. At pH 5, the electrostatic attraction was highest (or electrostatic repulsion was lowest). At pH 9, the electrostatic attraction was lowest (or electrostatic repulsion was highest). This could explain why the adsorption capacity was lowest at pH 9 and highest at pH 5.

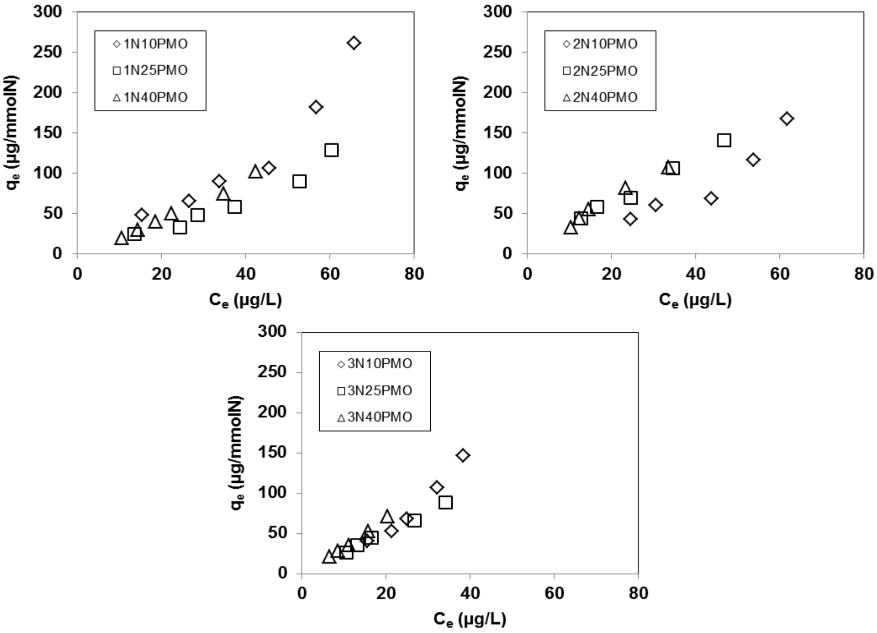

Figure 7.7 Adsorption capacity of PMOs with different surface functional group densities per nitrogen content (pH 7, 25 ^{o}C and IS 0.01M).

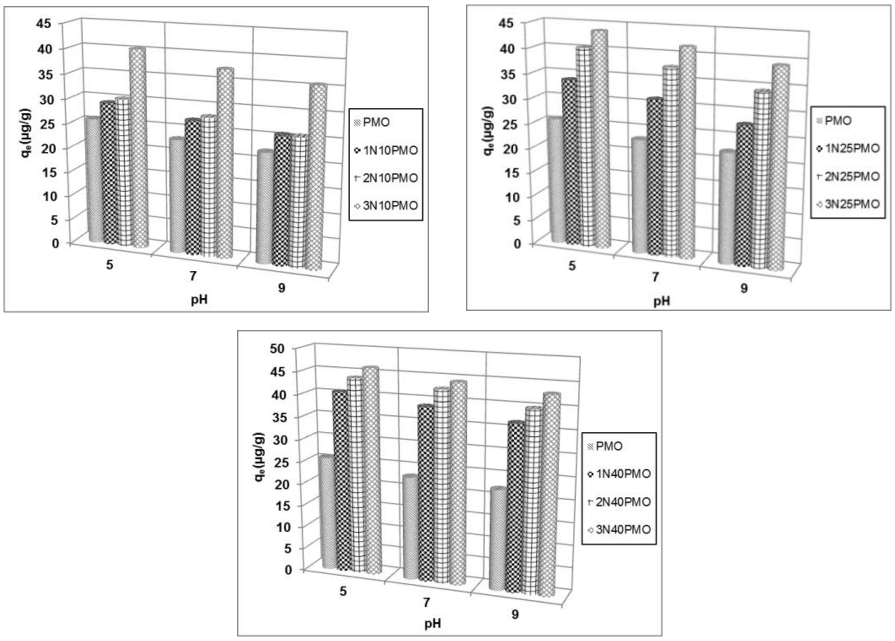

Figure 7.8 Adsorption capacity of PMOs at different pH (25 ^{o}C and IS 0.01M).

7.4 CONCLUSIONS

From the adsorption kinetics study, it was found that the adsorption of CFA onto all adsorbents decreased rapidly in the first 30 min and then gradually decreased thereafter until they reached equilibrium within 4 h. The adsorption of CFA onto the silicate materials is most likely represented by pseudo-second-order kinetics. Virgin PMO has the lowest initial adsorption rate. The initial adsorption rate of the adsorbents seemed to increase as the amount of added n-silane was increased. From the diffusion mechanism study, pore diffusion was found to be the rate-limiting step of the adsorption process for these adsorbents. Pore diffusion coefficient seemed to decrease as the concentration of added silane was increased. This reduction of pore coefficient could be explained by the reduction of the size of the pores as they were filled with organic molecules which were dispersed uniformly throughout the pores. From the adsorption isotherm data analysis, Langmuir isotherm model was found to be the best model to describe the adsorption of CFA onto PMO and functionalized PMOs. From the adsorption mechanism study, the adsorption capacity of functionalized PMO was found to be higher than the virgin PMO's. Surface modification with amine functional groups increased the adsorption capacity. This increase in adsorption capacity of functionalized PMOs after modification could be explained by either the enhancement of the electrostatic interaction or the reduction of the electrostatic repulsion between the CFA's and adsorbent's molecules. The adsorption capacity of the functionalized PMOs varied with the type and the density of the amine functional groups on the adsorbent's surface. The adsorption study of pharmaceuticals onto the adsorbents at various pH (5, 7 and 9) showed that the adsorption capacity of the periodic mesoporous organosilicas varied with pH. The adsorption capacity was highest at pH 5 and lowest at pH 9. The adsorption capacity of the adsorbent decreased when the pH of the solution was increased. This could be explained by electrostatic interaction between CFA and the adsorbents.

CHAPTER XIII
CONCLUSIONS AND RECOMMENDATONS

8.1 Conclusions

HMS, A-HMS, M-HMS, SBA-15, MCM-41, PMO and amino-functionalized PMOs were synthesized and characterized. All of the porous materials were synthesized via surfactant template method. A-HMS and M-HMS, were synthesized by modifying the surface of virgin HMS with two different types of organosilane, i.e. mercaptoprpyltrimethoxysilnae and aminopropyltriethoxysilane via direct co-condensation method. Functionalized PMOs were synthesized by surface modification of PMO with mono-, di- or triamino-organoalkoxysilane. The physicochemical properties of the synthesized materials were investigated by XRD, SEM, TEM, N_2 adsorption-desorption isotherm, TGA, DTA, elemental analysis, FTIR, acid/base titration, water contact angle and zeta potential analysis.

The physico-chemical properties of the synthesized materials were revealed. XRD patterns of the synthesized materials showed that they were porous materials with well ordered hexagonal framework. The SEM micrograph showed that HMS and M-HMS had similar morphology. Both had uniform aggregates of small distinct particles (diameter 0.1 to 0.2 micron). A-HMS had different morphology. It had particles which looked like sponge balls. These sponge balls consisted of aggregates of small particles. The small particles of A-HMS were a little bit smaller than those of HMS and M-HMS. The morphology of SBA-15 and MCM-41 were very different from those of HMS and HMS derivatives. SBA-15 had larger particles which looked like bundles of threads. These particles consisted of many ropelike domains of relatively uniform size which aggregated into wheat-like macrostructures. MCM-41 had mostly irregularly shaped particles. The morphology of PMO and functionalized PMO consisted mostly of irregularly shaped particles with smooth surface. The particle size of PMOs was around 1 to 10 micron. The TEM images confirmed that the synthesized PMO and PMO derivatives had well ordered meso-structure. The nitrogen gas adsorption-desorption isotherm showed that the pore sizes of the synthesized materials were in the mesoscale. The results of elemental and thermogravimetric analysis and FTIR spectra confirmed the presence of organic functional groups in the functionalized HMS that we synthesized. TGA and FTIR spectrum indicated that most of the surfactant templates in our synthesis of PMO were removed by the solvent extraction method. Surface characteristics of HMS were changed after functionalization with organic functional groups.

After the physico-chemical study, the synthesized materials were used in the adsorption study. HMS, A-HMS, M-HMS, SBA-15 and MCM-41 were used in the study on removal of low concentration of five pharmaceutical compounds (DCF, CBZ, NAP, CFA and ACT) from aqueous solution by adsorption. PMO and functionalized PMO were used for studying the removal of CFA from aqueous solution.

From adsorption kinetics study, adsorption of all pharmaceuticals onto all adsorbents was found to decrease rapidly in the first 30 min. and reached equilibrium within 10 h. The adsorption of all pharmaceuticals followed pseudo-second order kinetic model. Among HMS materials, M-HMS had the highest initial adsorption rate for DCF, CBZ and NAP. But for CFA and ACT adsorption, A-HMS had the highest initial adsorption rate. Among PMO materials, virgin PMO had the lowest initial adsorption rate. The initial adsorption rate of PMOs seemed to increase as the amount of added n-silane was increased. From diffusion mechanism study, intraparticle diffusion was not the only rate-limiting step in the adsorption process of HMS materials for DCF, CBZ, NAP and CFA. Rather, the external mass transfer played an important role in the adsorption process of these compounds. But in the adsorption process of ACT, pore diffsion was the rate-limiting step. For the adsorption process of CFA onto PMO materials, pore diffusion was the rate-limiting step. Pore diffusion coefficient seemed to decrease as the concentration of added silane was increased.

From the adsorption isotherm data analysis, it was found that the adsorption data of DCF, CBZ, NAP and CFA onto HMS materials best fitted the Linear isotherm model. But for the adsorption data of ACT, the Langmuir model was better correlated. Freundlich also fitted well and was the second best fitted model for the adsorption data of all pharmaceuticals. For the adsorption data of CFA onto PMO and functionalized PMOs, Langmuir isotherm was the best model to describe the adsorption data.

From the adsorption mechanism study, the adsorption capacity, at pH 7, of HMS materials for CBZ, DCF and NAP was found to be ranked (highest to lowest adsorption capacity) as M-HMS > HMS > A-HMS. The modification of HMS with mercapto functional group increased its adsorption capacity. For adsorption of CFA and ACT, the adsorption capacity was ranked in descending order as A-HMS > HMS > M-HMS. The adsorption capacity of HMS for these two pharmaceuticals was increased after modification with amino functional group. The adsorption capacity of functionalized PMOs for CFA was higher than the virgin PMO. Surface modification of PMO with amine functional group increased its adsorption capacity for this pharmaceutical. Comparative analysis of the adsorption capacity of HMS, SBA-15 and MCM-41 showed that the adsorption capacity of the pure silicate adsorbents varied directly with their surface areas. The adsorption capacity of functionalized PMOs varied with the type and density of the amine functional groups on the adsorbent's surface. The adsorption study of pharmaceuticals onto the adsorbents at variuos pH (5, 7 and 9) showed that the adsorption capacity of HMS, functionalized HMSs, PMO and functionalized PMOs varied with pH. There was no consistent relationship between the adsorption capacity of PAC with respect to pH changes. The adsorption capcity of PMOs for CFA was highest at pH 5 and lowest at pH 9. The adsorption capacity of PMOs decreased when the pH of the solution was increased.

The results of the study on the adsorption of HMS materials for pharmaceuticals in mixed solute solution suggested that in the process of adsorption of HMS and M-HMS for DCF, CBZ and NAP in which hydrogen bonding and hydrophobic interactions were the main mechanism of adsorption, there was a competition between each pharmaceutical to adsorb to M-HMS and HMS. The adsorption capacity in this case might be related to the molecular size of the adsorbates. But in case of selective adsorption of A-HMS for acidic pharmaceuticals such as DCF, NAP and CFA which have negatively charged molecules, the adsorption capacity varied with the pK_a values of the adsorbates.

8.2 Recommendations

1) To better understand the process of synthesis of organic-inorganic hybrid porous materials from silica based porous material (HMS), either surface modification with other organic functional groups (other than amino and mercapto functional groups) via direct co-condensation method or surface modification with amino and mercapto functional groups but via different method such as grafting should be tried.

2) To better understand the synthesis process of periodic mesoporous organosilica materials (PMO), we should try to synthesize other kinds of PMO using other types of silica source precursors.

3) To better understand the functionalization of periodic mesoporous organosilica materials (PMO), surface modifiction of PMO using other types of organic functional group should be tried.

4) The adsorption study should be expanded to evaluate the adsorption capacity of HMS and PMO materials for other substances such as heavy metals or dyes or other pharmaceuticals.

5) Selective or competitive adsorption study should be expanded by adding other substances commonly found in waste water into the mixed solute solution

6) Adsorption studies should be done using the materials to be synthesized in the future plan.

REFERENCES

Al-Ghouti, M.A., Khraisheh, M.A.M., Ahmad, M.N.M., and Allen, S.J. Adsorption behaviour of methylene blue onto Jordanian diatomite: A kinetic study, Journal of Hazardous Materials. 165 (2009): 589-598

Al-Muhtaseb, A., Ibrahim, K., Albadarin, A., Ali-khashman, O., Walker, G.M., and Ahmad, M.N.M. Remediation of phenol-contaminated water by adsorption using poly(methyl methacrylate) (PMMA). Chemical Engineering Journal. 168 (2011): 691-699.

Ahmad, M.A., and R. Alrozi. Optimization of preparation conditions for mangosteen peel- based activated carbons for the removal of remazol brilliant blue R using response surface methodology. Chemical Engineering Journal. 165 (2010): 883- 890.

Ahmad, M.A., and R. Alrozi. Removal of malachite green dye from aqueous solution using rambutan peel-based activated carbon: Equilibrium, kinetic and thermodynamic studies. Chemical Engineering Journal. 171 (2011): 510-516.

Allen, S.J., Gan, Q., Matthews, R., and Johnson, P.A. Comparison of optimised isotherm models for basic dye adsorption by kudzu. Bioresource Technology. 88 (2003) 143-152.

Asefa, T., MacLachlan, M.J., Coombs, Neil., and Ozin, G.A. Periodicmesoporous organosilicas with organic groups inside the channelwalls. Nature. 402 (1999): 867-871

Beck, J.S., Vartuli, J.C., Roth, W.J., Leonowicz, M.E., Kresge, C.T., Schmitt, K.D., Chu, C.T.W., Olson, D.H., Sheppard, E.W., Mccullen, S.B., Higgins, J.B., and Schlenker, J.L. A New family of mesoporous molecular sieves prepared with liquid crystal templates. Journal of American Chemical society. 114 (1992): 10834-10843.

Bendz, D., Paxeus, N.A., Ginn, T.R., and Loge, F.J. Occurrence and fate of pharmaceutically active compounds in the environment, a case study: Hoje river in Sweden. Journal of Hazardous Materials. 122 (2005): 195-204.

Boyd, G.E., Adamson, A.W., and Myers, L.S. The exchange adsorption of ions from aqueous solutions by organic zeolites. II. kinetics1. Journal of the American chemical society. 69 (1947): 2836-2848.

Boyd, G.R., Reemtsma, H., Grimm, D.A., and Mitra, S. Pharmaceuticals and personal care products (PPCPs) in surface and treated waters of Louisiana, USA and Ontario, Canada. Science of The Total Environment. 311 (2003): 135-149.

Brigante, M., and Schulz, P. Adsorption of the antibiotic adsorption of the antibiotic minocycline on cerium (IV) oxide: Effect of pH, ionic strength and temperature. Microporous and Mesoporous materials. 156 (2012): 138-144.

Brown, P.A., Brown, J.M., and Allen, S.J. The application of kudzu as a medium for the adsorption of heavy metals from dilute aqueous wastestreams, Bioresource Technology. 78 (2001): 195-201.

Bui, T.X., and Choi, H. Adsorptive removal of selected pharmaceuticals by mesoporous silica SBA-15. Journal of Hazardous Materials. 168 (2009): 602-608.

Bui, T.X., and Choi, H. Influence of ionic strength, anions, cations, and natural organic matter on the adsorption of pharmaceuticals to silica. Chemosphere. 80 (2010): 681-686.

Burleigh, M.C., Markowitz, M.A., Spector, M.S., and Gaber, B.P. Direct synthesis of periodic mesoporous organosilicas: Functional Incorporation by co-condensation with organosilanes. The Journal of Physical Chemistry B. 105 (2001): 9935-9942.

Burleigh, M.C., Markowitz, M.A., Spector, M.S., and Gaber, B.P. Amine-functionalized periodic mesoporous organosilicas. Chemistry of Materials. 13 (2001): 4760-4766.

Buser, H.R., Poiger, T., and Muller, M.D. Occurrence and fate of the pharmaceutical drug Diclofenac in surface waters: Rapid photodegradation in a Lake. Environmental Science & Technology. 32 (1998): 3449-3456.

Carballa, M., Omil, F., and Lema, J.M. Removal of cosmetic ingredients and pharmaceuticals in sewage primary treatment. Water Research. 39 (2005): 4790-4796.

Cheung, W.H., Szeto, Y.S., and Mckay, G. Intraparticle diffusion processes during acid dye adsorption onto chitosan. Bioresource Technology. 98 (2007): 2897-2904.

Clara, M., Strenn, B., and Kreuzinger, N. Carbamazepine as a possible anthropogenic marker in the aquatic environment: investigations on the behaviour of Carbamazepine in wastewater treatment and during groundwater infiltration. Water Research. 38 (2004): 947-954.

Coelho, A.D., Sans, C., Aguera, A., Gomez, M.J., Esplugas, S., and Dezotti, M. Effects of ozone pre-treatment on diclofenac: Intermediates, biodegradability and toxicity assessment. Science of the Total Environment. 407 (2009): 3572-3578.

Daughton, G.C., and Jones-Lepp, T.L. Pharmaceuticals and personal care products in the environment scientific and regulatory issues. (2011).

Dıaz, I., Alvarez, C.M., Mohino, F., Pariente, J.P., and Sastre, E. Combined alkyl and sulfonic acid functionalization of MCM-41-type silica. Journal of Catalysis. 193 (2000): 283–294.

Dickey, F.H. The preparation of specific adsorbents. Proc. Natl. Acad Sci. U.S.A. 35

Dimos, K., Stathi, P., Karakassides, M.A., and Deligiannakis, Y. Synthesis and characterization of hybrid MCM-41 materials for heavy metal adsorption. Microporous and Mesoporous Materials. 126 (2009): 65–71.

Dubinin, M.M., and Radushkevich, L.V. Equation of the characteristic curve of activated charcoal. Physical Chemestry Section: USSR. (1947): 331.

Dural, M.U., Cavas, L., Papageorgiou, S.K., and Katsaros, F.K. Methylene blue adsorption on activated carbon prepared from Posidonia oceanica (L.) dead leaves: Kinetics and equilibrium studies. Chemical Engineering Journal. 168 (2011): 77–85.

El Qada E.N, Allen, S.J., and Walker, G.M. Adsorption of methylene blue onto activated carbon produced from steam activated bituminous coal: A study of equilibrium adsorption isotherm. Chemical Engineering Journal. 124 (2006): 103-110.

El Qada, E.N., Allen, S.J., and Walker, G.M. Adsorption of basic dyes from aqueous solution onto activated carbons. Chemical Engineering Journal. 135 (2008): 174-184.

Esplugas, S., Bila, D. M., Krause, L. G. T., and Dezotti, M. Ozonation and advanced oxidation technologies to remove endocrine disrupting chemicals (EDCs) and pharmaceuticals and personal care products (PPCPs) in water effluents. Journal of Hazardous Materials. 149 (2007): 631-642.

Farre, M.L., Perez, S., Kantiani, L., and Barcelo, D. Fate and toxicity of emerging pollutants, their metabolites and transformation products in the aquatic environment. Trends in Analytical Chemistry. 27 (2008): 991-1007.

Fent, K., Weston, A. A., and Caminada, D. Ecotoxicology of human pharmaceuticals. Aquatic Toxicology. 76 (2006): 122-159.

Freundlich, H.M.F. Over the adsorption in solution. The Journal of Physical Chemistry. 57 (1906): 385-470.

Fu, L., Wang, J., Lu, H., Su, Y., and Ren, A. Comment on the removal of phenolic compounds from aqueous solutions by organophilic bentonite. Journal of Hazardous Materials. 151 (2008): 851-854.

Gebhardt, W., and Schroder, H.F. Liquid chromatography - (tandem) mass spectrometry for the follow-up of the elimination of persistent pharmaceuticals during wastewater treatment applying biological wastewater treatment and advanced oxidation. Journal of Chromatography A. 1160 (2007): 34-43.

Guan, W., Pan, J., Ou, H., Wang, X., Zou, X., Hu, W., Li, C., and Wu, X. Removal of strontium(II) ions by potassium tetratitanate whisker and sodium tritanate whisker from aqueous solution: Equibrium, kinetics and thermodynamics. Chemical Engineering Journal. 167 (2011): 215-222.

Han, X., Wang, W., and Ma, X. Adsorption characteristics of methylene blue onto low cost biomass material lotus leaf. Chemical Engineering Journal. 171 (2011): 1-8.

Ho, Y.S., and Mckay, G. Pseudo-second order model for sorption processes. Process Biochemistry. 34 (1999): 450-465.

Hobson, J.P. Physical adsorption isotherms extending from ultra-high vacuum to vapor pressure. Journal of Physical Chemistry, 73 (1969) 2720-2727.

Hua, W., Bennett, E.R., and Letcher, R.J. Ozone treatment and the depletion of detectable pharmaceuticals and atrazine herbicide in drinking water sourced from the upper Detroit River, Ontario, Canada. Water Research. 40 (2006): 2259-2266.

Inagaki, S., Guan, S., Fukushima, Y., Ohsuna, T., and Terasaki, O. Novel mesoporous materials with a uniform distribution of organic groups and inorganic oxide in their frameworks. Journal of American Chemical Society. 121 (1999): 9611-9614.

Ip A.W.M, Barford, J.P., and McKay, G. A comparative study on the kinetics and mechanisms of removal of Reactive Black 5 by adsorption onto activated carbons and bone char. Chemical Engineering Journal. 157 (2010): 434–442.

Isidori, M., Lavorgna, M., Nardelli, A., Parrella, A., Previtera, L., and Rubino, M. Ecotoxicity of Naproxen and its phototransformation products. Science of the Total Environment. 348 (2005): 93-101.

Kim, I., and Tanaka, H. Photodegradation characteristics of PPCPs in water with UV treatment. Environment International. 35 (2009): 793-802.

Kim, J.H., Tanabe, M., and Niwa, M. Characterization and catalytic activity of the AlMCM-41 prepared by a method of gel equilibrium adjustment. Microporous Materials. 10 (1997): 85-93.

Kimura, K., Hara, H., and Watanabe, Y. Removal of pharmaceutical compounds by submerged membrane bioreactors (MBRs). Desalination. 178 (2005): 135-140.

Kumar, D., Gaur, J.P., Chemical reaction- and particle diffusion-based kinetic modeling of metal biosorption by a Phormidium sp.-dominated cyanobacterial mat. Bioresource Technology, 102 (2011) 633-640.

Kummerer, K. Drugs in the environment: emission of drugs, diagnostic aids and disinfectants into wastewater by hospitals in relation to other sources - a review. Chemosphere. 45 (2001): 957-969.

Lagrega, M.D., Buckingham, P.L., Evans, J.C., and Environmental Resources Management. Hazardous waste management. McGraw-Hill. (2001).

Lagergren, S. Zurtheorie der sogenannten adsorption gelösterstoffe. Kungliga Svenska Vetenskapsakademiens Handlingar. 24 (1898): 1-39.

Langmuir, I. The constitution and fundamental properties of solids and liquids. Part 1. Solids. Journal of the American Chemical Society. 38 (1916): 2221-2295.

Lee, B., Kim, Y., Lee, H., and Yi, J. Synthesis of functionalized porous silicas via templating method as heavy metal ion adsorbents: the introduction of surface hydrophilicity onto the surface of adsorbents. Microporous and Mesoporous Materials. 50 (2001): 77-90.

Li, C., Liu, J., Shi, X., Yang, J., and Yang, Q. Periodic mesoporous organosilicas with 1,4-Diethylenebenzene in the mesoporous wall: Synthesis, characterization, and bioadsorption properties. Journal of American Chemical Society C. 111 (2007): 10948-10954.

Liu, J., Yang, Q., Zhang, L., Jiang, D., Shi, X., Yang, J., Zhong, H., and Li, C. Thioether-bridged mesoporous organosilicas: Mesophase rransformations induced by the bridged organosilane precursor. Advanced Functional Materials. 17 (2007): 569–576.

Lim, M.H., and Stein, A. Comparative studies of grafting and direct syntheses of inorganic-organic hybrid mesoporous materials. Chemistry of Materials. 11 (1999) 3285-3295.

Maria Chong, A.S., Zhao, X.S., Kustedjo, A.T., and Qiao, S.Z. Functionalization of large-pore mesoporous silicas with organosilanes by direct synthesis. Microporous and Mesoporous Materials. 72 (2004): 33-42.

Matamoros, V., Garcia, J., and Bayona, J.M. Organic micropollutant removal in a full-scale surface flow constructed wetland fed with secondary effluent. Water Research. 42 (2008): 653-660.

Mercier, L., and Pinnavaia, T.J. Direct synthesis of hybrid organicˆ inorganic nanoporous silica by a neutral amine assembly route: Structure - function control by stoichiometric incorporation of organosiloxane molecules. Chemistry of Materials. 12 (2000): 188-196.

Margolese, D., Melero, J.A., Christiansen, S.C., Chmelka, B.F., and Stucky. G.D. Direct syntheses of ordered SBA-15 mesoporous silica containing sulfonic acid groups. Chemistry of Materials. 12 (2000): 2448-2459.

Moller, K., Bein, T., and Fischer, R.X. Synthesis of ordered mesoporous methacrylate hybrid systems: Hosts for molecular polymer composites. Chemistry of Materials. 11 (1999): 665-673.

Mori, Y., and Pinnavaia, T.J. Optimizing organic functionality in mesostructured silica: direct assembly of mercaptopropyl groups in wormhole framework structures. Chemistry of Materials. 13 (2001): 2173-2178

Munoz, I., Rodriguez, A., Rosal, R., and Fernandez-Alba, A. R. Life cycle assessment of urban wastewater reuse with ozonation as tertiary treatment: A focus on toxicity-related impacts. Science of the Total Environment. 407 (2009): 1245-1256.

Ngah, W.S., and Hanafiah, M.A.K.M. Adsorption of copper on rubber (*Hevea brasiliensis*) leaf powder: Kinetic, equilibrium and thermodynamic studies. Biochemical Engineering Journal. 39 (2008): 521-530.

Pauly, T.R., and Pinnavaia, T.J. Pore size modification of mesoporous HMS molecular sieve silicas with wormhole framework structures. Chemistry of Materials.13 (2001): 987-993.

Pan, J., Zou, X., Wang, X., Guan, W., Li, C., Yan, Y., and Wu, X. Adsorptive removal of 2,4-didichlorophenol and 2,6-didichlorophenol from aqueous solution by B-cyclodextrin/attapulgite composites: Equilibrium, kinetics and thermodynamics. Chemical Engineering Journal. 166 (2011): 40-48.

Pan, J., Yao, H., Guan, W., Ou, H., Huo, P., Wang, X., Zou, X., and Li, C. Selective adsorption of 2,6-dichlorophenol by surface imprinted polymers using polyaniline/silica gel composites as functional support: Equilibrium, kinetics, thermodynamics modeling. Chemical Engineering Journal. 172 (2011): 847-855.

Park. S.S., Lee, C.H., Cheon, J.H., Choe, S.J. and Park, D.H. Morphological Control of Periodic Mesoporous Organosilica with Agitation. Bulletin of the Korean Chemical Society. 22 (2001): 948-952.

Pavlovic, D.M., Babic, S., Horvat, A.J.M., and Kastelan-Macan, M. Sample preparation in analysis of pharmaceuticals. Trends in Analytical Chemistry. 26 (2007): 1062-1075.

Paxeus, N. Removal of selected non-steroidal anti-inflammatory drugs (NSAIDs), Gemfibrozil, Carbamazepine, Beta-blockers, Trimethoprim and Triclosan in conventional wastewater treatment plants in five EU countries and their discharge to the aquatic environment. Water Science and Technology. 50 (2004): 253-60.

Prarat, P., Ngamcharussrivichai, C., Khaodhiar, S., and Punyapalakul, P. Adsorption characteristics of haloacetonitriles on functionalized silica-based porous materials in aqueous solution. Journal of Hazardous Materials. 192 (2011): 1210-1218.

Punyapalakul, P., Soonglerdsongpha, S., Kanlayaprasit, C., Ngamcharussrivichai, C., and Khaodhiar, S. Effects of crystalline structures and surface functional groups on the adsorption of haloacetic acids by inorganic materials. Journal of Hazardous Materials. 171 (2009): 491-499.

Punyapalakul, P., and Takizawa, S. Selective adsorption of nonionic surfactant on hexagonal mesoporous silicates (HMSs) in the presence of ionic dyes. Water Research. 40 (2006): 3177-3184.

Punyapalakul, P., and Sitthisorn, T. Removal of Ciprofloxazin and Carbamazepine by adsorption on functionalized mesoporous silicates, World Academy of Science. Engineering and Technology. 69 (2010).

Qiao, S.Z., Bhatia, S.K., and Zhao, X.S. Prediction of multilayer adsorption and capillary condensation phenomena in cylindrical mesopores. Microposous and Mesoporous Materials. 65 (2003): 287-298.

Quesada-Penate, I., Julcour-Lebigue, C., Jauregui-Haza, U.-*J*., Wilhelm, A.-M., and Delmas, H. Comparative adsorption of levodopa from aqueous solution on different activated carbons. Chemical Engineering Journal. 152 (2009): 183-188.

Quinn, B., Gagne, F., and Blaise, C. An investigation into the acute and chronic toxicity of eleven pharmaceuticals (and their solvents) found in wastewater effluent on the cnidarian, Hydra attenuata. Science of the Total Environment. 389 (2008): 306-314.

Rabiet, M., Togola, A., Brissaud, F., Seidel, J. L., Budzinski, H., and Elbaz-Poulichet, F. Consequences of treated water recycling as regards pharmaceuticals and drugs in surface and ground waters of a medium-sized Mediterranean catchment. Environmental Science and Technology. 40 (2006): 5282-5288.

Radjenovic, J., Petrovic, M., Ventura, F., and Barcelo, D. Rejection of pharmaceuticals in nanofiltration and reverse osmosis membrane drinking water treatment. Water Research. 42 (2008): 3601-3610.

Radjenovic, J., Petrovic, M., and Barcelo, D. Fate and distribution of pharmaceuticals in wastewater and sewage sludge of the conventional activated sludge (CAS) and advanced membrane bioreactor (MBR) treatment. Water Research. 43 (2009): 831-841.

Raman, N. K., Anderson, M. T., and Brinker, C. J. Template-based approaches to the preparation of amorphous, nanoporous silicas. Chemistry of Materials. 8 (1996): 1682-1701.

Reichenberg, D. Properties of ion exchange resins in relation to their structure. III. Kinetics of exchange. Journal of American Chemical Society. 75 (1953).

Richer, R., and Mercier, L. Direct synthesis of functionalized mesoporous silica by non-ionic alkylpolyethyleneoxide surfactant assembly. Chemical Communications. (1998): 1775-1776.

Ritchie, A.G. Alternative to the Elovich equation for the kinetics of adsorption of gases on solids. Journal of the Chemical Society, Faraday Transactions 1: Physical Chemistry in Condensed Phases. 73 (1977): 1650-1653.

Rosal, R., Rodriguez, A., Perdigon-Melon, J. A., Petre, A., Garcia-Calvo, E., Gomez, M. J., Aguera, A., and Fernandez-Alba, A. R. Occurrence of emerging pollutants in urban wastewater and their removal through biological treatment followed by ozonation. Water Research. 44 (2010): 578-588.

Saad, R., Hamoudi, S., and Belkacemi, K. Adsorption of phosphate and nitrate anions on ammonium-functionnalized mesoporous silicas. Journal of Porous Materials. 15 (2008): 315–323.

Samuel, D.F., and Osman, M.A. Adsorption process for water treatment. Boston. Butterworth Publishers. (1987).

Santos, L.H.M.L.M., Araujo, A.N., Fachini, A., Pena, A., Delerue-Matos, C., and Montenegro, M.C.B.S.M. Ecotoxicological aspects related to the presence of pharmaceuticals in the aquatic environment. Journal of Hazardous Materials. 175 (2010): 45-95.

Schnell, S., Bols, N.C., Barata, C., and Porte, C. Single and combined toxicity of pharmaceuticals and personal care products (PPCPs) on the rainbow trout liver cell line RTL-W1. Aquatic Toxicology. 93 (2009): 244-252.

Sim, W.J., Lee, J.W., and Oh, J.E. Occurrence and fate of pharmaceuticals in wastewater treatment plants and rivers in Korea. Environmental Pollution 158 (2010): 1938-1947.

Skadsen, J.M., Rice, B.L., and Meyering, D.J. The occurrence and fate of pharmaceuticals, personal care products and endocrine disrupting compounds in a municipal water use cycle: A case study in the city of Ann Arbor. Fleis & Vanden Brink Engineering, Inc. (2004).

Smart, M., Rada, R., and Donnermeyer, G. Determination of total nitrogen in sediments and plants using persulfate digestion. An evaluation and comparison with the kjeldahl procedure. Water Research. 17 (1983): 1207-1211.

Suarez, S., Lema, J. M., and Omil, F. Pre-treatment of hospital wastewater by coagulation-flocculation and flotation. Bioresource Technology. 100 (2009): 2138-2146.

Tanev, P.T., and Pinnavaia, T.J. Mesoporous silica molecular sieves prepared by ionic and neutral surfactant templating: A comparison of physical properties. Chemistry of Materials. 8 (1996): 2068-2079.

Tchobanoglous, G., Burtan, F., and Stensel, H. Wastewater engineering treatment and reuse. Forth edition by Metcalf&Eddy, Inc., Mc Grall Hill. (2004).

Temkin, M.J., and Pyzhev, V. Kinetics of ammonia synthesis on promoted iron catalysts. ActaPhysiochim. URSS. 12 (1940): 217-222.

Ternes, T.A. Occurrence of drugs in German sewage treatment plants and rivers. Water Research. 32 (1998): 3245-3260.

Thacker, P.D. Pharmaceutical data eludes environmental researchers. Environmental Science and Technology. 39 (2005): 193A-194A.

Thomas, K., and Hilton, M. The occurrence of selected human pharmaceutical compounds in UK esturies. Marine Pollution Bulletin. 49 (2004): 436-44.

Tixier, C., Singer, H., Oellers, S., and Muller, S. Occurrence and fate of Carbamazepine, Clofibric acid, Diclofenac, Ibuprofen, Ketoprofen, and Naproxen in surface waters. Environmental Science and Technology. 37 (2003): 1061-8.

Tong, K.S. Adsorption of copper ion from its aqueous solution by a novel biosorbent Uncaria gambir: Equilibrium, kinetics, and thermodynamic studies. Chemical Engineering Journal. 170 (2011): 145-153.

Triebskorn, R., Casper, H., Heyd, A., Eikemper, R., Kohler, H.R., and Schwaiger, J. Toxic effects of the non-steroidal anti-inflammatory drug Diclofenac: Part II. Cytological effects in liver, kidney, gills and intestine of rainbow trout (Oncorhynchus mykiss). Aquatic Toxicology. 68 (2004): 151-166.

Vermeulen, T. Theory for irreversible and constant pattern solid diffusion. Industrial and Engineering Chemistry Research. 45 (1953): 1664-1671.

Voegtlin, A.C.; Matijasic, A.; Patarin, J; Sauerland, C; Grillet, Y; Huve, L., Room-temperature synthesis of silicate mesoporous MCM-41-type materials: influence of the synthesis pH on the porosity of the materials obtained. Microporous Materials. 10 (1997): 137-147.

Wahab, M.A., Kim, I., and Ha, C.S. Hybrid periodic mesoporous organosilica materials prepared from 1,2-bis(triethoxysilyl)ethane and (3-cyanopropyl)triethoxysilane. Microporous and Mesoporous Materials. 69 (2004): 19–27.

Walcarius, A., Etienne, M., and Lebeau, B. Rate of access to the binding sites in organically modified silicates. 2. Ordered mesoporous silicas gafted with amine or thiol Groups. Chemistry of Materials. 15 (2003): 2161-2173.

Wang, G., Otuonye, A. N., Blair, E. A., Denton, K., Tao, Z., and Asefa, T. Functionalized mesoporous materials for adsorption and release of different drug molecules: A comparative study. Journal of Solid State Chemistry. 182 (2009): 1649-1660.

Weber, J.W., and Morris, J. Kinetics of adsorption on carbon from solution. J. Sanit. Eng. Div. ASCE. 89 (1963): 31-60.

Weiss, S., and Reemtsma, T. Membrane bioreactors for municipal wastewater treatment - A viable option to reduce the amount of polar pollutants discharged into surface waters. Water Research. 42 (2008): 3837-3847.

Yoshitake, H., Yokoi, T., and Tatsumi, T. Adsorption of Chromate and Arsenate by amino-functionalized MCM-41 and SBA-1. Chemistry of Materials. 14 (2002): 4603-4610.

Zhang, Y., Geiben, S.U., and Gal, C. Carbamazepine and Diclofenac: Removal in wastewater treatment plants and occurrence in water bodies. Chemosphere. 73 (2008): 1151-1161.

Zhang, L., Yang, Q., Zhang, W.H., Li, Y., Yang, J., Jiang, D., Zhu, G., and Li, C. Highly ordered periodic mesoporous ethanesilica synthesized under neutral Conditions. Journal of Materials Chemistry. 15 (2005): 2562–2568.

Zhang, W,G., Daly, B., Callaghan, J.O., Zhang, L., Shi, J.L., Li, C., Morris, M.A., and Holmes, J.D. Large pore methylene-bridged periodic mesoporous organosilicas: Synthesis, bifunctionalization and their use as nanotemplates. Chemistry of Materials. 17 (2005): 6407-6415.

Zhao, D., Feng, J., Huo, Q., Melosh, N., Fredrickson, G. H., Chmelka, B. F., and Stucky, G. D. Triblock copolymer syntheses of mesoporous silica with periodic 50 to 300 angstrom pores. Science. 279 (1998): 548-552.

Zhao, X. S., Huo, Q., Feng, J., Chmelka, B. F., and Stucky, G. D. Nonionic triblock and Star copolymer and oligomeric surfactant syntheses of highly ordered, hydrothermally stable, Mesoporous Silica Structure. Journal of American Chemical Society. 120 (1998): 6024-6036.

Zhao, X.S, Lu, G.Q., and Millar, G.J. Advances in mesoporous molecular sieve MCM-41. Industrial and Engineeing Chemistry Research. 35 (1996): 2075-2090.

Zhao, X.S., Lu, G.Q., Whittaker, A.K., Millar, G.J., and Zhu, H.Y. Comprehensive study of surface chemistry of MCM-41 using ^{29}Si CP/MAS NMR, FTIR, Pyridine-TPD, and TGA. The Journal of Physical Chemistry B. 101 (1997): 6525-6531.

Zhu, G., Yang, Q., Jiang, D., Yang, J., Zhang, L., Li, Y., and Li, C. Synthesis of bifunctionalized mesoporous organosilica spheres for high-performance liquid chromatography. Journal of Chromatography A. 1103 (2006): 257–264.

Zhu, G., Yang, Q., and Li., C. Synthesis of periodic Mesoporous ethanesilica and its application in high performance liquid chromatography. Chinese Journal of Chromatography. 25 (2007): 505–508.

Zhu, G., Yang, Q., Zhong, H., Jiang, D., and Li, C. Phase transformation of the periodic mesoporous organosilicas assisted by organotrialkoxysilane. Journal of Physical Chemistry B. 11 (2007): 8027-8033.

Zou, X., Pan, J., Ou, H. Wang, X., Guan, W., Li, C., Yan, Y., and Duan, Y. Adsorptive removal of Cr(III) and Fe(III) from aqueous solution by chitosan/attapulgite composites: Equilibrium, thermodynamics and kinetics. Chemical Engineering Journal. 167 (2011) 112-121.

APENDICES

APENDIX A

HPLC Chromatograms of pharmaceutical residues

APENDIX B

Experimental results for removal of trace pharmaceutical residues by adsorption on mesoporous silicas

Table B-1 Adsorption kinetics data of DCF adsorbed onto the different mesoporous silicates and PAC.

Time (min)	Pharmaceutical concentration (µg/L)					
	HMS	M-HMS	A-HMS	MCM-41	SBA-15	PAC
0	100.00	100.00	100	100	100.00	100.00
1	59.29	55.87	96.32	60.54	62.50	50.23
3	55.72	50.31	95.72	51.32	51.30	41.36
5	54.92	48.72	93.42	50.96	46.74	36.70
10	48.35	39.29	94.03	47.32	44.51	28.16
20	45.16	33.63	91.16	40.36	35.56	24.47
30	38.88	32.91	90.78	36.97	33.36	22.37
60	37.46	30.54	89.24	35.47	33.62	21.56
120	36.85	29.45	88.93	35.03	32.72	23.33
180	36.42	29.03	89.41	34.96	32.12	20.98
240	36.15	29.36	88.23	34.75	31.65	18.92

Time (min)	Adsorption capacity (µg/g)					
	HMS	M-HMS	A-HMS	MCM-41	SBA-15	PAC
0	0.00	0.00	0.00	0.00	0.00	0.00
1	20.36	22.07	1.84	19.73	18.75	24.89
3	22.14	24.85	2.14	24.34	24.35	29.32
5	22.54	25.64	3.29	24.52	26.63	31.65
10	25.83	30.36	2.99	26.34	27.75	35.92
20	27.42	33.19	4.42	29.82	32.22	37.77
30	30.56	33.55	4.61	31.52	33.32	38.82
60	31.27	34.73	5.38	32.27	33.19	39.22
120	31.58	35.28	5.54	32.49	33.64	38.34
180	31.79	35.49	5.30	32.52	33.94	39.51
240	31.93	35.32	5.89	32.63	34.18	40.54

Table B-2 Adsorption kinetics data of CBZ adsorbed onto the different mesoporous silicates and PAC.

Time (min)	**Pharmaceutical concentration (µg/L)**					
	HMS	**M-HMS**	**A-HMS**	**MCM-41**	**SBA-15**	**PAC**
0	100.00	100.00	100	100	100.00	100.00
1	64.70	60.27	94.95	67.42	62.47	55.32
3	55.05	51.55	94.52	56.87	52.28	48.65
5	47.74	42.82	93.5	49.06	45.26	40.74
10	46.99	37.57	92.14	46.9	43.52	32.98
20	45.67	35.27	90.36	43.38	41.25	27.85
30	45.37	33.28	89.94	42.69	40.75	24.82
60	45.62	32.78	89.81	41.87	39.81	20.41
120	45.32	31.14	89.46	41.02	38.68	18.32
180	45.16	30.57	89.36	40.47	38.47	17.09
240	44.82	30.43	89.28	40.15	38.14	16.27

Time (min)	**Adsorption capacity (µg/g)**					
	HMS	**M-HMS**	**A-HMS**	**MCM-41**	**SBA-15**	**PAC**
0	0.00	0.00	0.00	0.00	0.00	0.00
1	17.65	19.87	2.53	16.29	18.77	22.34
3	22.48	24.23	2.74	21.57	23.86	25.68
5	26.13	28.59	3.25	25.47	27.37	29.63
10	26.51	31.22	3.93	26.55	28.24	33.51
20	27.17	32.37	4.82	28.31	29.38	36.08
30	27.32	33.36	5.03	28.66	29.63	37.59
60	27.19	33.61	5.10	29.07	30.10	39.80
120	27.34	34.43	5.27	29.49	30.66	40.84
180	27.42	34.72	5.32	29.77	30.77	41.46
240	27.59	34.79	5.36	29.93	30.93	41.87

Table B-3 Adsorption kinetics data of NAP adsorbed onto the different mesoporous silicates and PAC.

Time (min)	**Pharmaceutical concentration (μg/L)**					
	HMS	**M-HMS**	**A-HMS**	**MCM-41**	**SBA-15**	**PAC**
0	100.00	100.00	100.00	100.00	100.00	100.00
10	82.47	56.32	93.25	78.45	74.23	55.74
20	80.41	54.86	92.14	75.36	71.65	49.68
30	78.26	47.64	91.75	74.14	68.23	32.65
60	77.29	36.72	88.65	73.35	67.69	28.45
120	76.65	32.65	85.67	71.42	65.65	29.72
180	75.47	31.41	84.36	70.83	63.25	25.04
240	74.89	30.74	80.54	70.17	61.74	22.62
300	73.36	28.63	78.25	69.36	60.36	20.36
360	73.71	27.63	77.46	67.65	60.85	18.45
420	73.86	29.69	75.63	66.86	61.63	18.14
480	73.24	28.41	75.45	64.82	60.02	17.39
540	72.54	25.32	75.82	64.67	59.87	16.84
600	71.66	25.66	75.25	63.97	59.63	16.36
660	71.02	25.98	74.71	63.85	58.42	16.32
720	70.78	25.13	74.36	63.42	58.02	16.25

Table B-3 Adsorption kinetics data of NAP adsorbed onto the different mesoporous silicates and PAC (continue).

Time (min)	**Adsorption capacity (µg/g)**					
	HMS	**M-HMS**	**A-HMS**	**MCM-41**	**SBA-15**	**PAC**
0	0.00	0.00	0.00	0.00	0.00	0.00
10	8.77	21.84	3.38	10.78	12.89	22.13
20	9.80	22.57	3.93	12.32	14.18	25.16
30	10.87	26.18	4.13	12.93	15.89	33.68
60	11.36	31.64	5.68	13.33	16.16	35.78
120	11.68	33.68	7.17	14.29	17.18	35.14
180	12.27	34.30	7.82	14.59	18.38	37.48
240	12.56	34.63	9.73	14.92	19.13	38.69
300	13.32	35.69	10.88	15.32	19.82	39.82
360	13.15	36.19	11.27	16.18	19.58	40.78
420	13.07	35.16	12.19	16.57	19.19	40.93
480	13.38	35.80	12.28	17.59	19.99	41.31
540	13.73	37.34	12.09	17.67	20.07	41.58
600	14.17	37.17	12.38	18.02	20.19	41.82
660	14.49	37.01	12.65	18.08	20.79	41.84
720	14.61	37.44	12.82	18.29	20.99	41.88

Table B-4 Adsorption kinetics data of CFA adsorbed onto the different mesoporous silicates and PAC.

Time (min)	**Pharmaceutical concentration (μg/L)**					
	HMS	**M-HMS**	**A-HMS**	**MCM-41**	**SBA-15**	**PAC**
0	100.00	100.00	100.00	100.00	100.00	100.00
10	88.25	95.63	65.87	85.41	83.63	72.45
20	85.36	93.14	62.45	83.33	80.42	70.82
30	82.61	91.05	58.26	81.47	78.67	67.36
60	79.66	88.61	56.32	79.62	72.31	62.36
120	78.74	87.54	42.78	76.78	69.69	63.24
180	77.62	85.69	39.17	74.37	67.24	61.02
240	76.21	84.25	35.87	72.55	66.63	57.36
300	75.14	83.32	33.14	69.63	64.57	55.36
360	74.98	80.44	32.68	68.14	64.10	55.47
420	74.85	79.65	32.41	67.85	63.76	54.96
480	74.74	79.44	31.48	67.62	63.53	54.58
540	74.68	79.32	30.68	67.41	63.24	54.72
600	74.62	78.96	30.74	66.95	62.96	54.23
660	74.58	78.74	30.42	66.54	62.42	54.17
720	74.41	78.63	30.36	66.47	62.17	53.36

Table B-4 Adsorption kinetics data of CFA adsorbed onto the different mesoporous silicates and PAC (continue).

Time (min)	**Adsorption capacity (µg/g)**					
	HMS	**M-HMS**	**A-HMS**	**MCM-41**	**SBA-15**	**PAC**
0	0.00	0.00	0.00	0.00	0.00	0.00
10	5.88	2.19	17.07	7.30	8.19	13.78
20	7.32	3.43	18.78	8.34	9.79	14.59
30	8.70	4.48	20.87	9.27	10.67	16.32
60	10.17	5.70	21.84	10.19	13.85	18.82
120	10.63	6.23	28.61	11.61	15.16	18.38
180	11.19	7.16	30.42	12.82	16.38	19.49
240	11.90	7.88	32.07	13.73	16.69	21.32
300	12.43	8.34	33.43	15.19	17.72	22.32
360	12.51	9.78	33.66	15.93	17.95	22.27
420	12.58	10.18	33.80	16.08	18.12	22.52
480	12.63	10.28	34.26	16.19	18.24	22.71
540	12.66	10.34	34.66	16.30	18.38	22.64
600	12.69	10.52	34.63	16.53	18.52	22.89
660	12.71	10.63	34.79	16.73	18.79	22.92
720	12.80	10.69	34.82	16.77	18.92	23.32

Table B-5 Adsorption kinetics data of ACT adsorbed onto the different mesoporous silicates and PAC.

Time (min)	**Pharmaceutical concentration (µg/L)**					
	HMS	**M-HMS**	**A-HMS**	**MCM-41**	**SBA-15**	**PAC**
0	100.00	100.00	100.00	100.00	100.00	100.00
10	94.65	96.36	85.36	92.85	92.24	79.58
20	92.14	95.25	76.74	91.56	90.14	72.25
30	88.23	93.85	71.14	87.89	87.62	65.25
60	86.17	92.21	66.47	85.41	85.41	61.63
120	84.52	91.69	63.68	83.63	83.66	60.17
180	84.74	87.87	61.04	81.55	81.20	59.66
240	83.58	84.36	60.62	81.21	78.28	59.41
300	81.36	83.95	60.36	79.37	75.66	58.25
360	80.32	82.74	59.25	76.65	74.56	58.17
420	78.98	82.69	58.96	76.21	74.32	57.63
480	79.62	80.74	58.84	75.44	74.21	57.89
540	78.74	80.56	58.68	75.12	74.08	56.85
600	78.47	80.63	58.39	74.94	73.85	56.41
660	78.56	80.21	58.25	74.87	73.74	56.85
720	78.45	80.14	57.85	74.66	73.62	56.17

Table B-5 Adsorption kinetics data of ACT adsorbed onto the different mesoporous silicates and PAC (continue).

Time (min)	**Adsorption capacity (µg/g)**					
	HMS	**M-HMS**	**A-HMS**	**MCM-41**	**SBA-15**	**PAC**
0	0.00	0.00	0.00	0.00	0.00	0.00
10	2.68	1.82	7.32	3.58	3.88	10.21
20	3.93	2.38	11.63	4.22	4.93	13.88
30	5.89	3.08	14.43	6.06	6.19	17.38
60	6.92	3.90	16.77	7.30	7.30	19.19
120	7.74	4.16	18.16	8.19	8.17	19.92
180	7.63	6.07	19.48	9.23	9.40	20.17
240	8.21	7.82	19.69	9.40	10.86	20.30
300	9.32	8.03	19.82	10.32	12.17	20.88
360	9.84	8.63	20.38	11.68	12.72	20.92
420	10.51	8.66	20.52	11.90	12.84	21.19
480	10.19	9.63	20.58	12.28	12.90	21.06
540	10.63	9.72	20.66	12.44	12.96	21.58
600	10.77	9.69	20.81	12.53	13.08	21.80
660	10.72	9.90	20.88	12.57	13.13	21.58
720	10.78	9.93	21.08	12.67	13.19	21.92

Table B-6 Adsorption capacity of HMS, M-HMS, A-HMS, MCM-41, SBA-15 and PAC for DCF.

Initial concentration (µg/L)	**Equilibrium concentration (µg/L)**	**Adsorption capacity (µg/g)**	**Equilibrium concentration (µg/L)**	**Adsorption capacity (µg/g)**	**Equilibrium concentration (µg/L)**	**Adsorption capacity (µg/g)**
		HMS		**M-HMS**		**A-HMS**
200	119.22	40.39	85.43	57.285	184.23	7.885
150	98.64	25.68	67.85	41.075	139.52	5.24
100	65.42	17.29	45.74	27.13	92.36	3.82
80	57.92	11.04	38.86	20.57	73.96	3.02
60	41.35	9.325	23.47	18.265	54.69	2.655
40	24.56	7.72	18.28	10.86	36.47	1.765

Initial concentration (µg/L)	**Equilibrium concentration (µg/L)**	**Adsorption capacity (µg/g)**	**Equilibrium concentration (µg/L)**	**Adsorption capacity (µg/g)**	**Equilibrium concentration (µg/L)**	**Adsorption capacity (µg/g)**
		MCM-41		**SBA-15**		**PAC**
200	113.95	43.025	101.87	49.065	36.28	81.86
150	95.86	27.07	85.52	32.24	30.44	59.78
100	63.74	18.13	57.73	21.135	24.45	37.775
80	55.48	12.26	50.68	14.66	17.1	31.45
60	40.62	9.69	39.65	10.175	-	-
40	24.22	7.89	23.16	8.42	-	-

Table B-7 Adsorption capacity of HMS, M-HMS, A-HMS, MCM-41, SBA-15 and PAC for CBZ.

Initial concentration (µg/L)	**Equilibrium concentration (µg/L)**	**Adsorption capacity (µg/g)**	**Equilibrium concentration (µg/L)**	**Adsorption capacity (µg/g)**	**Equilibrium concentration (µg/L)**	**Adsorption capacity (µg/g)**
		HMS		**M-HMS**		**A-HMS**
200	122.36	38.82	99.85	50.075	189.42	5.29
150	93.14	28.43	74.23	37.885	141.13	4.435
100	63.92	18.04	50.31	24.845	94.02	2.99
80	58.12	10.94	42.67	18.665	75.36	2.32
60	43.54	8.23	25.12	17.44	56.85	1.575
40	25.96	7.02	19.85	10.075	37.26	1.37

Initial concentration (µg/L)	**Equilibrium concentration (µg/L)**	**Adsorption capacity (µg/g)**	**Equilibrium concentration (µg/L)**	**Adsorption capacity (µg/g)**	**Equilibrium concentration (µg/L)**	**Adsorption capacity (µg/g)**
		MCM-41		**SBA-15**		**PAC**
200	119.47	40.265	104.24	47.88	52.36	73.82
150	90.22	29.89	79.76	35.12	41.36	54.32
100	62.15	18.925	54.94	22.53	26.62	36.69
80	54.8	12.6	47.38	16.31	18.54	30.73
60	41.89	9.055	37.85	11.075	-	-
40	25.03	7.485	22.72	8.64	-	-

Table B-8 Adsorption capacity of HMS, M-HMS, A-HMS, MCM-41, SBA-15 and PAC for NAP.

Initial concentration (µg/L)	**Equilibrium concentration (µg/L)**	**Adsorption capacity (µg/g)**	**Equilibrium concentration (µg/L)**	**Adsorption capacity (µg/g)**	**Equilibrium concentration (µg/L)**	**Adsorption capacity (µg/g)**
		HMS		**M-HMS**		**A-HMS**
200	141.44	29.28	78.36	60.82	179.36	10.32
150	102.36	23.82	61.34	44.33	132.13	8.935
100	78.25	10.875	40.47	29.765	85.87	7.065
80	61.36	9.32	31.73	24.135	70.42	4.79
60	45.69	7.155	21.36	19.32	52.32	3.84
40	26.63	6.685	15.87	12.065	34.56	2.72

Initial concentration (µg/L)	**Equilibrium concentration (µg/L)**	**Adsorption capacity (µg/g)**	**Equilibrium concentration (µg/L)**	**Adsorption capacity (µg/g)**	**Equilibrium concentration (µg/L)**	**Adsorption capacity (µg/g)**
		MCM-41		**SBA-15**		**PAC**
200	137.24	31.38	126.36	36.82	31.38	84.31
150	98.36	25.82	89.36	30.32	24.69	62.655
100	75.74	12.13	68.22	15.89	18.42	40.79
80	59.33	10.335	53.32	13.34	11.25	34.375
60	44.62	7.69	37.66	11.17	-	-
40	24.87	7.565	21.02	9.49	-	-

Table B-9 Adsorption capacity of HMS, M-HMS, A-HMS, MCM-41, SBA-15 and PAC for CFA.

Initial concentration (μg/L)	**Equilibrium concentration (μg/L)**	**Adsorption capacity (μg/g)**	**Equilibrium concentration (μg/L)**	**Adsorption capacity (μg/g)**	**Equilibrium concentration (μg/L)**	**Adsorption capacity (μg/g)**
		HMS		**M-HMS**		**A-HMS**
200	143.57	28.215	148.75	25.625	50.36	74.82
150	109.68	20.16	112.42	18.79	40.82	54.59
100	77.53	11.235	81.71	9.145	30.14	34.93
80	65.72	7.14	67.85	6.075	25.71	27.145
60	46.24	6.88	49.27	5.365	18.68	20.66
40	27.18	6.41	30.43	4.785	12.36	13.82

Initial concentration (μg/L)	**Equilibrium concentration (μg/L)**	**Adsorption capacity (μg/g)**	**Equilibrium concentration (μg/L)**	**Adsorption capacity (μg/g)**	**Equilibrium concentration (μg/L)**	**Adsorption capacity (μg/g)**
		MCM-41		**SBA-15**		**PAC**
200	137.63	31.185	129.65	35.175	101.45	49.275
150	105.74	22.13	98.32	25.84	72.23	38.885
100	74.66	12.67	69.25	15.375	56.41	21.795
80	61.25	9.375	56.74	11.63	41.86	19.07
60	43.11	8.445	40.36	9.82	30.96	14.52
40	25.27	7.365	22.36	8.82	22.14	8.93

Table B-10 Adsorption capacity of HMS, M-HMS, A-HMS, MCM-41, SBA-15 and PAC for ACT.

Initial concentration (µg/L)	**Equilibrium concentration (µg/L)**	**Adsorption capacity (µg/g)**	**Equilibrium concentration (µg/L)**	**Adsorption capacity (µg/g)**	**Equilibrium concentration (µg/L)**	**Adsorption capacity (µg/g)**
		HMS		**M-HMS**		**A-HMS**
200	168.25	15.875	173.5	13.25	124.5	37.75
150	132.14	8.93	137.47	6.265	89.47	30.265
100	87.13	6.435	89.69	5.155	59.69	20.155
80	70.38	4.81	72.82	3.59	45.82	17.09
60	51.82	4.09	54.15	2.925	34.15	12.925
40	33.75	3.125	35.63	2.185	22.63	8.685

Initial concentration (µg/L)	**Equilibrium concentration (µg/L)**	**Adsorption capacity (µg/g)**	**Equilibrium concentration (µg/L)**	**Adsorption capacity (µg/g)**	**Equilibrium concentration (µg/L)**	**Adsorption capacity (µg/g)**
		MCM-41		**SBA-15**		**PAC**
200	165.36	17.32	160.36	19.82	82.34	58.83
150	130.66	9.67	127.66	11.17	63.65	43.175
100	84.85	7.575	81.85	9.075	47.41	26.295
80	68.33	5.835	64.33	7.835	31.25	24.375
60	49.97	5.015	47.27	6.365	27.36	16.32
40	32.14	3.93	29.63	5.185	17.84	11.08

Table B-11 Adsorption capacity of HMS for DCF at pH 5, 7 and 9.

Initial concentration (µg/L)	HMS					
	pH 5		pH 7		pH 9	
	Equilibrium concentration (µg/L)	Adsorption capacity (µg/g)	Equilibrium concentration (µg/L)	Adsorption capacity (µg/g)	Equilibrium concentration (µg/L)	Adsorption capacity (µg/g)
200	107.82	46.09	119.22	40.39	130.26	34.87
150	85.41	32.29	98.64	25.68	104.65	22.67
100	57.36	21.32	65.42	17.29	73.85	13.07
80	44.25	17.87	57.92	11.04	61.47	9.265
60	32.64	13.68	41.35	9.325	47.52	6.24
40	20.83	9.58	24.56	7.72	31.65	4.17

Table B-12 Adsorption capacity of M-HMS for DCF at pH 5, 7 and 9.

Initial concentration (µg/L)	M-HMS					
	pH 5		pH 7		pH 9	
	Equilibrium concentration (µg/L)	Adsorption capacity (µg/g)	Equilibrium concentration (µg/L)	Adsorption capacity (µg/g)	Equilibrium concentration (µg/L)	Adsorption capacity (µg/g)
200	66.87	66.565	85.43	57.285	95.87	52.065
150	52.24	48.88	67.85	41.075	75.56	37.22
100	32.26	33.87	45.74	27.13	50.39	24.805
80	24.35	27.825	38.86	20.57	45.86	17.07
60	19.82	20.09	23.47	18.265	36.45	11.775
40	12.63	13.685	18.28	10.86	24.89	7.555

Table B-13 Adsorption capacity of A-HMS for DCF at pH 5, 7 and 9.

Initial concentration (µg/L)	**A-HMS**					
	pH 5		**pH 7**		**pH 9**	
	Equilibrium concentration (µg/L)	**Adsorption capacity (µg/g)**	**Equilibrium concentration (µg/L)**	**Adsorption capacity (µg/g)**	**Equilibrium concentration (µg/L)**	**Adsorption capacity (µg/g)**
200	175.02	12.49	184.23	7.885	187.26	6.37
150	135.14	7.43	139.52	5.24	143.48	3.26
100	89.56	5.22	92.36	3.82	96.82	1.59
80	69.33	5.335	73.96	3.02	78.24	0.88
60	52.24	3.88	54.69	2.655	57.19	1.405
40	33.74	3.13	36.47	1.765	38.53	0.735

Table B-14 Adsorption capacity of PAC for DCF at pH 5, 7 and 9.

Initial concentration (µg/L)	**PAC**					
	pH 5		**pH 7**		**pH 9**	
	Equilibrium concentration (µg/L)	**Adsorption capacity (µg/g)**	**Equilibrium concentration (µg/L)**	**Adsorption capacity (µg/g)**	**Equilibrium concentration (µg/L)**	**Adsorption capacity (µg/g)**
200	36.56	81.72	36.28	81.86	38.47	80.765
150	28.72	60.64	30.44	59.78	29.65	60.175
100	17.67	41.165	24.45	37.775	25.25	37.375
80	14.54	32.73	17.1	31.45	24.25	27.875
60	-	-	-	-	-	-
40	-	-	-	-	-	-

Table B-15 Adsorption capacity of HMS for CBZ at pH 5, 7 and 9.

Initial concentration (µg/L)	**HMS**					
	pH 5		**pH 7**		**pH 9**	
	Equilibrium concentration (µg/L)	**Adsorption capacity (µg/g)**	**Equilibrium concentration (µg/L)**	**Adsorption capacity (µg/g)**	**Equilibrium concentration (µg/L)**	**Adsorption capacity (µg/g)**
200	110.68	44.66	122.36	38.82	142.78	28.61
150	84.23	32.885	93.14	28.43	114.56	17.72
100	53.45	23.275	63.92	18.04	78.72	10.64
80	40.41	19.795	58.12	10.94	64.95	7.525
60	28.37	15.815	43.54	8.23	48.14	5.93
40	20.27	9.865	25.96	7.02	32.78	3.61

Table B-16 Adsorption capacity of M-HMS for CBZ at pH 5, 7 and 9.

Initial concentration (µg/L)	**M-HMS**					
	pH 5		**pH 7**		**pH 9**	
	Equilibrium concentration (µg/L)	**Adsorption capacity (µg/g)**	**Equilibrium concentration (µg/L)**	**Adsorption capacity (µg/g)**	**Equilibrium concentration (µg/L)**	**Adsorption capacity (µg/g)**
200	72.65	63.675	99.85	50.075	112.86	43.57
150	60.82	44.59	74.23	37.885	88.78	30.61
100	38.12	30.94	50.31	24.845	58.47	20.765
80	30.36	24.82	42.67	18.665	49.82	15.09
60	22.85	18.575	25.12	17.44	42.15	8.925
40	15.72	12.14	19.85	10.075	30.78	4.61

Table B-17 Adsorption capacity of A-HMS for CBZ at pH 5, 7 and 9.

Initial concentration (µg/L)	**A-HMS**					
	pH 5		**pH 7**		**pH 9**	
	Equilibrium concentration (µg/L)	**Adsorption capacity (µg/g)**	**Equilibrium concentration (µg/L)**	**Adsorption capacity (µg/g)**	**Equilibrium concentration (µg/L)**	**Adsorption capacity (µg/g)**
200	184.32	7.84	189.42	5.29	192.75	3.625
150	137.47	6.265	141.13	4.435	147.62	1.19
100	91.78	4.11	94.02	2.99	98.35	0.825
80	72.84	3.58	75.36	2.32	78.68	0.66
60	53.5	3.25	56.85	1.575	58.62	0.69
40	35.69	2.155	37.26	1.37	38.84	0.58

Table B-18 Adsorption capacity of PAC for CBZ at pH 5, 7 and 9.

Initial concentration (µg/L)	**PAC**					
	pH 5		**pH 7**		**pH 9**	
	Equilibrium concentration (µg/L)	**Adsorption capacity (µg/g)**	**Equilibrium concentration (µg/L)**	**Adsorption capacity (µg/g)**	**Equilibrium concentration (µg/L)**	**Adsorption capacity (µg/g)**
200	46.38	76.81	52.36	73.82	45.34	77.33
150	29.87	60.065	41.36	54.32	37.25	56.375
100	25.32	37.34	26.62	36.69	30.57	34.715
80	15.73	32.135	18.54	30.73	22.36	28.82
60	-	-	-	-	-	-
40	-	-	-	-	-	-

Table B-19 Adsorption capacity of HMS for NAP at pH 5, 7 and 9.

Initial concentration (µg/L)	HMS					
	pH 5		pH 7		pH 9	
	Equilibrium concentration (µg/L)	Adsorption capacity (µg/g)	Equilibrium concentration (µg/L)	Adsorption capacity (µg/g)	Equilibrium concentration (µg/L)	Adsorption capacity (µg/g)
200	132.63	33.685	141.44	29.28	152.22	23.89
150	95.47	27.265	102.36	23.82	116.37	16.815
100	62.36	18.82	78.25	10.875	85.41	7.295
80	44.63	17.685	61.36	9.32	69.42	5.29
60	35.72	12.14	45.69	7.155	53.96	3.02
40	20.33	9.835	26.63	6.685	33.21	3.395

Table B-20 Adsorption capacity of M-HMS for NAP at pH 5, 7 and 9.

Initial concentration (µg/L)	M-HMS					
	pH 5		pH 7		pH 9	
	Equilibrium concentration (µg/L)	Adsorption capacity (µg/g)	Equilibrium concentration (µg/L)	Adsorption capacity (µg/g)	Equilibrium concentration (µg/L)	Adsorption capacity (µg/g)
200	69.24	65.38	78.36	60.82	84.66	57.67
150	54.32	47.84	61.34	44.33	67.53	41.235
100	32.14	33.93	40.47	29.765	47.47	26.265
80	24.72	27.64	31.73	24.135	39.24	20.38
60	18.46	20.77	21.36	19.32	28.66	15.67
40	12.24	13.88	15.87	12.065	18.93	10.535

Table B-21 Adsorption capacity of A-HMS for NAP at pH 5, 7 and 9.

Initial concentration (µg/L)	**A-HMS**					
	pH 5		**pH 7**		**pH 9**	
	Equilibrium concentration (µg/L)	**Adsorption capacity (µg/g)**	**Equilibrium concentration (µg/L)**	**Adsorption capacity (µg/g)**	**Equilibrium concentration (µg/L)**	**Adsorption capacity (µg/g)**
200	168.53	15.735	179.36	10.32	183.24	8.38
150	121.86	14.07	132.13	8.935	136.27	6.865
100	78.34	10.83	85.87	7.065	89.36	5.32
80	59.78	10.11	70.42	4.79	73.41	3.295
60	45.23	7.385	52.32	3.84	54.37	2.815
40	27.36	6.32	34.56	2.72	36.25	1.875

Table B-22 Adsorption capacity of PAC for NAP at pH 5, 7 and 9.

Initial concentration (µg/L)	**PAC**					
	pH 5		**pH 7**		**pH 9**	
	Equilibrium concentration (µg/L)	**Adsorption capacity (µg/g)**	**Equilibrium concentration (µg/L)**	**Adsorption capacity (µg/g)**	**Equilibrium concentration (µg/L)**	**Adsorption capacity (µg/g)**
200	36.47	81.765	31.38	84.31	28.41	85.795
150	29.63	60.185	24.69	62.655	21.24	64.38
100	23.51	38.245	18.42	40.79	16.73	41.635
80	17.29	31.355	11.25	34.375	10.28	34.86
60	-	-	-	-	-	-
40	-	-	-	-	-	-

Table B-23 Adsorption capacity of HMS for CFA at pH 5, 7 and 9.

Initial concentration (µg/L)	HMS					
	pH 5		pH 7		pH 9	
	Equilibrium concentration (µg/L)	Adsorption capacity (µg/g)	Equilibrium concentration (µg/L)	Adsorption capacity (µg/g)	Equilibrium concentration (µg/L)	Adsorption capacity (µg/g)
200	134.41	32.795	143.57	28.215	157.24	21.38
150	97.32	26.34	109.68	20.16	119.63	15.185
100	61.53	19.235	77.53	11.235	87.81	6.095
80	46.61	16.695	65.72	7.14	71.29	4.355
60	37.28	11.36	46.24	6.88	55.44	2.28
40	22.85	8.575	27.18	6.41	35.72	2.14

Table B-24 Adsorption capacity of M-HMS for CFA at pH 5, 7 and 9.

Initial concentration (µg/L)	M-HMS					
	pH 5		pH 7		pH 9	
	Equilibrium concentration (µg/L)	Adsorption capacity (µg/g)	Equilibrium concentration (µg/L)	Adsorption capacity (µg/g)	Equilibrium concentration (µg/L)	Adsorption capacity (µg/g)
200	139.65	30.175	148.75	25.625	156.96	21.52
150	106.22	21.89	112.42	18.79	118.47	15.765
100	71.38	14.31	81.71	9.145	89.63	5.185
80	57.41	11.295	67.85	6.075	71.24	4.38
60	41.24	9.38	49.27	5.365	52.87	3.565
40	24.37	7.815	30.43	4.785	34.32	2.84

Table B-25 Adsorption capacity of A-HMS for CFA at pH 5, 7 and 9.

Initial concentration (µg/L)	**A-HMS**					
	pH 5		**pH 7**		**pH 9**	
	Equilibrium concentration (µg/L)	**Adsorption capacity (µg/g)**	**Equilibrium concentration (µg/L)**	**Adsorption capacity (µg/g)**	**Equilibrium concentration (µg/L)**	**Adsorption capacity (µg/g)**
200	42.74	78.63	50.36	74.82	56.96	71.52
150	33.62	58.19	40.82	54.59	52.14	48.93
100	26.41	36.795	30.14	34.93	37.66	31.17
80	20.38	29.81	25.71	27.145	31.25	24.375
60	16.47	21.765	18.68	20.66	26.42	16.79
40	11.45	14.275	12.36	13.82	19.73	10.135

Table B-26 Adsorption capacity of PAC for CFA at pH 5, 7 and 9.

Initial concentration (µg/L)	**PAC**					
	pH 5		**pH 7**		**pH 9**	
	Equilibrium concentration (µg/L)	**Adsorption capacity (µg/g)**	**Equilibrium concentration (µg/L)**	**Adsorption capacity (µg/g)**	**Equilibrium concentration (µg/L)**	**Adsorption capacity (µg/g)**
200	94.36	52.82	101.45	49.275	99.62	50.19
150	68.82	40.59	72.23	38.885	76.74	36.63
100	44.71	27.645	56.41	21.795	57.98	21.01
80	46.69	16.655	41.86	19.07	45.32	17.34
60	28.63	15.685	30.96	14.52	31.25	14.375
40	24.41	7.795	22.14	8.93	21.25	9.375

Table B-27 Adsorption capacity of HMS for ACT at pH 5, 7 and 9.

Initial concentration (µg/L)	**HMS**					
	pH 5		**pH 7**		**pH 9**	
	Equilibrium concentration (µg/L)	**Adsorption capacity (µg/g)**	**Equilibrium concentration (µg/L)**	**Adsorption capacity (µg/g)**	**Equilibrium concentration (µg/L)**	**Adsorption capacity (µg/g)**
200	159.23	20.385	168.25	15.875	172.88	13.56
150	122.87	13.565	132.14	8.93	136.46	6.77
100	75.53	12.235	87.13	6.435	90.14	4.93
80	61.92	9.04	70.38	4.81	72.48	3.76
60	42.85	8.575	51.82	4.09	54.26	2.87
40	26.28	6.86	33.75	3.125	34.48	2.76

Table B-28 Adsorption capacity of M-HMS for ACT at pH 5, 7 and 9.

Initial concentration (µg/L)	**M-HMS**					
	pH 5		**pH 7**		**pH 9**	
	Equilibrium concentration (µg/L)	**Adsorption capacity (µg/g)**	**Equilibrium concentration (µg/L)**	**Adsorption capacity (µg/g)**	**Equilibrium concentration (µg/L)**	**Adsorption capacity (µg/g)**
200	162.67	18.665	173.5	13.25	177.28	11.36
150	121.52	14.24	137.47	6.265	140.17	4.915
100	76.77	11.615	89.69	5.155	93.66	3.17
80	62.13	8.935	72.82	3.59	74.58	2.71
60	46.98	6.51	54.15	2.925	55.69	2.155
40	28.38	5.81	35.63	2.185	37.24	1.38

Table B-29 Adsorption capacity of A-HMS for ACT at pH 5, 7 and 9.

Initial concentration (µg/L)	**A-HMS**					
	pH 5		**pH 7**		**pH 9**	
	Equilibrium concentration (µg/L)	**Adsorption capacity (µg/g)**	**Equilibrium concentration (µg/L)**	**Adsorption capacity (µg/g)**	**Equilibrium concentration (µg/L)**	**Adsorption capacity (µg/g)**
200	104.46	47.77	124.5	37.75	129.36	35.32
150	76.87	36.565	89.47	30.265	92.47	28.765
100	44.36	27.82	59.69	20.155	64.39	17.805
80	37.82	21.09	45.82	17.09	48.25	15.875
60	27.13	16.435	34.15	12.925	37.86	11.07
40	15.67	12.165	22.63	8.685	26.4	6.8

Table B-30 Adsorption capacity of PAC for ACT at pH 5, 7 and 9.

Initial concentration (µg/L)	**PAC**					
	pH 5		**pH 7**		**pH 9**	
	Equilibrium concentration (µg/L)	**Adsorption capacity (µg/g)**	**Equilibrium concentration (µg/L)**	**Adsorption capacity (µg/g)**	**Equilibrium concentration (µg/L)**	**Adsorption capacity (µg/g)**
200	88.69	55.655	82.34	58.83	90.56	54.72
150	67.54	41.23	63.65	43.175	65.74	42.13
100	53.63	23.185	47.41	26.295	49.63	25.185
80	36.41	21.795	31.25	24.375	29.17	25.415
60	30.41	14.795	27.36	16.32	28.36	15.82
40	19.66	10.17	17.84	11.08	18.69	10.655

Table B-31 Adsorption capacity of HMS in mixed solute solution.

Initial concentration (µg/L)	**HMS**									
	DCF		**CBZ**		**NAP**		**CFA**		**ACT**	
	Equilibrium concentration (µg/L)	**Adsorption capacity (µg/g)**	**Equilibrium concentration (µg/L)**	**Adsorption capacity (µg/g)**	**Equilibrium concentration (µg/L)**	**Adsorption capacity (µg/g)**	**Equilibrium concentration (µg/L)**	**Adsorption capacity (µg/g)**	**Equilibrium concentration (µg/L)**	**Adsorption capacity (µg/g)**
200	111.25	44.375	119.61	40.195	160.36	19.82	148.12	25.94	170.42	14.79
150	81.36	34.32	90.85	29.575	122.41	13.795	115.26	17.37	136.96	6.52
100	52.24	23.88	58.41	20.795	82.63	8.685	75.74	12.13	89.78	5.11
80	47.25	16.375	53.63	13.185	66.51	6.745	59.63	10.185	72.24	3.88
60	32.36	13.82	37.57	11.215	48.62	5.69	46.24	6.88	53.37	3.315
40	18.24	10.88	20.56	9.72	30.36	4.82	24.52	7.74	35.36	2.32

Table B-32 Adsorption capacity of M-HMS in mixed solute solution.

Initial concentration (µg/L)	A-HMS									
	DCF		CBZ		NAP		CFA		ACT	
	Equilibrium concentration (µg/L)	Adsorption capacity (µg/g)	Equilibrium concentration (µg/L)	Adsorption capacity (µg/g)	Equilibrium concentration (µg/L)	Adsorption capacity (µg/g)	Equilibrium concentration (µg/L)	Adsorption capacity (µg/g)	Equilibrium concentration (µg/L)	Adsorption capacity (µg/g)
200	78.32	60.84	95.78	52.11	107.36	46.32	153.36	23.32	169.14	15.43
150	60.27	44.865	72.36	38.82	84.71	32.645	115.44	17.28	135.37	7.315
100	38.63	30.685	47.31	26.345	54.24	22.88	84.23	7.885	88.87	5.565
80	32.14	23.93	37.74	21.13	42.28	18.86	69.52	5.24	73.36	3.32
60	18.44	20.78	22.53	18.735	34.76	12.62	51.36	4.32	56.21	1.895
40	14.36	12.82	18.42	10.79	24.88	7.56	31.33	4.335	34.78	2.61

Table B-33 Adsorption capacity of A-HMS in mixed solute solution.

Initial concentration (µg/L)	A-HMS									
	DCF		CBZ		NAP		CFA		ACT	
	Equilibrium concentration (µg/L)	Adsorption capacity (µg/g)	Equilibrium concentration (µg/L)	Adsorption capacity (µg/g)	Equilibrium concentration (µg/L)	Adsorption capacity (µg/g)	Equilibrium concentration (µg/L)	Adsorption capacity (µg/g)	Equilibrium concentration (µg/L)	Adsorption capacity (µg/g)
200	183.54	8.23	186.63	6.685	175.86	12.07	60.68	69.66	142.36	28.82
150	141.23	4.385	137.19	6.405	128.25	10.875	49.74	50.13	109.74	20.13
100	90.44	4.78	92.74	3.63	83.41	8.295	36.52	31.74	65.28	17.36
80	71.85	4.075	72.89	3.555	67.78	6.11	32.32	23.84	54.62	12.69
60	53.41	3.295	52.11	3.945	49.63	5.185	20.66	19.67	39.65	10.175
40	34.14	2.93	34.93	2.535	33.26	3.37	15.41	12.295	24.41	7.795

Table B-34 Adsorption capacity of PAC in mixed solute solution.

Initial concentration (µg/L)	**PAC**									
	DCF		**CBZ**		**NAP**		**CFA**		**ACT**	
	Equilibrium concentration (µg/L)	**Adsorption capacity (µg/g)**	**Equilibrium concentration (µg/L)**	**Adsorption capacity (µg/g)**	**Equilibrium concentration (µg/L)**	**Adsorption capacity (µg/g)**	**Equilibrium concentration (µg/L)**	**Adsorption capacity (µg/g)**	**Equilibrium concentration (µg/L)**	**Adsorption capacity (µg/g)**
200	48.78	75.61	87.63	56.185	44.63	77.685	108.36	45.82	98.63	50.685
150	41.52	54.24	64.63	42.685	32.31	58.845	82.74	33.63	70.25	39.875
100	28.69	35.655	52.36	23.82	21.56	39.22	64.25	17.875	54.96	22.52
80	27.44	26.28	44.14	17.93	21.68	29.16	49.68	15.16	46.74	16.63
60	-	-	-	-	-	-	-	-	-	-
40	-	-	-	-	-	-	-	-	-	-

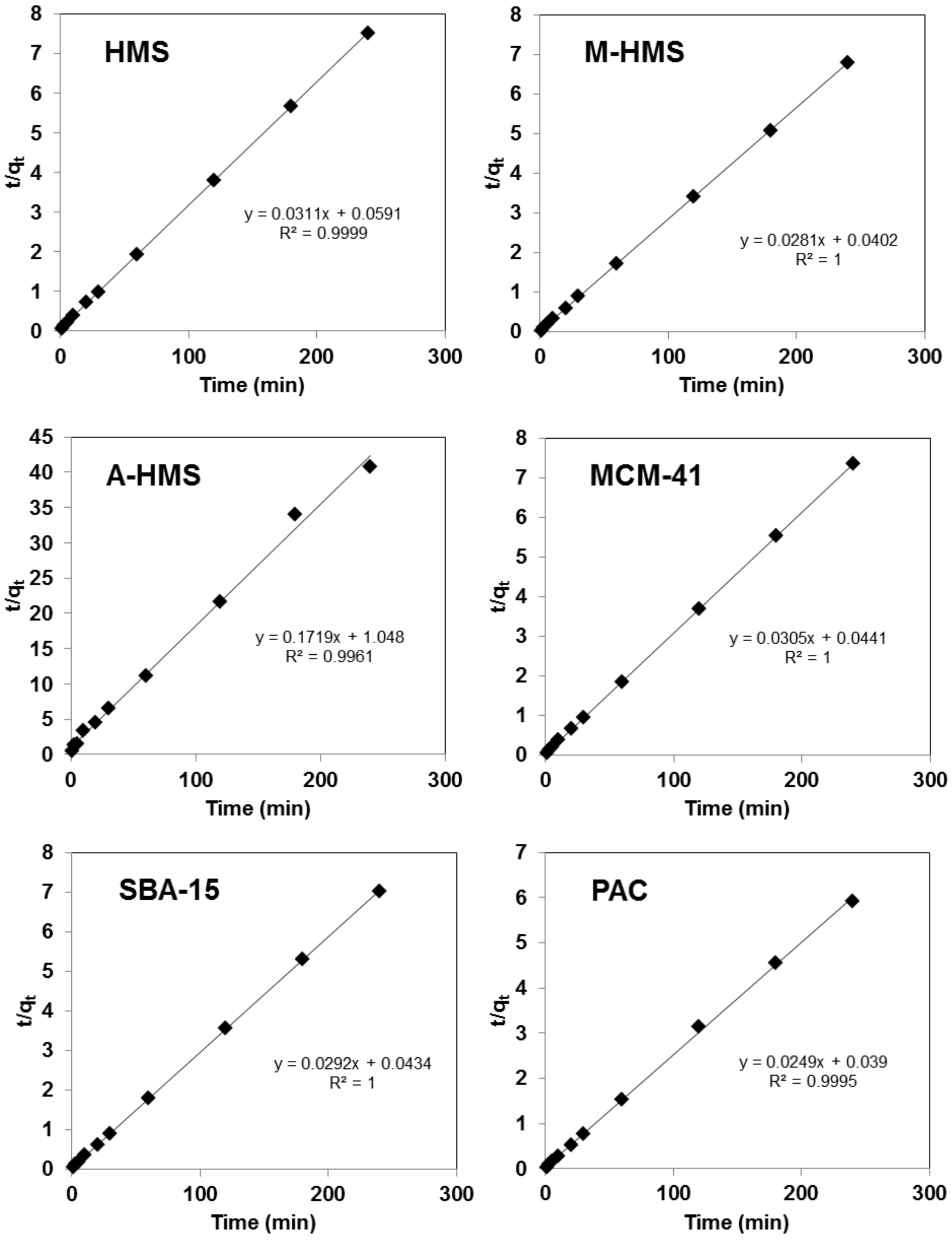

Figure B-1 Kinetic of DCF removal according to the pseudo 2nd order model (pH 7, 25 °C and IS 0.01M).

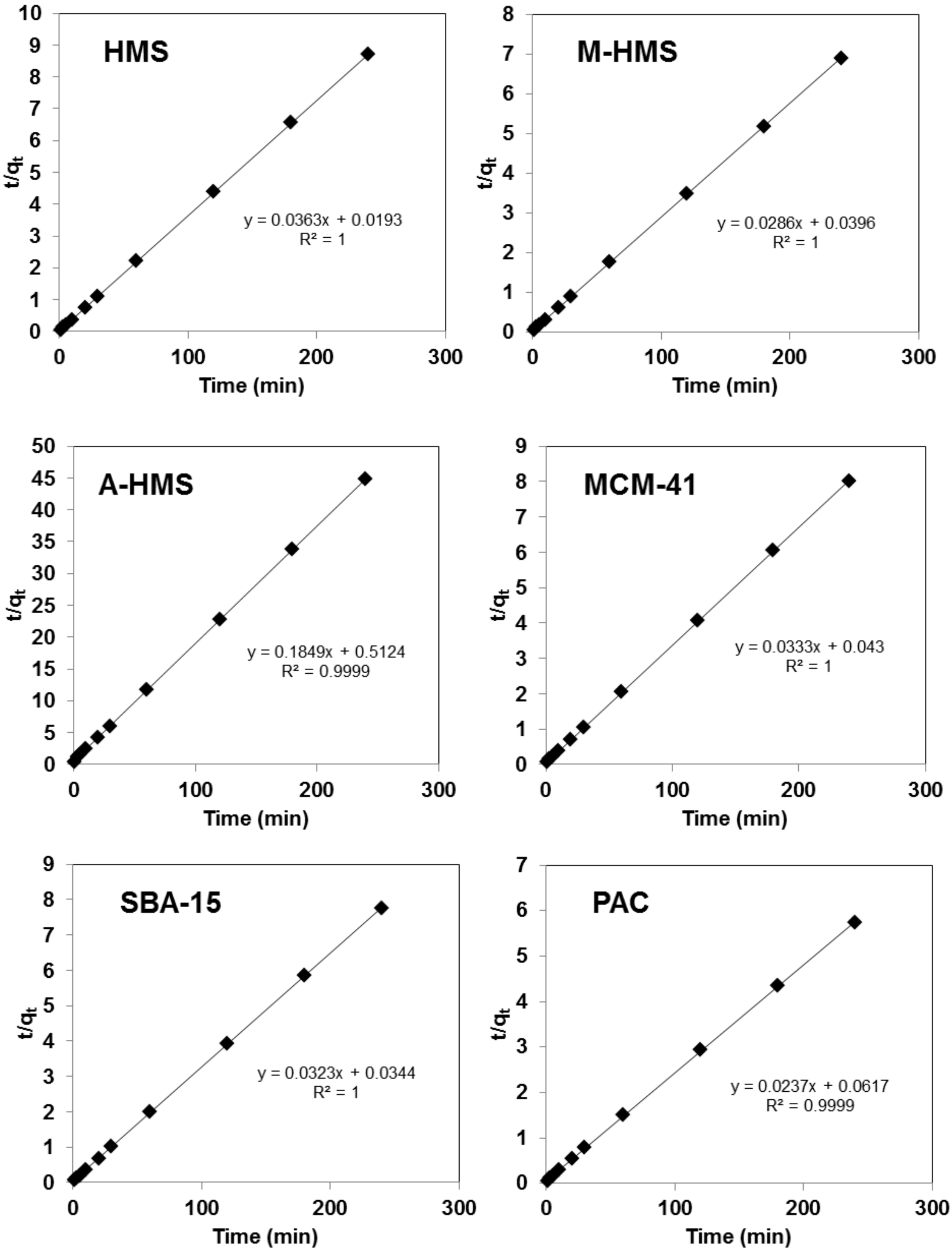

Figure B-2 Kinetic of CBZ removal according to the pseudo 2nd order model (pH 7, 25 ^{o}C and IS 0.01M).

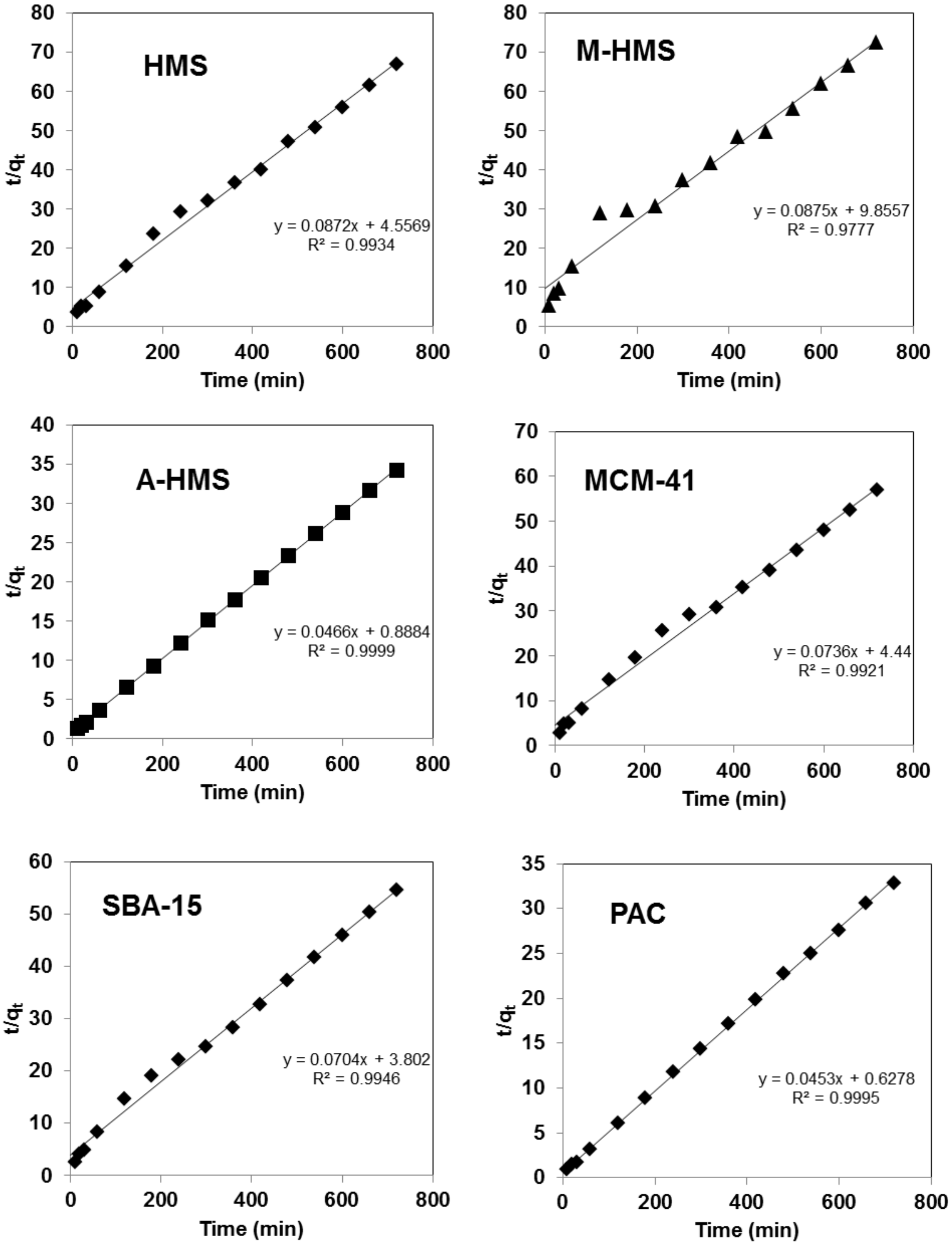

Figure B-5 Kinetic of ACT removal according to the pseudo 2nd order model (pH 7, 25 °C and IS 0.01M).

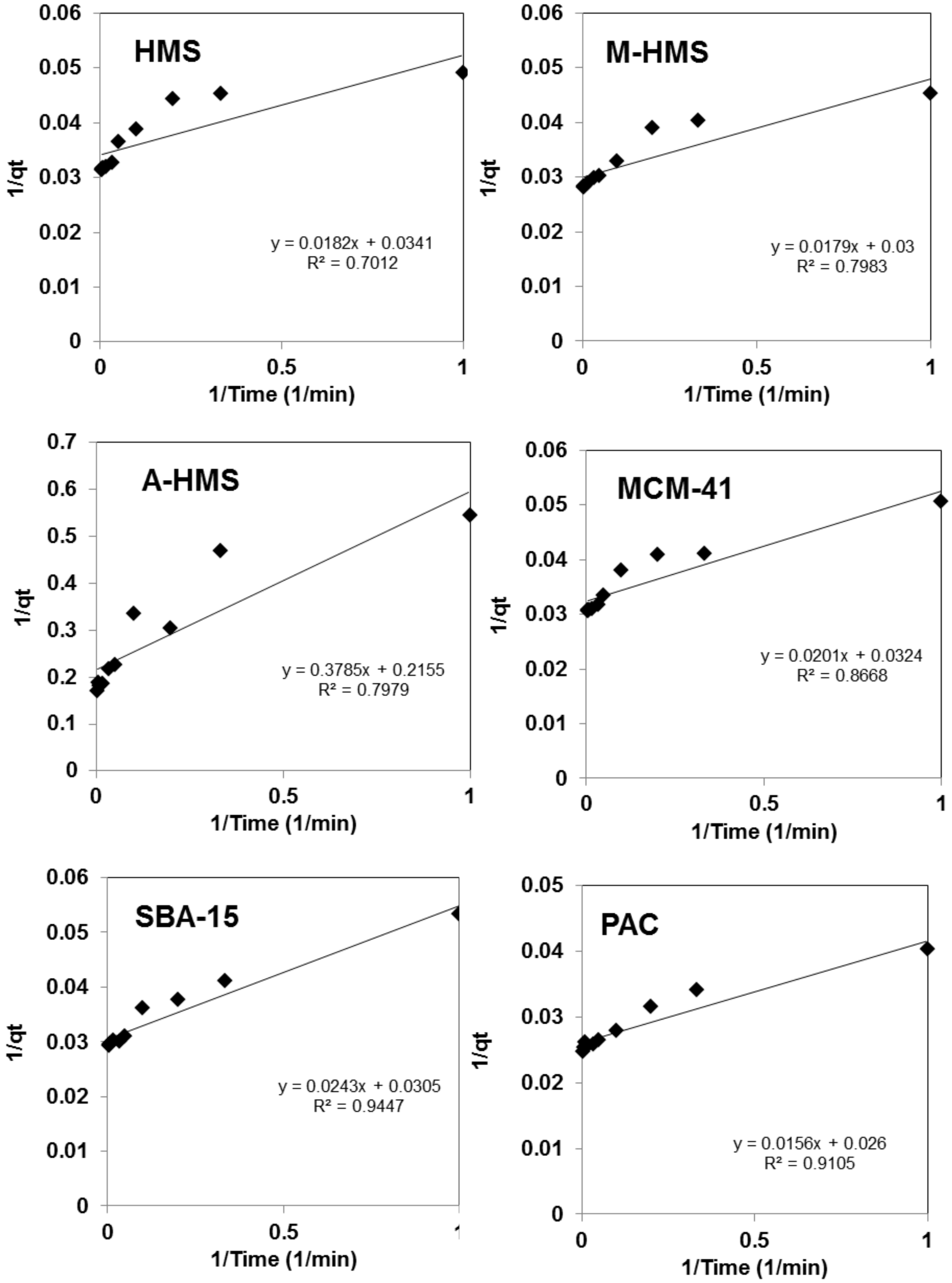

Figure B-6 Kinetic of DCF removal according to the Ritchie-second-order model (pH 7, 25 °C and IS 0.01M).

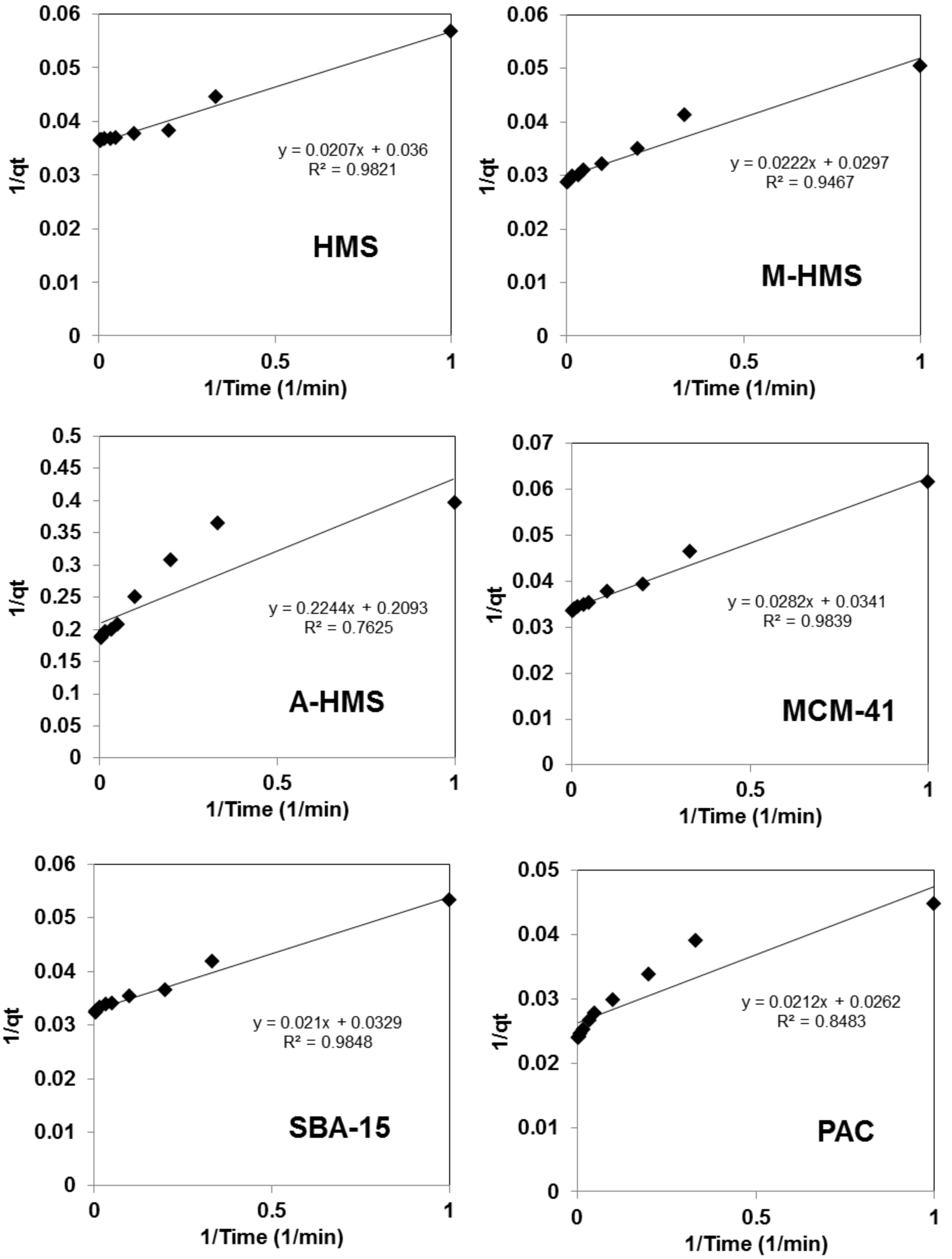

Figure B-7 Kinetic of CBZ removal according to the Ritchie-second-order model (pH 7, 25 °C and IS 0.01M).

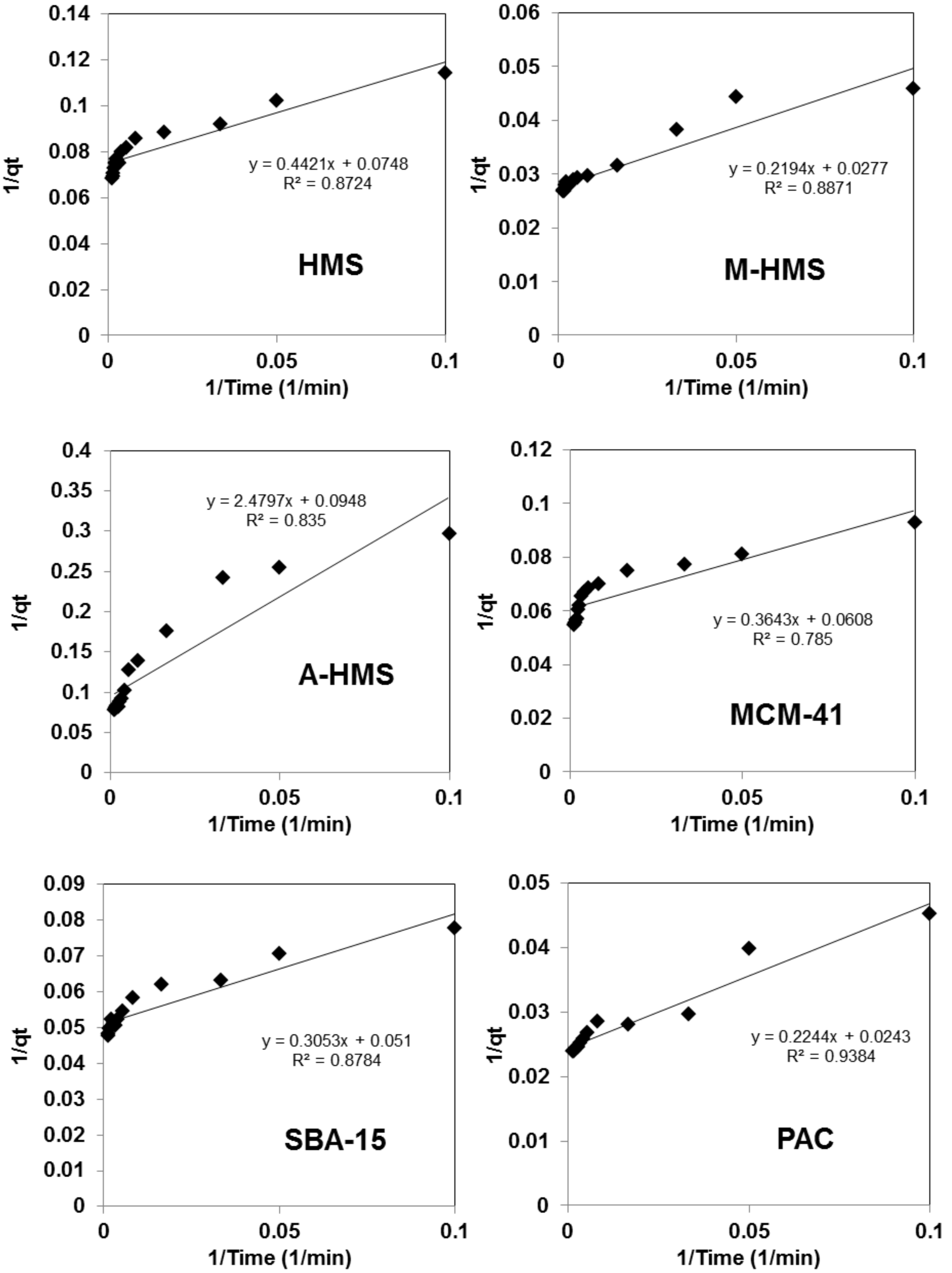

Figure B-8 Kinetic of NAP removal according to the Ritchie-second-order model (pH 7, 25 ^{o}C and IS 0.01M).

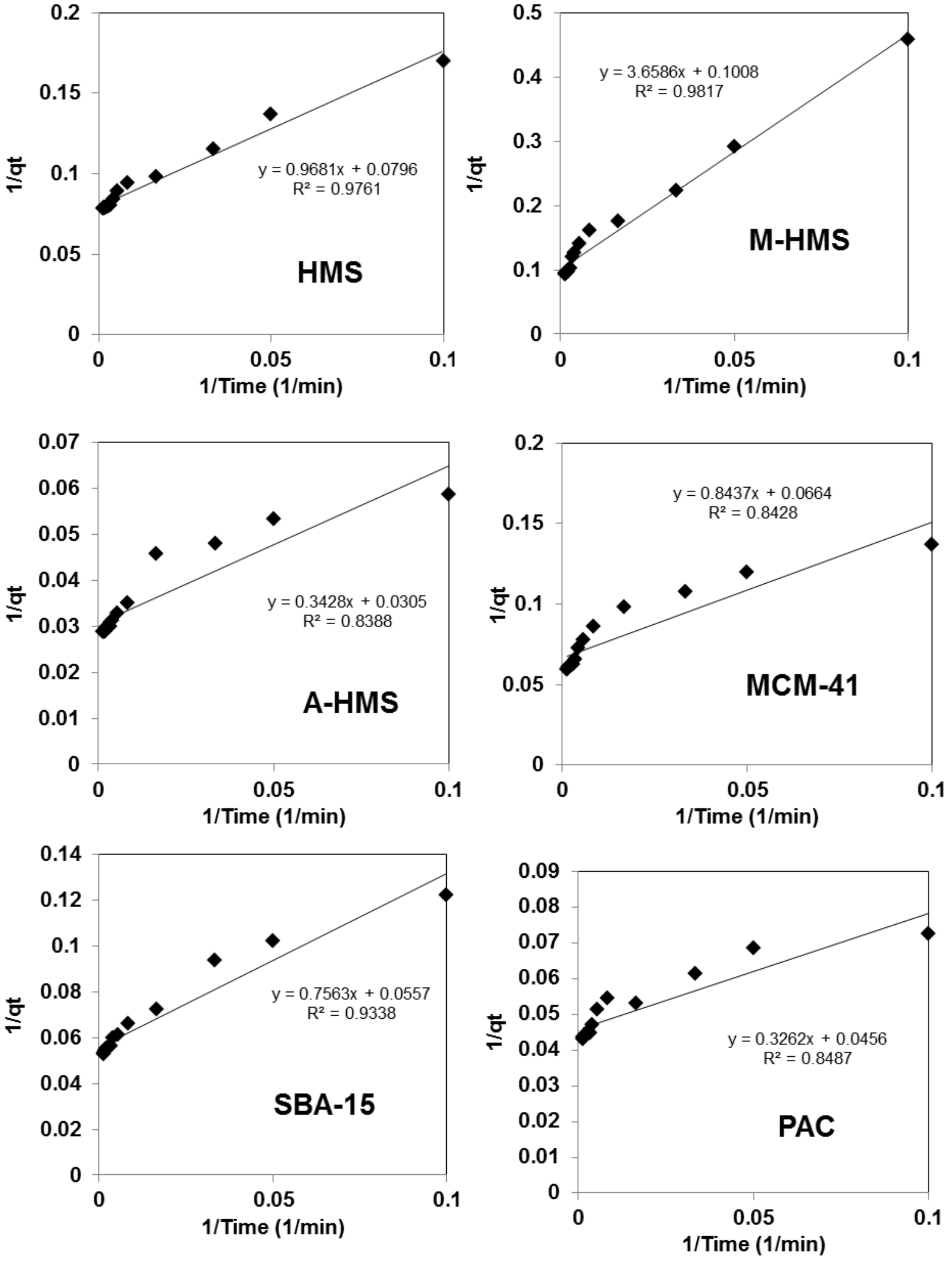

Figure B-9 Kinetic of CFA removal according to the Ritchie-second-order model (pH 7, 25 °C and IS 0.01M).

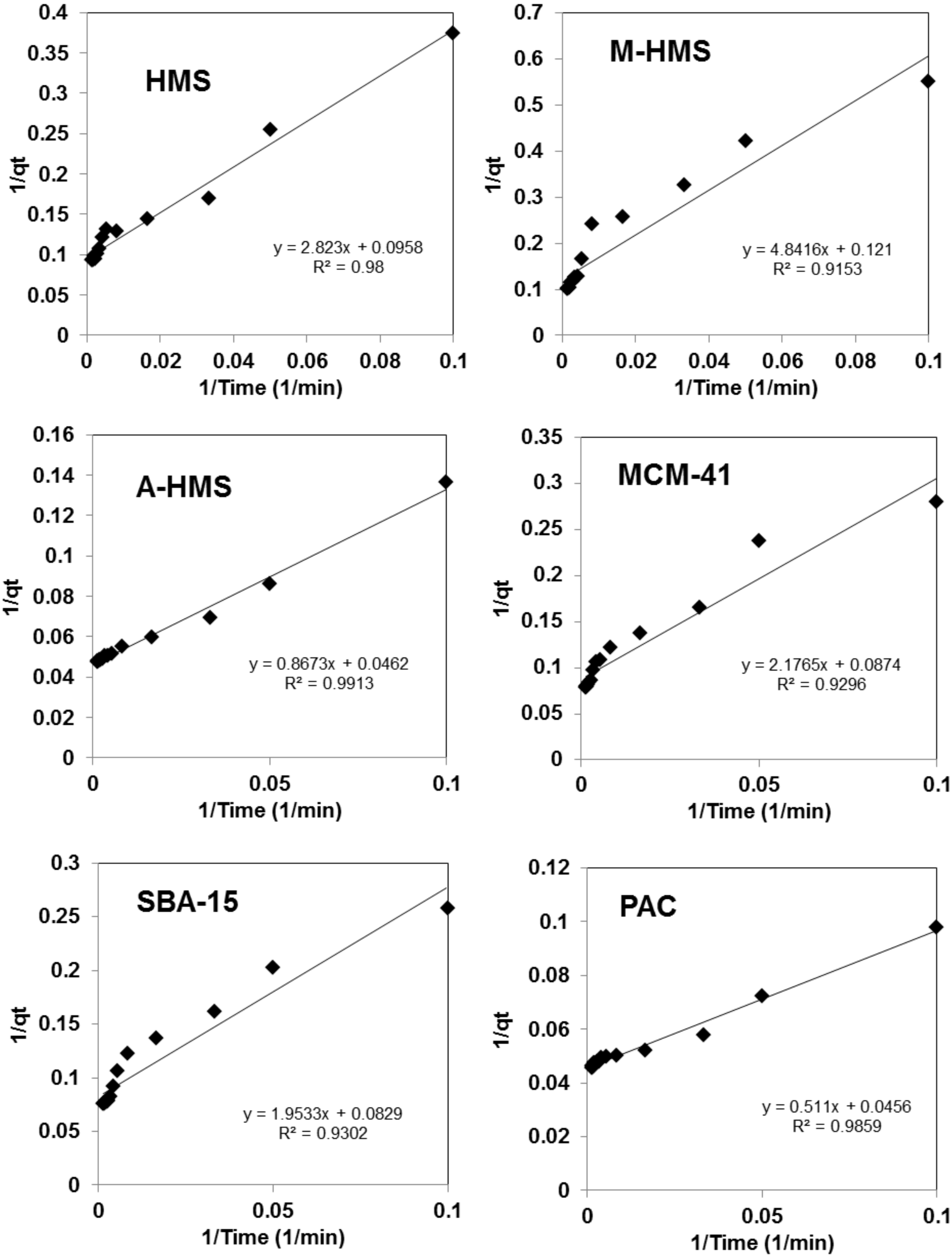

Figure B-10 Kinetic of ACT removal according to the Ritchie-second-order model (pH 7, 25 ^{o}C and IS 0.01M).

APENDIX C

Experimental results for removal of Clofibic acid by adsorption on periodic mesoporous organosilicas

Table C-1 Adsorption kinetics data of CFA adsorbed onto PMO and the functionalized PMO derivatives

Time (min)	**Pharmaceutical concentration (µg/L)**									
	PMO	**1N10PMO**	**1N25PMO**	**1N40PMO**	**2N10PMO**	**2N25PMO**	**2N40PMO**	**3N10PMO**	**3N25PMO**	**3N40PMO**
0	100.00	100.00	100.00	100.00	100.00	100.00	100.00	100.00	100.00	100.00
5	78.82	73.96	70.87	64.96	76.39	73.74	65.36	63.54	62.86	46.88
10	69.73	64.09	65.80	46.38	65.45	64.36	46.21	52.36	48.71	39.62
20	64.82	60.36	48.33	35.69	59.51	40.85	37.85	43.42	43.63	30.78
30	65.27	50.12	39.69	30.42	55.70	36.96	32.96	36.96	32.97	25.68
60	63.85	47.84	39.74	26.37	51.36	28.36	28.63	27.63	20.60	18.24
120	56.14	46.32	38.63	24.96	47.25	28.47	16.56	27.42	19.76	13.93
180	58.75	46.14	38.28	23.36	45.06	26.23	15.41	27.17	18.41	12.82
240	54.82	46.28	38.96	23.87	44.87	25.81	16.63	26.36	18.08	12.36
300	54.56	46.86	38.37	22.98	44.84	27.41	15.28	26.13	17.72	12.14
360	54.13	45.84	37.89	23.82	43.98	24.96	15.17	25.36	17.36	11.96
420	54.06	45.92	37.63	23.26	44.71	26.28	16.92	25.23	17.21	12.81
480	53.82	45.87	37.74	22.88	43.93	24.83	17.86	25.16	17.88	11.47
540	53.75	45.83	37.52	22.47	43.88	24.71	14.97	24.93	16.73	12.26
600	53.70	45.77	37.48	22.65	43.81	24.68	14.78	25.12	16.96	11.94
660	53.67	45.69	37.40	22.40	43.72	24.60	14.63	24.89	16.54	11.15

Table C-1 Adsorption kinetics data of CFA adsorbed onto PMO and the functionalized PMO derivatives (continue).

Time (min)	**Adsorption capacity (μg/g)**									
	PMO	**1N10PMO**	**1N25PMO**	**1N40PMO**	**2N10PMO**	**2N25PMO**	**2N40PMO**	**3N10PMO**	**3N25PMO**	**3N40PMO**
0	0.00	0.00	0.00	0.00	0.00	0.00	0.00	0.00	0.00	0.00
5	10.59	13.02	14.57	17.52	11.81	13.13	17.32	18.23	18.57	26.56
10	15.14	17.96	17.10	26.81	17.28	17.82	26.90	23.82	25.65	30.19
20	17.59	19.82	25.84	32.16	20.25	29.58	31.08	28.29	28.19	34.61
30	17.37	24.94	30.16	34.79	22.15	31.52	33.52	31.52	33.52	37.16
60	18.08	26.08	30.13	36.82	24.32	35.82	35.69	36.19	39.70	40.88
120	21.93	26.84	30.69	37.52	26.38	35.77	41.72	36.29	40.12	43.04
180	20.63	26.93	30.86	38.32	27.47	36.89	42.30	36.42	40.80	43.59
240	22.59	26.86	30.52	38.07	27.57	37.10	41.69	36.82	40.96	43.82
300	22.72	26.57	30.82	38.51	27.58	36.30	42.36	36.94	41.14	43.93
360	22.94	27.08	31.06	38.09	28.01	37.52	42.42	37.32	41.32	44.02
420	22.97	27.04	31.19	38.37	27.65	36.86	41.54	37.39	41.40	43.60
480	23.09	27.07	31.13	38.56	28.04	37.59	41.07	37.42	41.06	44.27
540	23.13	27.09	31.24	38.77	28.06	37.65	42.52	37.54	41.64	43.87
600	23.15	27.12	31.26	38.68	28.10	37.66	42.61	37.44	41.52	44.03
660	23.17	27.16	31.30	38.80	28.14	37.70	42.69	37.56	41.73	44.43

Table C-2 Adsorption capacity of PMO and the functionalized PMO derivatives for CFA.

Initial concentration (µg/L)	**Equilibrium concentration (µg/L)**	**Adsorption capacity (µg/g)**
		PMO
200	105.57	47.215
150	74.85	37.575
100	53.67	23.165
80	42.26	18.87
60	32.56	13.72
40	20.47	9.765

Initial concentration (µg/L)	**Equilibrium concentration (µg/L)**	**Adsorption capacity (µg/g)**	**Equilibrium concentration (µg/L)**	**Adsorption capacity (µg/g)**	**Equilibrium concentration (µg/L)**	**Adsorption capacity (µg/g)**
		1N10PMO		**1N25PMO**		**1N40PMO**
200	65.74	67.13	60.36	69.82	42.36	78.82
150	56.87	46.565	52.85	48.575	34.85	57.575
100	45.69	27.155	37.36	31.32	22.36	38.82
80	33.81	23.095	28.65	25.675	18.65	30.675
60	26.54	16.73	24.36	17.82	14.36	22.82
40	15.47	12.265	13.47	13.265	10.47	14.765

Table C-2 Adsorption capacity of PMO and the functionalized PMO derivatives for CFA (continue).

Initial concentration (µg/L)	**Equilibrium concentration (µg/L)**	**Adsorption capacity (µg/g)**	**Equilibrium concentration (µg/L)**	**Adsorption capacity (µg/g)**	**Equilibrium concentration (µg/L)**	**Adsorption capacity (µg/g)**
		2N10PMO		**2N25PMO**		**2N40PMO**
200	61.85	69.075	46.74	76.63	33.53	83.235
150	53.85	48.075	34.52	57.74	23.45	63.275
100	43.75	28.125	24.63	37.685	14.61	42.695
80	30.63	24.685	16.63	31.685	12.35	33.825
60	24.52	17.74	12.85	23.575	10.42	24.79
40	13.68	13.16	8.47	15.765	-	-

Initial concentration (µg/L)	**Equilibrium concentration (µg/L)**	**Adsorption capacity (µg/g)**	**Equilibrium concentration (µg/L)**	**Adsorption capacity (µg/g)**	**Equilibrium concentration (µg/L)**	**Adsorption capacity (µg/g)**
		3N10PMO		**3N25PMO**		**3N40PMO**
200	38.43	80.785	34.26	82.87	20.32	89.84
150	32.24	58.88	26.87	61.565	15.74	67.13
100	24.89	37.555	16.54	41.73	11.25	44.375
80	21.36	29.32	13.25	33.375	8.65	35.675
60	15.63	22.185	10.57	24.715	6.58	26.71
40	10.86	14.57	7.24	16.38	-	-

Table C-3 Adsorption capacity of PMOs with different surface functional group densities per surface area.

Initial concentration (μg/L)	Equilibrium concentration (μg/L)	Adsorption capacity (ng/m^2)
		PMO
200	105.57	37.71
150	74.85	30.01
100	53.67	18.50
80	42.26	15.07
60	32.56	10.96
40	20.47	7.80

Initial concentration (μg/L)	Equilibrium concentration (μg/L)	Adsorption capacity (ng/m^2)	Equilibrium concentration (μg/L)	Adsorption capacity (ng/m^2)	Equilibrium concentration (μg/L)	Adsorption capacity (ng/m^2)
		1N10PMO		1N25PMO		1N40PMO
200	65.74	57.08	60.36	63.73	42.36	72.54
150	56.87	39.60	52.85	44.34	34.85	52.99
100	45.69	23.09	37.36	28.59	22.36	35.73
80	33.81	19.64	28.65	23.44	18.65	28.23
60	26.54	14.23	24.36	16.27	14.36	21.00
40	15.47	10.43	13.47	12.11	10.47	13.59

Table C-3 Adsorption capacity of PMOs with different surface functional group densities per surface area (continue).

Initial concentration (µg/L)	**Equilibrium concentration (µg/L)**	**Adsorption capacity (ng/m^2)**	**Equilibrium concentration (µg/L)**	**Adsorption capacity (ng/m^2)**	**Equilibrium concentration (µg/L)**	**Adsorption capacity (ng/m^2)**
		2N10PMO		**2N25PMO**		**2N40PMO**
200	61.85	61.54	46.74	70.56	33.53	86.39
150	53.85	42.83	34.52	53.16	23.45	65.67
100	43.75	25.06	24.63	34.70	14.61	44.31
80	30.63	21.99	16.63	29.17	12.35	35.11
60	24.52	15.80	12.85	21.71	10.42	25.73
40	13.68	11.72	8.47	14.52	-	20.76

Initial concentration (µg/L)	**Equilibrium concentration (µg/L)**	**Adsorption capacity (ng/m^2)**	**Equilibrium concentration (µg/L)**	**Adsorption capacity (ng/m^2)**	**Equilibrium concentration (µg/L)**	**Adsorption capacity (ng/m^2)**
		3N10PMO		**3N25PMO**		**3N40PMO**
200	38.43	65.66	34.26	69.75	20.32	86.60
150	32.24	47.86	26.87	51.82	15.74	64.71
100	24.89	30.53	16.54	35.12	11.25	42.78
80	21.36	23.83	13.25	28.09	8.65	34.39
60	15.63	18.03	10.57	20.80	6.58	25.75
40	10.86	11.84	7.24	13.79	-	-

Table C-4 Adsorption capacity of PMOs with different surface functional group densities per nitrogen content.

Initial concentration (μg/L)	**Equilibrium concentration (μg/L)**	**Adsorption capacity (μg/mmol of N)**	**Equilibrium concentration (μg/L)**	**Adsorption capacity (μg/mmol of N)**	**Equilibrium concentration (μg/L)**	**Adsorption capacity (μg/mmol of N)**
		1N10PMO		**1N25PMO**		**1N40PMO**
200	65.74	261.06	60.36	128.08	42.36	101.24
150	56.87	181.09	52.85	89.11	34.85	73.95
100	45.69	105.60	37.36	57.45	22.36	49.86
80	33.81	89.81	28.65	47.10	18.65	39.40
60	26.54	65.06	24.36	32.69	14.36	29.31
40	15.47	47.70	13.47	24.33	10.47	18.96

Initial concentration (μg/L)	**Equilibrium concentration (μg/L)**	**Adsorption capacity (μg/mmol of N)**	**Equilibrium concentration (μg/L)**	**Adsorption capacity (μg/mmol of N)**	**Equilibrium concentration (μg/L)**	**Adsorption capacity (μg/mmol of N)**
		2N10PMO		**2N25PMO**		**2N40PMO**
200	61.85	167.02	46.74	140.57	33.53	106.91
150	53.85	116.24	34.52	105.92	23.45	81.27
100	43.75	68.01	24.63	69.13	14.61	54.84
80	30.63	59.69	16.63	58.12	12.35	43.44
60	24.52	42.89	12.85	43.25	10.42	31.84
40	13.68	31.82	8.47	28.92	-	-

Table C-4 Adsorption capacity of PMOs with different surface functional group densities per nitrogen content (continue).

Initial concentration (µg/L)	**Equilibrium concentration (µg/L)**	**Adsorption capacity (µg/mmol of N)**	**Equilibrium concentration (µg/L)**	**Adsorption capacity (µg/mmol of N)**	**Equilibrium concentration (µg/L)**	**Adsorption capacity (µg/mmol of N)**
		3N10PMO		**3N25PMO**		**3N40PMO**
200	38.43	146.03	34.26	88.70	20.32	70.54
150	32.24	106.43	26.87	65.90	15.74	52.71
100	24.89	67.89	16.54	44.67	11.25	34.84
80	21.36	53.00	13.25	35.72	8.65	28.01
60	15.63	40.10	10.57	26.45	6.58	20.97
40	10.86	26.34	7.24	17.53	-	-

Table C-5 Adsorption capacity of PMOs at different pH.

pH	Initial concentration (µg/L)	Equilibrium concentration (µg/L)									
		PMO	1N10PMO	1N25PMO	1N40PMO	2N10PMO	2N25PMO	2N40PMO	3N10PMO	3N25PMO	3N40PMO
5	**100**	48.32	41.44	32.15	18.69	39.43	19.26	12.21	19.36	12.41	7.52
7	**100**	53.67	45.69	37.36	22.36	43.75	24.63	14.61	24.89	16.54	11.25
9	**100**	55.39	48.32	44.41	26.55	48.36	31.33	20.14	28.44	21.36	13.77

pH	Initial concentration (µg/L)	Adsorption capacity (µg/g)									
		PMO	1N10PMO	1N25PMO	1N40PMO	2N10PMO	2N25PMO	2N40PMO	3N10PMO	3N25PMO	3N40PMO
5	**100**	25.84	29.28	33.93	40.66	30.29	40.37	43.90	40.32	43.80	46.24
7	**100**	23.17	27.16	31.32	38.82	28.13	37.69	42.70	37.56	41.73	44.38
9	**100**	22.31	25.84	27.80	36.73	25.82	34.34	39.93	35.78	39.32	43.12

BIOGRAPHY

Mr. Nakorn Suriyanon was born in 18 February 1978 in Chiang Mai, Thailand. He received his Bachelor degree (1999) and Master degree (2008) in Environmental Engineering from Chiang Mai University. After that he pursued his Ph.D study in environmental management at International Postgraduate programs in Environmental Management of National Center of Excellence for Environmental and Hazardous Waste Management, Chulalongkorn University, from 2009 to 2013.

Journal publications

1. N. Suriyanon, P. Punyapalakul, C. Ngamcharussrivichai, Mechanistic Study of Diclofenac and Carbamazepine Adsorption on Functionalized Silica-based Porous Materials, Chem. Eng. J. 214 (2013) 208-218.
2. S. Karnchanawong, N. Suriyanon, Household organic waste composting using bins with different types of passive aeration, Resources, Conservation and Recycling 55 (2011) 548–553.
3. นคร สุริยานนท์, สมใจ กาญจนวงศ์, การหมักขยะอินทรีย์ครัวเรือนในถังหมักที่มีการเติมอากาศด้วยวิธีแพสซีฟแบบต่างๆ, วารสารวิศวกรรมสิ่งแวดล้อมไทย ปีที่ 23 ฉบับที่ 3 เลขหน้า 127-137 ปีพ.ศ. 2552.

Employment:

Employer	**Position**	**Year**
1. Uthai Consultant Company Bangkok	Sanitary Engineer	2000-2001
2. Biogas Technology Center Chiang Mai University	Environmental Engineer	2001-2003
3. Chiang Mai Home Clinic Company	Civil Engineer	2005-2006